



universität  
wien

# DISSERTATION DOCTORAL THESIS

Titel der Dissertation  
Title of the Doctoral Thesis

**Quantum measurement and control of  
mechanical motion at room temperature**

verfasst von  
submitted by

**Lorenzo Magrini**

angestrebter akademischer Grad  
in partial fulfilment of the requirements for the degree of

**Doktor der Naturwissenschaften (Dr. rer. nat.)**

Wien, 2021/ Vienna, 2021

Studienkennzahl lt. Studienblatt

Degree programme code as it appears on the student

record sheet . . . . . UA 796 605 411

Dissertationsgebiet lt. Studienblatt

Field of study as it appears on the student record sheet . . . . . Physik

Betreut von / Supervisor . . . . . Univ.-Prof. Dr. Markus Aspelmeyer

Lorenzo Magrini

*Quantum measurement and control of mechanical motion at room temperature*,  
Doctoral Thesis, ©2021 University of Vienna.

WEBSITE:

<https://aspelmeyer.quantum.at/>

E-MAIL:

[lorenzo.magrini@univie.ac.at](mailto:lorenzo.magrini@univie.ac.at)

[lorenzomgrn@gmail.com](mailto:lorenzomgrn@gmail.com)

---

Image at page 20 by Lorenzo Magrini published as cover on *Optica*, 5(12), December 20th 2018. Reprinted with permission ©2018 The Optical Society of America

<https://www.osapublishing.org/optica/fulltext.cfm?uri=optica-5-12-1597&id=403090>

Image at page 42 by Lorenzo Magrini, published as cover on *Nature* 595(7867), July 15th 2021. Reprinted with permission ©2021 Nature

<https://www.nature.com/nature/volumes/595/issues/7867>

Image at page 88 by Mattia Balsamini, first published in the *Scientific American* article: “Quantum Gravity in the Lab” by Tim Folger. Reprinted with permission ©2019 Mattia Balsamini

<https://www.scientificamerican.com/article/quantum-gravity-in-the-lab/>  
<http://www.mattiabalsamini.com/>

“Vienna non è Austria, non è Alpi.  
È Danubio. Ed è, anche, la testa  
troppo grande di un corpo che non  
c’è più: l’impero.”

---

*Paolo Rumiz*

“Gestern früh war es schon am  
dämmernden Morgen so heiß, daß  
Arbeit – geistige Arbeit –  
hoffnungslos schien, ein  
gottgewollter Donautag zog  
herauf.”

---

*Konrad Lorenz*





# ABSTRACT

The Heisenberg uncertainty principle establishes the frontier to the quantum realm, where the act of observation plays a critical role. It poses a fundamental limit to our knowledge about a system: the position of a particle, the spin of an atom or the energy of a photon can only be known with finite precision. Realizing measurements and building sensors that approach this fundamental limit is a challenging effort, one that is suited to reveal the quantum properties of seemingly classical objects. In this thesis I describe how the motion of a levitated glass sphere at room temperature can be measured and controlled at this quantum limit.

In a first experiment the particle is trapped in the near-field of a photonic crystal demonstrating a measurement efficiency of 9%, two orders of magnitude larger than previously reported for levitated systems. With a tunable single-photon optomechanical coupling of up to  $g_0/2\pi = 9$  kHz, this represents an exciting interface for the study of optical fields in super resolution and the measurement of short range forces. In a second experiment the approach is different: here the particle is trapped in an optical tweezer in free space. The combination of a Heisenberg limited confocal measurement and optimal state estimation via Kalman filtering allows to track the state of the particle in phase space with an uncertainty of 1.3 times the zero point fluctuation. With optimal feedback the quantum harmonic oscillator is then stabilized to a mean occupation of  $n = 0.56 \pm 0.02$  quanta, realizing quantum ground state cooling in a room temperature environment. Finally, the generation of squeezed light is observed as the result radiation pressure (ponderomotive) forces driving the oscillating particle, for the first time without a cavity.

These results pave the way for quantum experiments with levitated solid-state objects, ranging from non-classical states of motion for tests of macroscopic quantum phenomena to the development of new force and impulse sensors for searches of new physics such as dark matter.

# ZUSAMMENFASSUNG

Die Heisenbergsche Unschärferelation markiert die Grenze zur Quantenwelt, in welcher der Akt der Beobachtung eine entscheidende Rolle spielt. Sie schränkt unser mögliches Wissen über ein System wesentlich ein: Die Position eines Teilchens, der Spin eines Atoms oder die Energie eines Photons können nur mit endlicher Genauigkeit bestimmt werden. Die Durchführung von Messungen und der Bau von Sensoren die sich dieser fundamentalen Grenze annähern, ist eine anspruchsvolle Aufgabe und eignet sich auch die Quanteneigenschaften scheinbar klassischer Objekte aufzudecken. In dieser Arbeit beschreibe ich, wie die Bewegung einer schwebenden Glaskugel bei Raumtemperatur an dieser Quantengrenze gemessen und kontrolliert werden kann.

In einem ersten Experiment wird das Teilchen im Nahfeld eines photonischen Kristalls gefangen und zeigt eine Messeffizienz von 9%. Dies entspricht einer Verbesserung um zwei Größenordnungen gegenüber vormals publizierten levitierten Systeme. Mit einer verstimmbaren optomechanischen Einzelphotonenkopplung von bis zu  $g_0/2\pi = 9$  kHz stellt dies eine spannende Schnittstelle für die Untersuchung optischer Felder in Superauflösung und die Messung von Kräften im Nahbereich dar. In einem zweiten Experiment wurde ein anderer Ansatz gewählt: Hier ist das Teilchen

in einer optischen Pinzette im freien Raum gefangen. Die Kombination aus einer Heisenberg-begrenzten konfokalen Messung und einer optimalen Zustandsbestimmung mittels Kalman-Filter ermöglichen es, den Zustand des Teilchens im Phasenraum mit einer Unsicherheit von 1.3 Nullpunktsfluktuation zu verfolgen. Mit Hilfe optimaler Rückkopplung wird der harmonische Quantenoszillator dann auf eine mittlere Besetzung von  $n = 0.56 \pm 0.02$  Quanten stabilisiert. Dies entspricht einer Kühlung in den Quantengrundzustand in einer Umgebung bei Raumtemperatur. Schließlich wird gequetschtes Licht erstmals ohne optische Cavity durch Strahlungsdruck erzeugt, der das oszillierende Teilchen antreibt (ponderomotorische Kräfte).

Diese Ergebnisse ebnen den Weg für Quantenexperimente mit schwebenden Festkörpern, deren Anwendung von der Erzeugung nicht-klassischer Bewegungszustände für Tests makroskopischer Quantenphänomene bis hin zur Entwicklung neuer Kraft- und Impulssensoren für die Suche nach neuer Physik wie dunkler Materie reichen.

# CONTENTS

ABSTRACT	v
PREFACE	1
1 INTRODUCTION	3
1.1 Why optical levitation?	4
1.2 Structure of this Thesis	4
2 QUANTUM MEASUREMENT	7
2.1 The measurement problem	7
2.2 Generalized measurements: effects and operations	8
2.3 Indirect measurements	9
2.4 Continuous linear measurements	10
2.4.1 In the Schrödinger picture: the quantum trajectory	11
2.4.2 In the Heisenberg picture: quantum filtering	12
2.4.3 "The route to reality"	12
2.5 The measurement limits: two simple examples	12
2.5.1 Measurement of a free particle	13
2.5.2 Measurement of an harmonic oscillator	14
2.5.3 The effect of a cavity on a measurement	15
2.6 Where does this thesis stand	17
3 NEAR-FIELD COUPLING OF A LEVITATED NANOPARTICLE TO A PHOTONIC CRYSTAL CAVITY	21
3.1 Abstract	23
3.2 Introduction	23
3.3 Methods	24
3.4 Results and Discussion	26
3.5 Conclusions	28
3.6 Supplementary Information	34
3.6.1 Cavity and fiber fabrication	34
3.6.2 Transfer of the photonic crystal cavity to the tapered fiber	34
3.6.3 Particle loading	35
3.6.4 Detection efficiency and sensitivity	35
3.6.5 Calibration of the optomechanical coupling	36
3.6.6 Cavity heating	38
3.6.7 Trapping distance simulation	39
3.6.8 Cavity field simulation	39
3.6.9 Optomechanical coupling simulation	41
4 REAL-TIME OPTIMAL QUANTUM CONTROL OF MECHANICAL MOTION AT ROOM TEMPERATURE	43
4.1 Abstract	45
4.2 Introduction	46
4.3 Quantum-limited measurement	46
4.4 Optimal quantum control	47
4.5 Results	50
4.6 Discussion and outlook	52
4.7 Supplementary Information	58
4.7.1 The complete experimental setup	58
4.7.2 Imprecision and backaction noise in an optical tweezer	58
4.7.3 Losses of information and photons	65
4.7.4 Contributions to the total force noise	67
4.7.5 Quantum equations of motion	70

4.7.6	Optimal feedback cooling . . . . .	76
4.7.7	Identification of the model parameters . . . . .	81
4.7.8	Raman scattering thermometry . . . . .	85
5	ROOM TEMPERATURE PONDEROMOTIVE SQUEEZING WITHOUT A CAVITY . . . . .	89
5.1	Theory . . . . .	90
5.1.1	The quantum langevin equations . . . . .	90
5.1.2	The system evolution . . . . .	91
5.1.3	The output field . . . . .	92
5.1.4	The motional spectrum of the quantum harmonic oscillator . . . . .	93
5.1.5	The spectrum of the output quadratures . . . . .	94
5.2	Experiment . . . . .	97
5.2.1	Heterodyne demodulation . . . . .	97
5.2.2	Detection . . . . .	97
5.2.3	Results . . . . .	98
6	CONCLUSIONS AND OUTLOOK . . . . .	101
	SOME MORE FIGURES . . . . .	103
	BIBLIOGRAPHY . . . . .	125
	CURRICULUM VITAE . . . . .	143

# LIST OF SYMBOLS

SYMBOL	DESCRIPTION	UNITS
$k_B$	$= 1.3806 \times 10^{-23}$ , the Boltzmann constant	$\frac{\text{m}^2\text{kg}}{\text{sK}}$
$R$	$= 8.314$ , the universal gas constant	$\frac{\text{J}}{\text{Kmol}}$
$h$	$= 6.626 \times 10^{-34}$ , the Plank constant	$\frac{\text{m}^2\text{kg}}{\text{s}}$
$\hbar$	$h/(2\pi)$ , the reduced Plank constant	$\frac{\text{m}^2\text{kg}}{\text{s}}$
$c$	$\sim 3 \times 10^8$ , the speed of light	$\frac{\text{m}}{\text{s}}$
$T$	temperature	K
$q = x, y, z$	direction of motion label	
$\omega, \Omega$	angular frequency, mostly $\Omega$ is used in low frequency approximations	$\frac{\text{rad}}{\text{s}}$
$m$	mass	kg
$\Omega_q$	mechanical angular frequency	$\frac{\text{rad}}{\text{s}}$
$\gamma$	mechanical damping	$\frac{\text{rad}}{\text{s}}$
$n, N$	quanta of excitation	
$n_{\text{th}}$	$= k_B T / \hbar \Omega_q$ quanta of excitation associated to the thermal bath	
$\dot{n}, \dot{N}$	rate of quanta, generally photon rate	Hz
$q_{\text{zpf}}$	$= \sqrt{\hbar/(2m\Omega_q)}$ position zero-point fluctuation	m
$p_{\text{zpf}}$	$= \sqrt{\hbar m \Omega_q / 2}$ momentum zero-point fluctuation	$\frac{\text{kg m}}{\text{s}}$
$\kappa$	cavity total loss rate	Hz
$G$	$= d\omega_{\text{cav}}/dx$ cavity optomechanical coupling, frequency shift per displacement	$\frac{\text{Hz}}{\text{m}}$
$g_0$	$= G q_{\text{zpf}}$ cavity single phonon single photon cavity optomechanical coupling	Hz
$\chi$	single photon measurement strength, phase shift per displacement (for a cavity $= 2G/\kappa$ )	$\frac{\text{rad}}{\text{s m}}$
$\eta_{\text{ld}}, \chi_0, \chi_F$	$= \chi q_{\text{zpf}}$ , Lamb-Dicke parameter	$\frac{\text{rad}}{\text{s}}$
$\eta_d$	information detection efficiency	
$\Gamma_{\text{meas}}$	$= \eta_d q_{\text{zpf}}^2 \chi^2 \dot{N}$ , measurement rate	$\frac{\text{rad}}{\text{s}}$
$\Gamma_{\text{ba}}$	$= q_{\text{zpf}}^2 \chi^2 \dot{N}$ , backaction decoherence rate	$\frac{\text{rad}}{\text{s}}$
$\Gamma_{\text{th}}$	$= \gamma n_{\text{th}}$ , thermal decoherence rate	$\frac{\text{rad}}{\text{s}}$
$\sqrt{\Gamma_{\text{ba}}}$	measurement strength	$\sqrt{\frac{\text{rad}}{\text{s}}}$
$C_q$	$= \Gamma_{\text{ba}}/\Gamma_{\text{th}}$ , measurement quantum cooperativity	

SYMBOL	DESCRIPTION	UNITS
$\eta_e$	$(1 + 1/C_q)$ , information efficiency due to loss to the thermal environment	
$\eta$	$= \eta_d \eta_e$ , total information efficiency	
$\eta^*$	photon detection efficiency	
$S_{XX}$	Power Spectral Density of variable X	$\frac{[X]^2}{\text{Hz}}$
$\bar{S}_{XX}$	$= \frac{1}{2} (S_{XX}(\Omega) + S_{XX}(-\Omega))$ Symmetrized PSD	"
$S_X$	$= 2\bar{S}_{XX}(\Omega > 0)$ single-sided PSD	"

## PREFACE

The basic elements of the experiments I will show in this thesis are quite simple: a glass nanoball is levitated in vacuum, held by light. In this trap it can move, it oscillates hundreds of thousands of times per second, as an harmonic oscillator, like a person on a swing. The same light that is trapping the particle also allows us to see it moving, and as a someone on a swing, if we see them moving we can time our pulls and pushes to slow them down, eventually stop the swing. But did we really stop the swing? Or is it still moving so little we cannot really tell? Quantum mechanics, specifically the Heisenberg uncertainty principle, poses an ultimate limit to the sensitivity of a measurement, and therefore the precision with which we can control a system. First because the energy of a quantum mechanical object is determined at the very least by its ground state energy, resulting a minimal amount of uncertainty of the measured quantities. It means that the particle cannot be stopped, it can be at best slowed down to its lowest ground state energy. Second because any quantum mechanical measurement apparatus (e.g. a Heisenberg microscope) will inevitably disturb the object that is being measured [Cav82]. For example, if we shine light onto an object to measure its position, we are also bombarding it with the tiny quantum elements of light, photons, modifying its state of motion. A quantum measurement entails a quantum backaction. In the words of Caves: “Quantum mechanics extracts its due twice” [Cav82]. If we look close enough we realize that the states of the particle and of light, are no longer distinguishable, separable. They are now part of a greater quantum system where a continuous dance of quantum (entangling) interactions takes place. But environmental disturbances tend to crush this kind of parties, and scramble the features of the quantum motion, burying it into a chaos of classical noise. The contact with a warm environment makes it very difficult to observe the quantum effects especially as objects become bigger. Big objects make huge parties. The challenge in the realization of a quantum measurement is to eliminate all unnecessary (classical) disturbances. This requires an efficient quantum measurement, and a good isolation from the environment [CGS03]. An exclusive quantum party.

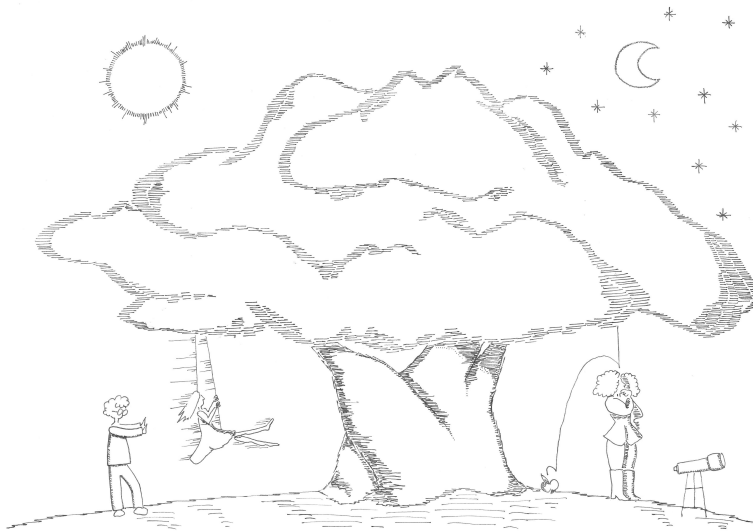


Figure 1: Ink on paper by Costanza Loricchio.





The motion of objects represents one of the most fundamental aspects of our perception of nature. Since ancient astronomy through the scientific revolution, to modern physics, the study of moving objects has been at the heart of some of the greatest scientific discoveries. Today, precise measurement of the motion of massive objects is still a widely used method to address open questions in fundamental physics. Prominent examples include searches for gravitational waves [Abb+16], as well as for signatures of physics beyond the current standard model such as dark matter, dark energy [MRG14; Car+20; MG21; GPK10; Ham+15; Ove+18; Lee+20], quantum gravity [Pik+12; Baw+15; Bel+16] and even string theory [Ger+08; Lee+20; Tan+20]. In 1975, observing the rapid advancements in the technology of precision measurements, and while contributing to the first ideas and prototypes for interferometric gravitational wave detectors, Braginsky posed a fundamental question: “Under what conditions in macroscopic experiments will the increase in sensitivity be limited by the quantum mechanical properties of the object?” [BV75]. This question did not only represent a practical concern, but implied critical epistemological consequences that addressed fundamental controversies at the core of the theories of modern physics. In this context, the modern formalism of continuous quantum measurements was developed [Bel80; BLP83; CM87; Car93], as well as the concept of the standard quantum limit of a measurement [BV75; Cav80; Cav+80; Yue83; Cav85; Oza89; CGS03; Cle+10], giving birth to the experimental field of quantum optomechanics. Realizing the conditions for which the quantum mechanical properties of a macroscopic object are relevant represents the achievement of the ultimate precision of a measurement and may provide insights about the action of quantum mechanics on macroscopic systems. Until recently, quantum measurements and control of the mechanical motion of macroscopic objects have required combinations of cryogenic and cavity cooling schemes [LaH+04; Teu+11; Cha+11; Ros+18; Del+20a]. Continuous sensing close to the quantum limit at room temperature has only been demonstrated in cold atoms experiments [Sch+14].

This thesis is about the experimental realization of quantum measurements and control of the motion of a macroscopic system at room temperature. Specifically, the system consists of a glass ball<sup>1</sup>, the size of a virus, that is trapped in vacuum by a focussed laser field: an optical tweezer.

Now the concept of macroscopicity is very a relative one and often source of controversy.<sup>2</sup> When referring to a sizeable extension (of objects or states) many will rightfully argue that a 150 nm glass ball is actually quite microscopic and even more so is its picometer-sized ground state! But bear with me for a moment. These are very *complex systems*: they are glass particles, made of  $10^9$  atoms, they are dirty, they are porous, not really symmetric, they get wet, they are hot... they interact strongly with the surrounding environment, they *behave* like very classical *macroscopic* objects. In this sense I might convince you, for now, that these particles have been, to me, very macroscopic! [to be continued...(at the end of the thesis)]

<sup>1</sup> more commonly called particle or sphere, I always believed ball was geometrically more appropriate, so i'll take my liberties just here!

<sup>2</sup> Quantifications of “macroscopicity” in quantum systems typically refer to the number of particles involved (or “size of the cat”) [Leg80; DSC02; Kor+07], the distance between the branches of a superposition [BM04; Kor+07; Sch+19], the degree of quantum coherence [LJ11; YV16] or the exclusion of theories that predict the failure of the superposition principle [NH13].

## 1.1 WHY OPTICAL LEVITATION?

Historically the motivation driving proposals [RI+10; BS10; Cha+10; RI+11b; RI+11a] and experiments [Gie+12; Kie+13; Ase+13; Jai+16] with optically levitated nanoparticles has been twofold: one quite technical, the second of fundamental nature. The technical reason was about bringing a mechanical system in the quantum regime, which requires “isolation”. As mentioned earlier, this is a fundamental ingredient that is required if one wishes to distinguish the quantum from the classical noise. It appeared that clamped mechanical systems such as micromirrors [Gig+06; Arc+06; KB06; Pog+07], membranes [Tho+08], and breathing structures [Arm+03; Sch+06] were doomed by their very nature to be dominated by both clamping and internal losses, and that levitation would naturally solve the problem. The development of phononic acoustic shields and soft clamping methods of outstanding performance made many of these limitations obsolete, and clamped mechanical oscillators have in some cases even surpassed [Ros+18; Mac+20] the photon-recoil limited quality factors that are expected for optically levitated systems, even at room temperature [Gha+18; GNG19]. The second argument for levitation, the fundamental one, is about what to do once the mechanical system is in a quantum state. One of the most intriguing possibilities is matter-wave interferometry [Kal+12], and the creation of large, massive, superposition states [RI+11a]. Experiments of this kind require, in the simplest of cases, some time of “free evolution”. Optical levitation can provide this. The real, fundamental advantage of optically levitated systems is that light, and only light, defines all of the relevant experimental parameters. It defines not only the measurement process and quantum decoherence rates, but also the function of the potential landscape in which the mechanical object lives. The result is an extremely versatile quantum system, which evolves in time according to a Hamiltonian that can be dynamically tuned in almost all of its degrees of freedom.

## 1.2 STRUCTURE OF THIS THESIS

This thesis takes the form of a cumulative thesis and is structured as follows. In chapter 2 I will present a brief theoretical background on quantum measurement. Starting from the basic definitions of a von Neumann measurement, its applicability and limitations, I will introduce the concept of generalized measurements, and their physical realizability as indirect measurements (Naimark’s theorem). I will extend the description to continuous sequences of measurements, show how the natural evolution of the system can be taken into account, leading to the equation of motion of a continuously monitored quantum state. I will briefly introduce the concepts of “quantum trajectory” used to define the state evolution in the Schrödinger picture, as well as the formalism of “quantum filtering” addressing the problem in the Heisenberg picture. Finally I will discuss the sensitivity limitations of a quantum measurement, and the effects of using optical cavities, described in terms of an enhanced measurement strength. In chapters 3 and 4 I will present my manuscripts on near field coupling of a levitated nanoparticle to a photonic crystal cavity [Mag+18] and ground state cooling by confocal detection and optimal control [Mag+21]. Both are preceded by a short introduction describing the most immediate scientific background, motivating the methodology of these experiments. As these chapters reflect the submission or publication format, the theoretical description and experimental details can be found in their respective supplementary material, also included here. In chapter 5 I describe the theory and experimental results regarding ongoing research on squeezing of light via optomechanical interaction (ponderomotive squeezing) at room temperature and in absence of a cavity. As the manuscript for this work is still in preparation, the structure of this chapter follows a more didactic

form: theory first. Finally in the conclusive chapter 6 I will summarize the results in a perspective for future developments.



# 2

## QUANTUM MEASUREMENT

In this chapter I give a brief overview of the basic concepts that are involved in defining the operational formalism of quantum measurements. The goal is give to draw a connection between some of the fundamental concepts of quantum mechanics and the practical realization of quantum measurements in real experiments.

### 2.1 THE MEASUREMENT PROBLEM

The concept of measurement, the interpretation of its outcomes and effects, or “the measurement problem” represents a central matter in quantum theory. What constitutes a measurement? What happens to the physical system during the measurement process? What does the collapse of the wave function mean? How does information about this quantum system permeate to our classical instruments “upon which we can lay our grubby classical hands on” [Cav82]? On a metaphysical level the quantum interpretation of a measurement, the quantum to classical transition, has been, and still is, subject of endless debate for physicists and philosophers. But dropping any ontological ambition [Mab05], the operational theory is clear, and for an experimentalist it is also enough! For now. A useful theory of measurement in quantum physics must satisfy two minimal requirements: First, it must relate the state of a quantum system to the physical quantities that are measured. Second, it must be able to predict the consequences of the measurement on the system [Mab05]. In the standard formalism of quantum measurements, as introduced by von Neumann [Neu32], the act of a measurement is represented by a projection operation of the state’s wavefunction onto an orthonormal basis of the Hilbert space defined by a specific observable determined by the measurement apparatus. The measurement outcome is given by the eigenvalue of the projection, while the state is left in the corresponding eigenvector, or eigenstate. The physicality of the measurement is ensured by the Born rule, linking the the state’s wavefunction  $|\psi\rangle$  to the probability amplitude  $p(x)$  of finding the system in a given eigenstate  $|x\rangle$ , and measuring the corresponding outcome  $x$ . Defining the projection operator in bracket notation as  $\Pi_x = |x\rangle\langle x|$ , a standard quantum projective measurement is defined by

*What do we want?*

$$\Pi_x |\psi\rangle = x |x\rangle, \quad \text{with} \quad p(x) = \langle\psi|\Pi_x|\psi\rangle = |\langle x|\psi\rangle|^2 \quad (1)$$

*a projective, von Neumann measurement*

And this is enough! It represents some statistical property of the system, and also predicts the state after the measurement. However, for quantum observables with a continuous spectrum, such as the position of a particle, there is no normalized basis of eigenstates. As a consequence, in this infinite dimensional Hilbert space, “an arbitrary precise measurement of position will require an arbitrary large amount of energy” [CM87], with devastating consequences on the system! Can we define a more practical and general class of measurements in quantum mechanics? [CM87] Can we describe the evolution of a system undergoing a measurement process and predict its post measurement state? A natural candidate for this job may be the Schrödinger equation. As a matter of fact this equation does define the dynamics and evolution of quantum systems:

$$i\hbar \frac{\partial |\psi\rangle}{\partial t} = H |\psi\rangle \quad (2)$$

*the Schrödinger equation*

and so it may seem that the problem is only about identifying a suited “measurement Hamiltonian”. But this equation is deterministic and also reversible, while a measurement is hardly so<sup>1</sup>! The Schrödinger equation alone is also not enough to describe a quantum measurement. A generalization of the standard measurement formalism for any open quantum system [GZo4] is necessary. We will see in the rest of this chapter how this can be done by opening the state space to a portion of the surrounding environment, connecting it to a quantum meter (or apparatus, or ancilla, or probe). A generalized measurement will be then the combination of a deterministic interaction of the quantum system and the quantum meter, described by the Schrödinger equation (2), followed by a dramatic (arbitrarily precise) von Neumann measurement (1) on the meter.

## 2.2 GENERALIZED MEASUREMENTS: EFFECTS AND OPERATIONS

Mixed states:  
 $\rho = \sum_j p_j |\psi_j\rangle\langle\psi_j|$

As we want to give a formal definition of a most general physical measurement, it makes sense to do so for the most general physical state. That is a mixture of  $j$  pure states  $|\psi_j\rangle$  weighted by the probability  $p_j$  of the system to be found in the corresponding state. Such a mixed state is conveniently described by a density operator  $\rho = \sum_j p_j |\psi_j\rangle\langle\psi_j|$ . As we said, in order to describe any physical and useful measurement, this must represent the statistical properties of the state being measured, and provide a means for predicting its post-measurement state. Formally this requires that any physical measurement must be represented by a set of measurement operators  $M_j$ , spanning the entire Hilbert space of the system (or complete), and normalized. Practically this means that we may have to accept a “minimum width” for the probability densities, a finite measurement precision (and backaction), that depends on the specific measurement apparatus [CM87]. The probability of measuring the outcome  $x$  can be written as

$$p(x) = \text{tr} [M_x \rho M_x^\dagger] = \text{tr} [M_x^\dagger M_x \rho]. \quad (3)$$

POVM

This satisfies the requirement of the measurement being a statistical representation of the state. In (3) the second identity follows the cyclic property of the trace. A Measurement associating a positive operator  $M_x^\dagger M_x$  with the probability of finding the system in the state  $x$  is commonly known as *Positive Operator Valued Measure* or *POVM*. As for the second requirement, the state after the measurement (conditioned on the outcome  $x$ ) must be of the form:

The conditional state

$$\rho \rightarrow \frac{M_x \rho M_x^\dagger}{\text{tr}[M_x \rho M_x^\dagger]} \equiv \hat{\rho} \quad (4)$$

where the  $\hat{\cdot}$ -symbol refers to the conditional (sometimes called “selective” [CM87]) state, in contrast to the unconditional (non-selective) post-measurement state that we have when disregarding the measurement outcome<sup>2</sup>:

The unconditional state

$$\rho \rightarrow \sum_x \frac{M_x \rho M_x^\dagger}{\text{tr}[M_x \rho M_x^\dagger]} \quad (5)$$

States, effects and operations

The measurement operator  $M_x$  therefore defines both its “effects” on the measurement apparatus (3) as well as the “operation” by which the initial state is transformed during the interaction with the apparatus itself (4) [Kra+83]. So how can one practically build a measuring apparatus that can satisfy equations (3) and (4)? A convenient way of doing so is through the concept of indirect measurements, as discussed in the following section.

<sup>1</sup> Except if the system is already in an eigenstate of the observable, but then eigenstates can be defined, and projective measurements would have worked just fine

<sup>2</sup> for example in the case of an inefficient measurement

## 2.3 INDIRECT MEASUREMENTS

An indirect measurement is a two-step process that involves two, initially distinct, quantum systems: the *object* of the measurement and the *meter*. In the first step these two systems are brought in “contact”, and correlations are established between their interacting degrees of freedom. The second step consists of a strong, projective measurement of a chosen observable of the quantum meter. The outcome of this measurement allows us to infer the statistical properties of the state of the quantum object. And the state after the measurement can be derived knowing the measurement outcome and the nature of the interaction with the probe. This is the beginning of what is known as a von Neumann chain. But what is the advantage? Have we not only shifted the quantum/classical cut (or “Heisenberg cut”) to a later moment? The advantage of such a decomposition lies in the fact that the quantum object only comes in contact with another known quantum system, and their state evolution is deterministically defined by the Schrödinger equation. We can deal with the mechanics of a “direct” projective measurement later. The meter takes it all! Imagine a photon (meter) probing the position of an electron (object) and then being smashed onto a highly sensitive photographic plate. Who cares about what happens to the photon, what is the chemistry involved in this “quantum-to-classical transition”; the quantum object is safe, and a new quantum meter can be prepared for a successive measurement. Formally the above considerations are justified by Naimark’s theorem, stating (broadly speaking) that any generalized measurement can be described as a von Neumann measurement on a larger Hilbert space and vice versa [Par12]. In order to highlight the connection between the experimental physical systems and the mathematical description of the measurement process, in the following I will go through the key steps of the proof of Naimark’s theorem. A complete statement of the theorem and a rigorous proof can be found in this useful tutorial on quantum measurement [Par12].

*Naimark’s theorem: Any generalized measurement can be viewed as a von Neumann measurement on a larger Hilbert space – and vice versa*

The state of the quantum object (or system, here denoted with the label “s”) is defined by its density operator  $\rho_s = \sum_i |\psi_i\rangle\langle\psi_i|$  on the Hilbert space  $\mathcal{H}_s$ . For simplicity we choose the meter (label “m”) to be in a pure quantum state<sup>3</sup>  $\rho_m = |\Upsilon\rangle\langle\Upsilon| \in \{|\Upsilon_n\rangle\}$  where  $\{|\Upsilon_n\rangle\}$  is an orthonormal basis for  $\mathcal{H}_m$ . Before the interaction of the object-meter state  $\rho_s\rho_m$  defined on  $\mathcal{H}_s \otimes \mathcal{H}_m$  is a separable state. Considering the interaction Hamiltonian  $H_I$ , defined on  $\mathcal{H}_s \otimes \mathcal{H}_m$ , the Schrödinger equation (2) allows to define the unitary Dyson operator in the interaction picture:

*the object is in a mixed state*

*the meter is in a pure state*

$$U_I = e^{-iH_I t/\hbar}. \quad (6)$$

The interaction introduces correlations between the two systems, entangling them, into an unseparable state  $\rho$  defined on the extended Hilbert space  $\mathcal{H}_s \otimes \mathcal{H}_m$ :

$$\rho = U_I \rho_s \rho_m U_I^\dagger. \quad (7)$$

At this point we perform a standard projective measurement of the meter on the basis of interest  $\{|x\rangle\} \in \mathcal{H}_m$ . Defining the projection operator  $\Pi_x = |x\rangle\langle x|$  the probability of measuring the value  $x$  can be derived adapting equation (1) in the density matrix representation:

$$\begin{aligned} p(x) &= \text{tr} [\rho \Pi_x] \\ &= \text{tr}_{sm} \left[ U_I \rho_s \rho_m U_I^\dagger |x\rangle\langle x| \right] \\ &= \text{tr}_s \left[ \rho_s \text{tr}_m \left[ \rho_m U_I^\dagger |x\rangle\langle x| U_I \right] \right] \\ &= \text{tr}_s \left[ \rho_s \sum_n \langle \Upsilon_n | \Upsilon \rangle \langle \Upsilon | U_I^\dagger |x\rangle\langle x| U_I | \Upsilon_n \rangle \right] \\ &= \text{tr}_s \left[ \rho_s \langle \Upsilon | U_I^\dagger |x\rangle\langle x| U_I | \Upsilon \rangle \right] = \text{tr}_s \left[ \rho_s M_x^\dagger M_x \right], \end{aligned} \quad (8)$$

<sup>3</sup> this is easy to do experimentally using light as a quantum meter

where we distinguish between the total trace operation  $\text{tr}$  (or equivalently  $\text{tr}_{\text{sm}}$ ) and the partial trace operations  $\text{tr}_s$  and  $\text{tr}_m$  over the subspaces of the object and meter, respectively. From (8) we immediately see how a standard measurement on an extended Hilbert space yields the same statistics as a generalized measurement on one of the subsystems, with a measurement operator defined on  $\mathcal{H}_s$  as:

$$M_x = \langle x | U_I | \Upsilon \rangle. \quad (9)$$

In addition we notice that the operator  $M_x^\dagger M_x$  is positive  $\forall x$ , and that for any pure state  $|\psi_s\rangle$  in  $\mathcal{H}_s$ :

$$\begin{aligned} \sum_x \langle \psi_s | M_x^\dagger M_x | \psi_s \rangle &= \sum_x \langle \psi_s | \langle \Upsilon | U_I^\dagger | x \rangle \langle x | U_I | \Upsilon \rangle | \psi_s \rangle \\ &= \langle \psi_s | \langle \Upsilon | U_I^\dagger U_I | \Upsilon \rangle | \psi_s \rangle = 1 \end{aligned} \quad (10)$$

and therefore  $\sum_x M_x^\dagger M_x = \mathbb{I}$  is a completely positive map, which guarantees the physicality of the measurement. In order to derive the post measurement state of the object conditioned on the measurement outcome  $x$ , we need to trace the density operator after the measurement over the meter subsystem. This reduces the density operator to the subspace  $\mathcal{H}_s$

$$\begin{aligned} \hat{\rho}_s &= \frac{1}{p(x)} \text{tr}_m \left[ U_I \rho_s \rho_m U_I^\dagger | x \rangle \langle x | \right] \\ &= \frac{1}{p(x)} \sum_n \langle \Upsilon_n | U_I \rho_s | \Upsilon \rangle \langle \Upsilon | U_I^\dagger | x \rangle \langle x | \Upsilon_n \rangle \\ &= \frac{1}{p(x)} \langle x | U_I | \Upsilon \rangle \rho_s \langle \Upsilon | U_I^\dagger | x \rangle = \frac{1}{p(x)} M_x \rho_s M_x^\dagger, \end{aligned} \quad (11)$$

fulfilling requirement (4).

## 2.4 CONTINUOUS LINEAR MEASUREMENTS

We have seen how to define the measurement operators given an appropriate choice of a quantum meter and its interaction with the measured object. The state of the system post measurement can now be calculated by conditioning upon the measurement outcome. In addition, it can also be measured again shortly after! One just has to prepare a new quantum probe, let it interact... We can then imagine to perform a sequence of measurements, that in turn generates a sequence of measurement outcomes and of post-measurement states, i.e. a *quantum trajectory*! One can write:

$$\rho_s \rightarrow \frac{1}{p(x_1)} M_{x_1} \rho_s M_{x_1}^\dagger \rightarrow \frac{1}{p(x_2|x_1)} M_{x_2} M_{x_1} \rho_s M_{x_1}^\dagger M_{x_2}^\dagger \rightarrow \dots \quad (12)$$

This trajectory is said to be driven by the measurement process: it only depends on the random measurement outcome and the effect of the system-meter interaction. But what if we want to monitor a particular observable in time, and how do we include the intrinsic dynamics of the system into this? We can consider a sequence of (instantaneous) measurements, separated by a time  $\tau$ . Between any 2 measurements, the system will evolve according to its free Hamiltonian  $H_0$ , by the unitary transformation

$$U_0 = e^{-iH_0\tau/\hbar}. \quad (13)$$

The state of the system after the  $n^{\text{th}}$  measurement is [CM87]

$$\hat{\rho}_s(t_n^+) = \frac{1}{p(\{x_i\})} \left( \prod_{i=1}^n M_{x_i} U_0 \right) \rho_s(0) \left( \prod_{i=1}^n M_{x_i} U_0 \right)^\dagger \quad (14)$$

a sequence of generalized  
measurements

a sequence of generalized  
measurements, and free  
evolutions



where the  $t_n^+$  indicates the time just after the measurement time  $t_n$ , and with

$$p(\{x_i\}) = \text{tr} \left[ \left( \prod_{i=1}^n M_{x_i} U_0 \right)^\dagger \left( \prod_{i=1}^n M_{x_i} U_0 \right) \rho_s(0) \right]. \quad (15)$$

It is important to keep in mind that the measurement results  $\{x_i\}$  are stochastic variables. For this reason, in the limit of  $\tau \rightarrow 0$ , the sequence (14) can be generalized to a stochastic differential equation driven by a continuous measurement  $x(t)$  [Mab05].

#### 2.4.1 In the Schrödinger picture: the quantum trajectory

This representation of the state evolution in the Schrödinger picture, where the continuously monitored quantum state evolves in time, driven by the operations and effects of the measurement process, was first given by Barchielli *et al.* [BLP82; BLP83]. In the following I provide a brief description of the main steps and key approximations required for the simplest derivation of the stochastic master equation describing the state evolution in the Schrödinger picture. The dynamics of the system is described by its variation in time, encompassed by the time derivative of the conditional state:

$$\frac{d\hat{\rho}_s(t)}{dt} = \lim_{\tau \rightarrow 0} \frac{\hat{\rho}_s(t_n^+) - \hat{\rho}_s(t_{n-1}^+)}{\tau} \quad (16)$$

which, using equations (14) and (15), becomes

$$\frac{d\hat{\rho}_s(t)}{dt} = \lim_{\tau \rightarrow 0} \frac{1}{\tau} \frac{M_{x_n} U_0 \hat{\rho}_s(t_{n-1}^+) U_0^\dagger M_{x_n}^\dagger - \hat{\rho}_s(t_{n-1}^+)}{p(x_n | \hat{\rho}_s(t_{n-1}^+))}. \quad (17)$$

*the Stochastic Differential Equation*

This differential equation depends on the stochastic processes defined by the measurement process. It is known as the Stochastic Master Equation (SME) of the system. The solution of this equation is in general a difficult problem as it is nonlinear in  $\hat{\rho}$  and depends on the statistical properties of the quantum probe. For this reason it is convenient to exploit the properties of a probe with Gaussian statistics<sup>4</sup>:

*the Stochastic Master Equation Gaussian noise*

$$p_Y(x) = |\langle x | Y \rangle|^2 = \frac{1}{\sqrt{2\pi\tau}} e^{-\frac{(x - \langle x \rangle)^2}{2\tau}}. \quad (18)$$

For linear systems, such as an harmonic oscillator, both the unitary evolution and the unitary measurement operation transform Gaussian states into Gaussian states, thereby greatly simplifying the problem [CM87]. The next step is usually an approximation: the measurement operator  $M_x$  is defined by plugging a second order Taylor-expansion of  $U_I$ , (6), into (9). This can be further simplified by use of (18), and keeping only the terms up to order  $\tau$  [JS06; Lam18].  $U_0$  is also approximated in a Taylor series up to the terms of order  $\tau$ . Finally with a bit of stochastic calculus and normalizations [JS06] one can find the conditional stochastic master equation for Gaussian linear system of the form:

$$d\hat{\rho}(t) = -i[H, \hat{\rho}(t)dt] + \mathcal{D}\hat{\rho}(t)dt + \sqrt{\eta}\mathcal{H}\hat{\rho}(t)dW(t) \quad (19)$$

where the first term represents the free evolution of the system, second term contributes to the diffusion of the system coupled to an external bath (defined by the measurement apparatus), and the third term accounts for the conditioning upon the measurement outcome, with  $\eta$  the efficiency of the measurement and  $dW$  a zero mean Gaussian stochastic process of variance  $dt$ . If the system couples also (as it is likely) to the environment through other mechanisms than the measurement process, this is modelled in (19) by additional dissipation terms. Equation (19) describes the quantum trajectory of the system under continuous measurement [Car93]

<sup>4</sup> This is an easy assumption to satisfy if using an electro-magnetic field as probe

### 2.4.2 In the Heisenberg picture: quantum filtering

The dynamics of the quantum system can equivalently be described in the Heisenberg picture. This approach, known as “quantum filtering” was developed by Belavkin [Bel95], extending the concepts of classical control theory and Kalman filtering to the quantum domain. While for a quantum physicist the “quantum trajectory” approach may seem the natural way to derive the quantum equation of motion, the quantum filtering approach allows us to appreciate the connections to the corresponding classical problem with a few restrictions. The core of this argument is that it is possible, under certain Markovianity conditions (descending from the statistical properties of the probe), to define a mapping from the operator-valued quantum observables to a classical, real-valued stochastic process, which describes the corresponding measurement signal [BVJ07; BVHJ09; EWP17; HH17].

In the Heisenberg picture, the extended state  $\rho = \rho_s \otimes \rho_m$  is independent of time, and the total Hamiltonian is given by  $H = H_s + H_m + H_I$  ( $\in \mathcal{H}_s \otimes \mathcal{H}_m$ ). The operators associated to the quantum observables absorb the time dependence defined by the Schrödinger equation:  $q_i(t) = e^{-iHt/\hbar} q_i e^{iHt/\hbar}$ . Their evolution is given by the Heisenberg equation:

$$\dot{q}_i(t) = \frac{i}{\hbar} [H, q_i(t)] \quad (20)$$

These, together with the statistical properties of the probe, allow derive the so-called input-output relations for the system dynamics and for the measurement process, and construct a state-space in perfect analogy with the classical case. The details of this derivation and the connection to Kalman filtering are fully described in Section 4.7.5.

### 2.4.3 "The route to reality"

In the above non-rigorous attempt of describing physical quantum measurements and their connections to the postulates of quantum mechanics we have rushed through the non-physical, yet reasonable assumption that the measurement occurs instantaneously. This cannot be true. It is only a fair approximation if a reasonable time-scale hierarchy is satisfied[BK95]<sup>5</sup>. In fact, “if a measurement is distributed in time the notion of a system’s quantum state evolving in time has no place” [Cav86]. Measurements distributed in time, require a more rigorous approach, “a route to reality”, that was introduced by Caves and makes use of a path-integral formulation and the so called “sum over histories” [Cav86; Cav87; CM87].

## 2.5 THE MEASUREMENT LIMITS: TWO SIMPLE EXAMPLES

We have seen how to operationally describe the dynamics of a system undergoing a continuous weak measurement by letting it interact with a quantum meter and a following strong measurement of it, resulting in the so-called state reduction. But with what precision can one measure the state of a system? The fundamental limits of a quantum measurement originate from the commutation relations of complementary operators, leading to the Heisenberg uncertainty principle. In this section we will derive, with some simple arguments, the limitations in accuracy that arise in the measurement of a quantum system using a quantum probe<sup>6</sup>. In particular, we focus on measurements of displacement using an electromagnetic field in the optical domain. The reasons are the two that ensured the extraordinary success of quantum optics in the past 40 years: first, it is easy to prepare pure quantum states of light, and second light is easy to measure! From the commutation relations of the

<sup>5</sup> The Heisenberg cut is much faster than the system meter interaction which is in turn much faster than the system dynamics

<sup>6</sup> For a rigorous and more general approach see for example Braginsky and Khalili [BK95].

electric field operator of a pure quantum state at different times, its easy to derive an uncertainty relation between the number of photons  $N$ , optical phase  $\varphi$  of the optical field [Lou00]:

$$\Delta N \Delta \varphi = \frac{1}{2} \quad (21)$$

### 2.5.1 Measurement of a free particle

What happens if we use this light to measure the position of a particle of mass  $m$  in space? Let's follow the gedankenexperiment known as the "Heisenberg microscope"[Hei27] combined with an interferometric measurement. As photons illuminate the particle, each one of them will disturb it by delivering a momentum  $p = 2\hbar k$ <sup>7</sup> (with  $k = \frac{2\pi}{\lambda}$  the magnitude of the wavevector and  $\lambda$  the optical wavelength). We use an interferometer to measure the phase of the scattered field. This quantity is related to the position of the particle  $x$  by  $\varphi = 2\frac{2\pi}{\lambda}x$ . Using these relations together with (21) we find that:

$$\Delta x_{\text{meas}} \Delta p_{\text{perturb}} = \frac{\hbar}{2}. \quad (22)$$

This means that, if at time  $t_0$  we measure the particle position with an accuracy of  $\Delta x_0$  we will necessarily perturb it by at least

$$\Delta p_0 = \frac{\hbar}{2\Delta x_0}, \quad (23)$$

which will result after a time interval  $\tau$  into an increased position uncertainty:

$$\Delta x = \sqrt{\Delta x_0^2 + \left(\frac{\Delta p_0 \tau}{m}\right)^2}. \quad (24)$$

We can now use the geometric inequality and (23), to finally define the Standard Quantum Limit (SQL) for the measurement of a free particle:

$$\Delta x \geq \sqrt{2\Delta x_0 \frac{\Delta p_0 \tau}{m}} = \sqrt{\frac{\hbar \tau}{m}} \quad (25)$$

Performing a second position measurement at time  $t_1 = t_0 + \tau$  one can compute the momentum that was delivered to the particle with the first measurement:  $p = m(x_1 - x_0)/\tau$ . Assuming arbitrary precision for the second measurement (we don't care of the consequences), the uncertainty over this estimation is:

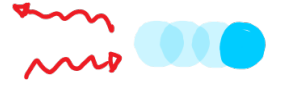
$$\Delta p \geq \sqrt{\frac{\hbar m}{\tau}} \quad (26)$$

The equality in equations (25) and (26) are valid if the initial measurement and associated perturbation are, respectively,  $\Delta x_0 = \Delta x_{\text{SQL}} = \sqrt{\hbar \tau / (2m)}$ , and  $\Delta p_0 = \Delta p_{\text{SQL}} = \sqrt{\hbar m / (2\tau)}$ . In this case the uncertainty contributions from the measurement imprecision and its back-action are equal (in equation (24)), and the total imprecision is minimized [BK95]<sup>8</sup>. These argument was first made by Braginsky [BV75], initiating a debate on the standard quantum limits, their meaning and fundamental nature [Cav+80; Yue83; Cav85; Oza89]. Indeed, in this derivation we have neglected the possibility of a negative correlation term in (24), arising from particular "contractive measurements" which could in principle allow sensitivities beyond the limitations imposed by the SQL [Yue83; Oza89].

<sup>7</sup> For simplicity we assume they are all perfectly reflected, the spherical geometry case with dipole-like emission is described in Section 4.7.2

<sup>8</sup> In literature the definitions of the SQL values are often differing by a factor  $\sqrt{2}$ . This depends on the definition of uncertainty/imprecision/accuracy of the measurement, and whether this is considered before or after the second measurement, whether the measurements are averaged or not, whether they are identical or not. But this is not a particular issue, the point is: there is a quantum limit to the precision of a measurement.

The Heisenberg Microscope



The Standard Quantum Limit

$$a^2 + b^2 \geq 2ab$$

### 2.5.2 Measurement of an harmonic oscillator



The same arguments stand if the particle is not free any more, but bound by a potential. Particularly interesting for us is the case of an harmonic potential of eigenfrequency  $\Omega_x$ . Equation (24) becomes :

$$\Delta x = \sqrt{\Delta x_0^2 + \left(\frac{\Delta p_0}{m\Omega_x}\right)^2} \geq \sqrt{\frac{\hbar}{m\Omega_x}}, \quad (27)$$

from which the SQL definitions  $\Delta x_{\text{SQL}} = \sqrt{\hbar/(2m\Omega_x)}$  and  $\Delta p_{\text{SQL}} = \sqrt{\hbar m\Omega_x/2}$ . It is important to notice that the standard quantum limit of a measurement (in its original formulation) is the consequence of the Heisenberg uncertainty principle applied to the measuring apparatus, in our case light. However, if measuring a quantum system such as an harmonically bound particle, one has to also consider the uncertainty (in position and momentum) that arises from its finite ground-state energy. This defines the quantum zero-point fluctuations of momentum and position of the harmonic oscillator:

$$x_{\text{zpf}} = \sqrt{\frac{\hbar}{2m\Omega_x}}, \quad \text{and} \quad p_{\text{zpf}} = \sqrt{\frac{\hbar\Omega_x m}{2}}. \quad (28)$$

Considering these quantum fluctuations the minimal displacement or momentum uncertainty, (again assuming no momentum position correlations) are given by the more stringent Quantum Limits (QL) [Cle+10]:

$$\begin{aligned} \Delta x_{\text{QL}} &= \sqrt{\Delta x_{\text{SQL}}^2 + x_{\text{zpf}}^2} = \sqrt{\frac{\hbar}{m\Omega_x}} \\ \Delta p_{\text{QL}} &= \sqrt{\Delta p_{\text{SQL}}^2 + p_{\text{zpf}}^2} = \sqrt{\hbar\Omega_x m}. \end{aligned} \quad (29)$$

We have seen how can one derive the sensitivity limits imposed by quantum mechanics on a two-measurements sequence for a free particle and of an harmonic oscillator. Can this be generalized to a continuous measurement monitoring the motion of the mechanical system? When performing a phase measurement of light in a coherent state (displaced vacuum) the phase and photon number uncertainty is governed by Poissonian statistics: these uncertainties are respectively  $\Delta\varphi = 1/(2\sqrt{N})$  and  $\Delta N = \sqrt{N}$ , where  $N$  is the measured number of photons during the time  $t$ <sup>9</sup>. The product of these uncertainties satisfies the relation (21). In the context of continuous measurements of stationary processes it is useful to reformulate these quantities in terms of a noise power spectral density. This is defined, for any variable, as the Fourier transform of its autocorrelation. Measuring a continuous flux of photons of average  $\bar{N}$ , we can now define  $S_{\varphi\varphi} = \Delta\varphi^2/t = 1/(4\bar{N})$  and  $S_{\dot{N}\dot{N}} = \Delta N^2/t = \bar{N}$ . Again, we have the uncertainty relation:

$$\sqrt{S_{\varphi\varphi} S_{\dot{N}\dot{N}}} = 1/2 \quad (30)$$

Leading to spectral density definitions for the imprecision of a position measurement  $S_{xx}^I = S_{\varphi\varphi}/(4k^2)$  and the random backaction force-noise  $S_{FF}^{ba} = 4\hbar^2 k^2 S_{\dot{N}\dot{N}}$  [Cle+10]. The uncertainty relation becomes:

$$\sqrt{S_{xx}^I S_{FF}^{ba}} = \hbar/2 \quad (31)$$

The response of a system to external forces is given by its mechanical response function or susceptibility. For an harmonic oscillator this is:  $\chi_m(\Omega) = [m(\Omega_x^2 - \Omega^2 + i\gamma\Omega)]^{-1}$  ( $m$  the mass of the particle,  $\Omega_x$ : the mechanical resonance frequency,  $\gamma$ : the total damping of the system). With this we can write the total displacement noise

<sup>9</sup> For  $N \gg 1$  the Poissonian distribution approaches a Gaussian distribution, for which our choice of meter is consistent with the Gaussian Noise approximations of the previous section

The power spectral density of a variable  $X$ :  $S_{XX}(\Omega) = \int_{-\infty}^{+\infty} e^{-i\Omega t} \langle X(0)X(t) \rangle dt$

that is measured as the sum of the contributions of the measurement imprecision, of the displacement response to the backaction force noise and of its intrinsic quantum fluctuations:

$$S_{xx}(\Omega) = S_{xx}^I + S_{FF}^{ba} |\chi_m(\Omega)|^2 + S_{xx}^{zpf}(\Omega), \quad (32)$$

where the ground-state displacement spectrum is given by [Cle+10]:

$$S_{xx}^{zpf}(\Omega) = x_{zpf}^2 \frac{\gamma/2}{(\Omega - \Omega_x)^2 + (\gamma/2)^2}. \quad (33)$$

The measurement-added noise is given by the sum of imprecision and backaction, and is minimized at the standard quantum limit:

$$S_{xx}^{SQL}(\Omega) = \min\{S_{xx}^I + S_{FF}^{ba} |\chi_m(\Omega)|^2\} = \hbar |\chi_m(\Omega)|. \quad (34)$$

Evidently, because of the frequency dependence of the response function, the optimal measurement strength that minimizes the added noise is not the same for all frequencies. In a real experiment two conditions may increase the measured displacement noise: inefficient detection and environmental force noise contributions. Defining the detection efficiency  $\eta_d \leq 1$ , the imprecision noise is increased to  $S_{xx}^{imp} = S_{xx}^I / \eta_d$ . On the other hand, an additional environmental force noise will result in a total force noise of  $S_{FF}^{tot} = S_{FF}^{ba} + S_{FF}^{th} = S_{FF}^{ba} (1 + 1/C_q)$  where  $C_q = S_{FF}^{ba} / S_{FF}^{th}$  is the measurement quantum cooperativity, defining the strength of the measurement compared to any other disturbance. The total displacement noise is then given by:

$$\begin{aligned} S_{xx}(\Omega) &= S_{xx}^{imp} + S_{FF}^{tot} |\chi_m(\Omega)|^2 + S_{xx}^{zpf}(\Omega) \\ &= \frac{S_{xx}^{imp}}{\eta_d} + S_{FF}^{ba} \left(1 + \frac{1}{C_q}\right) |\chi_m(\Omega)|^2 + S_{xx}^{zpf}(\Omega). \end{aligned} \quad (35)$$

It is evident that in order to measure and control a system at its quantum limits, the measurement must be both efficient ( $\eta_d \rightarrow 1$ ) and strong ( $C_q \rightarrow \infty$ ). We now define the measurement rate and the decoherence rate as the rate at which the measurement allows to resolve a displacement equivalent to the zero point motion of the oscillator ( $x_{zpf}$ ), and the decoherence rates due to the measurement backaction or thermal environment as

$$\Gamma_{meas} = \frac{x_{zpf}^2}{4S_{xx}^{imp}} = \eta_d \frac{x_{zpf}^2}{4S_{xx}^I}, \quad \text{and} \quad \Gamma_{ba,th} = \frac{S_{FF}^{ba,th}}{4p_{zpf}^2}. \quad (36)$$

The measurement cooperativity can then be rewritten as  $C_q = \Gamma_{ba} / \Gamma_{th}$ . Finally, using these definitions it is easy to see that in order to resolve the motion of the particle with a resolution that is smaller than the variance of  $n = 1$  phonon ( $\Delta x < \sqrt{2n+1} x_{zpf}$ ), and at a rate that is faster than the total decoherence rate we need [Gen+08; Sud+17a]:

$$\eta_d \left(1 + \frac{1}{C_q}\right) > \frac{1}{9} \quad (37)$$

### 2.5.3 The effect of a cavity on a measurement

We have seen how a quantum limited measurement must be both strong and efficient. A cavity can help with both. In particular, a cavity can amplify the coupling to a particular degree of freedom of the probe that we can detect efficiently. Cavity optomechanical systems, have been broadly studied in a variety of platforms and in many different settings [AKM14]. In particular, resonators do not only offer an enhanced light matter interaction, they allow to also select the type of interaction that is enhanced [Pal+13; Rie+16], and therefore coherently couple the mechanical

system to a tailored quantum bath [Cha+11; Teu+11; Wol+15; Del+20a]. Here I will briefly discuss the specific use of resonators to enhance the measurement strength for the position of a mechanical oscillator: that is in the condition of resonant drive in the “bad cavity” regime [MVT98; SN+13; Wil+15].

Using the definitions given above, we can define the measurement backaction as

$$\Gamma_{ba} = \chi^2 \chi_{zpf}^2 \dot{N} \quad (38)$$

where  $\chi$  is the optical phase shift per displacement of the particle. In free space  $\chi \leq 2\frac{2\pi}{\lambda}$ , where the equality holds if the mechanical oscillator is a perfectly reflecting flat mirror with light coming in parallel to its motion and perpendicular to its surface. Evidently, one can increase the measurement quantum cooperativity by having a laser with smaller wavelength or with stronger power. Often times the environmental force noise is so strong that one would end up needing a not so practical laser. In such cases an optical cavity helps. Broadly speaking, when the optomechanical interaction takes place within an optical cavity the photons are “recycled”, enhancing the interaction of each one by a factor given by the finesse of the resonator. Two parameters are crucial in defining a cavity that is suited for optomechanical experiments: the timescale of light being trapped into the cavity,  $\tau = \kappa^{-1}$ , and the coupling of the mechanical displacement on the cavity resonance,  $G = d\omega_{cav}/dx$ . If the mechanical oscillator is one of the end-mirrors of a Fabry-Perot cavity whose rest position is  $x_0$ , this is trivial: the position dependent resonance is  $\omega_{cav}(x) = 2\pi c/2L(x) \sim \omega_{cav}(x_0) + 2\pi c(x - x_0)/2 + \dots$ , where  $L$  is the cavity length, and the coupling is  $G = \pi c$ . Otherwise, if the mechanical oscillator is a dielectric object placed into the cavity [Tho+08; Kie+13], its non unity refractive index will determine a delay for the light travelling through, effectively increasing the cavity length. This delay will depend on the overlap of the cavity mode with the dielectric volume, which in turn will depend on its position resulting again in a position dependent resonance frequency. The position of the particle will be imprinted in the cavity output field. This can be derived knowing its optical response function, which for a single sided cavity is given by:

$$\chi_{cav}(\omega) = \frac{\sqrt{\kappa}}{\frac{\kappa}{2} - i(\omega - \omega_{cav}(x))}. \quad (39)$$

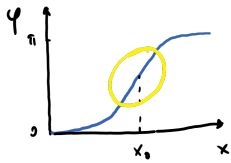
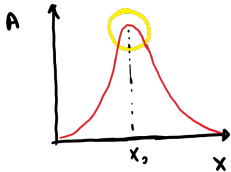
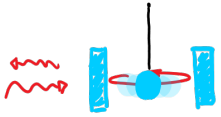
Here the real and imaginary parts of  $\chi_{cav}(\omega)$  represent the cavity’s phase and amplitude responses, respectively. From these relations is easy to see that a change in resonance frequency, caused for example by the displacement of the mechanical oscillator, detunes the cavity from the (resonant) input field, resulting in a phase delay of the output field:

$$\begin{aligned} \Delta x \rightarrow \Delta \omega_{cav} &= G \Delta x \\ \rightarrow \Delta \varphi &= \frac{2}{\kappa} \Delta \omega_{cav} = \frac{2G}{\kappa} \Delta x \end{aligned} \quad (40)$$

We can therefore define the optomechanical phase shift per displacement, or measurement strength, in presence of a cavity as  $\chi = 2G/\kappa$ . Additionally we can write the rate of photons leaving the cavity (for the detector) as the intracavity photon number times the cavity loss rate:  $\dot{N} = \sqrt{\kappa} N_{cav}$ . Finally, using equation (38) we find:

$$C_q = \frac{\Gamma_{ba}}{\Gamma_{th}} = \frac{\dot{N} \chi^2 \chi_{zpf}^2}{\Gamma_{th}} = \frac{4g_0^2 N_{cav}}{\kappa \Gamma_{th}} \quad (41)$$

with  $g_0 = G \chi_{zpf}$  the single-photon single-phonon optomechanical coupling [AKM14]. While the first two equalities in equation (41) are true in general for any optomechanical system, the third is specific to the use of a cavity.





## 2.6 WHERE DOES THIS THESIS STAND

In this thesis I study the motion of silica nano-balls that are trapped in an optical tweezer in vacuum and at room temperature. In particular I will show two main results on which I have been working. The first employing a cavity [Mag+18], the other one not [Mag+21]. At the time I started my PhD, in September 2015, optically levitated mechanical systems were trailing in the quest for the quantum regime, while clamped optomechanical systems [Pal+13; Wil+15; SN+13; Rie+16], with the benefit of cryogenic cooling and high mechanical frequencies, were steadily following in the footsteps of the atomic physics community. The “new” levitated particles had been hard to control and were often lost in UHV even with cavity sideband cooling [Kie+13] until the introduction of a measurement based parametric feedback cooling scheme by Gieseler *et al.* [Gie+12]. This allowed Jain *et al.* to reduce the thermal noise introduced by the residual gas and show for the first time the effect of radiation pressure shot noise on a levitated particle [Jai+16]. However, despite the strong backaction, the measurement efficiency was limited to about  $\eta_d \sim 10^{-3}$ , restricting control to the classical domain.

The idea of the first experiment I present here [Mag+18] was to improve this figure by strong evanescent coupling of the motion of particle to the optical mode of a photonic crystal cavity, which could be efficiently read out by coupling the structure to a tapered single mode fiber. We could show very high and tunable coupling (due to the small mode volume) and a detection efficiency of  $\eta_d = 0.09$ , two orders of magnitude better than previous results and just an inch from the minimal required limit of  $1/9$  for ground state cooling – and with room for improvement. However due to thermal and mechanical instabilities of the cavity this was only shown at a gas pressure of 1 mbar, hence limiting the measurement cooperativity to  $C_q \sim 10^{-9}$ ! On the other hand, as an added feature of the new experimental platform, we demonstrated imaging of the 3-dimensional nanophotonic near field gradient in super-resolution, and a promising platform for the measurement of short-range forces [Mon+21].

In the second experiment [Mag+21] we used a microscopy technique, a confocal interferometric detection, instead of a cavity. Measuring the photons that are

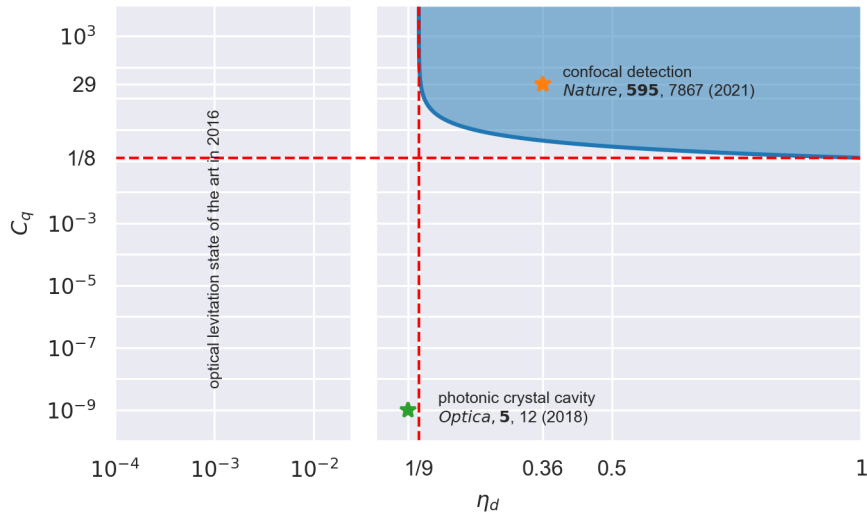


**Figure 2:** Performance of the published experiments with respect to the two main figures of merit: detection efficiency and quantum measurement cooperativity. The blue shaded area represents the parameter space where the measurement allows conditioning on to a state of uncertainty smaller than the extension of the first excited state. In other words where, with the appropriate feedback, ground state cooling ( $n < 1$ ) is possible.

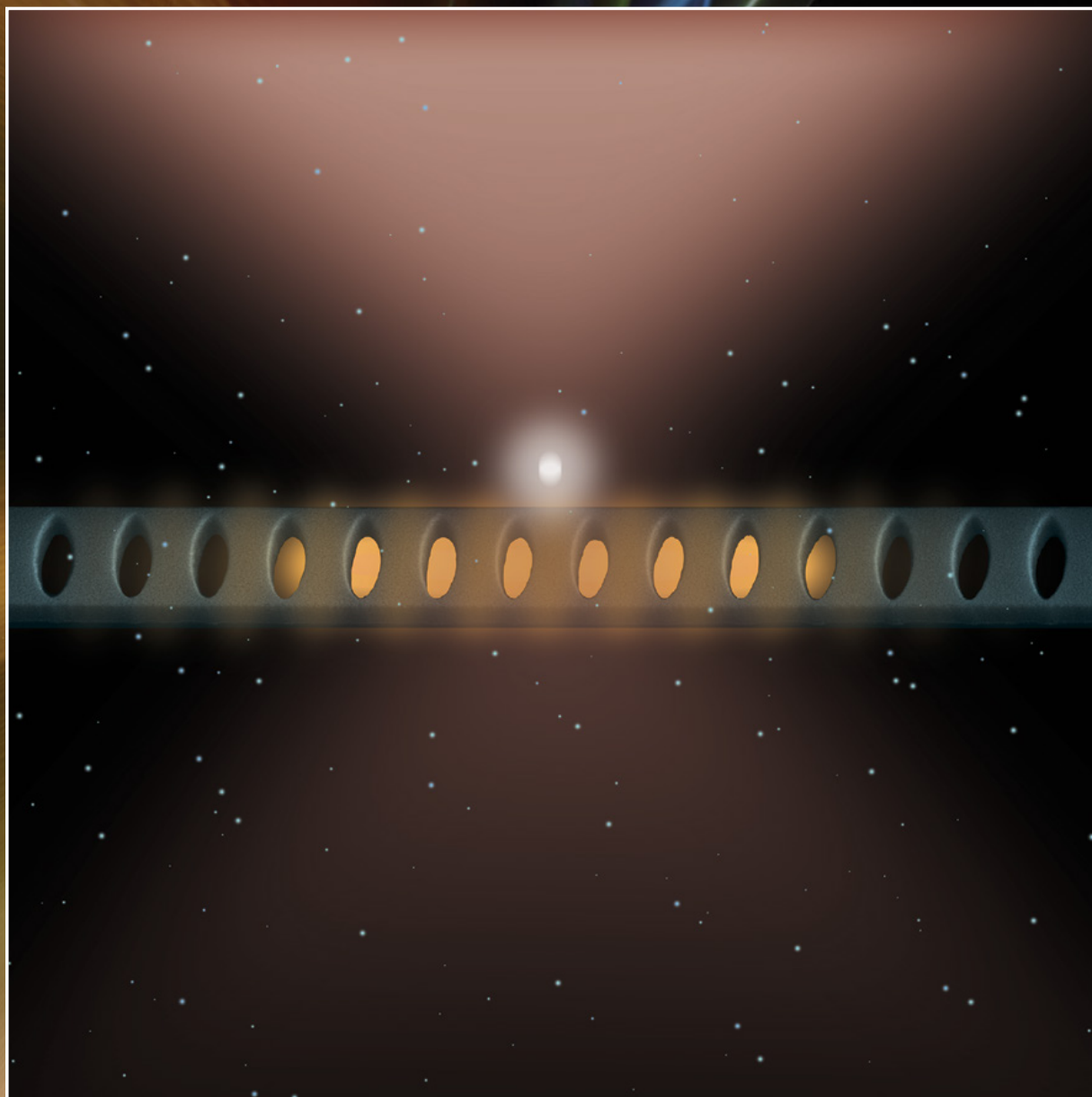
scattered backwards allows to only detect photons that have interacted with the levitated particle and discard those that do not carry any position information in the phase and would only contribute to an increased measurement shot noise. After all if they have not interacted they also do not contribute to the measurement backaction. It was also recently shown by Tebbejohanns *et al.* [TFN19] that the information distribution in the scattered optical field is not uniform, favouring (for one of the particle's degrees of freedom) the backscattered photons. Even better! The detection efficiency achieved in this experiment is  $\eta_d = 0.36$  with a measurement cooperativity of  $C_q = 29$  at a pressure of  $10^{-8}$  mbar, allowing us to measure the mechanical motion of the trapped particle at room temperature close to the SQL. We then use the quantum limited measurement in combination with a Kalman filter and optimal feedback control to track the quantum trajectory of the levitated particle conditioned on the measurement outcome in real time, and to stabilize it into the quantum ground state. In the last chapter, the same confocal measurement is used to observe correlations created by the mechanical motion into perpendicular optical quadratures and detect radiation-pressure induced optomechanical squeezing without a cavity and at room temperature.





# optica

Volume 5 • Issue 12 • December 2018



## 3

## NEAR-FIELD COUPLING OF A LEVITATED NANOPARTICLE TO A PHOTONIC CRYSTAL CAVITY

The diffraction limit defines the smallest volume that an electromagnetic field can be confined to. Beyond that limit, exponentially decaying evanescent (non propagating) components of the field will leak out of the boundaries of the confinement medium. This effect allows one to build nanophotonic devices that confine light within an extremely small volume, and still couple strongly to objects in the near-field. In this chapter I report on my first work in which I have demonstrated coupling an optically levitated dielectric particle to the evanescent field of a photonic crystal cavity. The results presented were first published as reference [Mag+18], and are here preceded by a short summary of the scientific context of the manuscript.

Shortly after the first proposals to use optically levitated particles for experiments in the quantum regime [Cha+10; RI+10; BS10], the first experiments appeared showing both measurement based feedback cooling [Gie+12; GNQ13] and passive cavity cooling [Kie+13; Ase+13; Kuh+15; Mil+15] of dielectric objects in vacuum. While cavity based schemes were struggling to operate in high vacuum, measurement based feedback control allowed to stabilize particles in UHV and to observe the effects of radiation pressure shot noise (or recoil heating) [Jai+16]. However, even in UHV the measurement efficiencies of far field detection were limited to around  $\eta_d \sim 10^{-3}$  restricting the control of the system to the classical domain. At the same time, nanophotonic structures had been used to demonstrate near-field coupling trapped [Vet+10; Tho+13; Tie+14] and flying [Alt+11; Jun+13] atoms, molecules [Qua+13], and clamped mechanical oscillators [Ane+09; GVK12; Wil+15], which allowed for strong and efficient measurements of the degrees of freedom of these systems. Inspired in particular by the results shown by Thompson *et al.* with atoms [Tho+13], the idea of this work was to bring the modern tools of nanophotonic devices to the domain levitated solid-state objects.

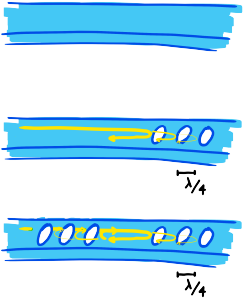
Why? In the context of a quantum measurement the macroscopic cavities used in previous experiments had two main problems. The first is a kind of luxury problem, but still crucial for the argument of pursuing a quantum measurement (as we introduced in chapter 2): being designed for passive sideband cooling [AKM14], macroscopic cavities are characterized by extremely low loss rates ( $\kappa/2\pi \sim 10^5$  Hz). In these conditions the time that light is confined into the cavity is comparable to the time scales of the mechanical oscillation ( $\kappa^{-1} \sim \Omega_q^{-1}$ ), invalidating the assumption of instantaneous measurements. The second issue arises from the natural trade off between low losses  $\kappa$  and high coupling  $g_0$ . One cannot just have it both ways, and experiments in levitated cavity-optomechanics operating in the regime of small linewidth were limited to optomechanical couplings of  $g_0/2\pi \sim 10^{-1}$  Hz [Del+20b]. For this reason we aimed for the opposite extreme: the smallest possible cavity volume, close to the diffraction limit, resulting in  $g_0/2\pi \sim 10^4$  Hz together with very high losses ( $\kappa/2\pi \sim 10^9$  Hz). In this way we have strongly shifted the coupling-linewidth trade-off in favour of a high coupling, allowing instantaneous measurements ( $\kappa^{-1} \ll \Omega_q^{-1}$ ), while keeping  $g_0/\kappa$  unchanged. The pursuit of enhanced light matter interaction by miniaturizing the optical cavities has greatly impacted the field of cavity-QED in the past 20 years. As a result a great variety of optical resonators is now available to the contemporary experimenter, all with different properties, advantages and disadvantages. They range from the most classical high-Q Fabry-Perot microcavity made of dielectric mirrors [HKY01] (with mode

volumes of a few  $\mu\text{m}^3$ ), etched silicon wafers [Kuh+17] or micropillars [Ger+96], over guided nanofiber resonators [Joh+19] and circular whispering gallery modes in micro -spheres [Kni+95], -toroids [KSV04] and -droplets [Qia+86], to photonic crystal cavities [Vuč+01] with the smallest demonstrated mode volumes ( $\sim \lambda^3$ ). It is a cavity of this last type that we have used in this experiment.

We demonstrate a detection efficiency of  $\eta_d = 0.09$ , which is an improvement over previous experiments by two orders of magnitude. In addition, precise control of the position of the particle with respect to the near-field of the photonic crystal enables tunable optomechanical coupling (up to  $g_0 = 9 \text{ kHz}$ ), and allows us to reconstruct the optical near field with a resolution of  $\sim 10 \text{ nm}$ . While this resolution is currently determined by the step size of our nanopositioner, it is fundamentally limited only by the extent of its motion. Finally this experiment provides an ideal platform for the measurement of forces at distances as low as  $50 \text{ nm}$ .

### A fast introduction to photonic crystal cavities for who has no idea

Photonic crystals are nanofabricated devices that exploit a modulation of the refractive index of the material on the order of the optical wavelength [Sako4]. If carefully engineered, this modulation can lead to constructive or destructive interference of the light that is scattered by the periodic structures. In analogy with solid-state semiconductors, where the crystalline arrangement of atoms define their electronic properties, a periodic modulation of the refractive index in an optical waveguide can be mapped into a primitive cell in momentum space describing the dispersion of the propagating optical modes. With this in mind we can take a thin silicon beam, where light is confined by total internal reflection as in a fiber, and, by etching holes at fixed distance into it, we will define a modulation of the refractive index resulting in high Bragg reflectivity for a specific wavelength with a defined bandwidth: a bandgap. By simply placing two of these Bragg mirrors one after the other light can be confined into a finite volume: we finally have a photonic crystal cavity [Vuc+02; EFV05].



# NEAR-FIELD COUPLING OF A LEVITATED NANOPARTICLE TO A PHOTONIC CRYSTAL CAVITY

Lorenzo Magrini<sup>1</sup>, Richard A. Norte<sup>2</sup>, Ralf Riedinger<sup>1</sup>, Igor Marinković<sup>2</sup>, David Grass<sup>1</sup>, Uroš Deliċ<sup>1</sup>, Simon Gröblacher<sup>2,\*</sup>, Sungkun Hong<sup>1,†</sup>, and Markus Aspelmeyer<sup>1,‡</sup>

<sup>1</sup> Vienna Center for Quantum Science and Technology (VCQ), Faculty of Physics, University of Vienna, A-1090 Vienna, Austria

<sup>2</sup> Kavli Institute of Nanoscience, Delft University of Technology, 2628CJ Delft, The Netherlands

\* s.groeblicher@tudelft.nl

† sungkun.hong@univie.ac.at

‡ markus.aspelmeyer@univie.ac.at

This is the author’s accepted version of the work. The definitive version was published in *Optica* “Near-field coupling of a levitated nanoparticle to a photonic crystal cavity”, volume 5, issue 12, pages 1597-1602 (13 December 2018).

doi: <https://doi.org/10.1364/OPTICA.5.001597>.

## 3.1 ABSTRACT

Quantum control of levitated dielectric particles is an emerging subject in quantum optomechanics. A major challenge is to efficiently measure and manipulate the particle’s motion at the Heisenberg uncertainty limit. Here we present a nanophotonic interface suited to address this problem. By optically trapping a 150 nm silica particle and placing it in the near field of a photonic crystal cavity, we achieve tunable single-photon optomechanical coupling of up to  $g_0/2\pi = 9$  kHz, three orders of magnitude larger than previously reported for levitated cavity optomechanical systems. An efficient collection and guiding of light through the nanophotonic structure results in a per-photon displacement sensitivity that is increased by two orders of magnitude compared to conventional far-field detection. The demonstrated performance shows a promising route for room temperature quantum optomechanics.

## 3.2 INTRODUCTION

Optical tweezers provide a remarkably simple, yet versatile platform for studying a plethora of intriguing problems in single molecule biophysics [Wan+97; Jia+17], thermodynamics [Bow+13; Li+10; Ron+17; Ric+17], sensing [Ran+16; Hem+17] or fundamental physics [GPK10; MRG14]. Realizing full quantum control of trapped nanoparticles will enable new insights into quantum-enhanced precision metrology as well as into fundamental aspects of quantum physics [RI+10; Kal+12]. The past few years have witnessed rapid progress towards the quantum regime of optically levitated nanoparticles through cavity- [Kie+13; Ase+13; Mil+15; Kuh+17] and feedback-assisted control schemes [LKR11; Gie+12; Jai+16; Vov+17]. The primary limitations lie either in small optomechanical coupling strengths to the cavity field, or, for the case of optical tweezers, in significant losses in the detection channel. As every scattered photon induces back-action noise on the particle motion, it

is crucial not to ‘lose’ any information carried by light [CGS03], especially in the regime where photon recoil is the dominant source of decoherence. Nanophotonic structures can provide a solution to these problems. Their small mode volumes and high quality factors result in strong optomechanical coupling [Ane+09; Cha+11]. These nanostructures can also be easily interfaced with a single-mode fiber, hence allowing for efficient collection and guiding of the light from the cavity [Bur+17]. Previously, optical nanodevices have been used, for example, to show strong coupling and super-radiance of trapped atoms [Tho+13; Gob+15], emission rate control of solid state quantum emitters [Eng+05; Hau+13], label-free single molecule detection [Qua+13], or trapping of colloidal particles in liquid [Des+13].

Here we use a nanophotonic cavity to efficiently couple the 3D mechanical motion of a levitated nanoparticle to a single optical mode. Specifically, by placing the particle at a distance of  $\sim 310$  nm from a photonic crystal cavity, and exploiting the dispersive coupling to the evanescent component of the strongly confined cavity field, information about the mechanical displacement is encoded into phase fluctuations of the cavity mode [Ane+09]. This signal is efficiently outcoupled and guided through single mode fibers to the detector, resulting in a real-time measurement of the particle motion at high bandwidth and high sensitivity. Our approach therefore complements previous experiments involving nanophotonic structures and colloidal particles, in which the structures are used mainly to trap the particle or to detect the presence of the particle without monitoring its precise position or motion [Qua+13; Des+13].

### 3.3 METHODS

Our experimental setup consists of an optical tweezer and a silicon nitride (SiN) photonic crystal cavity (Fig. 3(a)), both of which are situated inside a vacuum chamber. The cavity is impedance matched, with a fundamental resonance wavelength of  $\lambda_{\text{cav}} = 1538.72$  nm and an optical loss rate of  $\kappa/2\pi = 5.0$  GHz. The input/output mirror is adiabatically transitioned into a tapered waveguide that is interfaced with an open-end tapered fiber [Bur+17], yielding a fiber-to-cavity coupling efficiency of  $\eta_{\text{cav}} = 0.32$ . Taking into account all other losses in the setup, the total detection efficiency of photons approaching the cavity is  $\eta = 0.09$  (see Supplement 1). The fiber physically supports the nanocavity by van der Waals forces and can be positioned relative to the optical tweezer using a piezo-actuated three-axis translational stage. The optical tweezer is formed by tightly focusing the laser beam (wavelength  $\lambda_{\text{trap}} = 1064$  nm; trap power 150 mW) with a commercial dry objective lens (numerical aperture  $\text{NA} = 0.95$ ) inside the vacuum chamber. The location of the trap within the focal plane is controlled by steering the angle of incidence of the laser at the rear lens of the objective.

Ultimately, the particle is trapped in a standing wave potential formed by the interference of the focused trapping light with its reflection off the surface of the photonic crystal. To achieve this we first trap a neutral silica nanoparticle (nominal radius  $r = 71.5 \pm 2.0$  nm) with the optical tweezer at ambient pressure<sup>1</sup>. After reducing the pressure to 1.5 mbar, we bring the nanocavity in close proximity to the particle. During this process, the optical trap potential is transformed adiabatically from the single, nominally Gaussian, potential given by the focal spot of the tweezer, to the periodic potential induced by the standing wave [Tho+13] (Fig. 3(a)). The locations and actual shapes of the multiple lattice sites are determined by the wavelength of the trap beam and the thickness of the cavity (see Supplement 1 and [Tho+13; Die+18]). Our experimental parameters yield the first minimum of the trapping potential at  $z_0 \sim 380$  nm from the device surface, i.e. a surface-to-surface

<sup>1</sup> We note that in our experiment, most particles are generated without residual charges. This contrasts other experimental reports where tens of positive charges are observed after trapping [Fri+17], and is subject to further investigation.



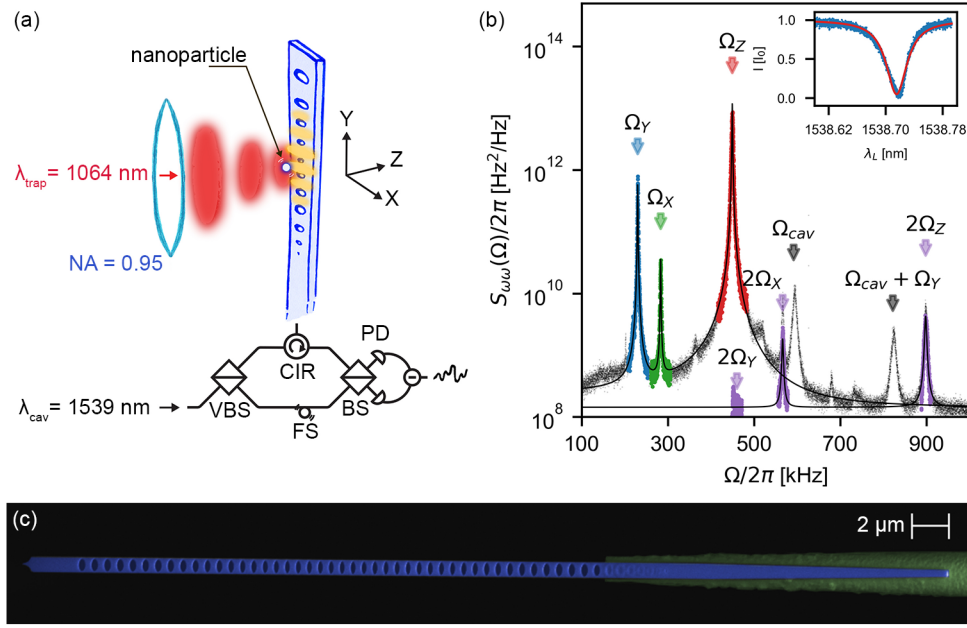


**Figure 3:** Nanophotonic interface. (a) Sketch of the setup: A dielectric nanoparticle is trapped inside the high intensity lobe formed by the reflection of the optical tweezer light ( $\lambda_{\text{trap}} = 1064 \text{ nm}$ ) from the surface of the nanophotonic cavity, at a distance of about  $310 \text{ nm}$ . A laser light resonant with the cavity ( $\lambda_{\text{cav}} = 1538.72 \text{ nm}$ ) is sent into a variable beam splitter (VBS) which splits it into a weak ( $260 \text{ nW}$ ) beam pumping the cavity, and a strong ( $1 \text{ mW}$ ) local oscillator. The cavity output is redirected by a circulator (CIR) towards a symmetric beam splitter (BS) at which it interferes with the local oscillator. The light in the two output ports is measured using a balanced photo-detector (PD). While the low frequency component of the signal is used to stabilize the interferometer via a fiber stretcher (FS), the high frequency part is directed to a signal analyzer. (b) The measured frequency power spectral density exhibits three mechanical peaks at  $\Omega_Y/2\pi = 228.3 \text{ kHz}$  (blue),  $\Omega_X/2\pi = 280.3 \text{ kHz}$  (green) and  $\Omega_Z/2\pi = 444.9 \text{ kHz}$  (red). The significantly higher frequency along  $z$ , which is the direction of the tweezer beam propagation, is caused by the standing wave confinement, and for the radial directions  $x$  and  $y$ , the degeneracy is broken due to the use of polarized light together with tight focusing. Nonlinearities in the trap potential as well as in the optomechanical couplings result in peaks at twice the mechanical frequencies (highlighted in purple). The mechanical vibration of the cavity/fiber assembly at around the frequency  $\Omega_{\text{cav}}/2\pi \sim 600 \text{ kHz}$  also induces additional peaks in the spectrum. The inset shows the cavity resonance measured by monitoring the light reflection from the cavity while scanning the pump laser wavelength. The slight asymmetry of the response arises from thermo-optic effects, as we are pumping the cavity at the limit of thermal stability (see [Supplement 1](#)). (c), False-colored scanning electron microscope image of the photonic crystal cavity (blue) attached to the tapered fiber (green).

separation between nanosphere and photonic crystal cavity of  $d = z_0 - r \sim 310 \text{ nm}$ . Due to the subwavelength transverse dimensions of the nanophotonic device, the cavity field exhibits a considerable evanescent component that decays exponentially with distance. In this region, the displacement of the particle results in a shift of the cavity resonance by  $\delta\omega_{\text{cav}} = G_\xi \delta\xi$ , where  $\xi = x, y, z$  is the direction of mechanical motion and  $G_\xi = \partial_\xi \omega_{\text{cav}} \propto \partial_\xi E^* E$  the optomechanical coupling ( $E$ : evanescent field amplitude). As  $G_\xi$  is proportional to the intensity gradient of the cavity field along the direction of motion, each mechanical mode couples to the cavity field with different strength. In particular, the small mode volume results in a large field variation and hence a significantly enlarged coupling when compared to standard levitated optomechanics configurations based on bulk optics [[Kie+13](#); [Ase+13](#); [Mil+15](#)].

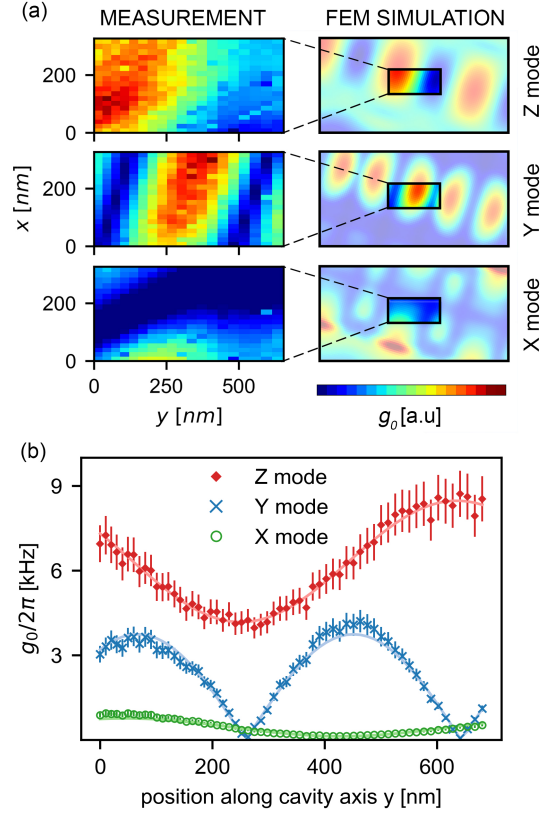


**Figure 4:** Optomechanical coupling. (a) Measured (left) and simulated (right) intensity map of the single-photon optomechanical coupling rates  $g_0$  for the three spatial modes. Because of heating from the tweezer light (see Supplement 1), at every position the cavity is reset on resonance before recording the interferometric signal. (b) Position scan of the single-photon optomechanical coupling rates along the  $y$  direction and close to the cavity center for the modes along  $x$  (green circles),  $y$  (blue crosses) and  $z$  (red diamonds). Solid lines are fits based on our cavity field model (see Supplement 1). As the scan was performed slightly off the cavity center, the coupling to the  $z$  mode is non-vanishing while we can suppress the  $x$  and  $y$  couplings. The main contribution to the error bars is given by the uncertainty in the shot noise level determined by the integration time of  $\sim 3$  seconds.

### 3.4 RESULTS AND DISCUSSION

When pumping the cavity on resonance, the position dependent frequency fluctuation is mapped onto the phase quadrature of the output field, which can then be measured via a shot-noise limited homodyne detection (Fig. 3(a)). We use this cavity-enhanced measurement to monitor the thermal motion of the trapped particle: the mechanical oscillations in the three spatial directions are observed as distinct frequency components in the homodyne signal (Fig. 3(b)). Using thermal noise of the particle motion and photon shot noise of the cavity light we calibrate both displacement and optomechanical coupling (see Supplement 1). We note that, by only injecting 260 nW of optical power into the cavity and at an overall detection efficiency of 9%, we achieve a displacement sensitivity of  $(3.3 \pm 0.5) \times 10^{-12} \text{ m}/\sqrt{\text{Hz}}$ , similar to what is measured in far field detection with 1 mW of detected light. This amounts to an increase in the position sensitivity per-photon by more than a factor of 100. At the optimal position we measure coupling rates along the  $z$ -direction of motion, i.e. orthogonal to the cavity surface, of  $G_z/2\pi = 3.6 \pm 0.4 \text{ MHz/nm}$ . This is consistent with our finite element method (FEM) simulation (see Supplement 1) and corresponds to a single-photon optomechanical coupling  $g_0/2\pi \equiv z_{\text{ZPF}} G_z/2\pi$  of  $9.3 \pm 0.9 \text{ kHz}$  ( $z_{\text{ZPF}} = (\hbar/2m\Omega_z)^{1/2}$ : mechanical zero point fluctuation of the particle motion in the  $z$  direction). Another intriguing feature of photonic crys-



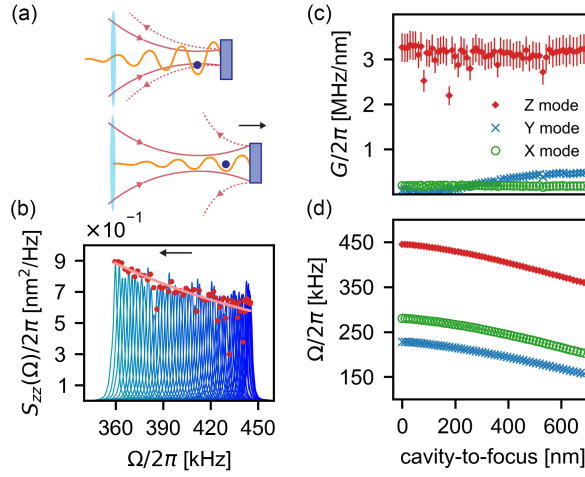


**Figure 5:** Position locking. (a) Sketch of the nanoparticle (blue dot), trapped in the standing wave potential (orange) formed by the reflection of the focused tweezer light (red) by the photonic crystal cavity (blue rectangle). The data is taken by moving the photonic crystal along the direction of propagation of the tweezer beam ( $z$ ). While the particle's distance to the cavity remains locked, the divergence of the tweezer causes a reduction of the trapping potential. (b) Position power spectral density for the  $z$  mode  $S_{zz}(\Omega)$  (blue) measured as cavity-focus increases (in direction of the arrow). The variance of the motion given by the peak integral (red dots  $\propto \int S_{zz}(\Omega) d\Omega$ ) changes with the mechanical frequency as stated by the equipartition theorem (pink solid line  $\propto 1/\Omega_z^2$ ). Deviation from the expected Lorentzian peak is given by the fluctuations during the integration time, which effectively reduce the peak height. (c) Frequency shift per displacement  $G$  plotted as a function of the cavity distance to the focal plane, for the  $z$  mode (red diamonds),  $y$  mode (blue crosses) and  $x$  mode (green circles). (d) Mechanical frequencies for the three modes as a function of the cavity distance to the focal plane.

tal cavities is the strong spatial variation of the cavity field  $E$ , which results in a significant position-dependent optomechanical coupling for all three spatial directions of motion. By changing the particle position relative to the cavity we can therefore tune the optomechanical coupling of all mechanical modes [Hry+15]. We experimentally demonstrate this by scanning the particle position in a plane perpendicular to the  $z$  axis while simultaneously monitoring the cavity signal. The observed strong modulations in all three coupling rates are in good agreement with FEM simulations (Fig. 4). As the motion of the levitated nanoparticle represents a sub-wavelength probe, this measurement allows us to image the three dimensional intensity gradient of the nanophotonic cavity mode in super-resolution, i.e. not limited by diffraction (Fig. 4). Compared to standard near-field scanning techniques, such as scanning near-field microscopy [RK14], our resolution is defined by the extent of the particle motion and not by the physical size of the probe. As a consequence, the imaging is fundamentally limited only by the ground state size of the trapped particle, i.e. to a resolution of some picometers. In spite of this position drifts and the accuracy of our positioner currently limit the imaging resolution to some tens of nanometers (Fig. 4(b)) in a field of view of half a micron square.

Our system also enables tunability of the mechanical frequencies without affecting the coupling strength to the cavity field. In other words, we can modify the trapping potential independent of the trapping distance. To demonstrate this we move the cavity along the  $z$  direction, away from the focus of the trapping beam (Fig. 5(a)). The optomechanical coupling stays constant (Fig. 5(c)), indicating that the relative distance between the particle and the cavity remains unchanged. This behavior can easily be understood when considering the formation of the standing wave by the cavity reflection. The positions of the anti-nodes are solely determined by the location of the cavity and its thickness, locking the trap position to the cavity. At the same time, the mechanical frequency is reduced because the high divergence

of the tightly focused optical tweezer leads to a sharp decrease of the intensity at the trap location (Figs. 5(b) and 5(d)).

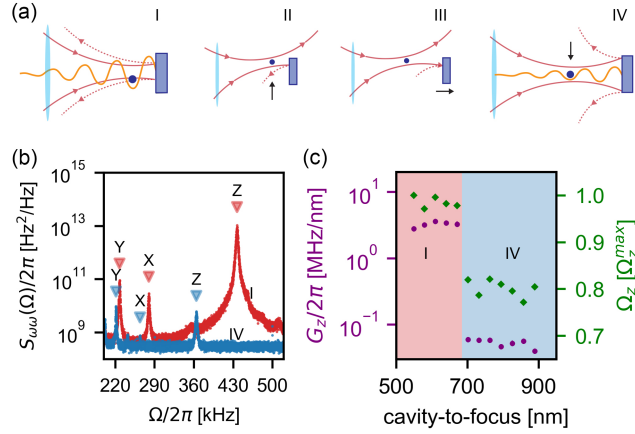


**Figure 6:** Loading of the particle into the lattice. (a) The particle is initially trapped in the closest of the cavity trap sites (I). We steer the tweezer away from the cavity (II) and subsequently change the cavity position (III). Finally the particle is steered back in front of the cavity (IV). Depending on the cavity-to-focus distance, the particle will slide into different sites. (b) Frequency power spectral densities measured in the case of the particle being in the first trapping site (red, I) or in the second (blue, IV). The small unlabeled peak in the blue spectrum is an electronic noise peak common to all measurements. (c) Optomechanical coupling (purple dots) and mechanical frequency (green diamonds) for the  $z$  mode as a function of the initial cavity-to-focus distance.

Finally, we demonstrate reliable, deterministic loading of the nanoparticle into the different standing wave optical lattice sites. This is achieved by a sequence of optical tweezer and cavity position control steps (Fig. 6(a)). We first terminate the standing wave by moving the particle to the side of the photonic crystal cavity. After displacing the cavity along the  $z$  axis, the particle is moved back and the standing wave is reestablished. When the cavity is sufficiently displaced, the particle will slide into the next trap location of the re-appearing standing wave. We observe this behavior when the cavity displacement is greater than  $\lambda_{\text{trap}}/4$  (Fig. 6(c)). At this second trap location, the optomechanical coupling rate is reduced by two orders of magnitude, consistent with FEM simulation (see Fig. 6(b) and Supplement 1).

### 3.5 CONCLUSIONS

In summary, we have realized a low-loss, and widely tunable hybrid optomechanical system combining optical levitation of a nanoparticle with a nanophotonic cavity via near-field coupling. The displacement sensitivity per photon of our platform is more than two orders of magnitude higher than what was shown using far-field detection [Jai+16]. This opens a direct route for quantum feedback control. Specifically, ground state cooling with feedback requires  $\eta > (1 + 1/C_q)/9$  with  $C_q$  the quantum cooperativity [Gen+08; Wil+15; Ros+18], yielding a minimally required value for the detection efficiency of  $\eta > 1/9 \approx 0.11$ . While far-field detection is currently limited at  $\eta \sim 10^{-3}$  [Jai+16], we here demonstrate  $\eta = 0.09$ , i.e. already close to the required bound. We anticipate that a more stringent screening process over multiple cavity transfer trials (see Supplement 1) will yield fiber-cavity assemblies with coupling efficiency exceeding  $\eta_{\text{cav}} = 0.96$ , as was previously shown by Burek *et al.* [Bur+17]. It would result in an overall detection efficiency of  $\eta > 0.3$ .

The other relevant figure of merit for quantum state control is the quantum cooperativity  $C_q = (4g_0^2 n_{\text{cav}})/(\kappa \Gamma_m n_{\text{th}})$ , where  $n_{\text{cav}}$  ( $n_{\text{th}}$ ) and  $\kappa$  ( $\Gamma_m$ ) are the cavity photon (mechanical phonon) occupation and loss rate, respectively [AKM14]. Our

current value ( $C_q \sim 10^{-9}$ ) is mainly limited by the fact that, in absence of feedback stabilization of the particle, the operating pressure cannot be decreased below  $\sim 1$  mBar (corresponding to mechanical loss rates  $\Gamma_m/2\pi$  of more than  $10^3$  Hz). Implementing stable feedback cooling will allow us to reach ultra-high vacuum levels ( $10^{-8}$  mbar and below) at which mechanical losses are limited by photon recoil to  $\Gamma_m/2\pi \approx 10^{-4}$  Hz. This will result in an immediate improvement of cooperativity by more than seven orders of magnitude. In the present configuration, the main bottleneck is the mechanical support of the cavity, which causes alignment drifts and hence limits feedback particle stabilization in ultra high vacuum. One workaround will be to use rigidly mounted on-chip (instead of fiber supported) cavities. This will also improve the thermal anchoring of the cavity and therefore enable a higher intra-cavity photon number  $n_{\text{cav}}$ , which is now limited to  $n_{\text{cav}} \sim 800$  because of thermo-optic heating. With a more careful design and fabrication, the cavity optical losses  $\kappa/2\pi$  can be reduced to as low as 20 MHz in silicon [Asa+17] and 1 GHz in SiN [Deb+17]. The cavity thickness directly affects the boundary condition for the standing wave trap formation such that, with an appropriately chosen thickness, the particle can be trapped within 200 nm from the cavity surface (see Supplement 1 and [Tho+13]). This would result in an increase of the optomechanical coupling rate by one order of magnitude. Incorporating all these improvements will allow to achieve  $C_q > 10$  and thus place the system deep into the strong cooperativity regime. This will enable a new generation of chip-based levitated quantum sensors operating at room temperature. For example, the high bandwidth of our system ( $\kappa \gg \Omega_m$ ) makes it an ideal platform for implementing measurement-based quantum state preparation using pulsed interactions [Van+11], which is a complementary approach to quantum control methods based on cavity sideband driving [AKM14]. The high coupling and relatively low frequencies place the system in reach of the non-linear optomechanical regime ( $g_0 \approx \Omega_m$ ) [Lei+17]. Exploiting the design capabilities for the spatial modes in photonic crystal cavities our system can also be used for studying effects of self-induced backaction and non-harmonic dynamics in both the classical and quantum regime [NQC15]. Also, the expected force noise of  $10^{-20}$  N/ $\sqrt{\text{Hz}}$  will allow a detailed study of short-range surface forces at sub-micron distances [GPK10; Ran+16; Hem+17].

## FUNDING

European Research Council (ERC) (QLev4G 649008, Strong-Q 676842); the Austrian Science Fund (FWF) (F40, P28172); the Foundation for Fundamental Research on Matter (FOM) (15PR3210); the Netherlands Organisation for Scientific Research (NWO/OCW).

## ACKNOWLEDGMENTS

We thank Ramon Moghadas Nia for valuable lab support, Eugene Straver, Michael J. Burek and Marko Lončar for their technical advice on the tapered fibers, and Nikolai Kiesel and Lukas Novotny for helpful discussions. L. M. is supported by the Vienna Doctoral School of Physics (VDS-P), R. R. is a recipient of a DOC fellowship of the Austrian Academy of Sciences at the University of Vienna and L. M., R. R., D. G. and U. D. are supported by the FWF under project W1210 (CoQuS).

## REFERENCES

These are the references cited in the author's version of the manuscript

- [AKM14] Markus Aspelmeyer, Tobias J. Kippenberg, and Florian Marquardt. "Cavity optomechanics". In: *Rev. Mod. Phys.* 86 (4 2014), pp. 1391–1452. DOI: [10.1103/RevModPhys.86.1391](https://doi.org/10.1103/RevModPhys.86.1391). URL: <https://link.aps.org/doi/10.1103/RevModPhys.86.1391> (cit. on pp. 15, 16, 21, 28, 29, 37, 81).
- [Ane+09] G. Anetsberger et al. "Near-field cavity optomechanics with nanomechanical oscillators". In: *Nature Physics* 5 (2009), p. 909. URL: <http://dx.doi.org/10.1038/nphys1425> (cit. on pp. 21, 24).
- [Asa+17] Takashi Asano et al. "Photonic crystal nanocavity with a Q factor exceeding eleven million". In: *Opt. Express* 25.3 (2017), pp. 1769–1777. DOI: [10.1364/OE.25.001769](https://doi.org/10.1364/OE.25.001769). URL: <http://www.opticsexpress.org/abstract.cfm?URI=oe-25-3-1769> (cit. on p. 29).
- [Ase+13] Peter Asenbaum et al. "Cavity cooling of free silicon nanoparticles in high vacuum". In: *Nature Communications* 4 (2013), p. 2743. URL: <http://dx.doi.org/10.1038/ncomms3743> (cit. on pp. 4, 21, 23, 25).
- [Bow+13] Richard W. Bowman et al. "Optical Trapping at Gigapascal Pressures". In: *Phys. Rev. Lett.* 110 (9 2013), p. 095902. DOI: [10.1103/PhysRevLett.110.095902](https://doi.org/10.1103/PhysRevLett.110.095902). URL: <https://link.aps.org/doi/10.1103/PhysRevLett.110.095902> (cit. on p. 23).
- [Bur+17] Michael J. Burek et al. "Fiber-Coupled Diamond Quantum Nanophotonic Interface". In: *Phys. Rev. Applied* 8 (2 2017), p. 024026. DOI: [10.1103/PhysRevApplied.8.024026](https://doi.org/10.1103/PhysRevApplied.8.024026). URL: <https://link.aps.org/doi/10.1103/PhysRevApplied.8.024026> (cit. on pp. 24, 28, 34–36).
- [CGSo3] A. A. Clerk, S. M. Girvin, and A. D. Stone. "Quantum-limited measurement and information in mesoscopic detectors". In: *Phys. Rev. B* 67 (16 2003), p. 165324. DOI: [10.1103/PhysRevB.67.165324](https://doi.org/10.1103/PhysRevB.67.165324). URL: <https://link.aps.org/doi/10.1103/PhysRevB.67.165324> (cit. on pp. 1, 3, 24, 62).
- [Cha+11] Jasper Chan et al. "Laser cooling of a nanomechanical oscillator into its quantum ground state". In: *Nature* 478 (2011), p. 89. URL: <http://dx.doi.org/10.1038/nature10461> (cit. on pp. 3, 16, 24).
- [Deb+17] Kapil Debnath et al. "Ultrahigh-Q photonic crystal cavities in silicon rich nitride". In: *Opt. Express* 25.22 (2017), pp. 27334–27340. DOI: [10.1364/OE.25.027334](https://doi.org/10.1364/OE.25.027334). URL: <http://www.opticsexpress.org/abstract.cfm?URI=oe-25-22-27334> (cit. on p. 29).
- [Des+13] Nicolas Deschannes et al. "Observation of Backaction and Self-Induced Trapping in a Planar Hollow Photonic Crystal Cavity". In: *Phys. Rev. Lett.* 110 (12 2013), p. 123601. DOI: [10.1103/PhysRevLett.110.123601](https://doi.org/10.1103/PhysRevLett.110.123601). URL: <https://link.aps.org/doi/10.1103/PhysRevLett.110.123601> (cit. on p. 24).
- [Die+18] Rozenn Diehl et al. "Optical potential mapping with a levitated nanoparticle at sub-wavelength distances from a membrane". In: *arXiv:1803.04917 [physics.optics]* (2018) (cit. on pp. 24, 35).
- [Eng+05] Dirk Englund et al. "Controlling the Spontaneous Emission Rate of Single Quantum Dots in a Two-Dimensional Photonic Crystal". In: *Phys. Rev. Lett.* 95 (1 2005), p. 013904. DOI: [10.1103/PhysRevLett.95.013904](https://doi.org/10.1103/PhysRevLett.95.013904). URL: <https://link.aps.org/doi/10.1103/PhysRevLett.95.013904> (cit. on p. 24).

- [Fri+17] Martin Frimmer et al. “Controlling the net charge on a nanoparticle optically levitated in vacuum”. In: *Phys. Rev. A* 95 (6 2017), p. 061801. DOI: [10.1103/PhysRevA.95.061801](https://doi.org/10.1103/PhysRevA.95.061801). URL: <https://link.aps.org/doi/10.1103/PhysRevA.95.061801> (cit. on pp. 24, 47, 58).
- [Gen+08] C. Genes et al. “Ground-state cooling of a micromechanical oscillator: Comparing cold damping and cavity-assisted cooling schemes”. In: *Phys. Rev. A* 77 (3 2008), p. 033804. DOI: [10.1103/PhysRevA.77.033804](https://doi.org/10.1103/PhysRevA.77.033804). URL: <https://link.aps.org/doi/10.1103/PhysRevA.77.033804> (cit. on pp. 15, 28).
- [Gie+12] Jan Gieseler et al. “Subkelvin Parametric Feedback Cooling of a Laser-Trapped Nanoparticle”. In: *Phys. Rev. Lett.* 109 (10 2012), p. 103603. DOI: [10.1103/PhysRevLett.109.103603](https://doi.org/10.1103/PhysRevLett.109.103603). URL: <https://link.aps.org/doi/10.1103/PhysRevLett.109.103603> (cit. on pp. 4, 17, 21, 23, 43).
- [Gob+15] A. Goban et al. “Superradiance for Atoms Trapped along a Photonic Crystal Waveguide”. In: *Phys. Rev. Lett.* 115 (6 2015), p. 063601. DOI: [10.1103/PhysRevLett.115.063601](https://doi.org/10.1103/PhysRevLett.115.063601). URL: <https://link.aps.org/doi/10.1103/PhysRevLett.115.063601> (cit. on p. 24).
- [GPK10] Andrew A. Geraci, Scott B. Papp, and John Kitching. “Short-Range Force Detection Using Optically Cooled Levitated Microspheres”. In: *Phys. Rev. Lett.* 105 (10 2010), p. 101101. DOI: [10.1103/PhysRevLett.105.101101](https://doi.org/10.1103/PhysRevLett.105.101101). URL: <https://link.aps.org/doi/10.1103/PhysRevLett.105.101101> (cit. on pp. 3, 23, 29).
- [Hau+13] B. J. M. Hausmann et al. “Coupling of NV Centers to Photonic Crystal Nanobeams in Diamond”. In: *Nano Letters* 13.12 (2013), pp. 5791–5796. DOI: [10.1021/nl402174g](https://doi.org/10.1021/nl402174g). eprint: <http://dx.doi.org/10.1021/nl402174g>. URL: <http://dx.doi.org/10.1021/nl402174g> (cit. on p. 24).
- [Hem+17] David Hempston et al. “Force sensing with an optically levitated charged nanoparticle”. In: *Applied Physics Letters* 111.13 (2017), p. 133111. DOI: [10.1063/1.4993555](https://doi.org/10.1063/1.4993555). eprint: <https://doi.org/10.1063/1.4993555>. URL: <https://doi.org/10.1063/1.4993555> (cit. on pp. 23, 29).
- [Hry+15] Aaron C. Hryciw et al. “Tuning of nanocavity optomechanical coupling using a near-field fiber probe”. In: *Optica* 2.5 (2015), pp. 491–496. DOI: [10.1364/OPTICA.2.000491](https://doi.org/10.1364/OPTICA.2.000491). URL: <http://www.osapublishing.org/optica/abstract.cfm?URI=optica-2-5-491> (cit. on p. 27).
- [Jai+16] Vijay Jain et al. “Direct Measurement of Photon Recoil from a Levitated Nanoparticle”. In: *Phys. Rev. Lett.* 116 (24 2016), p. 243601. DOI: [10.1103/PhysRevLett.116.243601](https://doi.org/10.1103/PhysRevLett.116.243601). URL: <https://link.aps.org/doi/10.1103/PhysRevLett.116.243601> (cit. on pp. 4, 17, 21, 23, 28, 36, 43, 83).
- [Jia+17] Junyi Jiao et al. “Single-Molecule Protein Folding Experiments Using High-Precision Optical Tweezers”. In: *Methods Mol Biol* 1486 (2017), pp. 357–390. ISSN: 1064-3745. DOI: [10.1007/978-1-4939-6421-5\\_14](https://doi.org/10.1007/978-1-4939-6421-5_14). URL: <http://www.ncbi.nlm.nih.gov/pmc/articles/PMC5508109/> (cit. on p. 23).
- [Kal+12] Rainer Kaltenbaek et al. “Macroscopic quantum resonators (MAQRO)”. In: *Experimental Astronomy* 34.2 (2012), pp. 123–164. ISSN: 1572-9508. DOI: [10.1007/s10686-012-9292-3](https://doi.org/10.1007/s10686-012-9292-3). URL: <https://doi.org/10.1007/s10686-012-9292-3> (cit. on pp. 4, 23).
- [Kie+13] Nikolai Kiesel et al. “Cavity cooling of an optically levitated submicron particle”. In: *Proceedings of the National Academy of Sciences* 110.35 (2013), pp. 14180–14185. DOI: [10.1073/pnas.1309167110](https://doi.org/10.1073/pnas.1309167110). eprint: <http://www.pnas.org/content/110/35/14180.full.pdf>. URL: <http://www.pnas.org/content/110/35/14180.abstract> (cit. on pp. 4, 16, 17, 21, 23, 25).



- [Kuh+17] Stefan Kuhn et al. “Nanoparticle detection in an open-access silicon microcavity”. In: *Applied Physics Letters* 111.25 (2017), p. 253107. DOI: [10.1063/1.5008492](https://doi.org/10.1063/1.5008492). eprint: <https://doi.org/10.1063/1.5008492>. URL: <https://doi.org/10.1063/1.5008492> (cit. on pp. 22, 23).
- [Lei+17] Rick Leijssen et al. “Nonlinear cavity optomechanics with nanomechanical thermal fluctuations”. In: *Nature Communications* 8 (2017), p. 16024. URL: <http://dx.doi.org/10.1038/ncomms16024> (cit. on p. 29).
- [Li+10] Tongcang Li et al. “Measurement of the Instantaneous Velocity of a Brownian Particle”. In: *Science* 328.5986 (2010), pp. 1673–1675. ISSN: 0036-8075. DOI: [10.1126/science.1189403](https://doi.org/10.1126/science.1189403). eprint: <http://science.sciencemag.org/content/328/5986/1673.full.pdf>. URL: <http://science.sciencemag.org/content/328/5986/1673> (cit. on p. 23).
- [LKR11] Tongcang Li, Simon Kheifets, and Mark G. Raizen. “Millikelvin cooling of an optically trapped microsphere in vacuum”. In: *Nature Physics* 7 (2011), p. 527. URL: <http://dx.doi.org/10.1038/nphys1952> (cit. on p. 23).
- [Mil+15] J. Millen et al. “Cavity Cooling a Single Charged Levitated Nanosphere”. In: *Phys. Rev. Lett.* 114 (12 2015), p. 123602. DOI: [10.1103/PhysRevLett.114.123602](https://doi.org/10.1103/PhysRevLett.114.123602). URL: <https://link.aps.org/doi/10.1103/PhysRevLett.114.123602> (cit. on pp. 21, 23, 25).
- [MRG14] David C. Moore, Alexander D. Rider, and Giorgio Gratta. “Search for Millicharged Particles Using Optically Levitated Microspheres”. In: *Phys. Rev. Lett.* 113 (25 2014), p. 251801. DOI: [10.1103/PhysRevLett.113.251801](https://doi.org/10.1103/PhysRevLett.113.251801). URL: <https://link.aps.org/doi/10.1103/PhysRevLett.113.251801> (cit. on pp. 3, 23).
- [NQC15] Lukas Neumeier, Romain Quidant, and Darrick E Chang. “Self-induced back-action optical trapping in nanophotonic systems”. In: *New Journal of Physics* 17.12 (2015), p. 123008. URL: <http://stacks.iop.org/1367-2630/17/i=12/a=123008> (cit. on pp. 29, 122).
- [Qua+13] Qimin Quan et al. “Single particle detection in CMOS compatible photonic crystal nanobeam cavities”. In: *Opt. Express* 21.26 (2013), pp. 32225–32233. DOI: [10.1364/OE.21.032225](https://doi.org/10.1364/OE.21.032225). URL: <http://www.opticsexpress.org/abstract.cfm?URI=oe-21-26-32225> (cit. on pp. 21, 24).
- [Ran+16] Gambhir Ranjit et al. “Zeptonewton force sensing with nanospheres in an optical lattice”. In: *Phys. Rev. A* 93 (5 2016), p. 053801. DOI: [10.1103/PhysRevA.93.053801](https://doi.org/10.1103/PhysRevA.93.053801). URL: <https://link.aps.org/doi/10.1103/PhysRevA.93.053801> (cit. on pp. 23, 29, 52).
- [RI+10] Oriol Romero-Isart et al. “Toward quantum superposition of living organisms”. In: *New Journal of Physics* 12.3 (2010), p. 033015. URL: <http://stacks.iop.org/1367-2630/12/i=3/a=033015> (cit. on pp. 4, 21, 23).
- [Ric+17] F. Ricci et al. “Optically levitated nanoparticle as a model system for stochastic bistable dynamics”. In: *Nature Communications* 8 (2017), p. 15141. URL: <http://dx.doi.org/10.1038/ncomms15141> (cit. on p. 23).
- [RK14] N. Rotenberg and L. Kuipers. “Mapping nanoscale light fields”. In: *Nature Photonics* 8 (2014), 919 EP. URL: <http://dx.doi.org/10.1038/nphoton.2014.285> (cit. on p. 27).
- [Ron+17] Loïc Rondin et al. “Direct measurement of Kramers turnover with a levitated nanoparticle”. In: *Nature Nanotechnology* 12 (2017), p. 1130. URL: <http://dx.doi.org/10.1038/nnano.2017.198> (cit. on p. 23).

- [Ros+18] Massimiliano Rossi et al. “Measurement-based quantum control of mechanical motion”. In: *Nature* 563.7729 (2018), pp. 53–58. ISSN: 1476-4687. DOI: [10.1038/s41586-018-0643-8](https://doi.org/10.1038/s41586-018-0643-8). URL: <https://doi.org/10.1038/s41586-018-0643-8> (cit. on pp. 3, 4, 28, 44, 46, 64, 69).
- [Tho+13] J. D. Thompson et al. “Coupling a Single Trapped Atom to a Nanoscale Optical Cavity”. In: *Science* 340.6137 (2013), pp. 1202–1205. ISSN: 0036-8075. DOI: [10.1126/science.1237125](https://doi.org/10.1126/science.1237125). eprint: <http://science.sciencemag.org/content/340/6137/1202.full.pdf>. URL: <http://science.sciencemag.org/content/340/6137/1202> (cit. on pp. 21, 24, 29, 39).
- [Van+11] M. R. Vanner et al. “Pulsed quantum optomechanics”. In: *Proceedings of the National Academy of Sciences* 108.39 (2011), pp. 16182–16187. DOI: [10.1073/pnas.1105098108](https://doi.org/10.1073/pnas.1105098108). eprint: <http://www.pnas.org/content/108/39/16182.full.pdf>. URL: <http://www.pnas.org/content/108/39/16182.abstract> (cit. on p. 29).
- [Vov+17] Jamie Vovrosh et al. “Parametric feedback cooling of levitated optomechanics in a parabolic mirror trap”. In: *J. Opt. Soc. Am. B* 34.7 (2017), pp. 1421–1428. DOI: [10.1364/JOSAB.34.001421](https://doi.org/10.1364/JOSAB.34.001421). URL: <http://josab.osa.org/abstract.cfm?URI=josab-34-7-1421> (cit. on p. 23).
- [Wan+97] M. D. Wang et al. “Stretching DNA with optical tweezers.” In: *Biophys J* 72.3 (1997), pp. 1335–1346. ISSN: 0006-3495. URL: <http://www.ncbi.nlm.nih.gov/pmc/articles/PMC1184516/> (cit. on p. 23).
- [Wil+15] D. J. Wilson et al. “Measurement-based control of a mechanical oscillator at its thermal decoherence rate”. In: *Nature* 524 (2015), p. 325. URL: <http://dx.doi.org/10.1038/nature14672> (cit. on pp. 16, 17, 21, 28, 64, 69).

### 3.6 SUPPLEMENTARY INFORMATION

This document provides supplementary information to “Near-field coupling of a levitated nanoparticle to a photonic crystal cavity”, <https://doi.org/10.1364/OPTICA.5.001597>.

#### 3.6.1 Cavity and fiber fabrication

Photonic crystal nanobeam patterns are exposed into a resist layer, on samples consisting of 350 nm films of LPCVD silicon nitride (SiN) deposited on Si substrates, using electron-beam lithography. We use a  $\text{CHF}_3/\text{O}_2$  directional plasma etch to transfer arrays of nanobeam structures into the SiN film. The surface is thoroughly cleaned using a (4:1) piranha solution and the chip then dipped into diluted hydrofluoric acid (HF) to remove oxidation from the exposed silicon surfaces. The SiN devices are released from the substrate using a  $\text{SF}_6$  plasma release. This method allows us to produce very clean and smooth surfaces with high yield. The nanobeams are designed to taper down into a thin bridge connecting it to the substrate (left side in Fig. 7(a) and (b)). This allows us to break the nanobeams off the substrate using a tapered fiber. These fibers are made by cleaving and stripping Corning SMF28 optical fibers and pulling them from a container of HF solution at a speed of  $0.2 \mu\text{m/s}$  for 70 minutes using computer controlled motors. A small amount of o-xylene is used as a thin protective layer on the surface of the HF in order to prevent HF vapor from etching (and roughening) other parts of the fiber as it is pulled from the beaker [Bur+17].

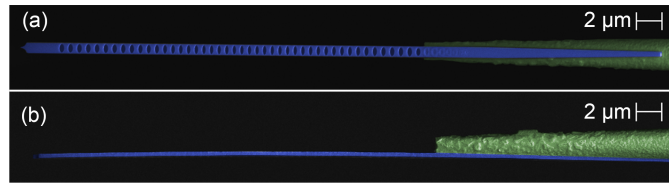


**Figure 7:** Scanning electron microscope (SEM) images of a device. Shown are top (a) and side (b) views of the photonic crystal cavity (blue) and the tapered fiber (green) assembly used in the experiments presented in the main text. The roughness of the tapered fiber is mitigated by UV glue coating, which improves the contact to the cavity and a stronger van der Waals adhesion.

#### 3.6.2 Transfer of the photonic crystal cavity to the tapered fiber

We image the tapered fiber clamped to its holder using an optical 50x microscope objective with a long working distance. The chip with arrays of the photonic crystal cavities is placed on a translational stage below the fiber. By controlling the chip position we can now move the fiber tip into contact with the tapered end of the photonic crystal cavity. Once a cavity with good resonance, coupling and optical  $Q$  is found, we break it off the chip by forcing the fiber against it. In most cases, the cavity remains on the fiber due to attractive van der Waals force. The violent cavity lift-off step, however, causes a displacement of the cavity on the fiber such that the light coupling efficiency between the two is reduced. Readjustment of the alignment is then carried out with the help of a tungsten tip placed perpendicular to the fiber on a separate stage. Although the coupling can be partially restored, we found that the full recovery of the coupling efficiency is extremely challenging due to yet limited control over the overlap length of the two structures after lift-off. This results in a relatively low yield in obtaining high efficiency fiber-cavity assemblies. For this reason, the present work was carried out with a  $\eta_{\text{cav}} = 0.32$ , while no fundamental issue will prevent us from being more selective in choosing assemblies with higher efficiencies.



Due to the HF tapering, the fiber surface is quite rough [Bur+17] and in order to increase the contact surface to the cavity and improve the connection strength, we dip the tapered fiber into UV glue and cure it before picking up the device. This results in a strong bond which does not affect the coupling efficiency and greatly reduces the chances to lose one of the photonic crystal cavities while transferring it into the vacuum chamber.

### 3.6.3 Particle loading

We load the nanoparticles into the tweezer trap at room pressure, keeping the cavity in vacuum in a separate chamber connected to the main chamber through a load lock valve. Once the particle is trapped and the main chamber is evacuated to around 1 mbar, we move the cavity positioner onto its holder in proximity to the trapping objective. Imaging through the trapping objective allows us to precisely control its position. Using a dichroic mirror, we can separate the trapping laser from the green ( $\lambda_{im} = 532$  nm) illumination light which is used to image the particle and the cavity at the same time. In order to obtain a well aligned trapping beam during the experiment, we tilt the last mirror, thereby moving the particle above the center of the objective field of view and center the cavity by controlling its nanopositioner (Fig. 8). Once the cavity is in place, we move the trapped particle in front of the

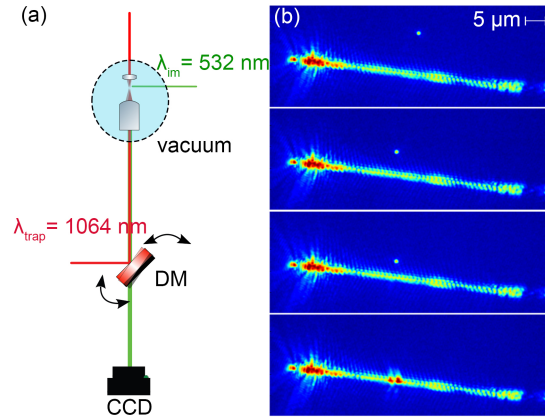


**Figure 8:** Position control of the levitated nanoparticle. (a) Position control of the trapped particle is achieved by tilting of the dichroic mirror (DM) just before the objective. As also shown by Diehl *et al.* [Die+18], the trapping objective is also used to image the particle and photonic crystal cavity by collection of scattered  $\lambda_{im} = 532$  nm light coming from the side. (b) Scattering images of the nanoparticle approaching the photonic crystal cavity as the trapping beam is tilted. When the particle is in front of the cavity, not perfect extinction of the reflected trapping light causes the camera to saturate hiding the particle.

cavity by tilting the mirror back into its original position. The cavity output signal allows us to measure the coupling strength and particle frequency, determining the particle position inside the lattice: if the particle is measured to be in the second or third lobe away from the cavity, we tilt the mirror away again, move the cavity closer into the microscope's focus and repeat the procedure until we observe large optomechanical coupling (Fig. 4 in the main text). After the particle is positioned in the first lobe, we define the lateral positioning in the cavity field, by moving the cavity itself in steps of  $\sim 10$  nm.

### 3.6.4 Detection efficiency and sensitivity

We pump the cavity with 260 nW laser power, and the output field is guided to homodyne detection. The total detection efficiency is  $\eta = \eta_{loss}\eta_q\kappa_{in}/\kappa = 0.09$ , with  $\kappa_{in}/\kappa = 0.5$  the ratio of cavity input to total energy decay rate,  $\eta_{loss} = 0.22$  the

transmission of all other optical components, and  $\eta_q = 0.85$  the detector quantum efficiency at  $\lambda = 1550$  nm. In contrast, for far-field detection, the trapping beam is re-collimated by a secondary objective together with the particle's scattered light and directed to a balanced detector where the common laser noise is cancelled. It is attenuated to typically 1 mW in order to stay in the linear regime of the photodetector. In this case the detection efficiency of the particle scattered light is estimated to be below  $\eta_F \sim 10^{-3}$  [Jai+16].

To compare the sensitivities of both detection schemes, we first acquire the power spectral densities of each methods in the presence (Fig. 9), as well as in the absence of the particle (not shown). The signal-to-noise ratio (SNR) can then be extracted by taking the ratio between integrated powers of these two spectra. SNR can be expressed as  $\sqrt{\text{SNR}} \propto \sqrt{\dot{n}_{\text{det}}}\chi$ , where  $\dot{n}_{\text{det}}$  is the rate of detected photons and  $\chi$  is the single-photon measurement strength. This gives us an estimate of the ratio

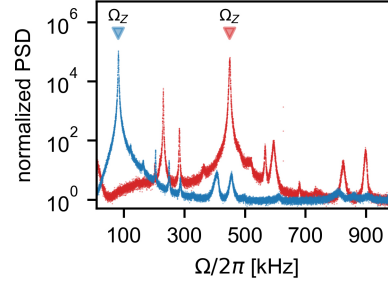


**Figure 9:** Measured power spectral densities of a particle's motion via far-field (blue) and cavity near-field (red) detection. The optical power detected in the far-field case is of about 1 mW, while in the case of cavity detection, the signal reaching the homodyne detection is of less than 60 nW. The significant difference in mechanical frequencies is due to the formation of a standing wave trap in the presence of the cavity device.

of single-photon measurement strengths for the two detection schemes,  $\chi_0/\chi_F \sim 10^2$ , with  $\chi_0$  and  $\chi_F$  the near- and far-field single-photon measurement strengths respectively.

$\chi_0$  can be independently calculated from  $\chi_0 = 2g_0/\kappa = 5.2 \times 10^{-6}$ . We note that it is already very close to the maximally allowed far-field single-photon measurement strength  $\chi_F^{\text{max}} = 4\pi\chi_{\text{ZPF}}/\lambda_{\text{trap}} = 2.0 \times 10^{-5}$  [Van+13]. It also shows that the large  $\chi_0/\chi_F$  ratio in the experiment is a result of the drastic difference between the near- and far-field detection efficiencies.

The detection efficiency can be further improved by reducing optical losses  $\eta_{\text{loss}} = \eta_{\text{cav}}\eta_{\text{path}}$ , where  $\eta_{\text{cav}}$  is the coupling efficiency between the photonic crystal's waveguide and the tapered fiber and  $\eta_{\text{path}}$  is the total transmission efficiency of the rest of the optical path. Currently,  $\eta_{\text{path}}$  includes the loss of many fiber connectors, which can be replaced by almost lossless splices. At the same time, while all measurements were performed with a device with  $\eta_{\text{cav}} = 0.32$ , we successively were able to pick up a device maintaining an efficiency of  $\eta_{\text{cav}} = 0.97$ , similarly to what shown by Burek *et al.* [Bur+17].

### 3.6.5 Calibration of the optomechanical coupling

The calibration of the frequency shift per displacement  $G = d\omega_{\text{cav}}/dx$  was carried out by evaluating the measured power spectral densities  $S_W(\Omega)$  compared to the measured shot-noise level  $S_W^{\text{sn}}$ . Using the known Poissonian statistics governing the photon shot noise, one can estimate the amount of detected photons and their contribution to the noise level. This allows us to calibrate the signal in units of

photons. The position spectral density of the particle is that of a damped harmonic oscillator subject to a stochastic Langevin force

$$S_{xx}(\Omega) = 2 \langle x^2 \rangle \frac{\Gamma \Omega_m^2}{(\Omega_m^2 - \Omega^2)^2 + \Gamma^2 \Omega^2}, \quad (42)$$

where the particle is in thermal equilibrium with its bath  $\langle x^2 \rangle = k_B T / m \Omega_m^2$ . The fluctuations of the cavity resonance are related to the particles position through  $G = d\omega_{\text{cav}}/dx$

$$S_{\omega\omega}(\Omega) = G^2 S_{xx}(\Omega). \quad (43)$$

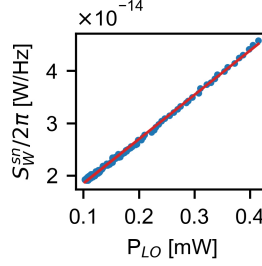


**Figure 10:** Shot-noise power dependence. Linear dependence of the shot-noise level as a function of optical power of the local oscillator.

Considering the optical annihilation operator  $\hat{a}$ , it is convenient to make use of the input-output formalism in order to evaluate the mechanically induced noise [AKM14]. The cavity field then reads

$$\hat{a} = \frac{\sqrt{\kappa_{\text{in}}}\hat{a}_{\text{in}} + \sqrt{\kappa_0}\hat{a}_0}{-i\Delta + \frac{\kappa}{2}}, \quad (44)$$

where  $\kappa_0$  is the intrinsic cavity decay rate,  $\Delta = \omega_L - \omega_{\text{cav}} + \delta\omega$  the detuning between the laser frequency  $\omega_L$  and the cavity resonance  $\omega_{\text{cav}}$ ,  $\delta\omega$  the mechanical induced frequency fluctuations,  $\hat{a}_0$  and  $\hat{a}_{\text{in}}$  the annihilation operators defining the environment vacuum and input field amplitudes respectively. The output field  $\hat{a}_{\text{out}}$  is given by

$$\begin{aligned} \hat{a}_{\text{out}} &= \hat{a}_{\text{in}} - \sqrt{\kappa_{\text{in}}}\hat{a} \\ &= \hat{a}_{\text{in}} - \sqrt{\kappa_{\text{in}}}(\sqrt{\kappa_{\text{in}}}\hat{a}_{\text{in}} + \sqrt{\kappa_0}\hat{a}_0) \left( \frac{\kappa/2}{\Delta^2 + (\frac{\kappa}{2})^2} + i \frac{\Delta}{\Delta^2 + (\frac{\kappa}{2})^2} \right) \\ &\sim -i \frac{2\delta\omega}{\kappa} \hat{a}_{\text{in}} - i \frac{2\delta\omega}{\kappa} \hat{a}_0 - \hat{a}_0, \end{aligned} \quad (45)$$

where the approximation arises when considering a resonant laser drive  $\omega_L = \omega_{\text{cav}}$ , and mechanical resonance fluctuations that are much smaller than the cavity linewidth  $\Delta = \delta\omega \ll \kappa$ . In addition, critical coupling  $\kappa/2 = \kappa_{\text{in}} = \kappa_0$  is also assumed to further reduce the parameter space. Using (45), considering a strong coherent input field  $\hat{a}_{\text{in}} \rightarrow \hat{a}_{\text{in}} + \alpha_{\text{in}}$  with  $\alpha_{\text{in}}$  real valued, the commutation relation  $[\hat{a}(t), \hat{a}^\dagger(t+\tau)] = \delta(\tau)$ , and defining the phase quadrature operator as  $\hat{Y} = \hat{a}_{\text{out}} - \hat{a}_{\text{out}}^\dagger/(\sqrt{2}i)$ , the phase quadrature spectral density can be computed:

$$\begin{aligned} S_{YY}(\Omega) &= \int_{-\infty}^{+\infty} d\tau e^{i\Omega\tau} \langle \hat{Y}(t+\tau) \hat{Y}(t) \rangle \\ &\sim 2 \frac{4\bar{\alpha}_{\text{in}}^2}{\kappa^2} \int_{-\infty}^{+\infty} d\tau e^{i\Omega\tau} \langle \delta\omega(t+\tau) \delta\omega(t) \rangle + \frac{1}{2} \int_{-\infty}^{+\infty} d\tau e^{i\Omega\tau} \delta(\tau) \\ &= 2 \frac{4\bar{\alpha}_{\text{in}}^2}{\kappa^2} S_{\omega\omega}(\Omega) + \frac{1}{2} = 2\bar{\alpha}_{\text{in}}^2 S_{\varphi\varphi}(\Omega) + \frac{1}{2}. \end{aligned} \quad (46)$$

The output signal is then attenuated by optical losses  $\eta_{\text{loss}}$ , and amplified by a strong local oscillator of amplitude  $\beta_0$  in a homodyne detection scheme. In addition, we consider the non unity quantum efficiency of the detectors yet as another attenuation channel  $\eta_q$ , affecting the expectation values of the field operator products ( $\alpha_{\text{in}} \rightarrow \sqrt{\eta_{\text{loss}}}\sqrt{\eta_q}\alpha_{\text{in}}$ ,  $\beta_0 \rightarrow \sqrt{\eta_q}\beta_0$ ) [Pau88]. At each detector the optical power spectral density is

$$S_{\text{PP}}(\Omega) = 4\eta_{\text{loss}}\eta_q^2\hbar^2\nu^2\bar{\alpha}_{\text{in}}^2\beta_0^2S_{\varphi\varphi}(\Omega) + S_{\text{PP}}^{\text{sn}}, \quad (47)$$

where  $S_{\text{PP}}^{\text{sn}} = \hbar^2\nu^2\eta_q\beta_0^2$  is the two-sided photon shot-noise level. When a photon is detected, it is converted into an electron current:  $i(t) = n(t)e$ , where  $n(t)$  is the number of detected photons and  $e$  the electron charge. Non unity of the quantum efficiency of detectors has been already considered in (47) as an effective optical loss [Pau88]. Photo-currents from each detector are subtracted and the DC component as well as classical laser noise are cancelled. The current can then be amplified and converted into a voltage signal via the transimpedance amplifier  $v(t) = g_t i_{\text{AC}}(t)$ . It is now convenient to define the lossless optical power to voltage conversion factor as

$$G_{\text{RF}} = \frac{g_t e}{\hbar\nu}. \quad (48)$$

Finally, the measured two-sided power spectral density reads:

$$S_W(\Omega) = \frac{G_{\text{RF}}^2}{R_L} 4S_{\text{PP}}(\Omega) = \frac{G_{\text{RF}}^2}{R_L} 4\eta_q^2\eta_{\text{loss}}P_{\text{in}}P_{\text{LO}} \frac{4G^2}{\kappa^2} S_{xx}(\Omega) + S_W^{\text{sn}}, \quad (49)$$

where  $P_{\text{in}} = \hbar^2\nu^2\bar{\alpha}_{\text{in}}^2$  ( $P_{\text{LO}} = \hbar^2\nu^2\beta_0^2$ ) is the cavity input (local oscillator) power,  $R_L$  is the input impedance of the measuring instrument, and  $S_W^{\text{sn}} = G_{\text{RF}}^2\eta_qP_{\text{LO}}\hbar\nu/R_L$  is the two-sided shot-noise level in the unit of  $\text{W/Hz}$ . The conversion factor  $G_{\text{RF}}$  can now be written in terms of measured quantities:

$$G_{\text{RF}} = \sqrt{\frac{S_W^{\text{sn}}R_L}{\eta_qP_{\text{LO}}\hbar\nu}}. \quad (50)$$

Substituting (50) into (49), we obtain

$$S_W(\Omega) = \frac{S_W^{\text{sn}}\eta_q}{\hbar\nu} 4\eta_{\text{loss}}P_{\text{in}} \frac{4G^2}{\kappa^2} S_{xx}(\Omega) + S_W^{\text{sn}}. \quad (51)$$

The optomechanical coupling can now be derived by integrating the power spectral density

$$G = \sqrt{\frac{\int_{-\infty}^{+\infty} S_W(\Omega) \frac{d\Omega}{2\pi} \frac{\kappa^2\hbar\nu}{\frac{k_B T}{m\Omega_m^2}}}{S_W^{\text{sn}} 8\eta_{\text{loss}}\eta_qP_{\text{in}}}}. \quad (52)$$

In (52) the negative contribution arising from the shot-noise is neglected as it is orders of magnitude lower due to the large optomechanical coupling rate.

### 3.6.6 Cavity heating

The cavity resonance strongly depends on heating, arising both from the optical field of the tweezer and the cavity pump field. Heating effects are particularly evident in vacuum, where heat dissipation is less efficient. The heating from the tweezer field results in a static frequency shift of the cavity, where the amount of the shift varies depending on the position of the cavity relative to the tweezer beam. We therefore scan the wavelength of the cavity pump laser at each position of the cavity (Fig. 11(a)) and set the laser on resonance, which is the optimal condition

for homodyne readout of the motion. Heating arising from the cavity pump field strongly depends on the wavelength of the pump laser which defines the intra-cavity photon population, leading to a thermo-optic instability. These effects are visible when scanning the pump wavelength: the expected Lorentzian response in the reflected signal shows an asymmetry due to dynamic heating effects when the power is too high (Fig. 11(b)). We run the experiments with  $P_{\text{in}} \sim 260$  nW ( $n_{\text{cav}} \sim 800$ ), far below the input powers where a sizable deviation from the Lorentzian line shape can be observed.

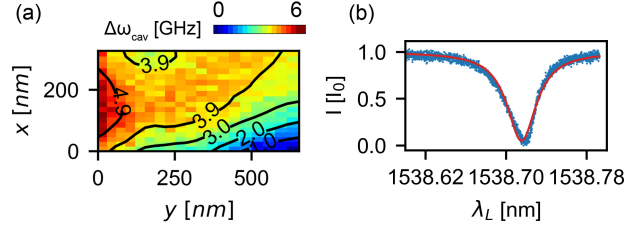


**Figure 11:** Static and dynamic cavity heating. (a) Cavity heating induced by the tweezer field at different positions: the resonance is shifted by up to 5 GHz, while the shape and the width of the cavity response function remain unaffected. This map was taken during the scan in Fig. 2(b) in the main text. (b) Cavity heating induced by the intra-cavity field causes an asymmetry in the cavity response function. Above a certain threshold, the pump will cause dynamic instability of the cavity.

### 3.6.7 Trapping distance simulation

As shown in Thompson *et al.* [Tho+13], the lattice formation, particularly the trapping locations with respect to the photonic crystal's surface are defined by the thickness of the slab  $L$ :

$$z_i = -\frac{\phi}{4\pi}\lambda_{\text{trap}} + i\frac{\lambda_{\text{trap}}}{2}, \quad i = 0, 1, 2, \dots \quad (53)$$

with

$$\phi = \tan^{-1} \left( \frac{2n \cos(nkL)}{(1+n^2) \sin(nkL)} \right), \quad (54)$$

where  $k = 2\pi/\lambda_{\text{trap}}$  is the optical wavevector and  $n$  the refractive index in silicon nitride. The measured thickness of our photonic crystal cavity is 310 nm, corre-

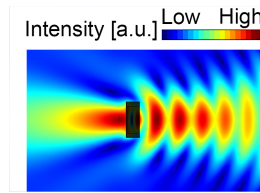


**Figure 12:** Optical lattice. FEM simulation of the trap formation from the reflection of the tweezer light focused from the left on to the photonic crystal cavity (dark shaded area).

sponding to  $z_0 \sim 380$  nm. With a particle size of  $r \sim 70$  nm, the surface-to-surface distance is  $d_0 = z_0 - r \sim 310$  nm. Fig. 13 shows how, by reducing the cavity thickness to about 200 nm, the trapping position can be reduced to  $z_0 \sim 220$  nm, corresponding to a surface-to-surface distance of  $d_0 \sim 150$  nm.

### 3.6.8 Cavity field simulation

The design of the photonic crystal cavity is based on finite element method (FEM) simulation. This also allows us to predict the amount of evanescent field and optimize the optomechanical coupling. For a qualitative understanding, we use a

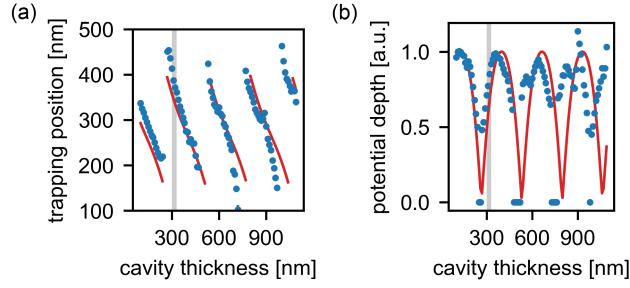


**Figure 13:** Trap position simulation. (a) FEM simulation of the trapping position  $z_0$  as a function of the cavity thickness. (b) Potential depth simulation as a function of the cavity thickness. Red solid lines show the theoretical expected value considering a plane incident wave. Gray shaded areas indicate our experimental conditions: thickness of 310nm, measured by SEM imaging.

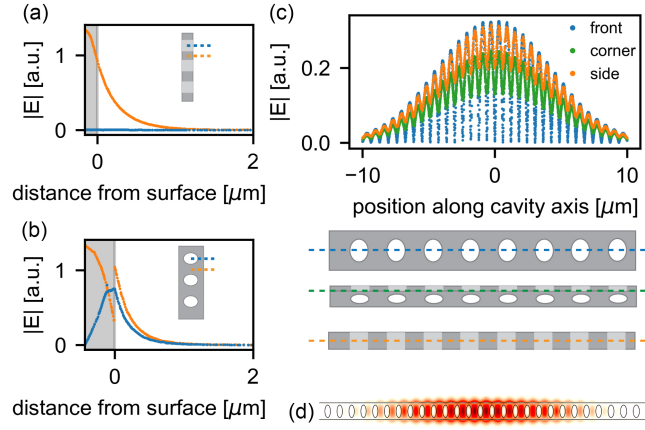


**Figure 14:** FEM simulation of the cavity field. (a) Depicted is the cavity field as a function of a distance from the cavity surface moving away from its wide side, in correspondence of a hole (blue) or of the matter region (orange). The shaded area indicates the cavity extension. (b) Cavity field simulation as a function of distance from its narrow side in correspondence of a hole (blue) or matter (orange). (c) Simulation of the evanescent cavity field evaluated at 250 nm distance from the surface, and in front of the cavity (blue), at a corner (green) and at the side of the cavity (orange). Whenever one moves away from the cavity axis, the contrast of the oscillation is reduced and the field never vanishes. (d) Heat map of the simulated cavity field intensity.

simple model of the cavity field as described in the following equation:

$$E^*E = E_0^2 e^{-\frac{y^2}{2\sigma_y^2}} e^{-\frac{x^2}{2\sigma_x^2}} e^{-\beta\sqrt{x^2+z^2}} \sin^2\left(\frac{2\pi}{\lambda}y\right). \quad (55)$$

This model considers a standing wave with an intensity oscillation period of  $\lambda/2$ , Gaussian mode confinement in all directions (parameterized by  $\sigma_x$  and  $\sigma_y$ ) inside the material and exponential evanescent field decay (parameterized by  $\beta$ ) outside. We note that it does not account for the details of the photonic structure, only the dominant mode shape. Polarization and surface scattering are not considered as well. Close to the cavity axis ( $y$  axis), our model agrees well with the simulation (blue line in Fig. 14(c)). However, as one moves away from the center of the cavity, surface effects give rise to a more complex  $x$  dependence, reducing the contrast of the field oscillations as shown in FEM simulation (Fig. 14). Nevertheless, one can derive single-photon optomechanical couplings for all three spatial mechanical modes from the model:

$$g_0^z(y) \propto |\partial_z E^*E| \propto \left| 1 - \cos\left(2\frac{2\pi}{\lambda}y\right) \right|, \quad (56)$$

$$g_0^y(y) \propto |\partial_y E^* E| \propto \left| \sin \left( 2 \frac{2\pi}{\lambda} y \right) \right|, \quad (57)$$

$$g_0^x(y) \propto |\partial_x E^* E| \propto \left| 1 - \cos \left( 2 \frac{2\pi}{\lambda} y \right) \right|. \quad (58)$$

The deduced equations show qualitative agreements to the measurements shown in Fig. 2(b) in the main text. For instance, (57) correctly predicts the shape of the modulation presented in the measured  $g_0^y(y)$ . (56) and (58) also capture the overall sinusoidal modulations in the measured data although they fail to predict the existence of non-zero offsets. These non-vanishing couplings are due to the fact that the particle is placed off from the cavity axis, which already led to the deviation of the model from the simulation in Fig. 14(c).

### 3.6.9 Optomechanical coupling simulation

A study of the expected coupling was carried out by FEM simulation in a static fashion. The expected cavity resonances were evaluated by placing a 75 nm radius nanoparticle at a given distance from the cavity surface. Simulations have been run at different distances both on the side and in front of the cavity. The result is fitted to an exponential decay of the cavity field. Assuming small particle displacements, the optomechanical coupling can be estimated in the linearized case:

$$G = \frac{\partial \omega_{\text{cav}}}{\partial z} \Big|_{z=d} + \mathcal{O}(\delta \omega_{\text{cav}}^2). \quad (59)$$

At a distance of  $d = z_0 - r \sim 310$  nm, expected optomechanical couplings are 11 MHz/nm and 7 MHz/nm respectively for the case of the particle in front and on the side of the cavity (Fig. 15). The measured value (3.6 MHz/nm; see Fig. 2(b) in the main text) are lower than the simulation result, and can be explained by the fact that measurements were made slightly off the cavity axis as discussed previously.

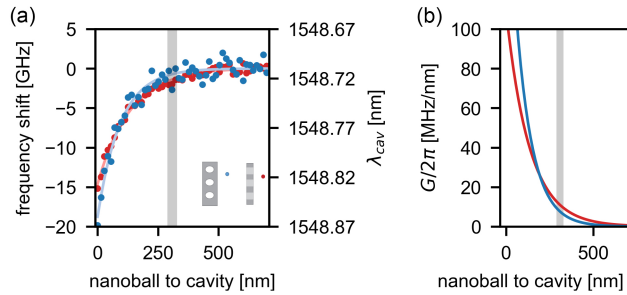


**Figure 15:** Optomechanical frequency shift simulation. (a) FEM simulation of the cavity frequency shift as a function of the particle surface to cavity surface distance. The plot shows simulation results for the case of the particle in front (red) and on the side (blue) of the cavity. A gray shaded area indicates our experimental conditions: trapping at  $z_0 \sim 380$  nm results in surface-to-surface distance of  $d_0 \sim 310$  nm. An exponential decay follows the evanescent field amplitude. (b) An estimated frequency shift per displacement as a function of  $d$ .



The international journal of science / 15 July 2021

**outlook**  
Autoimmune  
disease

# nature

## QUANTUM MOTION

Precise measurement of trapped nanosphere  
enables cooling to ground state

### **Coronavirus**

Genetic association  
studies reveal links  
to COVID risk

### **Climate imbalance**

Deforestation turns  
part of Amazonia from  
carbon sink to source

### **Internal exam**

Probing microbial  
metabolism in the  
microbiome of the gut

Vol. 595, No. 7867  
£10.00 nature.com





## 4

REAL-TIME OPTIMAL QUANTUM CONTROL  
OF MECHANICAL MOTION AT ROOM  
TEMPERATURE

A quantum measurement is a very particular operation. As discussed in chapter 2 this can be represented (in the general case) by a two-step process: a deterministic interaction of the object with a quantum meter followed by a probabilistic projective measurement of the meter. A sequence of measurements of this type leads to the definition of a quantum trajectory of the state of the quantum object that is now driven by the stochastic quantum properties of the probe. In this chapter I report on my work on real-time control of the quantum trajectory of a levitated particle at room temperature. The work was published as reference [Mag+21] and is here preceded by a brief introduction of the scientific context.

The requirements for a quantum limited measurement are a high detection efficiency and a strong measurement cooperativity. In the previous chapter high detection efficiency was achieved by coupling to a photonic crystal cavity. However thermal and mechanical instabilities had set us back on the second requirement, demanding further technological development in the design of stable photonic structures. In this work we took a different approach to the measurement of a levitated particle by going back to the fundamentals of microscopy. Far-field measurements of levitated particles typically rely on the collection of light after the trap [Gie+12; Gie+14; Jai+16]. This technique is particularly convenient as the “forward scattered light” by the particle is naturally overlapped with unperturbed tweezer light, which acts as a phase-stable reference oscillator that provides a linear measurement of the particle position. Despite its robustness, this method presents two fundamental limits. First because the motion of the particle along the beam propagation is strongly coupled to the light that is scattered backwards [TFN19; SR20], making forward detection an intrinsically inefficient measurement. Second because the poor mode overlap between the forward scattered light and the tweezer light results in a low interferometric visibility. In other words, the detector is almost completely saturated by light that had not interacted with the particle and therefore only contributes to an increased of the noise. In microscopy this is a well-known problem, associated with its simplest technique: bright-field microscopy. For this reason more sophisticated designs have been developed over the past century (and a half), mostly driven by biological applications. Prominent examples are the dark-field and phase-contrast microscopes, which allow to suppress and amplify light scattered by the sample by using spatially structured optical modes. In this work we implement a confocal microscope which was patented by Minsky at MIT for the improvement of signal to noise in neural tissue imaging [Min61]. This technique is particularly suited for the experiment presented here: first, because it works in reflection, meaning that the strongly interacting light can be efficiently detected; second, the overlap with the local oscillator can be optimized, thereby maximizing visibility and reducing the background contribution; finally, confocal spatial filtering allows strong suppression of stray light at the detector. The resulting total detection efficiency of  $\eta_d = 0.35$  allows for a measurement of the position of the particle that is less than a factor 2 away from the Heisenberg limit.

We also reconstruct and control in real time the conditional quantum state of the levitated particle: its quantum trajectory. We apply the concepts of quantum filtering [Bel95; BVJo7] introduced in chapter 1 to our specific experimental conditions by implementing a Kalman filter [Kal60] and an optimal controller [Kal+60].

Optimal estimation and control algorithms, originally developed for trajectory estimation and navigation of aerospace technology during the Cold War and first used during the Apollo mission to the Moon [GA10], have become ubiquitous in modern technology [ÅW13]. In the quantum domain, feedback control has been used for the stabilization of optical [Say+11] and microwave [Vij+12] photonic states, cold atoms [GSMo4] and mechanical oscillators [Ros+18], while Kalman (quantum-)filtering had only been demonstrated to track and stabilize the phase of a squeezed optical field [Yon+12]. Here we apply optimal quantum filtering and control to the motion of a solid state object at room temperature. Combined with measurements of the system close to the Heisenberg limit allows us to reconstruct the state of the particle in real time with an uncertainty of 1.3 times its zero point fluctuations. The employment of Kalman filtering and optimal control algorithms in quantum systems represents a crucial step in the development of modern quantum technologies and quantum limited sensors. It also brings the quantum theory of measurement and its experimental implementation closer together, hopefully encouraging and easing future dialogue between quantum physicists and control engineers.

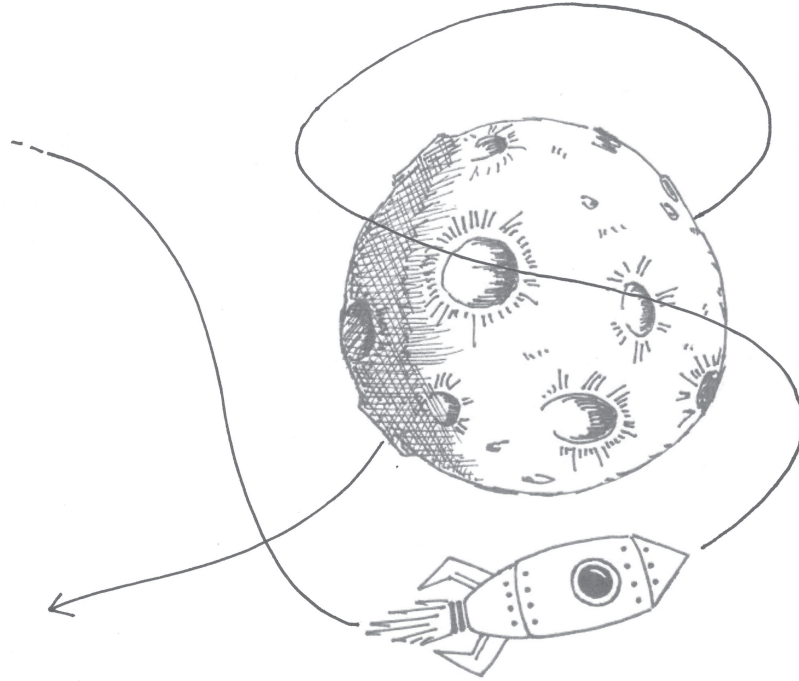


Figure 16: Ink on paper by Costanza Loricchio.

# REAL-TIME OPTIMAL QUANTUM CONTROL OF MECHANICAL MOTION AT ROOM TEMPERATURE

Lorenzo Magrini<sup>1,\*</sup>, Philipp Rosenzweig<sup>2</sup>, Constanze Bach<sup>1</sup>, Andreas Deutschmann-Olek<sup>2</sup>, Sebastian G. Hofer<sup>1</sup>, Sungkun Hong<sup>3</sup>, Nikolai Kiesel<sup>1</sup>, Andreas Kugi<sup>2,4</sup>, and Markus Aspelmeyer<sup>1,5,†</sup>

<sup>1</sup> Vienna Center for Quantum Science and Technology (VCQ), Faculty of Physics, University of Vienna, A-1090 Vienna, Austria

<sup>2</sup> Automation and Control Institute (ACIN), TU Wien, 1040 Vienna, Austria

<sup>3</sup> Institute for Functional Matter and Quantum Technologies (FMQ) and Center for Integrated Quantum Science and Technology (IQST), University of Stuttgart, 70569 Stuttgart, Germany

<sup>4</sup> Austrian Institute of Technology (AIT), Center for Vision, Automation & Control 1040, Vienna, Austria

<sup>5</sup> Institute for Quantum Optics and Quantum Information (IQOQI), Austrian Academy of Sciences, 1090 Vienna, Austria.

\* lorenzo.magrini@univie.ac.at

† markus.aspelmeyer@univie.ac.at

This is the author's accepted version of the work. The definitive version was published in *Nature* "Real-time optimal quantum control of mechanical motion at room temperature", volume 595, issue 7867, pages 373–377 (14 July 2021).

doi: <https://doi.org/10.1038/s41586-021-03602-3>.

## 4.1 ABSTRACT

The ability to accurately control the dynamics of physical systems by measurement and feedback is a pillar of modern engineering [ÅW13]. Today, the increasing demand for applied quantum technologies requires to adapt this level of control to individual quantum systems [Ger+03; Gla+15]. Achieving this in an optimal way is a challenging task that relies on both quantum-limited measurements and specifically tailored algorithms for state estimation and feedback [WM10]. Successful implementations thus far include experiments on the level of optical and atomic systems [Say+11; Yon+12; JM+18]. Here we demonstrate real-time optimal control of the quantum trajectory [Car93] of an optically trapped nanoparticle. We combine confocal position sensing close to the Heisenberg limit with optimal state estimation via Kalman filtering to track the particle motion in phase space in real time with a position uncertainty of 1.3 times the zero point fluctuation. Optimal feedback allows us to stabilize the quantum harmonic oscillator to a mean occupation of  $n = 0.56 \pm 0.02$  quanta, realizing quantum ground state cooling from room temperature. Our work establishes quantum Kalman filtering as a method to achieve quantum control of mechanical motion, with potential implications for sensing on all scales. In combination with levitation, this paves the way to full-scale control over the wavepacket dynamics of solid-state macroscopic quantum objects in linear and nonlinear systems.

## 4.2 INTRODUCTION

The Kalman filter is an iterative real-time state estimation algorithm that combines measurement records with a mathematical description of the system dynamics. At each time step, it provides a state estimate that is conditioned on the knowledge acquired from earlier observations [Kal60]. This *conditional state* can then serve as the basis for feedback control methods that steer the system and stabilize it in a desired target state [Kal+60]. For Gaussian systems, the Kalman filter is optimal in a mean-square-error sense. As many physical systems can be approximated by Gaussian dynamics it is being used in a broad variety of applications ranging from bio-medical signal processing [SC92] over navigation [BSLK04] to mechanical sensing [Rup+16]. In particular for the last case, high-precision experiments employing mechanical sensors are now approaching a regime in which quantum effects of the object itself become relevant [Ros+18; Ros+19]. Any estimation or control approach therefore has to incorporate a full quantum description [WM10]. In analogy with the classical case, the dynamics of an open quantum system undergoing continuous measurement can be generally understood as a non-linear quantum filtering problem, giving rise to the concept of *conditional quantum states*. It was shown by Belavkin [Bel95] that for Gaussian systems the quantum filter reduces to the classical Kalman-filter form. Critically, however, quantum mechanics places restrictions on the underlying physical model, in particular to reflect the intrusive nature of the measurement. The challenge in realizing real-time (optimal) quantum control is then two-fold: First, the measurement process has to be quantum limited, i.e., imprecision and backaction of the measurement must saturate the Heisenberg uncertainty relation. This is achieved only for a high detection efficiency and if the decoherence of the system is dominated by the quantum backaction of the measurement process. Second, quantum filtering has to be implemented in real time and connected to a feedback architecture that allows to stabilize the desired quantum state. For mechanical devices, these requirements have thus far only been realized independently in separate experiments. In a cryogenic environment, ground-state feedback cooling [Ros+18] and offline quantum filtering [Ros+19] were demonstrated for a micromechanical resonator. In a regime driven by thermal forces, Kalman filtering was implemented for classical feedback on a gram-scale mirror [Iwa+13], offline state estimation of micromechanical motion [Wie+15], and real-time state estimation and feedback of nanomechanical systems [Set+18; Lia+19]. In a backaction dominated regime, feedback was used to cool mechanical motion close to the quantum ground state with suspended nanobeams [Sud+17a] and levitated nanoparticles [Teb+20; Kam+21]. As of yet, optimal control at the quantum level has not been achieved. Our work combines all relevant elements in a single experiment, specifically optimal state estimation based on near-Heisenberg limited measurement sensitivity at room temperature with optimal control of the quantum trajectory. Consequently, we can stabilize the unconditional quantum state of a levitated nanoparticle to a position uncertainty of 1.3 times the ground state extension. This contrasts cavity-based cooling schemes for levitated nanoparticles [Win+19; Del+19; RSMQ21] that also achieve ground-state cooling [Del+20a] but without requiring quantum-limited read-out sensitivity. In comparison, real-time optimal control as presented here avoids the overhead of cavity stabilization and can tolerate colored environmental noise by including it directly in the state-space model [Wie+15].

## 4.3 QUANTUM-LIMITED MEASUREMENT

We use an optical tweezer ( $\text{NA} = 0.95$ ,  $\lambda_0 = 1064 \text{ nm}$ , power  $\approx 300 \text{ mW}$ , linearly polarized) to trap a silica nanosphere of  $71.5 \text{ nm}$  radius ( $\approx 2.8 \times 10^{-18} \text{ kg}$ ) in ultra-high vacuum (Figure 17a). The particle oscillates at frequencies of  $\Omega_z/2\pi = 104 \text{ kHz}$ ,

$\Omega_y/2\pi = 236$  kHz and  $\Omega_x/2\pi = 305$  kHz, where we use the trapping beam to define a coordinate system with  $z$  along the beam axis and  $x$  and  $y$  parallel and perpendicular to its polarization, respectively. The motion in the  $x$ - and  $y$ -direction is stabilized by an independent parametric feedback to occupations of about  $10^3$ , allowing us to suppress any effect due to thermal nonlinearities or measurement cross-coupling [GNQ13][SI]. Most trapped particles carry excess charges, which allows us to apply a calibrated force through an external electric field. In our case, we control the  $z$ -motion by a voltage applied to an electrode in front of the grounded tweezer objective [Fri+17]. The position of the particle is encoded in the optical phase of the scattered tweezer light, which is collected and measured by optical homodyning. Note that the position information contained in the scattered light is not uniformly distributed [TFN19; SR20]. For the  $z$ -direction, almost all information is carried by the backscattered photons, which is why we restrict ourselves to backplane detection using a fiber-based confocal microscope [Vam+07]. Here the collected light is spatially filtered by a single-mode fiber, which suppresses contributions from stray light by almost a factor  $10^3$  while maximizing the overlap between the spatial modes of the scattering dipole and the fiber ( $\eta_m = 0.71$ ) [SI]. Our measurement operates close to the quantum limit. In the ideal case, imprecision and backaction noise of the measurement saturate the Heisenberg uncertainty relation  $\sqrt{S_z^I(\Omega)S_F^{ba}(\Omega)} = \hbar$  for all frequencies  $\Omega$  ( $S_{z,F}(\Omega)$ : one-sided noise power spectral densities of position ( $z$ ) and force ( $F$ ) [SI]). Losses degrade this performance: experimental losses in the detection channel ( $\eta_d$ ) increase the imprecision noise to  $S_z^{imp} = S_z^I/\eta_d$ , while additional environmental interactions, for example scattering of gas molecules, increase the total force noise to  $S_F^{tot} = S_F^{ba}/\eta_e$ . This results in  $\sqrt{S_z^{imp}(\Omega)S_F^{tot}(\Omega)} = \hbar/\sqrt{\eta}$ , where  $\eta = \eta_d\eta_e$  amounts to an effective collection efficiency of the overall phase-space information available from the system. In our case, the efficient and low-noise confocal detection scheme results in a displacement sensitivity of  $\sqrt{S_z^{imp}} = 2.0 \times 10^{-14}$  m/ $\sqrt{\text{Hz}}$ , allowing us to resolve displacements of the size of the zero-point motion of the particle ( $z_{zpf} = \sqrt{\hbar/(2m\Omega_z)}$ ) at a rate of  $\Gamma_{\text{meas}} = z_{zpf}^2/2S_z^{imp} = 2\pi \cdot 6.6$  kHz [Cle+10]. By performing re-heating measurements at different background pressures, we can directly determine the decoherence rates of the particle due to backaction,  $\Gamma_{ba} = 2\pi \cdot 18.8$  kHz, and due to residual gas molecules,  $\Gamma_{th} = 2\pi \cdot 0.6$  kHz at the minimal operating pressure of  $9.2 \times 10^{-9}$  mbar, providing us with a quantum cooperativity of  $C_q = \Gamma_{ba}/\Gamma_{th} = 30$  [SI]. The resulting information collection efficiency [Cle+10]  $\eta = \Gamma_{\text{meas}}/(\Gamma_{ba} + \Gamma_{th}) = 0.34$  is consistent with the value obtained from the independently measured loss contributions in the experimental setup [SI]. This yields an imprecision-backaction product of  $\hbar/\sqrt{\eta} = 1.7\hbar$ , which is less than a factor of 2 from its fundamental limit, and more than one order of magnitude better than previously shown for mechanical systems at room temperature [Abb+09; Bus+13; Teb+20; Kam+21]. Note that this also enables measurements close to the standard quantum limit (SQL), where the effects of imprecision and backaction force noise on the displacement spectrum are equal. Figure 17b shows the different noise contributions for a measurement performed at moderate feedback gain, where a sensitivity of 1.76 times the SQL is reached at frequencies of  $\sim 22$  kHz above resonance.

## 4.4 OPTIMAL QUANTUM CONTROL

The idea of optimal feedback is to find a control input that renders the closed-loop system stable and optimizes a pre-defined cost function. In our case, the goal is to minimize the particle's energy. This task can be broken down into two steps: an estimation step to provide an optimal estimate of the system's quantum state in real time, here in the form of a Kalman filter; and a control step that computes the

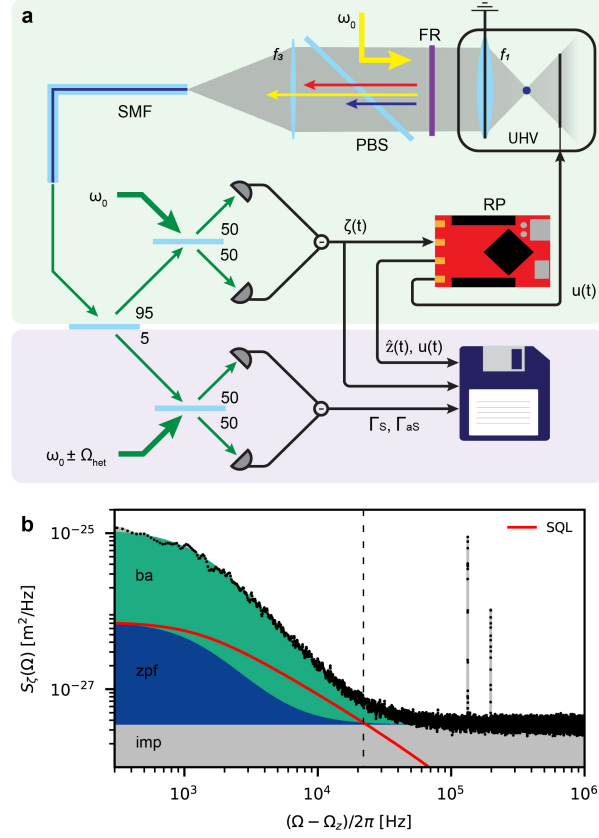


**Figure 17: Experimental setup.** **a**, Scheme of the experimental setup. The particle is trapped in an optical tweezer (laser frequency:  $\omega_0$ ), and oscillates in an ultra-high vacuum (UHV), along the z direction, at a frequency of  $\Omega_z/2\pi = 104$  kHz. The backscattered light is collected by the tweezer objective lens ( $f_1$ ), separated from the tweezer light by the combination of a Faraday rotator (FR) and polarizing beam-splitter (PBS) and spatially filtered by focusing ( $f_3$ ) onto a single mode fiber (SMF) in a confocal arrangement. It is then split into two paths: an in-loop homodyne detection and an out-of-loop heterodyne detection. The homodyne detection is used for the efficient position measurement ( $\zeta(t)$ ), and is directed to the Red-Pitaya (RP) board, where the LQG is implemented in real time. Both the state estimate ( $\hat{z}(t)$ ) and the control signal ( $u(t)$ ) can be recorded. The control signal is applied to the electrode in the vacuum chamber. The heterodyne detection (local oscillator at a frequency of  $\omega_0 \pm \Omega_{\text{het}}$ ) employs only 5% of the light and performs an out-of-loop measurement of the particle's energy via Raman scattering thermometry by measurement of the ratio of the Stokes and anti-Stokes scattering rates ( $\Gamma_s, \Gamma_{as}$ ). **b**, Contributions to the measured position power spectral density by the measurement imprecision (imp), the measurement backaction (ba), and the mechanical quantum fluctuations (zpf) in the homodyne detection, at a control gain of  $g_{fb}/2\pi = 2$  kHz and occupation  $\langle n \rangle = 8.3 \pm 0.09$ . The dashed line indicates the frequency ( $\sim \Omega_z + 2\pi \cdot 22$  kHz) at which imprecision and backaction contribute equally to the total added noise. Here the measured noise is only a factor 1.76 above the SQL (red line).



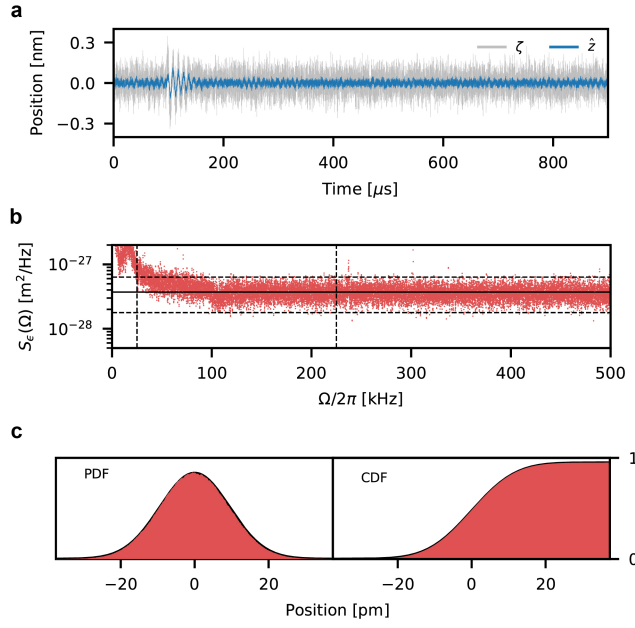


**Figure 18: Kalman filter and verification.** **a**, Time trace of the measurement (gray) and estimation (blue) sequences at  $g_{fb}/2\pi = 16 \text{ kHz}$ ,  $n = 1.68 \pm 0.09$ . At around  $t = 100 \mu\text{s}$ , a (rare,  $\sim 10p_{zpf}$ ) disturbance to the particle is highlighted by the filter. **b**, Power spectral density of the innovation sequence. Horizontal lines indicate the white noise model (solid) and the 95% confidence region of the expected  $\chi^2$  distribution (dashed) [Wie+15]. The low frequency phase noise ( $< 25 \text{ kHz}$ ) and the narrow noise peaks due to residual  $x$  – and  $y$  – modes coupling ( $> 225 \text{ kHz}$ ) are not considered in our noise model. **c**, Experimental probability density function (PDF) and cumulative density function (CDF) of a 10 ms innovation sequence. A 4th order  $f_c = 10 \text{ kHz}$  highpass filter is used to reduce the low frequency contributions that are not considered in our model. The black lines are Gaussian fits to the data.

optimal feedback, here in the form of a linear–quadratic regulator (LQR). Both steps require an adequate mathematical model of the experimental setup, and together form the so-called linear–quadratic–Gaussian (LQG) control problem. To this end, we define a quantum stochastic model that allows us to construct the dynamical equations for the conditional quantum state  $\hat{\rho}$ . We model the levitated particle as a one-dimensional quantum harmonic oscillator coupling to two environments, the electromagnetic field in the vacuum state and the residual gas in a thermal state. Both environments are treated in a Markovian approximation, which means they effectively act as Gaussian white noise sources. By measuring the electromagnetic field we realize a (continuous) measurement of the particle position. As under this model the system state is Gaussian at all times,  $\hat{\rho}$  is fully characterized by the first two moments of the state vector  $\mathbf{z} = [z, p]^T$  ( $z$  and  $p$  being the particle’s position and momentum operators in the  $z$ -direction), given by  $\hat{\mathbf{z}}(t) = \text{tr}(\mathbf{z}\hat{\rho}(t))$  and  $\hat{\Sigma}(t) = \text{Re}[\text{tr}(\mathbf{z}\mathbf{z}^T\hat{\rho}(t))] - \hat{\mathbf{z}}(t)\hat{\mathbf{z}}(t)^T$ . Here we follow the notation where the  $\hat{\cdot}$ -symbol refers to the quantities of the conditional state. The corresponding equations of motion for  $\hat{\mathbf{z}}$  and  $\hat{\Sigma}$  are then equivalent to the classical Kalman–Bucy filter [Bel95; DJ99][SI], which takes the noisy measurement signal  $\zeta(t)$  as an input. The particle’s motion is controlled by a control input  $u(t)$ , which defines the feedback force that is applied to the particle via an external electric field:  $F_{fb} = qE_{fb}(t) = \hbar u(t)/z_{zpf}$  ( $q$ : the charge of the particle,  $E_{fb}(t)$ : the electric field.) In order to find the optimal control input  $u(t) = -\mathbf{k}^T(t)\hat{\mathbf{z}}(t)$  ( $\mathbf{k}^T(t)$  being the feedback vector) that minimizes the particle’s energy, we solve the (deterministic) LQR problem [Kal+60; DJ99][SI]. The solution depends on the control effort, which can be parametrized by the feedback gain  $g_{fb}$ . Adjusting this degree of freedom allows us to shape the closed-loop dynamics and steer the particle into the desired thermal state. The corresponding closed-loop covariance matrix of  $\mathbf{z}$  is given by  $\Sigma(t) = \hat{\Sigma}(t) + \langle \hat{\mathbf{z}}(t)\hat{\mathbf{z}}(t)^T \rangle_{cl}$ , where

$\langle \cdot \rangle_{\text{cl}}$  denotes the expectation value with respect to the classical stochastic process induced by the measurement. In the long term limit ( $t \gg 1/\Gamma_{\text{meas}}$ ), both  $\Sigma(t)$  and  $\hat{\Sigma}(t)$  converge to a steady state, which we denote by  $\Sigma^{\text{ss}}$  and  $\hat{\Sigma}^{\text{ss}}$  respectively. Then  $\hat{\Sigma}^{\text{ss}}$  can be obtained by solving the stationary Riccati equation. Finally, we combine the stationary LQR and Kalman filter into a single time-discrete transfer function that solves the optimal quantum feedback problem in real time. It is implemented as a digital filter with a sampling time of  $T_s = 32 \text{ ns}$  in a Red Pitaya board equipped with a Xilinx Zynq 7010 FPGA. A key element of optimal estimation and control is the accurate mathematical description of the experimental setup including external noise processes, which relies on a careful calibration of the position readout. We calibrate our readout using Raman sideband thermometry from an out-of-loop heterodyne detection, which provides an absolute energy measurement that is compared to the simultaneously recorded homodyne position measurement. To avoid any possible distortion in the closed-loop position detection that may result in noise squashing [Pog+07], we perform the calibration at low feedback gains [SI]. This allows us to quantify all relevant noise processes and to calibrate the feedback force applied via the electrodes [SI]. We ensure the accuracy of the conditional state computed by the Kalman filter by performing a thorough model verification. This is a crucial aspect, in particular because the dynamical equations for  $\hat{\Sigma}$  do not depend on the measurements but only on the model. Verification is done by computing the innovation sequence  $\epsilon(t) = \zeta(t) - \hat{z}(t)$ , which describes the difference between the position predicted by the Kalman filter  $\hat{z}(t)$  and the actual measurement outcome  $\zeta(t)$ . For an optimally working filter,  $\epsilon$  is a Gaussian zero-mean white noise process. We confirm this to be the case for our experiment, (see Figure 18b-c).

## 4.5 RESULTS

The closed-loop dynamics can be influenced by adjusting the feedback gain  $g_{\text{fb}}$ . At each gain setting, we record the measurement sequence  $\zeta(t)$ , the state's conditional expectation value  $\hat{z}(t)$  and the control input  $u(t)$ . Figure 19c shows the quantum trajectory of the particle, which is tracked by the Kalman filter in phase space with the uncertainties in position and momentum given by the diagonal values of the steady-state conditional covariance matrix  $\sigma_z = \sqrt{\hat{\Sigma}_{zz}^{\text{ss}}} = 1.30 z_{\text{zpf}}$ ,  $\sigma_p = \sqrt{\hat{\Sigma}_{pp}^{\text{ss}}} = 1.35 p_{\text{zpf}}$  ( $p_{\text{zpf}} = \sqrt{\hbar m \Omega_z / 2}$ : momentum ground-state uncertainty). To obtain the motional energy of the particle, we evaluate the closed-loop steady-state covariance matrix  $\Sigma^{\text{ss}}$ . For increasing control gain, the mean particle energy  $\langle E \rangle = \hbar \Omega_z (\langle n \rangle + 1/2) = \hbar \Omega_z \text{tr}(\Sigma^{\text{ss}})/2$  ( $n$ : motional quanta) decreases and quantum ground state cooling ( $\langle n \rangle < 1$ ) is achieved for gain levels larger than  $2\pi \cdot 40 \text{ kHz}$  (Figure 18d). The estimated occupation values  $\langle n \rangle$  agree well with the analytic solution of the LQG problem. We independently confirm these results by Raman sideband thermometry in an out-of-loop heterodyne measurement by mixing the backscattered light with a local oscillator field that is detuned from the trapping field by  $\Omega_{\text{het}} = \pm 2\pi \cdot 9.2 \text{ MHz}$  (Figure 17a). This allows us to spectrally resolve the Stokes and anti-Stokes components originating from inelastic scattering off the particle. The scattering rates of these two processes ( $\Gamma_S$ ,  $\Gamma_{\text{aS}}$ ) correspond to the powers detected in the sidebands of the heterodyne measurement. They contain a fundamental asymmetry due to the fact that anti-Stokes scattering, which removes energy from the system, cannot occur from a motional quantum ground state. This is captured by a non-zero difference  $\Gamma_S - \Gamma_{\text{aS}}$  of the scattering rates that is independent of the thermal occupation  $\langle n \rangle$  [SI] (Figure 19b). On the other hand, their ratio  $\Gamma_{\text{aS}}/\Gamma_S = \langle n \rangle / (\langle n \rangle + 1)$  provides us a direct, calibration-free measure of  $\langle n \rangle$  [SN+12]. To exclude other sources of asymmetry that may falsify the measurement, we independently characterize and subtract all (potentially non-white) noise sources (e.g.,



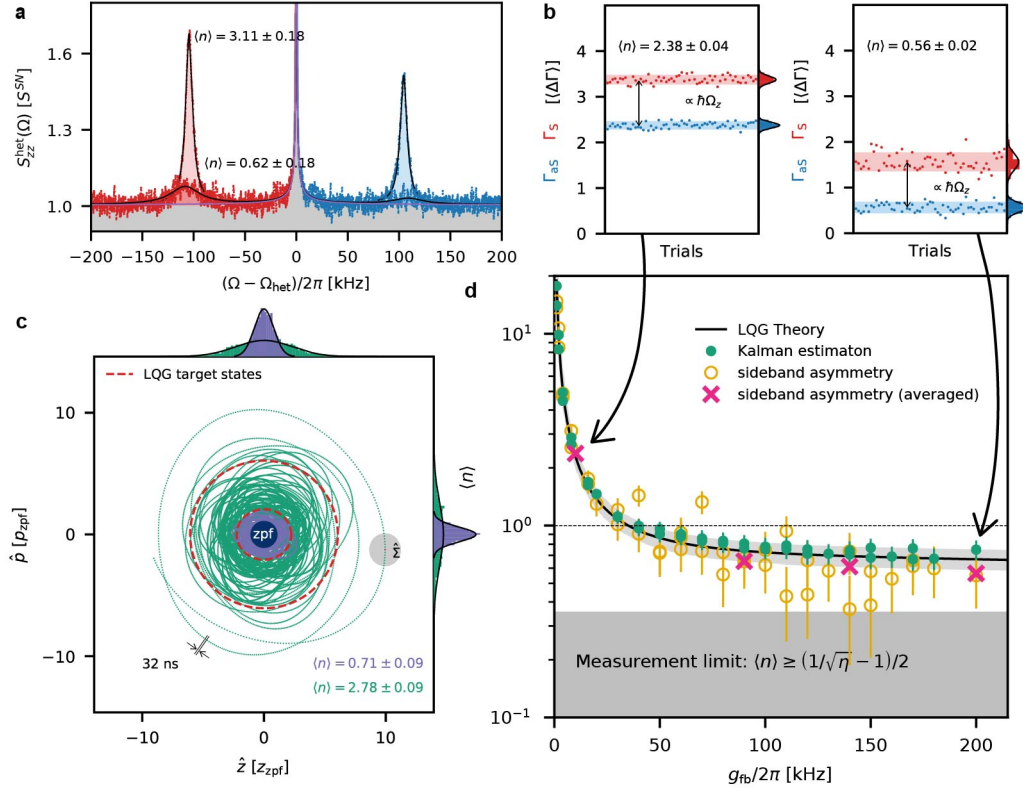


**Figure 19: Quantum optimal control.** **a**, Heterodyne power spectral density at  $g_{\text{fb}}/2\pi = 8$  kHz (large narrow peaks) and  $g_{\text{fb}}/2\pi = 110$  kHz (small broad peaks), where we distinguish the spectral contributions from Stokes (red) and anti-Stokes (blue) scattering. The asymmetry of the peaks is a signature of the quantization of the energy levels of the harmonic oscillator. **b**, Statistical fluctuations of Stokes (red) and anti-Stokes (blue) scattering rates at  $g_{\text{fb}}/2\pi = 10$  kHz and  $g_{\text{fb}}/2\pi = 200$  kHz. Each point is evaluated by integrating a single PSD as shown in **a**, and normalizing by the average value of their difference over all of the measurements ( $\langle \Delta\Gamma \rangle = \langle \Gamma_s - \Gamma_{\text{as}} \rangle$ ). **c**, Phase space plot of the quantum trajectory of the particle at the steady state, for  $g_{\text{fb}}/2\pi = 8$  kHz (green),  $g_{\text{fb}}/2\pi = 110$  kHz (purple) and the corresponding solutions of the LQG closed-loop system (red dashed). Both traces display about 750  $\mu\text{s}$  of evolution. Highlighted is the uncertainty given by the steady-state conditional covariance matrix  $\hat{\Sigma}^{\text{ss}}$  as given by the Kalman filter. For comparison, we show the phase space volume occupied by the zero-point fluctuations in dark blue. Here the data is filtered with a high-order bandpass (25 to 225 kHz), attenuating the contributions of the noise sources at high and low frequencies that are not considered by the model. **d**, Occupation at different feedback gains as estimated by the Kalman filter (green dots) and independently measured by heterodyne asymmetry (yellow circles). The magenta crosses show the four points at which 60 repeated measurements were performed for reduction of statistical fluctuations as in **b**. Error bars represent the standard deviation of the measured value. The solid line is the analytic closed-loop solution of the LQG, showing the expected occupancy given by our experimental parameters and their uncertainties. The gray area shows the cooling limit set by the efficiency of our measurement.

optical phase noise, detector dark noise) and normalize the data to shot noise, thereby taking into account also the frequency-dependent detector response [SI]. For consistency, we perform all measurements at both positive and negative heterodyne frequencies. For each gain setting, both measurements agree within the statistical error (Figure 19b-c [SI]). All data points are also in good agreement with the LQG theory. At maximum gain, we measure a maximal averaged asymmetry of 0.35, corresponding to an occupation of  $\langle n \rangle = 0.56 \pm 0.02$ . This establishes quantum ground state cooling of a nanoparticle from room temperature by real-time optimal quantum control. In the ideal case, the lowest energy can be achieved at infinite feedback gain and is limited by the steady-state conditional covariance to  $\langle n \rangle = 0.34$ . In our experiment, the cooling performance is limited by the computational resources of the Red Pitaya, restricting the trade-off between the complexity of the model, the accuracy of the fixed-point arithmetic and the sampling frequency of the implementation. In practice, this generates a significant risk of numerical overflow when the control output is increased above  $g_{fb} = 2\pi \cdot 200\text{kHz}$ .

## 4.6 DISCUSSION AND OUTLOOK

We have demonstrated real-time optimal quantum control of a levitated nanoparticle. Our experiment combines two features: First, using a near Heisenberg-limited confocal measurement scheme, we realize – at room temperature – the conditions for which the quantum-mechanical properties of the particle can no longer be neglected [BV75]. Second, real-time implementation of both a Kalman filter and a linear quadratic regulator (LQR) provides the required algorithms for optimal state estimation and control. As a result, we achieve feedback cooling to the motional quantum ground state ( $\langle n \rangle = 0.56 \pm 0.02$ ) in a room temperature environment. An immediate application is mechanical sensing of weak stationary [Ran+16; Mon+20a; MG21] or transient [Mon+20b; Car+20; MG21] forces. While neither real-time optimal filtering or feedback cooling improves the signal-to-noise ratio [MG21], our real-time state estimation can discriminate momentum kicks to the particle as small as  $\Delta p = \sqrt{\sigma_p^2 + p_{zpf}^2} = 1.2\sqrt{\hbar m \Omega_z} = 1.6 \times 10^{-23} \text{ kg m/s}$  (29 keV/c), only a factor 1.2 away from the fundamental quantum limit for continuous sensing [Car+20]. This is comparable to the momentum imparted by the inelastic collision with a hydrogen molecule travelling at about 800 m/s, and smaller than the momentum (in a single dimension) of almost 10% of the gas molecules at room temperature. Interestingly, this sensitivity is only a factor of 60 above the latest bounds in the search for gravitationally interacting particle-like candidates for dark matter [Mon+20b]. In other words, extending our method to particle sizes beyond  $1\mu\text{m}$  would enable the search for these exotic particles in new parameter regimes. From a more general perspective, the ability to drive seemingly classical room temperature objects into genuine quantum states of motion simply by measurement and feedback offers unique possibilities to study quantum phenomena in hitherto unexplored macroscopic parameter regimes [Lego2; Che13]. Extending our current scheme to a more complex system dynamics may enable the preparation of genuinely non-classical states including squeezed [Gen+15] or, in combination with non-linear filtering and anharmonic potential landscapes [Ral+18; RF19], even non-Gaussian states of motion.

## ACKNOWLEDGEMENTS

We thank José Manuel Leitão for his introduction to optimal control, and Paolo Vezio, Hans Hepach and Tobias Westphal for discussions and their help in the lab. L. M. thanks Arno Rauschenbeutel for the discussion inspiring the confocal

detection scheme. This project was supported by the European Research Council (ERC CoG QLev4G), by the ERA-NET programme QuantERA, QuaSeRT (Project No. 11299191; via the EC, the Austrian ministries  $\text{mathbf{DW}}$  and  $\text{mathbf{BWF}}$  and research promotion agency FFG), and by the Austrian Science Fund (FWF, Project TheLO, AY0095221, START). L. M. is supported by the Vienna Doctoral School of Physics (VDS-P) and by the FWF under project W1210 (CoQuS).

## AUTHOR CONTRIBUTIONS

L. M. designed and built the experiment, P. R. designed and programmed the filter and controller. L. M. and C. B. performed the measurements. L. M., P. R. and C. B. analyzed the data and all authors contributed to writing and editing of the paper.

## REFERENCES

These are the references cited in the author’s version of the manuscript

- [Abb+09] B. Abbott et al. “Observation of a kilogram-scale oscillator near its quantum ground state”. In: *New Journal of Physics* 11 (2009), pp. 0–13. ISSN: 13672630. DOI: [10.1088/1367-2630/11/7/073032](https://doi.org/10.1088/1367-2630/11/7/073032). URL: <http://iopscience.iop.org/1367-2630/11/7/073032> (cit. on pp. 47, 62).
- [ÅW13] Karl J Åström and Björn Wittenmark. *Computer-controlled systems: theory and design*. Courier Corporation, 2013 (cit. on pp. 44, 45, 76).
- [Bel95] VP Belavkin. “Quantum filtering of Markov signals with white quantum noise”. In: *Quantum communications and measurement*. Springer, 1995, pp. 381–391 (cit. on pp. 12, 43, 46, 49, 76).
- [BSLK04] Yaakov Bar-Shalom, X Rong Li, and Thiagalingam Kirubarajan. *Estimation with applications to tracking and navigation: theory algorithms and software*. John Wiley & Sons, 2004 (cit. on p. 46).
- [Bus+13] P. Bushev et al. “Shot-Noise-Limited Monitoring and Phase Locking of the Motion of a Single Trapped Ion”. In: *Phys. Rev. Lett.* 110 (13 2013), p. 133602. DOI: [10.1103/PhysRevLett.110.133602](https://doi.org/10.1103/PhysRevLett.110.133602). URL: <https://link.aps.org/doi/10.1103/PhysRevLett.110.133602> (cit. on pp. 47, 62).
- [BV75] Vladimir B Braginskii and Yurii I Vorontsov. “Quantum-mechanical limitations in macroscopic experiments and modern experimental technique”. In: *Soviet Physics Uspekhi* 17.5 (1975), pp. 644–650. DOI: [10.1070/pu1975v017n05abeh004362](https://doi.org/10.1070/pu1975v017n05abeh004362). URL: <https://doi.org/10.1070/pu1975v017n05abeh004362> (cit. on pp. 3, 13, 52).
- [Car+20] Daniel Carney et al. “Mechanical quantum sensing in the search for dark matter”. In: *Quantum Science and Technology* (2020). URL: <http://iopscience.iop.org/article/10.1088/2058-9565/abcfd> (cit. on pp. 3, 52, 101).
- [Car93] Howard Carmichael. *An open systems approach to quantum optics: lectures presented at the Université Libre de Bruxelles, October 28 to November 4, 1991*. Vol. 18. Springer Science & Business Media, 1993 (cit. on pp. 3, 11, 45, 76).

- [Che13] Yanbei Chen. “Macroscopic quantum mechanics: theory and experimental concepts of optomechanics”. In: *Journal of Physics B: Atomic, Molecular and Optical Physics* 46.10 (2013), p. 104001. ISSN: 0953-4075. DOI: [10.1088/0953-4075/46/10/104001](https://doi.org/10.1088/0953-4075/46/10/104001). arXiv: [arXiv: 1302.1924v1](https://arxiv.org/abs/1302.1924v1). URL: <http://stacks.iop.org/0953-4075/46/i=10/a=104001?key=crossref.f6fb280b25ca177dd9c80e4daf9cd4e0> (cit. on p. 52).
- [Cle+10] A. A. Clerk et al. “Introduction to quantum noise, measurement, and amplification”. In: *Rev. Mod. Phys.* 82 (2 2010), pp. 1155–1208. DOI: [10.1103/RevModPhys.82.1155](https://doi.org/10.1103/RevModPhys.82.1155). URL: <https://link.aps.org/doi/10.1103/RevModPhys.82.1155> (cit. on pp. 3, 14, 15, 47, 58, 59, 62, 85).
- [Del+19] Uroš Delić et al. “Cavity Cooling of a Levitated Nanosphere by Coherent Scattering”. In: *Phys. Rev. Lett.* 122 (12 2019), p. 123602. DOI: [10.1103/PhysRevLett.122.123602](https://doi.org/10.1103/PhysRevLett.122.123602). URL: <https://link.aps.org/doi/10.1103/PhysRevLett.122.123602> (cit. on p. 46).
- [Del+20a] Uroš Delić et al. “Cooling of a levitated nanoparticle to the motional quantum ground state”. In: *Science* 367.6480 (2020), pp. 892–895. ISSN: 0036-8075. DOI: [10.1126/science.aba3993](https://doi.org/10.1126/science.aba3993). eprint: <https://science.sciencemag.org/content/367/6480/892.full.pdf>. URL: <https://science.sciencemag.org/content/367/6480/892> (cit. on pp. 3, 16, 46).
- [DJ99] A. C. Doherty and K. Jacobs. “Feedback control of quantum systems using continuous state estimation”. In: *Physical Review A - Atomic, Molecular, and Optical Physics* 60.4 (1999), pp. 2700–2711. ISSN: 10941622. DOI: [10.1103/PhysRevA.60.2700](https://doi.org/10.1103/PhysRevA.60.2700). arXiv: [9812004](https://arxiv.org/abs/9812004) (cit. on pp. 49, 76).
- [Fri+17] Martin Frimmer et al. “Controlling the net charge on a nanoparticle optically levitated in vacuum”. In: *Phys. Rev. A* 95 (6 2017), p. 061801. DOI: [10.1103/PhysRevA.95.061801](https://doi.org/10.1103/PhysRevA.95.061801). URL: <https://link.aps.org/doi/10.1103/PhysRevA.95.061801> (cit. on pp. 24, 47, 58).
- [Gen+15] Marco G Genoni et al. “Quantum cooling and squeezing of a levitating nanosphere via time-continuous measurements”. In: *New Journal of Physics* 17.7 (2015), p. 073019. ISSN: 1367-2630. DOI: [10.1088/1367-2630/17/7/073019](https://doi.org/10.1088/1367-2630/17/7/073019). arXiv: [1503.05603](https://arxiv.org/abs/1503.05603). URL: <https://iopscience.iop.org/article/10.1088/1367-2630/17/7/073019> (cit. on p. 52).
- [Ger+03] JM Geremia et al. “Quantum Kalman Filtering and the Heisenberg Limit in Atomic Magnetometry”. In: *Phys. Rev. Lett.* 91 (25 2003), p. 250801. DOI: [10.1103/PhysRevLett.91.250801](https://doi.org/10.1103/PhysRevLett.91.250801). URL: <https://link.aps.org/doi/10.1103/PhysRevLett.91.250801> (cit. on p. 45).
- [Gla+15] Steffen J. Glaser et al. “Training Schrödinger’s cat: quantum optimal control”. In: *The European Physical Journal D* 69.12 (2015), p. 279. ISSN: 1434-6079. DOI: [10.1140/epjd/e2015-60464-1](https://doi.org/10.1140/epjd/e2015-60464-1). URL: <https://doi.org/10.1140/epjd/e2015-60464-1> (cit. on p. 45).
- [GNQ13] Jan Gieseler, Lukas Novotny, and Romain Quidant. “Thermal nonlinearities in a nanomechanical oscillator”. In: *Nature Physics* 9 (2013), p. 806. URL: <http://dx.doi.org/10.1038/nphys2798> (cit. on pp. 21, 47, 70).
- [Iwa+13] Kohjiro Iwasawa et al. “Quantum-Limited Mirror-Motion Estimation”. In: *Phys. Rev. Lett.* 111 (16 2013), p. 163602. DOI: [10.1103/PhysRevLett.111.163602](https://doi.org/10.1103/PhysRevLett.111.163602). URL: <https://link.aps.org/doi/10.1103/PhysRevLett.111.163602> (cit. on p. 46).

- [JM+18] Ricardo Jiménez-Martínez et al. “Signal Tracking Beyond the Time Resolution of an Atomic Sensor by Kalman Filtering”. In: *Phys. Rev. Lett.* 120 (4 2018), p. 040503. DOI: [10.1103/PhysRevLett.120.040503](https://doi.org/10.1103/PhysRevLett.120.040503). URL: <https://link.aps.org/doi/10.1103/PhysRevLett.120.040503> (cit. on p. 45).
- [Kal+60] Rudolf Emil Kalman et al. “Contributions to the theory of optimal control”. In: *Boletín de la Sociedad Matemática Mexicana* 5.2 (1960), pp. 102–119 (cit. on pp. 43, 46, 49, 76).
- [Kal60] Rudolph Emil Kalman. “A new approach to linear filtering and prediction problems”. In: *J. Basic Eng.* 82 (1960), pp. 35–45 (cit. on pp. 43, 46, 76).
- [Kam+21] M. Kamba et al. “Recoil-limited feedback cooling of single nanoparticles near the ground state in an optical lattice”. In: *Phys. Rev. A* 103 (5 2021), p. L051701. DOI: [10.1103/PhysRevA.103.L051701](https://doi.org/10.1103/PhysRevA.103.L051701). URL: <https://link.aps.org/doi/10.1103/PhysRevA.103.L051701> (cit. on pp. 46, 47, 62).
- [Leg02] A J Leggett. “Testing the limits of quantum mechanics: motivation, state of play, prospects”. In: *J. Phys. Condens. Matter* 14 (2002), R415–R451 (cit. on p. 52).
- [Lia+19] J. Liao et al. “FPGA Implementation of a Kalman-Based Motion Estimator for Levitated Nanoparticles”. In: *IEEE Transactions on Instrumentation and Measurement* 68.7 (2019), pp. 2374–2386 (cit. on p. 46).
- [MG21] David C. Moore and Andrew A. Geraci. “Searching for new physics using optically levitated sensors”. In: *Quantum Sci. Technol.* 6 (2021), p. 014008. URL: <https://doi.org/10.1088/2058-9565/abcf8a> (cit. on pp. 3, 52).
- [Mon+20a] Fernando Monteiro et al. “Force and acceleration sensing with optically levitated nanogram masses at microkelvin temperatures”. In: *Phys. Rev. A* 101 (5 2020), p. 053835. DOI: [10.1103/PhysRevA.101.053835](https://doi.org/10.1103/PhysRevA.101.053835). URL: <https://link.aps.org/doi/10.1103/PhysRevA.101.053835> (cit. on p. 52).
- [Mon+20b] Fernando Monteiro et al. “Search for Composite Dark Matter with Optically Levitated Sensors”. In: *Phys. Rev. Lett.* 125 (18 2020), p. 181102. DOI: [10.1103/PhysRevLett.125.181102](https://doi.org/10.1103/PhysRevLett.125.181102). URL: <https://link.aps.org/doi/10.1103/PhysRevLett.125.181102> (cit. on pp. 52, 101).
- [Pog+07] M. Poggio et al. “Feedback Cooling of a Cantilever’s Fundamental Mode below 5 mK”. In: *Phys. Rev. Lett.* 99 (1 2007), p. 017201. DOI: [10.1103/PhysRevLett.99.017201](https://doi.org/10.1103/PhysRevLett.99.017201). URL: <https://link.aps.org/doi/10.1103/PhysRevLett.99.017201> (cit. on pp. 4, 50, 69, 81).
- [Ral+18] Jason F Ralph et al. “Dynamical model selection near the quantum-classical boundary”. In: *Physical Review A* 98.1 (2018), p. 010102. ISSN: 2469-9926. DOI: [10.1103/PhysRevA.98.010102](https://doi.org/10.1103/PhysRevA.98.010102). URL: <https://link.aps.org/doi/10.1103/PhysRevA.98.010102> (cit. on p. 52).
- [Ran+16] Gambhir Ranjit et al. “Zeptonewton force sensing with nanospheres in an optical lattice”. In: *Phys. Rev. A* 93 (5 2016), p. 053801. DOI: [10.1103/PhysRevA.93.053801](https://doi.org/10.1103/PhysRevA.93.053801). URL: <https://link.aps.org/doi/10.1103/PhysRevA.93.053801> (cit. on pp. 23, 29, 52).
- [RF19] Andrey A Rakhubovsky and Radim Filip. “Stroboscopic high-order nonlinearity in quantum optomechanics”. In: *arXiv:1904.00773v1 [physics.optics]* 1 (2019), pp. 1–9. eprint: [arXiv:1904.00773v1](https://arxiv.org/abs/1904.00773v1) (cit. on p. 52).



- [Ros+18] Massimiliano Rossi et al. “Measurement-based quantum control of mechanical motion”. In: *Nature* 563.7729 (2018), pp. 53–58. ISSN: 1476-4687. DOI: [10.1038/s41586-018-0643-8](https://doi.org/10.1038/s41586-018-0643-8). URL: <https://doi.org/10.1038/s41586-018-0643-8> (cit. on pp. 3, 4, 28, 44, 46, 64, 69).
- [Ros+19] Massimiliano Rossi et al. “Observing and Verifying the Quantum Trajectory of a Mechanical Resonator”. In: *Phys. Rev. Lett.* 123 (16 2019), p. 163601. DOI: [10.1103/PhysRevLett.123.163601](https://link.aps.org/doi/10.1103/PhysRevLett.123.163601). URL: <https://link.aps.org/doi/10.1103/PhysRevLett.123.163601> (cit. on p. 46).
- [RSMQ21] Andrés de los Ríos Sommer, Nadine Meyer, and Romain Quidant. “Strong optomechanical coupling at room temperature by coherent scattering”. In: *Nature Communications* 12.1 (2021), p. 276. ISSN: 2041-1723. DOI: [10.1038/s41467-020-20419-2](https://doi.org/10.1038/s41467-020-20419-2). URL: <https://doi.org/10.1038/s41467-020-20419-2> (cit. on p. 46).
- [Rup+16] M. G. Ruppert et al. “A Kalman Filter for Amplitude Estimation in High-Speed Dynamic Mode Atomic Force Microscopy”. In: *IEEE Transactions on Control Systems Technology* 24.1 (2016), pp. 276–284. DOI: [10.1109/TCST.2015.2435654](https://doi.org/10.1109/TCST.2015.2435654) (cit. on p. 46).
- [Say+11] Clément Sayrin et al. “Real-time quantum feedback prepares and stabilizes photon number states”. In: *Nature* 477.7362 (2011), pp. 73–77. ISSN: 1476-4687. DOI: [10.1038/nature10376](https://doi.org/10.1038/nature10376). URL: <https://doi.org/10.1038/nature10376> (cit. on pp. 44, 45).
- [SC92] Dean F. Sittig and Kei-Hoi Cheung. “A parallel implementation of a multi-state Kalman filtering algorithm to detect ECG arrhythmias”. In: *International journal of clinical monitoring and computing* 9.1 (1992), pp. 13–22. ISSN: 0167-9945. DOI: [10.1007/BF01145898](https://doi.org/10.1007/BF01145898). URL: <https://doi.org/10.1007/BF01145898> (cit. on p. 46).
- [Set+18] Ashley Setter et al. “Real-time Kalman filter: Cooling of an optically levitated nanoparticle”. In: *Phys. Rev. A* 97 (3 2018), p. 033822. DOI: [10.1103/PhysRevA.97.033822](https://link.aps.org/doi/10.1103/PhysRevA.97.033822). URL: <https://link.aps.org/doi/10.1103/PhysRevA.97.033822> (cit. on p. 46).
- [SN+12] Amir H. Safavi-Naeini et al. “Observation of Quantum Motion of a Nanomechanical Resonator”. In: *Phys. Rev. Lett.* 108 (3 2012), p. 033602. DOI: [10.1103/PhysRevLett.108.033602](https://link.aps.org/doi/10.1103/PhysRevLett.108.033602). URL: <https://link.aps.org/doi/10.1103/PhysRevLett.108.033602> (cit. on p. 50).
- [SR20] T. Seberston and F. Robicheaux. “Distribution of laser shot-noise energy delivered to a levitated nanoparticle”. In: *Phys. Rev. A* 102 (3 2020), p. 033505. DOI: [10.1103/PhysRevA.102.033505](https://link.aps.org/doi/10.1103/PhysRevA.102.033505). URL: <https://link.aps.org/doi/10.1103/PhysRevA.102.033505> (cit. on pp. 43, 47, 58, 60, 84).
- [Sud+17a] V. Sudhir et al. “Appearance and Disappearance of Quantum Correlations in Measurement-Based Feedback Control of a Mechanical Oscillator”. In: *Phys. Rev. X* 7 (1 2017), p. 011001. DOI: [10.1103/PhysRevX.7.011001](https://link.aps.org/doi/10.1103/PhysRevX.7.011001). URL: <https://link.aps.org/doi/10.1103/PhysRevX.7.011001> (cit. on pp. 15, 46, 64, 87, 89).
- [Teb+20] Felix Tebbenjohanns et al. “Motional Sideband Asymmetry of a Nanoparticle Optically Levitated in Free Space”. In: *Phys. Rev. Lett.* 124 (1 2020), p. 013603. DOI: [10.1103/PhysRevLett.124.013603](https://link.aps.org/doi/10.1103/PhysRevLett.124.013603). URL: <https://link.aps.org/doi/10.1103/PhysRevLett.124.013603> (cit. on pp. 46, 47, 62, 81).

- [TFN19] Felix Tebbenjohanns, Martin Frimmer, and Lukas Novotny. “Optimal position detection of a dipolar scatterer in a focused field”. In: *Phys. Rev. A* 100 (4 2019), p. 043821. DOI: [10.1103/PhysRevA.100.043821](https://doi.org/10.1103/PhysRevA.100.043821). URL: <https://link.aps.org/doi/10.1103/PhysRevA.100.043821> (cit. on pp. [18](#), [43](#), [47](#), [60](#), [61](#)).
- [Vam+07] A. N. Vamivakas et al. “Phase-sensitive detection of dipole radiation in a fiber-based high numerical aperture optical system”. In: *Opt. Lett.* 32.8 (2007), pp. 970–972. DOI: [10.1364/OL.32.000970](https://doi.org/10.1364/OL.32.000970). URL: <http://ol.osa.org/abstract.cfm?URI=ol-32-8-970> (cit. on pp. [47](#), [65](#)).
- [Wie+15] Witlief Wieczorek et al. “Optimal State Estimation for Cavity Optomechanical Systems”. In: *Phys. Rev. Lett.* 114 (22 2015), p. 223601. DOI: [10.1103/PhysRevLett.114.223601](https://doi.org/10.1103/PhysRevLett.114.223601). URL: <https://link.aps.org/doi/10.1103/PhysRevLett.114.223601> (cit. on pp. [46](#), [49](#), [79](#), [80](#)).
- [Win+19] Dominik Windey et al. “Cavity-Based 3D Cooling of a Levitated Nanoparticle via Coherent Scattering”. In: *Phys. Rev. Lett.* 122 (12 2019), p. 123601. DOI: [10.1103/PhysRevLett.122.123601](https://doi.org/10.1103/PhysRevLett.122.123601). URL: <https://link.aps.org/doi/10.1103/PhysRevLett.122.123601> (cit. on p. [46](#)).
- [WM10] Howard M. Wieseman and Gerard J. Milburn. *Quantum measurement and control*. Cambridge: Cambridge University Press, 2010 (cit. on pp. [45](#), [46](#), [75](#)).
- [Yon+12] Hidehiro Yonezawa et al. “Quantum-Enhanced Optical-Phase Tracking”. In: *Science* 337.6101 (2012), pp. 1514–1517. ISSN: 0036-8075. DOI: [10.1126/science.1225258](https://doi.org/10.1126/science.1225258). eprint: <https://science.sciencemag.org/content/337/6101/1514.full.pdf>. URL: <https://science.sciencemag.org/content/337/6101/1514> (cit. on pp. [44](#), [45](#)).

## 4.7 SUPPLEMENTARY INFORMATION

This document provides supplementary information to “Real-time optimal quantum control of mechanical motion at room temperature”, <https://doi.org/10.1038/s41586-021-03602-3>.

### 4.7.1 The complete experimental setup

We include the complete experimental details of the experiment. The core of the experiment is the optical tweezer: a microscope objective of  $\text{NA} = 0.95$  to tightly focusing  $\sim 300 \text{ mW}$  of light at  $\lambda = 1064 \text{ nm}$  ( $\omega_0 = c2\pi/\lambda$ : optical frequency) in ultra-high vacuum. Before reaching the optical trap, part of the light is diverted to a couple of acousto-optic modulators (AOMs) oriented to scatter in positive and negative first order. In order to avoid slow intensity drifts due to interference between the parametric feedback and the optical tweezer, the parametric feedback cooling is implemented with light at optical frequencies of  $\omega_{\text{pfb}} = \omega_0 + 2\pi \cdot 205 \text{ MHz}$  while the light shifted by the second AOM at a frequency of  $\omega_{\text{het}} = \omega_0 \pm 2\pi \cdot 9.2 \text{ MHz}$  is used as local oscillator for the heterodyne measurement. The polarization in the tweezer is controlled by a half and a quarter waveplate (HWP,QWP). This allows us to excite the rotational degree of freedom and its precession about the z-axis in ultra-high vacuum to frequencies above 100 MHz by briefly applying an optical torque to the levitated particle, avoiding disturbance at the frequencies of interest. The back scattered light is selected by a Faraday rotator (FR) and a polarizing beam-splitter (PBS) and routed to the confocal fiber filtering. Here a lens ( $f_3$ ) focuses light into a single-mode fiber (green). A variable ratio coupler (VRC) is used to split the light between homodyne and heterodyne detection. The use of these tunable VRCs, also in the actual interferometric measurement, allows us to balance the splitting ratio with a precision below 0.5%. The slow phase drift of the homodyne signal is stabilized by use of a low-pass filter (LP) and PID controller driving a fiber stretcher constituted of a bare fiber wrapped around a cylindrical piezo. The signal is then directed to the Red-Pitaya (RP) board which calculates the state estimates and a calibrated control signal. The control signal is applied to the holder of a collection lens which serves as electrode and is placed in front of the tweezer objective which is grounded [Fri+17]. The homodyne and heterodyne measurement sequences as well as the state estimates and control signals are recorded simultaneously. After the tweezer, light is collected by a lens and used for 3D forward split-detection (BS: beam splitter). This low quality measurement serves to implement the parametric feedback of all 3 modes: a phase lock loop (PLL) allows to track the phase of each mode and stabilize its motion by modulating the optical spring at twice the mechanical frequency via an electro-optic modulator (EOM) and overlayed with the tweezer light by a PBS. During the experiment, the parametric feedback for the z-mode is switched off. A green laser is shined from the side onto the particle for imaging of the dipole scattering through a dichroic mirror (DM) onto a CCD sensor.

### 4.7.2 Imprecision and backaction noise in an optical tweezer

We describe the effects of quantum noise in a measurement process following the description by Clerk *et al.* [Cle+10] for a flat mirror moving in one dimension. We then extend this to the geometry of an optically levitated particle, along the lines of the analysis showed by Seberon and Robischeaux [SR20]. A full quantum description of the open quantum system in terms of the quantum Langevin equations and input-output formalism will be derived in Section 4.7.5.

When performing a phase measurement of light in a coherent state (displaced vacuum) the phase and photon number uncertainty is governed by Poissonian statistics: these uncertainties are respectively  $\Delta\phi = 1/(2\sqrt{N})$  and  $\Delta N = \sqrt{N}$ , where  $N$  is the



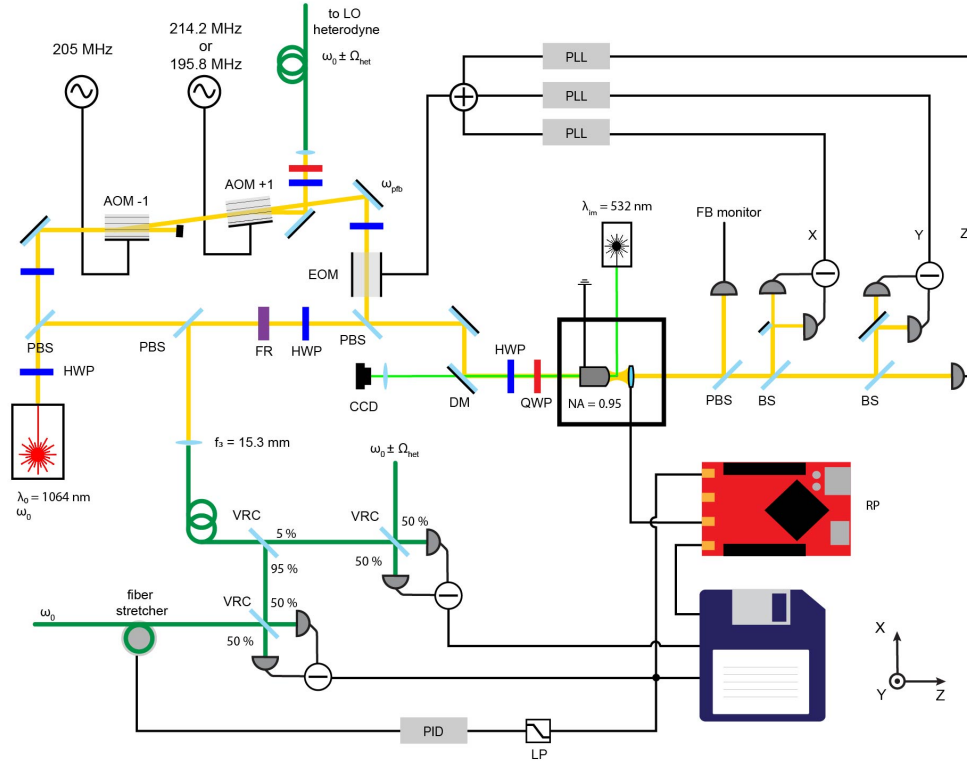


**Figure 20: The experimental setup.** **a**, The complete experimental setup as described in section 4.7.1. **b**, The scattering geometry: we define the scattering angle  $\theta$  as the angle between the  $z$  axis and the scattering direction.

measured number of photons during the time  $t$ . The product of these uncertainties satisfies the relation  $\Delta N \Delta \varphi = 1/2$  [Lou00]. In the context of continuous measurements of stationary processes it is useful to reformulate these quantities in terms of a noise power spectral density. This is defined, for a variable  $X$ , as the Fourier transform of its autocorrelation:

$$S_{XX}(\Omega) = \int_{-\infty}^{+\infty} e^{-i\Omega t} \langle X(0)X(t) \rangle dt \quad (60)$$

Measuring a continuous flux of photons of average  $\bar{N}$ , we can now define  $S_{\varphi\varphi} = (\Delta\varphi)^2/t = 1/(4\bar{N})$  and  $S_{\dot{N}\dot{N}} = (\Delta N)^2/t = \bar{N}$ . Again, we have the uncertainty relation:

$$\sqrt{S_{\varphi\varphi} S_{\dot{N}\dot{N}}} = 1/2 \quad (61)$$

### Measuring the displacement of a flat mirror

As a first example of optical measurement, we study the one dimensional case of a photon bouncing off a mirror, measuring its displacement  $x$ . The phase shift gained by each photon is two times the phase shift acquired in  $x$  distance:  $\varphi = 2kx$ . The momentum transferred to the mirror by elastic scattering is twice the photon momentum  $p = 2\hbar k$ . These lead to spectral density definitions for imprecision of position measurement and random backaction force-noise:  $S_{xx}^I = S_{\varphi\varphi}/(4k^2)$  and  $S_{FF}^{ba} = 4\hbar^2 k^2 S_{\dot{N}\dot{N}}$  [Cle+10]. The uncertainty relation becomes:

$$\sqrt{S_{xx}^I S_{FF}^{ba}} = \hbar/2 \quad (62)$$

### The case of a levitated particle

The case of a levitated particle is qualitatively equivalent. The main difference to consider is that the direction of incoming and scattered photons is not necessarily parallel to the direction of the particle's motion that we are interested in measuring. The total optomechanical interaction is distributed to the different degrees of freedom ( $x, y, z$ ), reducing the average coupling to each mode. We follow the same steps and notation as described by Seberston and Robicheaux [SR20] to derive the imprecision noise and measurement backaction for our system. A photon of initial wave-vector  $\vec{k}_i = k\hat{k}_i = (k_{ix}, k_{iy}, k_{iz}) = k(\hat{k}_{ix}, \hat{k}_{iy}, \hat{k}_{iz})$  scatters elastically off a particle at position  $\vec{r}$ , initial velocity  $\vec{v}_i$  and mass  $m$ . The phase shift acquired by the photon and the final velocity of the particle are given by:

$$\varphi = \vec{k}_i \vec{r} - \vec{k}_f \vec{r} \quad \text{and} \quad \vec{v}_f = \vec{v}_i + \frac{\hbar}{m} (\vec{k}_i - \vec{k}_f), \quad (63)$$

where  $\vec{k}_f$  is the final wave-vector. The squared phase shift resulting from a displacement along the direction  $j = (x, y, z)$  is:

$$\varphi_j^2 = (k_{ij} r_j - k_{fj} r_j)^2 = k^2 r_j^2 (\hat{k}_{ij} - \hat{k}_{fj})^2, \quad (64)$$

and similarly the square momentum exchanged with the particle's mode  $j$  is:

$$p_j^2 = (mv_{fj} - mv_{ij})^2 = \hbar^2 k^2 (\hat{k}_{ij} - \hat{k}_{fj})^2, \quad (65)$$

where we have used the fact that  $\langle v_j \rangle = 0$  for harmonic motion. As the phase and

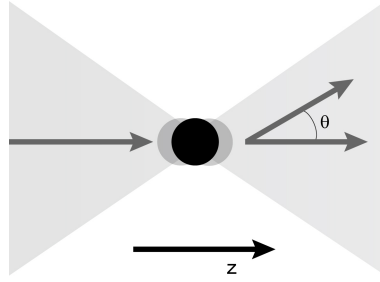


**Figure 21: Scattering angle.** We define the scattering angle  $\theta$  as the angle between the  $z$  axis and the scattering direction.

momentum depend on the incidence and scattering directions, in order to compute second moments of momentum and phase fluctuations we have to consider the scattering probability distribution defined for a dipole emitter. The probability of a photon emitted by a dipole being scattered in direction  $\hat{k}_f$  is [SR20; TFN19]:

$$P(\hat{k}_f) = \frac{3}{8\pi} (\cos^2 \theta \cos^2 \phi + \sin^2 \phi), \quad (66)$$

where the spherical coordinate system is defined such that the scattered photon has the direction  $\hat{k}_f = (\sin \theta \cos \phi, \sin \theta \sin \phi, \cos \theta)$ . Note that  $\int_{4\pi} P(\hat{k}_f) d\Omega = 1$ . For each direction of motion, the square optical phase shift and momentum exchange, averaged over the scattering probability distribution is then given by:

$$\langle \varphi_j^2 \rangle = \int_{4\pi} P(\hat{k}_f) \varphi_j^2 d\Omega \quad \text{and} \quad \langle p_j^2 \rangle = \int_{4\pi} P(\hat{k}_f) p_j^2 d\Omega. \quad (67)$$

We consider the case for  $j = z$ , which is the direction of interest of this paper. The other directions follow trivially and are discussed in [SR20; TFN19]. If considering

an incident plane wave, the incidence and scattering wave vectors are defined as  $\hat{k}_{iz} = 1$  and  $\hat{k}_{fz} = \cos \theta$ , respectively. As we are dealing with a tightly focused beam we have to modify the value of the initial wave vector to be  $\hat{k}_{iz} = A \leq 1$ , where  $A$  is a geometrical factor arising from the Gouy phase shift in the focal field which depends on the trapping NA and can be computed following [TFN19]. In our case  $A = 0.71$ . Inserting (64) and (65) into (67), and projecting on  $z$ ,

$$\langle \varphi_z^2 \rangle = k^2 z^2 \int_{4\pi} P(\hat{k}_f) (A - \cos \theta)^2 d\Omega \quad \text{and} \quad \langle p_z^2 \rangle = \hbar^2 k^2 \int_{4\pi} P(\hat{k}_f) (A - \cos \theta)^2 d\Omega \quad (68)$$

The mean square phase shift and square momentum exchange along  $z$  become:

$$\langle \varphi_z^2 \rangle = \left( A^2 + \frac{2}{5} \right) k^2 z^2 \quad \text{and} \quad \langle p_z^2 \rangle = \left( A^2 + \frac{2}{5} \right) \hbar^2 k^2 \quad (69)$$

As for the one dimensional case we can now express the interaction in terms of spectral densities for position imprecision and force noise, extending the averaging to the time domain:

$$S_{zz}^I = \frac{S_{\varphi\varphi}}{\left( A^2 + \frac{2}{5} \right) k^2} \quad \text{and} \quad S_{FF}^{ba} = \left( A^2 + \frac{2}{5} \right) \hbar^2 k^2 S_{\dot{N}\dot{N}} \quad (70)$$

and in terms of optical scattered power,  $P_{\text{scatt}} = \hbar \omega \bar{N} = \hbar c k \bar{N}$ :

$$S_{zz}^I = \frac{\hbar c}{\left( A^2 + \frac{2}{5} \right) 4k P_{\text{scatt}}} \quad \text{and} \quad S_{FF}^{ba} = \left( A^2 + \frac{2}{5} \right) \frac{\hbar k P_{\text{scatt}}}{c}, \quad (71)$$

which also fulfills the Heisenberg uncertainty relation (62).

As we measure real signals, it is useful to consider the one-sided power spectral density, defined for a real signal  $X$ , at positive frequencies as:

$$S_X(\Omega \geq 0) = (S_{XX}(\Omega) + S_{XX}(-\Omega)) \quad (72)$$

where the variance of the signal  $X$  is:

$$\langle X^2 \rangle = \frac{1}{2\pi} \int_{-\infty}^{+\infty} S_{XX}(\Omega) d\Omega = \frac{1}{2\pi} \int_0^{+\infty} S_X(\Omega) d\Omega \quad (73)$$

which for a real white process simply reduces to  $S_X = 2S_{XX}$ . In terms of single-sided power spectral densities, the uncertainty relation becomes:

$$\sqrt{S_z^I S_F^{ba}} = \hbar \quad (74)$$

In real experiments the backaction-imprecision product is degraded by losses. On the one hand, there are losses of information in the detection channel  $\eta_d$ . They increase the imprecision noise while leaving the backaction force noise unaltered; The detected imprecision noise becomes  $S_z^{\text{imp}} = S_z^I / \eta_d$ . On the other hand, there are losses of information by interactions with the environment  $\eta_e$ . Environmental force noise contributions include scattering of gas molecules, feedback noise, black-body radiation; All having the effect of exchanging momentum with the system, without contributing to the measurement. The total force noise becomes  $S_F^{\text{tot}} = \sum_i S_F^i = S_F^{ba} / \eta_e$  and the imprecision-backaction product can be written as:

$$\sqrt{S_z^{\text{imp}} S_F^{\text{tot}}} = \frac{\hbar}{\sqrt{\eta}} \geq \hbar \quad (75)$$

where  $\eta = \eta_d \eta_e$  considers information losses in the detection and into the environment. In the following sections (4.7.3, 4.7.4), we will analyze losses in the detection channel and discuss additional force noise contributions to the backaction term.

### The standard quantum limit for the harmonic oscillator

The response of a system to external forces is given by its mechanical susceptibility, defined, for a harmonic oscillator, as:  $\chi_m(\Omega) = [m(\Omega_z^2 - \Omega^2 + i\gamma\Omega)]^{-1}$  ( $m$  the mass of the particle,  $\Omega_z$ : the mechanical resonance frequency,  $\gamma$ : the total damping of the system). The relation between imprecision and backaction (equation (74)) defines a minimal added noise to the measured displacement spectrum that is known as the standard quantum limit. This limit is achieved, at a given frequency, when the strength of measurement is such that the contributions of imprecision and response to backaction are equal [Mas+19]:

$$S_z^{\text{SQL}}(\Omega) = \min\{S_z^{\text{I}} + S_F^{\text{ba}}|\chi_m(\Omega)|^2\} = 2\hbar|\chi_m(\Omega)| \quad (76)$$

In a real measurement one has to consider not only losses in the detection and environmental force noise contributions, but also the oscillator's quantum fluctuations of position  $z_{\text{zpf}} = \sqrt{\hbar/(2m\Omega_z)}$ , resulting in a ground state displacement spectrum [Cle+10]:

$$S_z^{\text{zpf}}(\Omega) = z_{\text{zpf}}^2 \frac{\gamma}{(\Omega - \Omega_z)^2 + (\gamma/2)^2}. \quad (77)$$

The particle motional spectrum is:

$$S_z(\Omega) = S_F^{\text{tot}}|\chi_m(\Omega)|^2 + S_z^{\text{zpf}}(\Omega) \quad (78)$$

and the total measured displacement noise then becomes:

$$S_\zeta(\Omega) = S_z^{\text{imp}} + S_F^{\text{tot}}|\chi_m(\Omega)|^2 + S_z^{\text{zpf}}(\Omega) \quad (79)$$

where  $\zeta = z + v$  is the sum of the actual motion of the particle together the position equivalent measurement noise. It is evident that, in the case of weak damping, backaction and quantum fluctuations have a large contribution to the total noise on resonance, and the added noise is much larger than the SQL (Supplementary Figure 22a, 22c). Off resonance however it is possible to find frequencies where the noise is closest to the SQL (Supplementary Figure 22b). Up to a certain degree it is also possible to suppress the backaction contribution on resonance, and redistribute the quantum zero point fluctuation noise contribution to a larger frequency band. This is done by feedback cooling which increases damping and modifies the mechanical susceptibility (Supplementary Figure 22c, 22d and Section 4.7.4). In our system, with an information efficiency of  $\eta = 0.34$ , we distinguish 2 regimes: the weakly cooled regime where we achieve (off resonance) a displacement noise of 1.76 times the SQL, and a strongly cooled regime, where by strongly suppressing backaction we are able to achieve (on resonance) a displacement noise that is 2.7 times the SQL (Supplementary Figure 23). Note that for the resonant case, even at zero temperature the contribution of the zero point fluctuations limits the displacement noise to 2 times the SQL. These results show an improvement of more than one order of magnitude for a mechanical system at room temperature [Abb+09; Bus+13; Sch+16; Teb+20; Kam+21].

### Measurement and decoherence rates

The resolution of a noisy measurement increases with measurement time. A quantum limited measurement however necessarily disturbs the system, limiting the time for which one can measure a quantum state before it is completely destroyed by the measurement itself [CGSo3]. We introduce rates of measurement and decoherence to quantify these processes. We define the measurement rate as the rate at which our measurement is able to resolve a displacement equivalent to the zero point motion of the particle ( $z_{\text{zpf}}$ ):

$$\Gamma_{\text{meas}} = \frac{z_{\text{zpf}}^2}{4S_{zz}^{\text{imp}}} = \frac{z_{\text{zpf}}^2}{2S_z^{\text{imp}}} = \eta_d \frac{z_{\text{zpf}}^2}{2S_z^{\text{I}}} \quad (80)$$

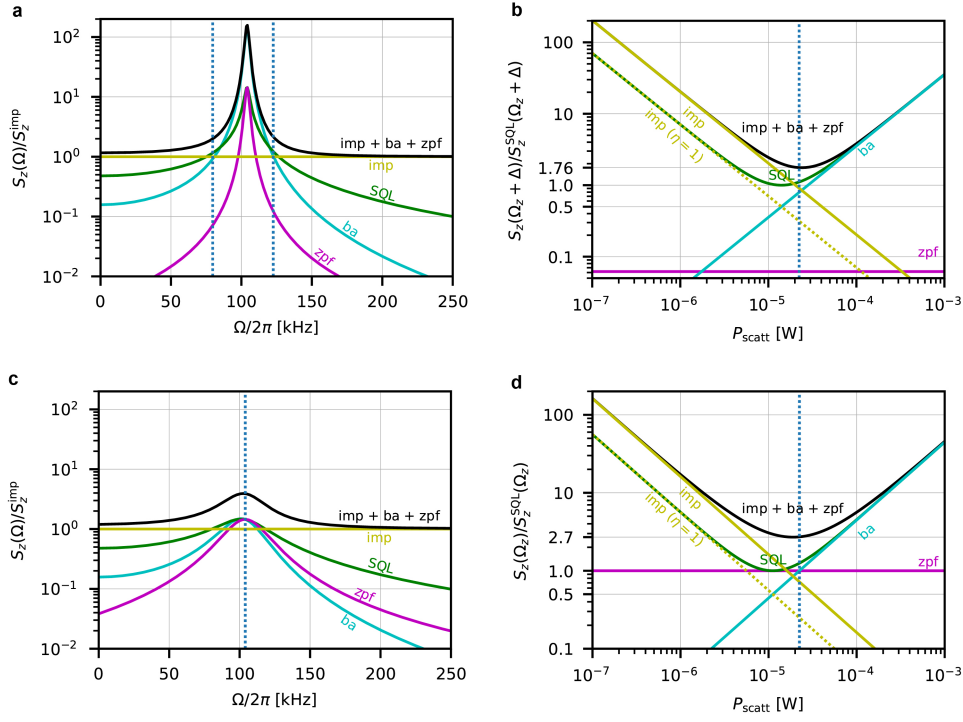


**Figure 22: The standard quantum limit.** **a**, Contribution to the measured power spectral density of imprecision (imp), backaction (ba), and zero point fluctuation (zpf), compared to the SQL as a function of frequency, in a regime of weak cooling ( $\Gamma_{fb} = \Gamma_{ba}/5$ ). **b**, Contribution to the total noise, evaluated at  $\Omega_z \pm \Delta$  (vertical dotted line in **a**), as a function of the scattered power (measurement strength). In the case of weak cooling, the contributions of backaction and zero point fluctuation are concentrated on resonance, allowing perfect balancing of imprecision and backaction when  $\Delta \approx 2\pi \times 22$  kHz, and resulting in a total added noise that is only a factor 1.76 from the SQL. **c**, Contributions to the measured power spectral density in a regime of strong cooling ( $\Gamma_{fb} = 2\Gamma_{ba}$ ). In this case, the contributions of backaction and the zero point fluctuations are broadened in frequency, allowing on resonance (vertical dotted line), a suppression of the added noise to a factor of 2.7 from SQL (in **d** as a function of the scattered power). Note that in the case of optical tweezers, **b** and **d** do not represent a complete set of experimentally available conditions, and are only valid at a fixed scattered power (vertical dotted lines). A variation of this would necessarily come along with a change in the mechanical frequency, and a redefinition of the system parameters. This representation is however useful to understand the operating conditions of the system with respect to the SQL.

Similarly, the decoherence rate, defined as the rate of energy quanta delivered to the oscillator by the measurement process, is

$$\Gamma_{ba} = \frac{S_{FF}^{ba}}{4p_{zpf}^2} = \frac{S_F^{ba}}{8p_{zpf}^2} \quad (81)$$

where  $p_{zpf} = \sqrt{\hbar m \Omega_z / 2}$  momentum ground-state uncertainty. With the help of equation (74), we can compute the ratio of measurement rate and backaction-induced decoherence rate:

$$\frac{\Gamma_{meas}}{\Gamma_{ba}} = \eta_d \leq 1. \quad (82)$$

Decoherence in the system, however, does not only originate from the measurement process, but also from other environmental interactions. We define the rate of decoherence induced by the environment (commonly thermal) as  $\Gamma_{th}$ . The strength of a measurement with respect to other environmental interactions is known as the measurement quantum cooperativity:  $C_q = \Gamma_{ba}/\Gamma_{th}$ . Finally, using equation (82) it

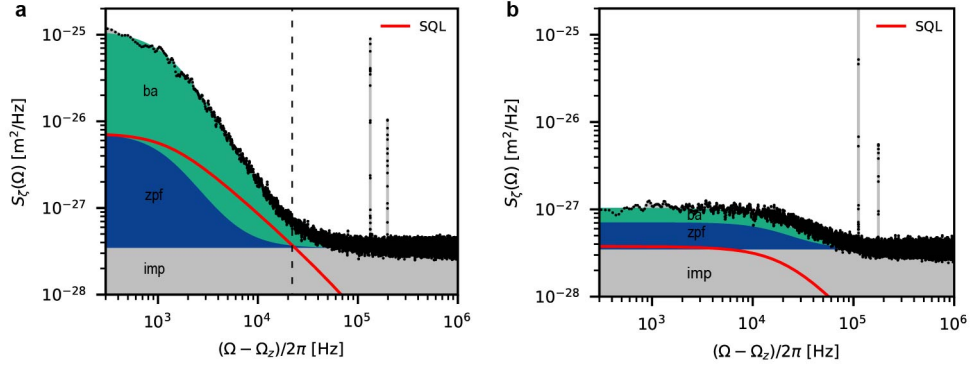


**Figure 23: The measured noise.** Measured displacement power spectral density (black) showing the contributions by imprecision (imp, gray), backaction (ba, green), and the zero point fluctuations (zpf, blue), compared to the SQL (red). **a**, A feedback gain of  $g_{fb}/2\pi = 2$  kHz results in an occupation of  $n = 8.3 \pm 0.09$ . The almost perfect balancing of imprecision and backaction at 22 kHz above resonance (vertical dashed line) results in a measurement that is only a factor 1.76 from the ideal SQL. **b**, In the case of strong cooling ( $g_{fb}/2\pi = 110$  kHz), and occupation of  $n = 0.71 \pm 0.09$ , we achieve a total added noise on resonance that is a factor 2.7 higher than the SQL.

is possible to define the measurement information efficiency, which summarizes the quality of a measurement process:

$$\eta = \frac{\Gamma_{\text{meas}}}{\Gamma_{\text{ba}} + \Gamma_{\text{th}}} = \eta_d \frac{\Gamma_{\text{ba}}}{\Gamma_{\text{ba}} + \Gamma_{\text{th}}} = \eta_d \left(1 + \frac{1}{C_q}\right)^{-1} = \eta_d \eta_e \quad (83)$$

#### Noise equivalent occupation

When monitoring the position of a harmonic oscillator, often the quantities of imprecision and force noise are considered in units of energy quanta. We can assign an apparent thermal occupation to the imprecision noise [Wil+15; Sud+17a; Ros+18]:

$$n_{\text{imp}} = \frac{S_z^{\text{imp}}}{2S_z^{\text{zpf}}(\Omega_z)} = S_z^{\text{imp}} \frac{\gamma}{8z_{\text{zpf}}^2} \quad (84)$$

On the other hand we can assign an occupancy to the bath associated with the force noise driving the oscillator. Assuming energy equipartition this is:

$$n_{\text{tot}} = \frac{1}{2\pi} \int_0^\infty \frac{S_F^{\text{tot}} |\chi_m(\Omega)|^2}{2z_{\text{zpf}}^2} d\Omega = \frac{S_F^{\text{tot}}}{8p_{\text{zpf}}^2 \gamma} \quad (85)$$

where the last identity in equation (85) is only valid in the case of a white force noise. The effect of backaction associated to any quantum measurement process seemingly would prohibit any kind of quantum control. However, the effects of this noise are directly captured by the measurement, and can be counteracted by feedback control schemes. We can then write the minimal achievable occupancy in presence of an ideal feedback as [Wil+15]:

$$n_{\text{min}} = 2\sqrt{n_{\text{imp}} n_{\text{tot}}} - \frac{1}{2} \quad (86)$$

Note that equation (86) is an asymptotic value, requiring an experimentally impractical infinite bandwidth feedback (see also Section 4.7.6). Given the parameters in our system we estimate  $n_{\text{min}} = 0.34$ .

### 4.7.3 Losses of information and photons

As we have seen in the previous section 4.7.2 information is not uniformly distributed across the dipole scattered light. Whenever there are spatially dependent losses, there are mismatches between the loss of photons and the actual loss of information. In other words, there are losses and the are losses. We will refer to efficiency that is complementary to information loss with  $\eta$  and efficiency that is complementary to photon loss with  $\eta^*$ .

#### Microscope collection

The collection efficiency by the microscope objective of dipole scattered photons is:

$$\eta_{d,c}^* = \frac{\int_{\Omega_{\text{coll}}} P(\hat{\mathbf{k}}_f) d\Omega}{\int_{4\pi} P(\hat{\mathbf{k}}_f) d\Omega}, \quad (87)$$

which results in a photon collection efficiency of  $\eta_{d,c}^* = 0.375$ . On the other hand, the information collection efficiency by the microscope objective is the ratio of the imprecision noise calculated for a limited collection angle  $\Omega_{\text{coll}}$  over the ideal imprecision noise defined in equation (68)

$$\eta_{d,c} = \frac{\int_{\Omega_{\text{coll}}} P(\hat{\mathbf{k}}_f) (A - \cos \theta)^2 d\Omega}{\int_{4\pi} P(\hat{\mathbf{k}}_f) (A - \cos \theta)^2 d\Omega}. \quad (88)$$

With an NA of 0.95 this leads to an information collection efficiency of  $\eta_{d,c} = 0.84$ .

#### Confocal mode-matching

After being collected by the microscope objective, light needs to be matched to the local oscillator. We implement a fiber based confocal dipole detection [Vam+07]. This has two advantages: first it allows easy and efficient mode matching of the dipole scattered light to the local oscillator, second, confocal filtering by the fiber allows to suppress stray reflections in the trapping-detection path. Following the description by Vamivakas *et al.* [Vam+07] we compute the mode overlap between the electric dipole far field  $E_{\text{dip}}$  imaged at the fiber boundary and the fiber mode profile  $E_{\text{fm}}$  in cylindrical coordinates as a function of magnification  $M = f_3/f_1$ . Here  $f_1$  and  $f_3$  are the focal lengths of the objective lens and the imaging lens respectively. The mode overlap efficiency is defined as:

$$\eta_{d,m}^*(M) = \frac{|\int \vec{E}_{\text{dip}}^*(\vec{r}_3) \vec{E}_{\text{fm}}^x(\vec{r}_3) dA_3|^2}{\int |\vec{E}_{\text{dip}}^x(\vec{r}_3)|^2 dA_3 \int |\vec{E}_{\text{fm}}^x(\vec{r}_3)|^2 dA_3}, \quad (89)$$

where the dipole is oriented along  $\hat{x}$  with its origin in the focal point of a 0.95 NA microscope objective and the fiber mode superscript  $x$  indicates the  $x$  polarized solution. We integrate the overlap of dipole image and fiber mode over the fiber tip surface  $dA_3$  at the focal position. A maximal collection efficiency of 0.76 can be achieved with a magnification of  $f_3/f_1 \approx 7.7$ . In our case a magnification of  $M = 8.5$  leads to a mode matching efficiency of  $\eta_{d,m}^* = 0.75$ . We manage to couple up to  $\eta_{d,m}^* = 0.71$ .

For comparison, we also calculate the overlap integral for the dipole image in paraxial approximation, where the collection angle  $\theta \rightarrow 0$ . The  $x$  component of the dipole image becomes:

$$E_{\text{dip}}^x(\rho_3, M) = \theta_1 \frac{M}{k_3 \rho_3} J_1(k_3 \rho_3 \theta_1 / M), \quad (90)$$



where  $\rho_3$  is the distance from the fiber axis,  $J_1$  is the first order Bessel function of the first kind,  $\theta_1 = \arcsin \text{NA}/n_1$ , with  $n_1 = 1$  the refractive index before the microscope objective and  $k_3 = n_1 2\pi/\lambda$ . All other contributions vanish. We insert equation (90) into equation (89) and integrate numerically at different magnifications. The result can be found in Supplementary Figure 24b. Approximating the dipole image as a Bessel function (without any azimuthal dependence) increases the maximal coupling efficiency and shifts it to higher magnification. While qualitative behaviour remains similar, it is evident that in our configuration the approximate solution is no longer valid. As the dipole scatterer is treated as a point source, once the light is collected by the microscope objective and imaged onto the fiber, information is distributed uniformly over the mode. For this reason the information collection efficiency will, from this point on, coincide with the photon collection efficiency. Even though a higher NA leads to an increased information collection by the microscope, it also causes a reduced overlap of the collected light with a Gaussian single mode. Therefore it is the efficiency of the combined system that has to be considered and maximized (Supplementary Figure 24c). Still, computing the product of the maximal information collection efficiency  $\eta_c$  for each NA we notice that the overall information collection efficiency is still maximized at the highest NA.

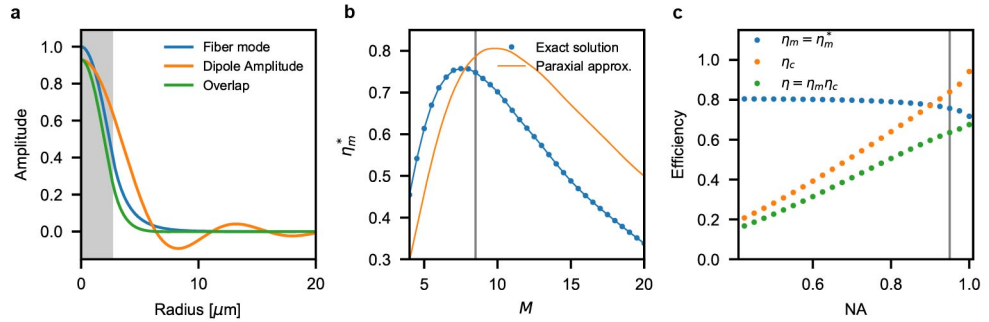


**Figure 24: Fiber-dipole mode overlap.** **a**, Numerical calculation of the dipole mode (orange) at a fixed angle imaged at the fiber interface by our confocal microscope system, fiber mode (blue), and their overlap (green) as a function of the distance to the center of the fiber. The gray shaded area represents the fiber core. **b**, Overlap efficiency as a function of magnification of the optical system. The gray vertical line shows our operating point, not far from the optimal value. **c**, Information collection efficiency by the microscope objective (orange dots), maximum fiber mode matching (blue dots) and the product of the two (green dots) as a function of the objective NA. The gray line is our operating point.

### Objective transmission

We measure the transmission efficiency of the microscope objective to be  $\eta_{d,obj}^* = \eta_{d,obj} = 0.84$ , assuming uniform loss, which is in good agreement with the producers specified value at this wavelength.

### Heterodyne splitting

After mode-matching to the fiber we split 5% by use of a variable ratio coupler of the signal to contribute to the out-of-loop heterodyne measurement (Supplementary Figure 20). We have  $\eta_{d,hel}^* = \eta_{d,hel} = 0.95$ .

### Homodyne balancing

As the interferometric measurement is performed in fiber, the visibility is degraded by the imperfect splitting ratios of the variable ratio couplers. These tunable beam-splitters can be adjusted to a mismatch of about 0.1%, with thermal fluctuations of less than 0.5%. This results in an efficiency  $\eta_{d,hom}^* = \eta_{d,hom} = 0.99$ .



### Detector efficiency

Together with the microscope transmissivity this is the second largest loss. We use a commercial balanced detector, where the current difference between the 2 diodes is amplified by a transimpedance gain. We calibrate the detector responsivity defined as  $R(\nu) = \eta_{d,q}^* e/h\nu$  with  $e$  the electron charge, by measuring the dc voltage at each diode monitor port and extrapolate the efficiency of  $\eta_{d,q}^* = \eta_{d,q} = 0.85$  for both diodes.

### Detector dark noise

The last detection noise source is the detector dark noise. We measure the dark noise at the relevant frequencies to be 11 dB below the shot noise level, resulting in  $\eta_{d,dn} = 0.924$ .

### Digital noise

After detection there are further noise sources to be considered which reduce the collected information: The Red-Pitaya board has 14-bit analog to digital and digital to analog converters. This results in a limitation of the dynamic range of operation. In our settings this results in an effective information loss of 2% ( $\eta_{d,rp} = 0.98$ ).

### Environmental information loss

We here consider the information loss to interactions with gas molecules. This contributes the dominant environmental loss in  $\eta_e$ . As already discussed in Section 4.7.2, a gas molecule colliding with the particle performs a measurement which information we cannot read. The associated efficiency is:

$$\eta_e = \frac{S_F^{ba}}{S_F^{tot}} = 0.97 \quad (91)$$

Values for the force noise contributions are calculated in Section 4.7.4. As discussed in Section 4.7.4 we can define the cooperativity  $C_q = S_F^{ba}/S_F^{th} = \Gamma_{ba}/\Gamma_{th}$ :

$$\eta_e = \left(1 + \frac{1}{C_q}\right)^{-1} \quad (92)$$

### The total loss budget

We finally derive a total photon detection efficiency of  $\eta^* = 0.178$  while the total information detection efficiency is as high as  $\eta = 0.347$  (Supplementary Table 1). This estimation of the total information collection efficiency is in excellent agreement (less than 1% unaccounted for) with the value of  $\eta = 0.342$  directly calculated from the ratio of measurement to decoherence rates.

#### 4.7.4 Contributions to the total force noise

We here estimate the expected force noise contributions given the parameters of our system. Actual values are measured in Section 4.7.7. While the backaction and thermal force noise contributions are defined and fixed by the physical system, the contribution from the feedback strongly depend on the chosen control algorithm.

#### Backaction force noise

The backaction force noise, resulting from photons scattering off the particle was derived in Section 4.7.2. In order to estimate its contribution, we must consider the experimental details of the optical tweezer. The power scattered by the particle

Loss source	$\eta^*$	$\eta$
Microscope collection (d)	0.375	0.84
Microscope transmissivity (d)	0.84	0.84
Confocal mode-matching (d)	0.71	0.71
Heterodyne split (d)	0.95	0.95
Homodyne balancing (d)	0.99	0.99
Detector efficiency (d)	0.85	0.85
Detector dark-noise (d)	-	0.92
Kalman digital noise (d)	-	0.98
Environmental information loss (e)	-	0.96
Total	0.178	0.347

**Table 1: Measurement efficiency.** The total efficiency budget for photon and information loss. All loss sources are considered in both the detection and electronic line (d), and information loss to the environment (e).

is  $P_{\text{scatt}} = I_0 \sigma$ , where  $I_0$  is the tweezer intensity and  $\sigma = \frac{8\pi}{3} \left( \frac{\alpha k^2}{4\pi\epsilon_0} \right)^2$  the scattering cross section ( $\alpha$ : polarizability of the particle  $\epsilon_0$ : vacuum permittivity). The tweezer intensity  $I_0 = 2P/\pi w$  depends on the trapping power  $P$  and on the effective beam waist  $w$  calculated for a tightly focused beam at the particle position, taking into account the displacement due to the scattering force contribution [NHo6]. We calculate a scattered power by the dipole of  $P_{\text{scatt}} = 22.4 \mu\text{W}$ . The expected single-sided backaction force noise therefore is:

$$S_F^{\text{ba}} = 2 \left( A^2 + \frac{2}{5} \right) \frac{\hbar k P_{\text{scatt}}}{c} = 8.4 \cdot 10^{-41} \text{ N}^2/\text{Hz}, \quad (93)$$

In the absence of feedback center of mass motion of the particle would thermalize to a temperature defined by competing effects of photon recoil heating and radiation damping [Nov17]:  $T_{\text{opt}} = \hbar\omega_0/(4k_B)$  ( $\omega_0$ : the optical laser frequency). This is equivalent to  $n_{\text{ba}} = 6.8 \cdot 10^8$  quanta of occupation of the harmonic oscillator. We cannot directly observe this in the experiment as it would lead to the particle loss due to the finite optical trap depth.

#### Thermal force noise

The thermal force noise is the noise contribution arising from interaction with the surrounding gas. At a temperature  $T$  of 292 K and pressure of  $10^{-8}$  mbar, we calculate:

$$S_F^{\text{th}} = 4k_B T \gamma_{\text{th}} m = 3.9 \cdot 10^{-42} \text{ N}^2/\text{Hz} \quad (94)$$

where  $k_B$  is the Boltzmann constant and  $\gamma_{\text{th}}$  is the damping due to residual gas molecules (for definition see also Section 4.7.7). This force noise contributes to an occupancy of  $n_{\text{th}} = 6.0 \cdot 10^7$ .

#### Feedback force noise

Measurement-based feedback control relies on a typically noisy measurement to control the dynamics of the system. The measurement noise is therefore fed back to the controller whose output drives the system, adding a new contribution to the force noise term, and setting a lower bound to the accuracy of the control. The force noise arising from feedback imprecision noise is:

$$S_F^{\text{fb}}(\Omega) = |h_{\text{fb}}(\Omega)|^2 S_z^{\text{imp}}, \quad (95)$$

where  $h_{fb}(\Omega)$  is the controller transfer function in the feedback path. Closing the feedback loop the susceptibility of the system becomes:

$$\chi_{eff}(\Omega) = \frac{\chi_m(\Omega)}{1 + \chi_m(\Omega)h_{fb}(\Omega)}, \quad (96)$$

which allows us to write the closed-loop spectral density of the position ( $z$ ) and measurement outcome ( $\zeta$ ):

$$S_z(\Omega) = |\chi_{eff}(\Omega)|^2 \left( S_F^{tot} + |h_{fb}(\Omega)|^2 S_z^{imp} \right) \quad (97a)$$

$$S_\zeta(\Omega) = |\chi_{eff}(\Omega)|^2 \left( S_F^{tot} + |\chi_m(\Omega)|^{-2} S_z^{imp} \right) \quad (97b)$$

From (95),(96) and (97a), we see how the controller transfer function  $h_{fb}(\Omega)$  influences the closed-loop power spectral densities (PSDs). The controller should minimize the PSD by respecting the constraints of the control input and render the closed-loop stable. For linear Gaussian systems such as the one considered in this paper, the linear-quadratic Gaussian (LQG) controller fulfills these demands in an optimal way, as will be discussed in detail in the next sections. We here discuss the simple example of a *differentiation filter*, as it is the most common form of feedback cooling applied in most optomechanical experiments. The feedback transfer function for the differentiation filter is:

$$h_{fb}^d(\Omega) = i m \Omega \gamma g_{fb} \quad (98)$$

where  $\gamma$  is the natural damping of the system associated to the bath (of temperature  $T$ ) it is coupled to, and  $g_{fb}$  the feedback gain. Evaluating the total energy as a function of the gain  $g_{fb}$  makes it evident that at some point the imprecision noise will start to be fed back into the system, heating the motion of the particle:

$$\langle z^2 \rangle = \frac{1}{2\pi} \int_0^\infty S_z(\Omega) d\Omega = \frac{1}{1 + g_{fb}} \frac{k_B T}{m \Omega_z^2} + \frac{g_{fb}^2}{1 + g_{fb}} \frac{\gamma}{2} \frac{S_z^{imp}}{2}. \quad (99)$$

This effect appears in the measured spectral density  $S_\zeta(\Omega)$  in the form of noise squashing, as the particle motion is driven to minimize the total noise in the measurement outcome [Pog+07; Ros+18; Wil+15]. It is important to notice that, in practical applications, the controller transfer function defined in (98) is not realistic as exact differentiation would require infinite bandwidth and knowledge of the future, producing unbounded control signals. When limiting the bandwidth of the differentiation filter, the qualitative behaviour of (99) is preserved, albeit with a reduced performance (see Supplementary Figure 25b).

### Coupling of the transverse degrees of freedom

The finite temperature of the transverse modes may in principle affect the cooling performance in the  $z$ -direction in two ways:

- Coupling of the transverse degrees of freedom through the measurement. In this case, displacements along the transverse directions are transduced into the backscattered signal. This effect would reduce the information efficiency of the  $z$ -measurement, just as any other noise source, in turn reducing the cooling performance. For a specific measurement geometry, the noise power contributed by each mode  $i = (x, y, z)$  can be written as  $P_i \propto \Gamma_i^{meas} (\langle 2n_i \rangle + 1)$ , where  $\Gamma_i^{meas}$  are the measurement rates for each mode, and  $\langle n_i \rangle$  the average occupation of each mode. Concretely, for our setup, we find  $\Gamma_{x,y}^{meas} / \Gamma_z^{meas} \sim 10^{-5}$ , which means that the residual coupling of the transverse modes is about 5 orders of magnitude weaker than for the  $z$ -mode. Using parametric feedback via an independent forward detection scheme (Figure S1), the transverse modes are cooled to occupations of  $\langle n_{x,y} \rangle \sim 10^3$ . This yields a relative noise

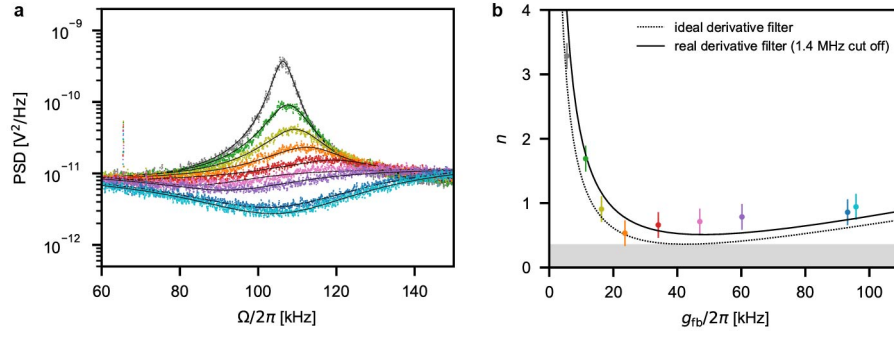


**Figure 25: Derivative feedback performance.** **a**, Noise squashing in the closed-loop measurement PSD resulting from leakage of measurement noise in the closed-loop system. **b**, Occupation number measured in heterodyne detection as a function of the feedback gain of a derivative feedback. The different colours correspond to the PSDs in **a**. A qualitative approximation of this behaviour can be obtained by tuning the Kalman gains (defined in Section 4.7.6) of our controller to a value that is a factor  $10^5$  larger than the optimal one, and reducing the controller transfer function to be white over a large frequency band. In this setting the filter ignores the model and bases its feedback solely on the measurement. It is important to notice that the ideal differentiation filter would reach occupations as low as those determined by the measurement uncertainty as defined in (86). However this is not a practical solution, as it would require an infinite bandwidth controller.

power contribution of the two transverse modes, when  $\langle n_z \rangle \sim 1$ , of about  $P_{x,y}/P_z \sim 10^{-2}$ , which is a negligible contribution. In addition, since the feedback signal for cooling is confined to the spectral region around  $\Omega_z$ , the spectral separation between transverse motion and z-motion further suppresses the unwanted cross-coupling effect.

- Coupling between the modes through the nonlinearity of the potential. The optical tweezer presents a Duffing nonlinearity of the order  $\xi_i = -2/w_i^2$  with  $i = (x, y, z)$  and  $w_i$  the beam characteristic length scale (i.e. the waist for the transverse directions  $(x, y)$  and the Rayleigh length for the  $z$ -direction). As a consequence, the force along each direction of motion becomes coupled to the position in the other directions [GNQ13]:

$$F_i = -k_i x_i \left( 1 + \sum_{j=x,y,z} \xi_j x_j^2 \right). \quad (100)$$

For small displacements,  $|x| \ll |\xi_i|^{-1/2}$ , this coupling becomes negligible and the modes decouple. Specifically, in this experiment, we have  $|\xi_i|^{-1/2} \geq 4 \times 10^{-7} \text{ m}$  and the root mean square displacement along each direction is given by  $x_i^{\text{rms}} = x_i^{\text{zpf}} \sqrt{2n_i + 1}$ . While the  $z$ -motion is cooled to  $\langle n_z \rangle \sim 0.5$ , the motion along the other modes is parametrically cooled to  $\langle n_{x,y} \rangle \sim 10^3$ . This is enough to have  $x_{x,y}^{\text{rms}} \sim 10^{-10} \text{ m}$ . It is evident that even with limited cooling on the transverse modes the expected energy contribution to the  $z$ -mode due to nonlinear coupling is negligible.

#### 4.7.5 Quantum equations of motion

In this section we derive the quantum Langevin equations for the nanosphere, describing its motion in the harmonic trap formed by the tweezer field, together with the corresponding input-output relations. These equations form the basis for the state-space model used for the Kalman filter.

### Hamiltonian

The effective Hamiltonian for the center-of-mass motion of the nanosphere in the tweezer field and the coupling to the electromagnetic field can be derived following [GB+19] (which treats a more general system), assuming a linear, isotropic dielectric medium and the validity of the long-wavelength assumption. (That is, the typical extension of the mechanical state is much smaller than the tweezer wavelength  $\lambda_0$ ).

We describe the center-of-mass motion of the nanosphere in direction  $j \in \{x, y, z\}$  by annihilation and creation operators  $b_j$  and  $b_j^\dagger$  with commutation relations  $[b_i, b_j^\dagger] = \delta_{ij}$ . The light field is expanded into a continuum of plane-wave modes labeled by the wavevector  $\mathbf{k} \in \mathbb{R}^3$  and an index  $\lambda$  that determines the mode's polarisation. The corresponding annihilation and creation operators are denoted by  $a_\lambda(\mathbf{k})$  and  $a_\lambda^\dagger(\mathbf{k})$ , respectively. Their commutation relations are given by  $[a_\lambda(\mathbf{k}), a_{\lambda'}^\dagger(\mathbf{k}')] = \delta_{\lambda\lambda'}\delta(\mathbf{k} - \mathbf{k}')$ , where  $\delta(\cdot)$  is the Dirac  $\delta$ -function and  $\delta_{\lambda\lambda'}$  is the Kronecker  $\delta$ . For the system discussed here we find the Hamiltonian

$$H = \hbar \sum_{j=x,y,z} \Omega_j b_j^\dagger b_j + \hbar \sum_{\lambda} \int d^3k \Delta_k a_\lambda^\dagger(\mathbf{k}) a_\lambda(\mathbf{k}) + \hbar \sum_{j=x,y,z} \sum_{\lambda} \int d^3k [g_{j\lambda}(\mathbf{k}) a_\lambda^\dagger(\mathbf{k}) (b_j + b_j^\dagger) + \text{H.c.}], \quad (101)$$

where  $\Omega_j$  is the mechanical frequency in direction  $j$ ,  $\Delta_k = \omega_k - \omega_0$ , and  $\omega_k = \|\mathbf{k}\|c$ . The coupling constants  $g_{j\lambda}(\mathbf{k})$  are given by

$$g_{j\lambda}(\mathbf{k}) = i \frac{G_0^\lambda(\mathbf{k})}{2} (k_j - k_0 \delta_{jz}) r_{0j}, \quad (102)$$

$$G_0^\lambda(\mathbf{k}) = \alpha E_0 \sqrt{\frac{\omega_k}{2\hbar\epsilon_0(2\pi)^3}} \mathbf{e}_x \cdot \mathbf{e}_\lambda(\mathbf{k}), \quad (103)$$

where  $r_{0j}$  is the mechanical ground-state extension in direction  $j$ ,  $\alpha$  is the nanosphere's polarisability, and  $E_0$  is the electric field strength of the tweezer. Symbols  $\mathbf{e}_x$  and  $\mathbf{e}_\lambda(\mathbf{k})$  denote unit vectors in  $x$ -direction and the direction of (linear) polarization for the  $(\mathbf{k}, \lambda)$  field mode respectively, and  $\mathbf{e}_x \cdot \mathbf{e}_\lambda$  denotes their scalar product in  $\mathbb{R}^3$ .

### Quantum Langevin Equations

Starting from the Hamiltonian above we now derive the quantum-optical Langevin equations for the mechanical system following the procedure introduced in [GC85]. Here we neglect relativistic effects [Nov17] and, for now, also mechanical damping effects due to residual gas which will be added later. We first find the Heisenberg equations for  $b_j$  and  $a_\lambda(\mathbf{k})$ , yielding

$$\dot{a}_\lambda(\mathbf{k}, t) = -i\Delta_k a_\lambda(\mathbf{k}, t) - i \sum_j g_{j\lambda}(\mathbf{k}) (b_j + b_j^\dagger), \quad (104a)$$

$$\dot{b}_j(t) = -i\Omega_j b_j(t) - i \sum_{\lambda} \int d^3k [g_{j\lambda}(\mathbf{k}) a_\lambda^\dagger(\mathbf{k}, t) + \text{H.c.}]. \quad (104b)$$

We formally solve (104a), which gives

$$a_\lambda(\mathbf{k}, t) = e^{-i\Delta_k t} a_\lambda(\mathbf{k}, 0) - i \sum_{j=x,y,z} g_{j\lambda}(\mathbf{k}) \int_0^t ds e^{-i\Delta_k(t-s)} [b_j(s) + b_j^\dagger(s)], \quad (105)$$

and plug it into (104b). We find

$$\begin{aligned} \dot{b}_j(t) = & -i\Omega_j b_j(t) - i \sum_{\lambda} \int d^3k [g_{j\lambda}(\mathbf{k}) e^{i\Delta_k t} a_\lambda^\dagger(\mathbf{k}, 0) + \text{H.c.}] \\ & + \sum_{l=x,y,z} \int_0^t ds [b_j(s) + b_j^\dagger(s)] \int d^3k \sum_{\lambda} [g_{j\lambda}(\mathbf{k}) g_{l\lambda}^*(\mathbf{k}) e^{i\Delta_k(t-s)} - \text{H.c.}]. \end{aligned} \quad (106)$$

We now make the (typical) assumptions [ZG97] that (i) the interaction with the field is restricted to a frequency interval  $[\omega_0 - \theta, \omega_0 + \theta]$ , where  $\theta$  is a cutoff frequency that fulfills  $\omega_0 \gg \theta \gg \Omega_j$ , and (ii) the coupling constants  $g_{j\lambda}$  are approximately constant across this interval. These assumptions will allow us to employ a Markov approximation (taking the limit  $\theta \rightarrow \infty$ ), making the resulting equation local in time, and considerably simplify equation (106).

We first take a look at the second term in (106), which describes the interaction of the mechanical system with (unnormalized) light modes  $\int d^3k g_{j\lambda}^*(k) e^{-i\Delta_k t} a_\lambda(k, 0)$ , where  $t$  should be interpreted as the time at which the incoming light-field interacts with the nanosphere. For our purposes it is convenient to decompose this mode into two orthogonal modes, one of which is monitored in the experiment. The corresponding mode function, denoted by  $h$ , is determined by the measurement setup. We write

$$\int d^3k g_{l\lambda}^*(k) e^{-i\Delta_k t} a_\lambda(k, 0) = \sqrt{2\pi K_{ll}^\lambda} \left\{ \sqrt{\eta_{l\lambda}} c_\lambda(t) + \sqrt{1 - \eta_{l\lambda}} c_{l\lambda}^\perp(t) \right\},$$

where we defined the light modes

$$c_\lambda(t) = (2\pi I)^{-\frac{1}{2}} \int d^3k h^*(k) e^{-i\Delta_k t} a_\lambda(k, 0), \quad (107a)$$

$$c_{l\lambda}^\perp(t) = [2\pi K_{ll}^\lambda (1 - \eta_{l\lambda})]^{-\frac{1}{2}} \int d^3k [g_{l\lambda}^*(k) - (J_{l\lambda}^*/I) h^*(k)] e^{-i\Delta_k t} a_\lambda(k, 0), \quad (107b)$$

and the constants

$$I = \int d\Omega_k \frac{\omega_0^2}{c^3} \left| h\left(\frac{\omega_0}{c} \mathbf{e}_k\right) \right|^2, \quad (108)$$

$$J_{l\lambda} = \int d\Omega_k \frac{\omega_0^2}{c^3} h^*\left(\frac{\omega_0}{c} \mathbf{e}_k\right) g_{l\lambda}\left(\frac{\omega_0}{c} \mathbf{e}_k\right), \quad (109)$$

$$K_{jl}^\lambda = \int d\Omega_k \frac{\omega_0^2}{c^3} g_{j\lambda}\left(\frac{\omega_0}{c} \mathbf{e}_k\right) g_{l\lambda}^*\left(\frac{\omega_0}{c} \mathbf{e}_k\right). \quad (110)$$

Here  $d\Omega_k$  denotes the integration with respect to the angular degrees of freedom of  $k$  and  $\mathbf{e}_k$  is a unit vector in the direction of  $k$ . The parameter  $\eta_{l\lambda} = |J_{l\lambda}|^2 / K_{ll}^\lambda I \in [0, 1]$  determines the overlap between the measured mode function  $h$  and the scattering profile  $g_{l\lambda}$  at the tweezer frequency  $\omega_0$  and takes the role of a measurement efficiency. Note that for  $h = g_{l\lambda}$  we have  $\eta_{l\lambda} = 1$ . The parameter  $K_{ll}^\lambda$  on the other hand effectively describes the coupling strength between the nanosphere's motion in direction  $l$  and the mode light mode defined by  $g_{l\lambda}$ . Plugging the expressions for  $g_{l\lambda}$  into the definition of  $K_{jl}^\lambda$  one can show that  $K_{jl}^\lambda = K_{ll}^\lambda \delta_{jl}$ .

Assuming that  $h$  is (similarly to  $g$ ) restricted to a frequency interval around  $\omega_0$  and roughly flat and taking the Markovian limit ( $\theta \rightarrow \infty$ ) we can show that  $c_\lambda$ ,  $c_\lambda^\perp$  describe zero-mean white-noise fields that obey

$$[c_\lambda(t), c_{\lambda'}^\dagger(s)] = [c_{l\lambda}^\perp(t), (c_{l\lambda'}^\perp)^\dagger(s)] = \delta_{\lambda\lambda'} \delta(t - s), \quad (111a)$$

$$[c_\lambda(t), (c_{l\lambda'}^\perp)^\dagger(s)] = 0, \quad (111b)$$

and, assuming the electromagnetic field is initially in the vacuum state, the correlation functions

$$\langle c_\lambda(t) c_{\lambda'}^\dagger(s) \rangle = \langle c_{l\lambda}^\perp(t) (c_{l\lambda'}^\perp)^\dagger(s) \rangle = \delta_{\lambda\lambda'} \delta(t - s), \quad (112a)$$

$$\langle c_\lambda(t) (c_{l\lambda'}^\perp)^\dagger(s) \rangle = 0, \quad (112b)$$

where  $\langle \cdot \rangle$  refers to the expectation value with respect to system plus environment. In deriving relations (111) and (112) we find integrals of the following form, which can be approximated using the assumptions (i) and (ii) from above:

$$\int d^3k g_{j\lambda}(k) g_{l\lambda}^*(k) e^{i\Delta_k(t-s)} \stackrel{(i),(ii)}{\approx} \int_{\omega_0-\theta}^{\omega_0+\theta} d\omega e^{i(\omega-\omega_0)(t-s)} \int d\Omega_k \frac{\omega_0^2}{c^3} g_{j\lambda}\left(\frac{\omega_0}{c}e_k\right) g_{l\lambda}^*\left(\frac{\omega_0}{c}e_k\right) \quad (113)$$

$$\xrightarrow{\theta \rightarrow \infty} 2\pi K_{jl}^\lambda \delta(t-s)$$

Plugging this back into equation (106) we see that, under this approximation, the second line vanishes identically as  $K_{lj}^\lambda \in \mathbb{R}$ . Using this, the quantum Langevin equations for the motion of the nanosphere (in a Markov approximation) take the form

$$\dot{b}_l(t) = -i\Omega_l b_l(t) - i \sum_{\lambda} \sqrt{2\pi K_{ll}^\lambda} \left\{ \sqrt{\eta_{l\lambda}} [c_\lambda(t) + c_\lambda^\dagger(t)] + \sqrt{1-\eta_{l\lambda}} [c_\lambda^\perp(t) + (c_\lambda^\perp(t))^\dagger] \right\}. \quad (114)$$

Alternatively we can rewrite (114) in terms of position  $r_j = (b_j + b_j^\dagger)/\sqrt{2}$  and momentum  $p_j = (b_j - b_j^\dagger)/\sqrt{2}i$

$$\dot{r}_l(t) = \Omega_l p_l(t), \quad (115a)$$

$$\dot{p}_l(t) = -\Omega_l r_l(t) - \sum_{\lambda} \sqrt{4\pi K_{ll}^\lambda} \left\{ \sqrt{\eta_{l\lambda}} x_\lambda(t) + \sqrt{1-\eta_{l\lambda}} x_{l\lambda}^\perp(t) \right\}, \quad (115b)$$

where we introduced the amplitude quadratures  $x_\lambda = c_\lambda + c_\lambda^\dagger$ .

Up to now we have neglected two important points in our treatment: the nanosphere's interaction with residual gas, which constitutes an additional thermal environment, and the feedback force. The former we model as *Brownian motion damping* [GZ04], but treat it in a Markov approximation. We thus introduce an additional Gaussian noise operator  $f_l$  that obeys

$$\langle f_l(t) \rangle = 0, \quad (116a)$$

$$\langle f_l(t) f_l(t') + f_l(t') f_l(t) \rangle = (2\bar{n}_l + 1) \delta(t - t'), \quad (116b)$$

where  $\bar{n}_l = \hbar\Omega_l/k_B T$ . The corresponding damping rate we denote by  $\gamma$ . The additional energy contribution by the feedback we write as  $H_{fb} = -qE_{fb}(t)r_{0z}r_z = -\hbar u(t)r_z$ , where  $q$  is the charge of the particle and  $E_{fb}(t)$  is the time-dependent electric field that is used to apply the feedback signal (also see Section 4.7.7). Putting this all together the modified Langevin equations take the form

$$\dot{r}_l(t) = \Omega_l p_l(t), \quad (117a)$$

$$\dot{p}_l(t) = -\Omega_l r_l(t) - \gamma p_l(t) + u(t) + \sqrt{2\gamma} f_l(t) - \sum_{\lambda} \sqrt{4\pi K_{ll}^\lambda} \left\{ \sqrt{\eta_{l\lambda}} x_\lambda(t) + \sqrt{1-\eta_{l\lambda}} x_{l\lambda}^\perp(t) \right\}. \quad (117b)$$

A relativistic treatment of the optomechanical interaction would as well show a radiation-damping contribution to the particle dynamics [Nov17]. Together with the radiation-pressure shot noise (described by the last term in (117b)) this defines, similarly to the thermal environment, a fluctuation–dissipation balance and a thermalization temperature associated with the optical bath. In our experiment both damping mechanisms (residual gas and radiation damping) are negligible in the presence of feedback. The experimental decoherence rates for the thermal and optical interactions are characterized in Section 4.7.7.



### Input–Output relations

To compute the scattered field after the interaction with the nanosphere (that is what we measure) we go back to equation (105) which, in a first step, we multiply by  $h^*(k)$  and integrate over  $k$ , leading to

$$\begin{aligned} \int d^3k h^*(k) a_\lambda(k, t) &= \sqrt{2\pi\Gamma} c_\lambda(t) - i \sum_{l=x,y,z} \int d^3k h^*(k) g_{l\lambda}(k) \int_0^t ds e^{-i\Delta_k(t-s)} [b_l(s) + b_l^\dagger(s)] \\ &\approx \sqrt{2\pi\Gamma} c_\lambda(t) - 2i\pi \sum_{l=x,y,z} J_{l\lambda} \int_0^t ds \delta(t-s) [b_l(s) + b_l^\dagger(s)] \\ &= \sqrt{2\pi\Gamma} c_\lambda(t) - i\pi \sum_{l=x,y,z} J_{l\lambda} [b_l(t) + b_l^\dagger(t)] \end{aligned} \quad (118)$$

Note again that  $c_\lambda(t)$  refers to the light field *before* the interaction. To connect this to its state *after* the interaction, we again formally integrate (104a), this time specifying  $a(k, T)$  at some (distant) final time  $T > t$ :

$$a_\lambda(k, t) = e^{i\Delta_k(T-t)} a_\lambda(k, T) + i \sum_{j=x,y,z} g_{j\lambda}(k) \int_t^T ds e^{-i\Delta_k(t-s)} [b_j(s) + b_j^\dagger(s)]. \quad (119)$$

Applying the same procedure as before we find

$$\int d^3k h^*(k) a_\lambda(k, t) = \sqrt{2\pi\Gamma} c_\lambda^{\text{out}}(t) + i\pi \sum_{l=x,y,z} J_{l\lambda} [b_l(t) + b_l^\dagger(t)], \quad (120)$$

where we interpret  $c_\lambda^{\text{out}}(t) = \int d^3k h^*(k) e^{i\Delta_k(T-t)} a_\lambda(k, T) / \sqrt{2\pi\Gamma}$  as the field (at the time  $T$ ) after the interaction. We can combine equations (120) and (118) to obtain the usual input–output relation (with  $\varphi_{l\lambda} = \arg J_{l\lambda}$ )

$$c_\lambda^{\text{out}}(t) = c_\lambda(t) - i \sum_{l=x,y,z} \sqrt{2\pi\eta_{l\lambda} K_{ll}^\lambda} e^{i\varphi_{l\lambda}} [b_l(t) + b_l^\dagger(t)]. \quad (121)$$

Note that the choice of  $h$  and thus the value of  $\eta_{l\lambda}$  determines which direction of the nanosphere’s motion can be monitored by measuring the scattered light. In the experiment we use homodyne detection to monitor (amplitude and phase) quadratures ( $x_{j\lambda}^{\text{out}}$  and  $y_{j\lambda}^{\text{out}}$ ) of the scattered field. The corresponding input–output relations are given by

$$x_\lambda^{\text{out}}(t) = [c_\lambda^{\text{out}}(t) + (c_\lambda^{\text{out}}(t))^\dagger] = x_\lambda(t) + \sum_{l=x,y,z} \sin \varphi_{l\lambda} \sqrt{16\pi\eta_{l\lambda} K_{ll}^\lambda} r_l(t), \quad (122a)$$

$$y_\lambda^{\text{out}}(t) = -i[c_\lambda^{\text{out}}(t) - (c_\lambda^{\text{out}}(t))^\dagger] = y_\lambda(t) - \sum_{l=x,y,z} \cos \varphi_{l\lambda} \sqrt{16\pi\eta_{l\lambda} K_{ll}^\lambda} r_l(t). \quad (122b)$$

As in our experiment  $\varphi_{z\lambda} \approx 0$  the amplitude quadrature  $x_\lambda^{\text{out}}$  only carries noise, while the phase quadrature  $y_\lambda^{\text{out}}$  contains information about the nanosphere’s position. We thus only monitor the phase quadrature. Also, (122b) shows that, depending on the value of  $\eta_{l\lambda}$  and thus on the definition of the measured mode  $h$ ,  $y_\lambda^{\text{out}}$  contains contributions from the particle displacement along all directions. In the experiment  $h$  is such that the contributions from the  $x$  and  $y$  directions are heavily suppressed (i.e.,  $\eta_{x\lambda}, \eta_{y\lambda} \ll \eta_{z\lambda}$ ). Additional imperfections in the experimental setup will determine the effective measurement efficiency, which will result in effective values for  $\eta_{l\lambda}$  (see Section 4.7.3).

### Quantum Langevin equations in vector form

In analogy to the *state-space models* commonly used in classical control theory, we can rewrite the quantum Langevin equations (117) and the input–output relations

(122) in vector form. These definitions will enable us to compactly write the Kalman filter equations in the next section.

We start by defining  $\mathbf{z}(t) = [r_z(t) \ p_z(t)]^T$ . Here and in the following sections, we assume that we measure the phase quadrature  $y_{\lambda_0}^{\text{out}}(t)$  for a single polarisation  $\lambda_0$ . We can then write

$$\dot{\mathbf{z}}(t) = \mathbf{A}\mathbf{z}(t) + \mathbf{b}u(t) + \mathbf{w}(t), \quad (123a)$$

$$y_{\lambda_0}^{\text{out}}(t) = \mathbf{c}^T \mathbf{z}(t) + y_{\lambda_0}(t), \quad (123b)$$

with

$$\mathbf{A} = \begin{bmatrix} 0 & \Omega_z \\ -\Omega_z & -\gamma \end{bmatrix}, \quad \mathbf{b} = [0 \ 1]^T, \quad \mathbf{c}^T = \sqrt{16\pi\eta_{z\lambda_0} K_{zz}^{\lambda_0}} [1 \ 0]. \quad (124)$$

and  $\mathbf{w}(t) = \mathbf{g}w(t) = [0 \ 1]^T w(t)$ ,

$$w(t) = \left\{ \sqrt{2\gamma} f_z(t) - \sum_{\lambda} \sqrt{4\pi K_{zz}^{\lambda}} \left[ \sqrt{\eta_{z\lambda}} x_{\lambda}(t) + \sqrt{1 - \eta_{z\lambda}} x_{z\lambda}^{\perp}(t) \right] \right\}. \quad (125)$$

As the light field is assumed to be in the vacuum state both  $\mathbf{w}$  and  $y_{\lambda_0}$  are zero-mean Gaussian processes. Their symmetrized (cross-)correlation matrices are

$$\langle y_{\lambda_0}(t) y_{\lambda_0}(t') \rangle = \delta(t - t'), \quad (126a)$$

$$\text{Re}\langle \mathbf{w}(t) y_{\lambda_0}(t') \rangle = \mathbf{M}\delta(t - t') = 0, \quad (126b)$$

$$\text{Re}\langle \mathbf{w}(t) \mathbf{w}^T(t') \rangle = \mathbf{N}\delta(t - t') = \text{diag}\left(0, \gamma(2\bar{n}_z + 1) + 4\pi \sum_{\lambda} K_{zz}^{\lambda}\right) \delta(t - t'), \quad (126c)$$

which follows from (112) and (116).

#### Connection to the stochastic master equation and Kalman filtering

Equations (117) and (122) define a quantum stochastic model of the experimental setup. This model also allows us to construct the dynamical equations for the so-called *conditional quantum state*  $\hat{\rho}$ , which describes the nanosphere's motional state in  $z$ -direction conditioned on the classical output of the measurement of  $y_{\lambda_0}^{\text{out}}$ . The time evolution of  $\hat{\rho}$  is (approximately) given by the Ito stochastic master equation (see, e.g., [WM10] for an introduction to the formalism). Assuming  $\varphi_{z\lambda_0} = 0$ :

$$\begin{aligned} d\hat{\rho}(t) = & -i[\Omega_z b_z^{\dagger} b_z - u(t)r_z, \hat{\rho}(t)]dt \\ & + \gamma(\bar{n} + 1)\mathcal{D}[b_z]\hat{\rho}(t)dt + \gamma\bar{n}\mathcal{D}[b_z^{\dagger}]\hat{\rho}(t)dt \\ & + \sum_{\lambda} \mathcal{D}[s_{z\lambda}]\hat{\rho}(t)dt + \sqrt{\eta_{z\lambda_0}}\mathcal{H}[s_{z\lambda_0}]\hat{\rho}(t)dW(t), \end{aligned} \quad (127a)$$

$$\mathcal{D}[s]\hat{\rho} = s\hat{\rho}s^{\dagger} - \frac{1}{2}(s^{\dagger}s\hat{\rho} + \hat{\rho}s^{\dagger}s), \quad (127b)$$

$$\mathcal{H}[s]\hat{\rho} = [s - \text{tr}(s\hat{\rho})]\hat{\rho} + \hat{\rho}[s - \text{tr}(s\hat{\rho})]^{\dagger}, \quad (127c)$$

where  $s_{z\lambda} = -i\sqrt{2\pi K_{zz}^{\lambda}}(b_z + b_z^{\dagger})$ . The second and third term in (127a) describe damping and decoherence effects due to the residual gas, while the fourth term describes diffusion due to the coupling to the electromagnetic field. The last term effects conditioning on the homodyne measurement, where  $W$  is a classical Wiener process corresponding to the innovation process denoted as  $\epsilon$  in the main text. We can (formally) write for the Wiener increments  $dW(t) = \epsilon(t)dt$ .

In deriving this equation, we assumed that the measured mode  $h$  couples only weakly to the particle motion in  $x$ - and  $y$ -direction and thus neglected measurement terms scaling with  $\sqrt{\eta_{x\lambda_0}}$  and  $\sqrt{\eta_{y\lambda_0}}$  (which show up as sharp resonances in the measured spectrum, see Figure 1b in main text). Also note that this formulation of

mechanical damping due to residual gas does not strictly correspond to Brownian motion damping as used above. The two formulations are connected by a rotating-wave approximation (see [GZ04]), which is a good approximation for oscillators with a high quality factor.

For Gaussian systems, such as ours, it was shown [Bel95; EB05] that the evolution of the conditional quantum state  $\hat{\rho}$  can be mapped to the well-known *Kalman–Bucy filter* from classical estimation theory. In this case,  $\hat{\rho}$  is completely determined by the first and second moment of  $\mathbf{z} = [r_z, p_z]$  (an operator in the Schrödinger picture), which we denote as

$$\hat{\mathbf{z}}(t) = \text{tr}[\hat{\rho}(t)\mathbf{z}], \quad (128a)$$

$$\hat{\Sigma}(t) = \text{Re} \left\{ \text{tr}[\hat{\rho}(t)\mathbf{z}\mathbf{z}^T] \right\} - \hat{\mathbf{z}}(t)\hat{\mathbf{z}}^T(t). \quad (128b)$$

Using the definitions from Section 4.7.5 the dynamical equations determining the evolution of  $\hat{\mathbf{z}}(t)$  and  $\hat{\Sigma}(t)$  can be written as the classical Kalman–Bucy filter [Bel95; Bel98; DJ99; EB05]

$$\dot{\hat{\mathbf{z}}}(t) = \mathbf{A}\hat{\mathbf{z}}(t) + \mathbf{b}u(t) + \hat{\mathbf{k}}(t)[\zeta(t) - \mathbf{c}^T\hat{\mathbf{z}}(t)], \quad (129a)$$

$$\dot{\hat{\Sigma}}(t) = \mathbf{A}\hat{\Sigma}(t) + \hat{\Sigma}(t)\mathbf{A}^T + \mathbf{N} - [\hat{\Sigma}(t)\mathbf{c} + \mathbf{M}][\hat{\Sigma}(t)\mathbf{c} + \mathbf{M}]^T, \quad (129b)$$

$$\dot{\hat{\mathbf{k}}}(t) = \hat{\Sigma}(t)\mathbf{c} + \mathbf{M}, \quad (129c)$$

where  $\zeta(t) \in \mathbb{R}$  denotes the measurement signal resulting from a measurement of  $y_{\lambda_0}^{\text{out}}(t)$ . These equations are correct for general Gaussian systems that can be described by quantum Langevin equations of the form (123), in particular also for systems where  $\mathbf{M} \neq 0$ . Note that although these equations are derived from a quantum description of the experiment, they are classical (stochastic) differential equations that involve classical quantities (the moments of  $\mathbf{z}$  under  $\hat{\rho}$ , the measurement signal  $\zeta$ ) only and can thus be readily implemented on a classical signal processor.

The results presented above show that the quantum filtering problem for Gaussian systems described by a quantum Langevin equation (123a) (together with the output equation (123b)) is formally equivalent to the classical filtering problem for the corresponding classical Langevin equation when using the correct noise properties (126) that arise from a quantum description. For the details of the derivation in the framework of quantum filtering see [HH17].

Additional to the approach taken in quantum filtering theory [BVJ07], complementary approaches exist to describe the dynamics of a (Gaussian) quantum system under continuous measurement. These include a fully Gaussian treatment in a phase-space description [GLS16] and the well-known quantum trajectories formalism [Car93] which describes the stochastic evolution of the wave function.

#### 4.7.6 Optimal feedback cooling

Online (optimal) estimation [Kal60] and automatic control [Kal+60; Ste94] techniques have become ubiquitous in modern technology [DFT13; ÅW13; MP09]. Due to the required level of control they are also becoming an increasingly important tool in quantum research and quantum technologies.

Here we design an optimal feedback controller in order to cool the particle's motion into the quantum ground state. For linear (quantum) systems driven by Gaussian white noise, an optimal output feedback law can be obtained by solving the linear quadratic gaussian regulator (LQG) problem. Its solution consists of the combination of a Kalman filter and a linear quadratic regulator, which can be designed independently of each other, as stated by the separation principle [BHo8], breaking the design of the LQG down into an estimation step and a control step. The regulator computes the optimal feedback for a given state by solving an optimization problem in order to minimize the energy of the system. Since the system state is in general not completely measurable, a Kalman filter is designed to provide

optimal state estimates based on noisy measurements. The basis of the design process of the LQG is the mathematical description of the experimental setup detailed in the sections above. The experimental characterization of the involved quantities is described in detail in Section 4.7.7.

### Discretized time evolution

While physical systems are usually considered in continuous time, estimation and control algorithms are necessarily implemented in a time-discrete manner. The resulting effects of the discretization process can be considered for linear dynamical systems by deriving a time-discrete formulation of the state-space model, evaluating it at times  $t_k = kT_s$ . To this end, we integrate (123) over a sampling time  $T_s = t_{k+1} - t_k$  (which we assume is short on all system time scales), defining  $\mathbf{z}_k = \mathbf{z}(t_k)$ ,  $\mathbf{u}_k = \mathbf{u}(t_k)$ , and the fundamental solution  $\Phi(t) = \exp(\mathbf{A}t)$ . We find

$$\begin{aligned} \mathbf{z}(t_{k+1}) &= \Phi(T_s)\mathbf{z}(t_k) + \int_{t_k}^{t_{k+1}} d\tau \Phi(t_{k+1} - \tau)[\mathbf{b}\mathbf{u}(\tau) + \mathbf{w}(\tau)] \\ &= \mathbf{A}_d\mathbf{z}(t_k) + \mathbf{b}_d\mathbf{u}(t_k) + \bar{\mathbf{w}}_k, \end{aligned} \quad (130)$$

where we assumed that  $\mathbf{u}(t)$  is piecewise constant over the sampling time, i.e.,  $\mathbf{u}(t) = \mathbf{u}_k$  for  $t \in [t_k, t_{k+1}]$  (zero-order hold used as a model for the digital-to-analog converter) and we introduced the matrices  $\mathbf{A}_d = \exp(\mathbf{A}T_s)$  and  $\mathbf{b}_d = \int_0^{T_s} \exp(\mathbf{A}\tau) \mathbf{b} d\tau$ . The discretized noise process  $\bar{\mathbf{w}}_k$  is given by  $\bar{\mathbf{w}}_k = \int_{t_k}^{t_{k+1}} d\tau \Phi(t_{k+1} - \tau)\mathbf{w}(\tau)$ .

To describe the measurement, we define the time-averaged operator  $\bar{y}_{\lambda_0,k}^{\text{out}} := \frac{1}{T_s} \int_{t_k}^{t_{k+1}} ds y_{\lambda_0}^{\text{out}}(s)$  together with a corresponding expression for  $\bar{y}_{\lambda_0,k}$ . Assuming that  $\mathbf{z}(t)$  likewise is approximately constant over the sampling time  $T_s$  we find the discretized quantum state-space model

$$\mathbf{z}_{k+1} = \mathbf{A}_d\mathbf{z}_k + \mathbf{b}_d\mathbf{u}_k + \bar{\mathbf{w}}_k, \quad (131a)$$

$$\bar{y}_{\lambda_0,k}^{\text{out}} = \mathbf{c}^T\mathbf{z}_k + \bar{y}_{\lambda_0,k}. \quad (131b)$$

In analogy to (126) the (cross-) correlations for the noise processes  $\bar{\mathbf{w}}_k$  and  $\bar{y}_{\lambda_0,k}$  are given by

$$\langle \bar{y}_{\lambda_0,k} \bar{y}_{\lambda_0,k'} \rangle = \bar{R} \delta_{kk'} = (1/T_s) \delta_{kk'}, \quad (132a)$$

$$\text{Re} \langle \bar{\mathbf{w}}_k \bar{y}_{\lambda_0,k'} \rangle = \bar{\mathbf{M}} \delta_{kk'} = 0, \quad (132b)$$

$$\text{Re} \langle \bar{\mathbf{w}}_k \bar{\mathbf{w}}_{k'}^T \rangle = \bar{\mathbf{N}} \delta_{kk'} \approx \mathbf{N} T_s \delta_{kk'}, \quad (132c)$$

where the relation  $\bar{\mathbf{N}} \approx \mathbf{N} T_s$  is true only if the sampling time is much shorter than all system time scales.

### Discrete-time Kalman Filter

The Kalman filter for the state-space system (131) is given by [EB03]

$$\hat{\mathbf{z}}_{k+1} = \mathbf{A}_d\hat{\mathbf{z}}_k + \mathbf{b}_d\mathbf{u}_k + \hat{\mathbf{k}} \left( \zeta_k - \mathbf{c}^T\hat{\mathbf{z}}_k \right), \quad (133)$$

where  $\zeta_k$  is the discretized measurement signal corresponding to  $\bar{y}_{\lambda_0,k}^{\text{out}}$  and the observer gain  $\hat{\mathbf{k}}$  of the Kalman filter results from

$$\hat{\mathbf{k}} = \left( \mathbf{A}_d \hat{\Sigma}_d^{\text{ss}} \mathbf{c} + \bar{\mathbf{M}} \right) \left( \mathbf{c}^T \hat{\Sigma}_d^{\text{ss}} \mathbf{c} + \bar{R} \right)^{-1}. \quad (134)$$

The (time-discrete) steady state error covariance matrix  $\hat{\Sigma}_d^{\text{ss}}$  is computed by solving the discrete algebraic Riccati equation

$$\hat{\Sigma}_d^{\text{ss}} = \mathbf{A}_d \hat{\Sigma}_d^{\text{ss}} \mathbf{A}_d^T + \bar{\mathbf{N}} - \left( \mathbf{A}_d \hat{\Sigma}_d^{\text{ss}} \mathbf{c} + \bar{\mathbf{M}} \right) \left( \mathbf{c}^T \hat{\Sigma}_d^{\text{ss}} \mathbf{c} + \bar{R} \right)^{-1} \left( \mathbf{A}_d \hat{\Sigma}_d^{\text{ss}} \mathbf{c} + \bar{\mathbf{M}} \right)^T. \quad (135)$$

Note that the Kalman filter (133) with the observer gain (134) and the discrete algebraic Riccati equation (135) is the time-discrete description of the Kalman–Bucy filter (129) and therefore describes the motional quantum state of the nanosphere conditioned on the measurement, as shown in Section 4.7.5. In the limit of  $T_s \rightarrow 0$  we recover the Kalman–Bucy equations (129) and  $\hat{\Sigma}_d^{ss} \rightarrow \hat{\Sigma}^{ss}$ . As written, the Kalman filter is also valid for general systems with  $\bar{\mathbf{M}} \neq 0$ .

### Linear Quadratic Gaussian Regulator

The concept of optimal feedback control consists of finding the optimal control inputs such that the system is stably operated at minimum cost. The optimal control input  $u_k$  is obtained by minimizing the expected cost

$$J(u_k) = \lim_{N \rightarrow \infty} \left\langle \frac{1}{N} \sum_{k=0}^{N-1} \left( \mathbf{z}_k^T \mathbf{Q} \mathbf{z}_k + r u_k^2 \right) \right\rangle \quad (136)$$

with respect to (131), where  $\langle \cdot \rangle$  refers to the quantum expectation value with respect to the initial state of the system and environment. Here, the first term with weighting matrix  $\mathbf{Q} = \text{diag} \left( \frac{\Omega_z}{2}, \frac{\Omega_z}{2} \right)$  represents the total energy of the particle while the second term penalizes the required control effort scaled by  $r = \Omega_z / g_{fb}^2$ , with the feedback gain  $g_{fb}$  in units of  $\text{rad s}^{-1}$ . The control law that minimizes the cost function (136) is given by [EB03]

$$u_k = -\mathbf{k}^T \hat{\mathbf{z}}_k. \quad (137)$$

The feedback vector  $\mathbf{k}^T$  is calculated by

$$\mathbf{k}^T = \left( r + \mathbf{b}_d^T \Omega^{ss} \mathbf{b}_d \right)^{-1} \mathbf{b}_d^T \Omega^{ss} \mathbf{A}_d \quad (138)$$

where  $\Omega^{ss}$  is determined by the discrete algebraic Riccati equation

$$\Omega^{ss} = \mathbf{Q} + \mathbf{A}_d^T \Omega^{ss} \mathbf{A}_d - \mathbf{A}_d^T \Omega^{ss} \mathbf{b}_d \left( r + \mathbf{b}_d^T \Omega^{ss} \mathbf{b}_d \right)^{-1} \mathbf{b}_d^T \Omega^{ss} \mathbf{A}_d. \quad (139)$$

The solution of the quantum LQG problem is thus formally identical to the one of the classical LQG problem for a classical state-space model of the form (131) and cost function of the form (136) (when interpreting  $\langle \cdot \rangle$  as an appropriate classical expectation value). In general, the observer gain  $\hat{\mathbf{k}}$  and the feedback vector  $\mathbf{k}^T$  are time variant and they are calculated by solving the discrete Riccati equation for  $\hat{\Sigma}_k$  forwards in time and for  $\hat{\Sigma}_k$  backwards in time for a finite time horizon. If the time goes to infinity, the stationary solution  $\hat{\Sigma}_{k+1} = \hat{\Sigma}_k = \hat{\Sigma}_d^{ss}$  and  $\Omega_{k+1} = \Omega_k = \Omega^{ss}$  of the corresponding discrete algebraic Riccati equation has to be calculated (see (139)) and (135)). Thus, the LQG becomes time invariant. The transfer function of the time invariant LQG, combining (137) and the Kalman filter (133), is given by

$$G(z) = \frac{u_z(z)}{\zeta_z(z)} = -\mathbf{k}^T \left( z\mathbf{I} - \left( \mathbf{A}_d - \mathbf{b}_d \mathbf{k}^T - \hat{\mathbf{k}} \mathbf{c}^T \right) \right)^{-1} \hat{\mathbf{k}} \quad (140)$$

where  $u_z(z)$  and  $\zeta_z(z)$  are the  $\mathcal{Z}$ -transform of the control input and measurement signal,  $u_z(z) = \mathcal{Z}\{u_k\}$  and  $\zeta_z(z) = \mathcal{Z}\{\zeta_k\}$ , respectively, and  $\mathbf{I}$  is the identity matrix. The time discrete transfer function (140) is implemented as a digital filter with a sampling time of  $T_s = 32 \text{ ns}$  on the Red Pitaya board which is equipped with a Xilinx Zynq 7010 FPGA. The effects of the low frequency  $1/f$  phase noise and the intrinsic delay of the controller of about 300ns are negligible in a fairly large frequency band around resonance, and at most of the feedback gains we are operating at. For this reason we do not include these effects into the model, in favour of a larger dynamic range for the output. We observe, however, a drift in

the oscillation frequency for increasing feedback gains which is caused presumably by nonlinear effects not captured by the mathematical model. This error leads to the appearance of color in the innovation sequence and a decreasing cooling performance (Supplementary Figure 26c). The calibration of the measurement signal and feedback force, as well as the characterization of the noise processes  $\bar{y}_{\lambda_0,k}$  and  $\bar{w}_k$  are presented in the following section.

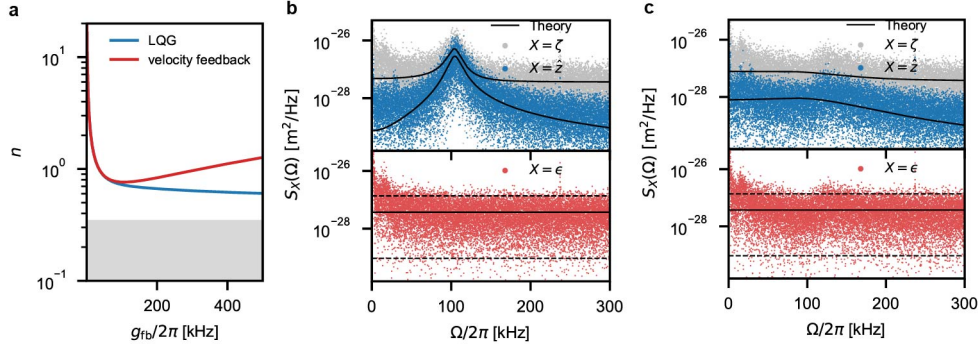


**Figure 26: LQG performance.** Comparison of the analytic solution of the occupation for optimal (LQG) and non-optimal (velocity) control and estimation methods. Despite the use of an optimal state estimator the closed-loop solution of the velocity feedback (red) is diverging for high feedback gains, contrary to the LQG (blue). This shows the importance of using the complete state vector in the feedback in order to minimize the energy of the system. **b - c**, Power spectral densities of the measurement (gray), Kalman estimation (blue), innovation (red) and the analytic solution of the mathematical description (black line) at  $g_{fb}/2\pi = 16$  kHz and  $g_{fb}/2\pi = 180$  kHz. The black lines in the innovation plot indicate the white noise model (solid) and the 95% confidence region of the expected  $\chi^2$  distribution (dashed) [Wie+15].

### Colored Noise Model

Although the effects of low frequency noise are negligible compared to the white noise level, we have seen that this model mismatch is amplified by the controller, and would eventually be limiting the closed-loop performance at feedback gains larger than 200kHz. For this reason, we also extend the state-space model (123) by an appropriate colored noise model. The Kalman filter is designed on the basis of an extended state-space model given by:

$$\dot{\tilde{\mathbf{z}}}(t) = \tilde{\mathbf{A}}\tilde{\mathbf{z}}(t) + \tilde{\mathbf{b}}u(t) + \tilde{\mathbf{G}}\tilde{\mathbf{w}}(t), \quad \tilde{\mathbf{x}}(0) = \tilde{\mathbf{x}}_0 \quad (141a)$$

$$y_{\lambda_0}^{\text{out}}(t) = \tilde{\mathbf{c}}^T\tilde{\mathbf{z}}(t) + y_{\lambda_0}(t) \quad (141b)$$

with the extended state vector  $\tilde{\mathbf{z}}(t) = [\mathbf{z}(t)^T \quad \boldsymbol{\xi}(t)^T]^T$ , and the process noise input vector  $\tilde{\mathbf{w}}(t) = [w(t) \quad \mu(t)]^T$ , where  $\mu(t)$  is white Gaussian noise, which drives the chosen noise model. The extended system matrix  $\tilde{\mathbf{A}}$ , the extended input vector of the control input  $\tilde{\mathbf{b}}$ , the extended input matrix of the process noise  $\tilde{\mathbf{G}}$  and the extended output vector  $\tilde{\mathbf{c}}^T$  are defined as

$$\tilde{\mathbf{A}} = \begin{bmatrix} \mathbf{A} & \mathbf{0} \\ \mathbf{0} & \mathbf{A}_n \end{bmatrix}, \quad \tilde{\mathbf{b}} = \begin{bmatrix} \mathbf{b} \\ \mathbf{0} \end{bmatrix}, \quad \tilde{\mathbf{G}} = \begin{bmatrix} \mathbf{g} & \mathbf{0} \\ \mathbf{0} & \mathbf{g}_n \end{bmatrix}, \quad \tilde{\mathbf{c}}^T = [\mathbf{c}^T \quad \mathbf{c}_n^T],$$

with the dynamic matrix of the noise model  $\mathbf{A}_n$ , the input vector of the noise model  $\mathbf{g}_n$  and the output vector of the noise model  $\mathbf{c}_n^T$ . As proposed in [Wie+15], Brownian noise is a good approximation for the non-white amplitude and phase noise of a laser, which is modeled by the state-space system (141) with  $\mathbf{A}_n = 0$  and  $\mathbf{g}_n = \mathbf{c}_n^T = 1$ . This model (green line in Supplementary Figure 27a) provides a good approximation of the low frequency noise that we observe. Nevertheless, it has a limited hardware feasibility as the magnitude of the noise becomes large in the



lower frequency range and the slow dynamics lead to numerical issues in the fixed-point implementation, resulting in drift and overflows, and can even destabilize the closed-loop system. For a practical hardware implementation we model the noise as a low-pass filter driven by white noise  $\mu(t)$ . Thereby,  $\mathbf{A}_n$ ,  $\mathbf{g}_n$  and  $\mathbf{c}_n^T$  are obtained from the state-space representation of the low-pass filter  $G_{lp}(s) = 1/(1 + s/\omega_c)$ , with the cutoff frequency  $\omega_c = 3.5$  kHz. In Supplementary Figure 27b, we show the power spectral densities of the measurement (gray), the Kalman estimation (blue), the innovation (orange) in good agreement with the analytic solution of the mathematical description (black line) of the LQG based on the proposed low-pass noise model for  $g_{fb}/2\pi = 40$  kHz. Nevertheless, for high gain feedback  $g_{fb}/2\pi = 150$  kHz (Supplementary Figure 27c) the performance decreases significantly due to the reduced dynamic range of the hardware implementation to fit the more complex filter on the FPGA. The use of a more powerful hardware would overcome such implementation issues of the Kalman filter using colored noise models and has the potential to further increase the performance.

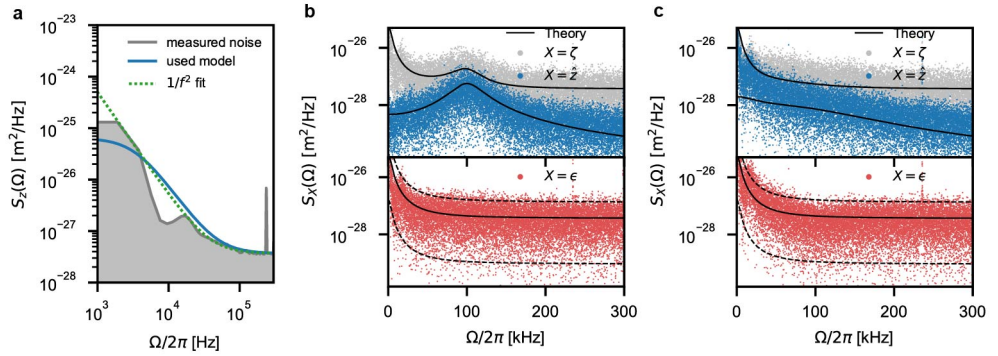


**Figure 27: Colored noise model.** **a**, Comparison of the power spectral densities of the Brownian noise model (green) and the low-pass noise model (blue) the power spectral densities of the innovation (gray). **b - c**, Power spectral densities of the measurement (gray), Kalman estimation (blue), innovation (red) and the analytic solution of the mathematical description (black line) at  $g_{fb}/2\pi = 40$  kHz and  $g_{fb}/2\pi = 150$  kHz. The extension with an appropriate noise model brings along more accurate estimates of the state. The black lines in the innovation plot indicate the colored noise model (solid) and the 95% confidence region of the expected  $\chi^2$  distribution (dashed) [Wie+15].

### FPGA implementation

The designed LQG is implemented on a Red Pitaya board equipped with a Xilinx Zynq 7010 FPGA. The base design of the Vivado Design Suite project of the Red Pitaya is based on the tutorial provided by Anton Potočník [Pot16], modified to suit our purposes. The time-invariant transfer function of the LQG (140) is implemented in MATLAB/SIMULINK as digital filter with the Xilinx System Generator for DSP. Thereby, hardware-in-the-loop simulations can be performed in MATLAB/SIMULINK, capturing the exact behavior of the real implementation on the FPGA of the Red Pitaya. This provides the possibility to quickly identify and fix issues with the fixed-point arithmetic and quantization. The Xilinx System Generator for DSP allows automatic code generation of the designed filter, considering the resource limitations and timing constraints of the FPGA. The obtained VHDL code (IP Core) is inserted in the base design of the FPGA in the Vivado Design Suite and the bitstream file of the FPGA is generated. Parameters can be changed online via communication with the AXI-bus. The low frequency output noise of the Red Pitaya has been improved by removing the 2 resistors and disconnecting the noisy output offset [Lne16].



#### 4.7.7 Identification of the model parameters

The identification of the system parameters is crucial for a properly tuned model based Kalman filter and linear quadratic regulator (LQR) design. Direct measurement of most of the system parameters depends on a proper calibration of the measurements.

##### *Calibration of the measurement transduction coefficient*

In this section, we measure the calibration factor ( $C_{mV}$  [m/V]) for our homodyne detection. One possibility is thermometry in an environment in which the nanoparticle thermalizes to a room-temperature gas [Heb+18]. Given the high resolution of our position measurement, the limited dynamic range of our detector and data acquisition board this method cannot be implemented directly, but would require multiple steps of amplification. In addition, the accuracy of this approach was verified only up to a factor of 2 [Teb+20]. To reconstruct the relation between the displacement of the particle in meters and the homodyne time traces in volts we take advantage of the simultaneous out-of-loop measurement of the particle's energy via Raman thermometry (see Section 4.7.8) at different feedback gains. To minimize the effects of noise squashing [Pog+07] due to imprecision noise driving the motion of the particle via the feedback, we restrict calibration to low values of the feedback gain. We perform the calibration in an iterative way, where we alternate evaluation of the calibration factor and update of the controller setting. The variance of the particles motion can be estimated from a measurement of energy in units of motional quanta  $\langle n \rangle$  by  $\langle z^2 \rangle = z_{zpf}^2 (2 \langle n \rangle + 1)$ . We compare this value with the variance of the signal  $V(t)$  obtained from the homodyne noisy position measurement:

$$\langle V^2 \rangle = C_{mV}^{-2} (\langle z^2 \rangle + \langle v^2 \rangle) = \int_0^{+\infty} S_z(\Omega) \frac{d\Omega}{2\pi}. \quad (142)$$

Where  $v(t)$  is the measurement noise and  $C_{mV}$  the calibration factor converting the measured voltage into the corresponding displacement in meters. We fit a linear function (Supplementary Figure 28b), where the offset indicates the measurement noise and the slope determines the calibration factor:

$$C_{mV} = (8.0 \pm 0.3) \times 10^{-9} \text{ m/V} \quad (143)$$

We also verify the consistency of the measured calibration factor by considering all transduction coefficients composing the measurement. The phase-shift induced by the particle's displacement on to the fraction of collected light defines the measurement strength of our detection (what in cavity-optomechanics you would call  $2G/\kappa$  [AKM14]):

$$\chi = \frac{\partial \varphi}{\partial z} = \sqrt{\frac{\eta_{d,c}}{\eta_{d,c}^*}} \sqrt{\left(A^2 + \frac{2}{5}\right)} \kappa \quad [\text{rad/m}] \quad (144)$$

In a homodyne detection the signal light beam is interfered with a strong local oscillator, and phase shifts are transduced to a power variation by  $G_{\text{HOM}} = 2\sqrt{P_S P_{\text{LO}}}$  [W/rad], where  $P_S = P_{\text{scatt}} \eta^* / \eta_{d,q}^*$  is the signal light just before the detector,  $P_{\text{LO}}$  is the local oscillator power,  $\eta_d^*$  the photon detection efficiency and  $\eta_{d,q}^*$  the detector quantum efficiency as defined in Section 4.7.3. Optical power is converted into an electron current at the photodiodes via the detector responsivity is  $R_{\text{det}} = -e \eta_{d,q} / \hbar \omega_0$  [A/W], and finally the transimpedance gain  $g_t = 250 \times 10^3$  [V/A] converts this current to a voltage. Impedance matching to the detector's  $50 \Omega$  output attenuates the signal by 3 dB. We can now convert measured voltage to meters by:

$$C_{mV} = \frac{\hbar \omega_0}{(-e) \eta_{d,q} g_t \sqrt{P_S P_{\text{LO}}}} = 7.8 \times 10^{-9} \text{ m/V} \quad (145)$$

which is in good agreement with the measured value.

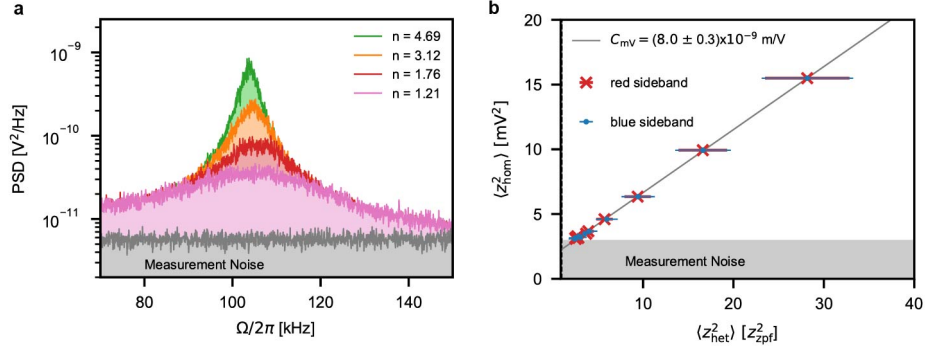


**Figure 28: Position calibration.** **a**, Measurement of the displacement power spectral densities at different feedback gains and labelled by the occupation measured independently by Raman thermometry. **b**, Integrated voltage variance from the homodyne measurement plotted as a function of position variance estimated from the heterodyne measurement. Red crosses and blue dots represent the position variance estimated by the Stokes and anti-Stokes sidebands respectively. A linear fit provides the calibration factor for the homodyne measurement.

### Evaluation of the measurement noise

From the calibrated PSD, we can measure the measurement noise level at the relevant frequencies. While the detector bandwidth is about 75 MHz, the Red Pitaya has a measurement bandwidth of 31.25 MHz. We include an anti-aliasing analog low pass filter with cut off at 11 MHz, below the sampling Nyquist frequency. This allows to minimize the aliasing of high frequency noise at the relevant frequencies. We measure the imprecision noise  $S_z^{\text{imp}}$  dominated by photon shot noise of the local oscillator by covering the signal beam. This results in a variance of measurement noise (assuming a white noise model) of

$$\sigma_z^2 = S_z^{\text{imp}} \frac{f_s}{2} = (5.4 \pm 0.2) \times 10^{-21} \text{ m}^2 \quad (146)$$

where  $f_s = 1/T_s = 31.25$  MHz is Red-Pitaya sampling frequency. The measurement noise can likewise be estimated by evaluating the signal variance from independently characterized experimental parameters. This includes contributions of photon shot noise and detector dark noise:

$$\langle V^2 \rangle = \left[ \left( \frac{g_t}{2} e \sqrt{\frac{P_{\text{LO}} \eta_q}{\hbar \omega_0}} \right)^2 + \left( \frac{g_t}{2} \text{NEC} \right)^2 \right] f_s \quad (147)$$

where the factor 2 below  $g_t$  arises from the coupling of the detector to  $50 \Omega$  load and NEC is the noise equivalent current. The noise equivalent position variance is therefore:

$$\sigma_z^2 = C_{\text{mV}}^2 \langle V^2 \rangle = 5.3 \times 10^{-21} \text{ m}^2 \quad (148)$$

in good agreement with the measured value.

### Calibration of the applied force

With the position calibration at hand, we can further map the applied voltage to the control electrode on the force acting on the charged nanoball. We drive the particle by applying a sinusoidal signal of known amplitude and frequency. In the case of strong off-resonant drive force  $F_d(t)$ , with spectral density  $S_F^d$ , if at a particular drive frequency  $\Omega_d$ , having  $S_F^d(\Omega_d) \gg S_F^{\text{tot}}(\Omega_d)$ , the driven motion is related to the drive by:

$$S_z(\Omega_d) = S_F^d(\Omega_d) |m(\Omega_d)|^2 + S_z^{\text{imp}} \quad (149)$$

which in the simple case of  $F_d(t) = F_{d0} \sin(\Omega_d t)$ , and  $\Omega_d/\gamma \gg 1$  results in:

$$\langle z_d^2 \rangle = \frac{1}{2\pi} \int_{\Omega_d - \epsilon}^{\Omega_d + \epsilon} (S_z(\Omega) - S_z^{\text{imp}}) d\Omega = \frac{\langle F_d^2 \rangle}{(m(\Omega_z^2 - \Omega_d^2))^2} = \frac{F_{d0}^2/2}{(m(\Omega_z^2 - \Omega_d^2))^2}. \quad (150)$$

The variance of the displacement is again obtained by integrating over the symmetrized spectral density around the driving frequency subtracting the background imprecision noise. As the driving force is proportional to the applied voltage  $F_d(t) = C_{NV}V(t)$ , we can use the relation (150) to calibrate this to the applied force in newton and identify the transduction coefficient  $C_{NV}$ . We perform the measurement at different values of drive frequency and amplitude, and plot the standard deviation of the calibrated force  $\sqrt{\langle F_v^2 \rangle} = m\sqrt{\langle z^2 \rangle (\Omega_z^2 - \Omega_d^2)}$  versus the standard deviation of the applied signal. The slope gives a factor of  $C_{NV} = (1.98 \pm 0.06) \times 10^{-15} \text{ N/V}$ . The measurements at the two different frequencies result in perfectly overlapping values (Supplementary Figure 29).

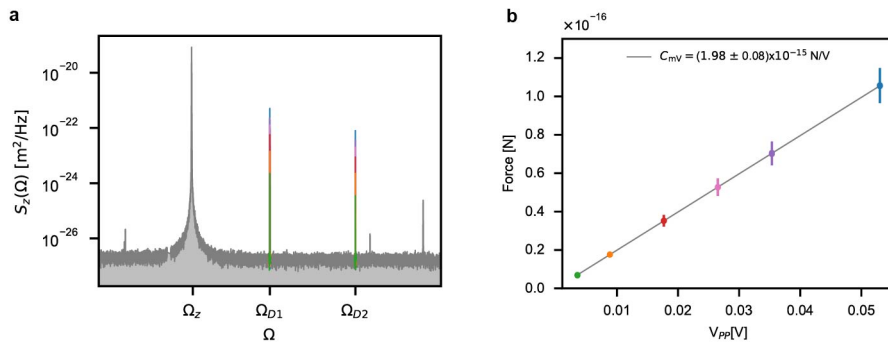


**Figure 29: Force calibration.** To map the applied voltage [V] to a force [N], we drive the particle with a series of sinusoidal signals of different amplitude and frequency and measure the particles response in the calibrated position PSD.

### Measurement of the thermal and backaction decoherence rates

We define the decoherence rates originating from thermal force noise and measurement backaction as the average rate of phonons delivered to the particle. To determine the decoherence rate induced by measurement backaction and interactions with the thermal environment, we perform a set of re-heating measurements of the particle's energy. We do so by switching off the feedback, observing the relaxation trace. Ensemble averaging over many cycles allows to extract the average heating rates [Gie+14; Jai+16] (Supplementary Figure 30a). To distinguish contributions from photon recoil (backaction) and gas collisions (thermal force), this is done at various pressures (Supplementary Figure 30b). When switching the feedback off, the energy  $E$ , or level of excitation of the oscillator  $n = E/\hbar\Omega_z$  increases on average as:

$$n(t) = n_0 + n_{\text{th}}(1 - e^{-\gamma_{\text{th}} t}) + n_{\text{ba}}(1 - e^{-\gamma_{\text{ba}} t}) \stackrel{t \ll \frac{1}{\gamma_{\text{th,ba}}}}{\approx} n_0 + n_{\text{th}}\gamma_{\text{th}} t + n_{\text{ba}}\gamma_{\text{ba}} t = n_0 + (\Gamma_{\text{th}} + \Gamma_{\text{ba}})t, \quad (151)$$

where  $n_0$  is the initial occupation and  $n_{\text{th}}$  and  $n_{\text{ba}}$  are the occupations associated to the thermal and optical baths respectively,  $\gamma_{\text{th}}$  is the gas damping and  $\gamma_{\text{ba}}$  the radiation damping that results from relativistic effects [Nov17]. The decoherence rates are now written as:

$$\Gamma_{\text{th}} = \gamma_{\text{th}} n_{\text{th}} \quad \text{and} \quad \Gamma_{\text{ba}} = \gamma_{\text{ba}} n_{\text{ba}}, \quad (152)$$

The thermal heating rate is derived by considering a thermal bath of energy  $E_{\text{th}} = k_B T$  and temperature of 292 K and a damping rate given by [BCF90]:

$$\gamma_{\text{th}} = \frac{6\pi\eta_v r}{m} \left( \frac{\text{Kn}}{0.619 + \text{Kn}} \right) \left( 1 + \frac{0.310\text{Kn}}{\text{Kn}^2 + 1.152\text{Kn} + 0.785} \right), \quad (153)$$

where  $\eta_v$  is the dilute gas shear viscosity,  $\text{Kn} = \lambda_{\text{gas}}(P)/L$  the Knudsen number,  $\lambda_{\text{gas}}(P)$  the pressure dependent molecule mean free path,  $L = V/A = 4r/3$  the particle's characteristic length,  $V$  its volume and  $A$  its cross section. In the low pressure limit,  $\text{Kn} \gg 1$ , eq. (153) can be approximated by:

$$\gamma_{\text{th}} = \frac{64}{3} \frac{r^2 P}{m \bar{v}_{\text{gas}}}, \quad (154)$$

where  $\bar{v}_{\text{gas}} = \sqrt{8RT/(\pi m_{\text{gas}})}$  is the mean gas velocity,  $r$  and  $m$  the particle radius and mass respectively,  $P$  the pressure (expressed in Pascal, SI),  $R = k_B N_A = 8,3144 \text{ J}/(\text{mol K})$  the universal gas constant, and  $m_{\text{gas}}$  the molar mass of the gas. Up to 1 mbar, this approximation exhibits a deviation of less than  $10^{-2}$  from the real value for the particles we are considering. Following the treatment by Sebersson and Robicheaux [SR20], we can also derive the contribution of photon recoil to the heating rate:

$$\Gamma_{\text{ba},z} = \left( A^2 + \frac{2}{5} \right) \frac{\omega_0 P_{\text{scatt}}}{2\Omega_z m c^2} \quad (155)$$

At a pressure of  $1.6 \times 10^{-8}$  mbar we directly measure a minimal total heating rate

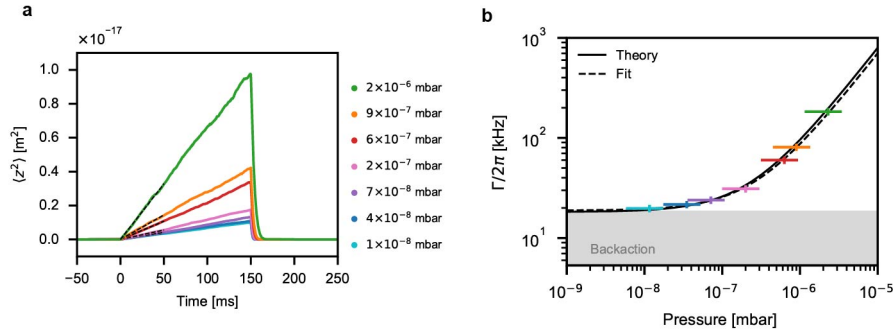


**Figure 30: Heating rate.** The backaction and thermal contribution to the force noise are directly measured by performing re-heating measurements. We restrict the measurement to short (150 ms) re-heating periods. Longer ring up measurements may lead to the loss of the particle when mainly coupled to the high temperature photon bath. **a**, At each pressure we release the feedback and observe the heating dynamics of the particle 1000 times. The ensemble average of the variance of these traces represents the average energy increase rate. **b**, Pressure dependence of the heating rate. At pressures below  $1 \times 10^{-8}$  mbar the contribution to the total force noise is dominated by the photon recoil, or measurement backaction. Horizontal error bars are given by the 50% accuracy specified by the pressure gauge producer.

of:

$$\Gamma_{\text{tot}} = \Gamma_{\text{th}} + \Gamma_{\text{ba}} = 2\pi \cdot (19.7 \pm 1.5) \text{ kHz} \quad (156)$$

With a linear fit to the pressure dependent data (Supplementary Figure 30b) we can extrapolate the contributions of thermal noise and measurement backaction at all pressures, finding them in excellent agreement with the values estimated using equations 154 and 155 in our experimental settings (Supplementary Figure 30b). At the minimal operating pressure  $9.2 \times 10^{-9}$  mbar, we find the process noise to be (for the Kalman filter)

$$\sigma_F^2 = \langle F_{\text{tot}}^2 \rangle = S_F^{\text{tot}} \frac{f_s}{2} = 4\hbar\Omega_z m \Gamma_{\text{tot}} \frac{f_s}{2} = (1.5 \pm 0.1) \times 10^{-33} \text{ N}^2 \quad (157)$$

#### 4.7.8 Raman scattering thermometry

The optomechanical interaction exhibits both energy and momentum exchange between the oscillating particle and the electromagnetic field. While elastic scattering (Rayleigh) leave the energy of the scattered photons unaltered, the side-bands of  $n^{\text{th}}$  order in the absorption and fluorescence spectra due to inelastic scattering (Raman) are interpreted as transitions between the quantized energy levels of the harmonic oscillator [JD96]. The elastic and inelastic scattering rates can be calculated using Fermi's golden rule:

$$\Gamma_{n \rightarrow n+\Delta n} = \frac{2\pi}{\hbar} M_{n,n+\Delta n} \rho(n+\Delta n) \quad (158)$$

where  $\rho(n+\Delta n)$  the population density of occupation  $n+\Delta n$  state of the particle motion and  $M_{n,n+\Delta n}$  the transition matrix element given by the cross term in the dipole-field interaction [RI+11b; SS20]:

$$M_{n,n+\Delta n} = |\langle n+\Delta n | \hat{H}_I | n \rangle|^2 \propto |\langle n+\Delta n | (\chi z_{\text{zpf}}(b+b^\dagger))^{\Delta n} | n \rangle|^2 = (\chi z_{\text{zpf}})^{2\Delta n}. \quad (159)$$

Here  $\hat{H}_I \propto \hat{a} e^{-i\chi \hat{z}} + \text{H.c.}$  with  $\hat{z} = z_{\text{zpf}}(\hat{b} + \hat{b}^\dagger)$ , and  $\chi$  the mean momentum transferred to the particle by a photon scattered into the detection mode [JD96]. As the transition matrix element is symmetric, the asymmetry of the scattering rates into the Stokes and anti-Stokes sideband arises from population differences between the vibrational states. Moreover, considering a thermal steady state, the ratio between first order ( $\Delta n = 1$ ) transition rates is given by the detailed balance  $\Gamma_S \rho(n) = \Gamma_{aS} \rho(n+1)$  [Cle+10]:

$$\frac{\Gamma_{aS}}{\Gamma_S} = \frac{\Gamma_{n+1 \rightarrow n}}{\Gamma_{n \rightarrow n+1}} = \frac{\rho(n)}{\rho(n+1)} = e^{\frac{\hbar \Omega_z}{k_B T}} = R. \quad (160)$$

From this ratio one can extract the average occupation for a thermal state defined as:

$$\langle n \rangle = \frac{1}{e^{\frac{\hbar \Omega_z}{k_B T}} - 1} = \frac{R}{R - 1} \quad (161)$$

In absence of a cavity, the motion of the mechanical oscillator interacts with a white continuum vacuum state, and the mechanical power spectral density is linearly transduced to the output optical state. The measured heterodyne optical power spectral density describes the ability of the optical field to absorb (yield) energy from (to) the mechanical oscillator [Wei+14]. The first order power spectral density for the quantum harmonic oscillator is [Cle+10; HMD15]:

$$S_{zz}(\Omega) = z_{\text{zpf}}^2 \gamma \left[ \frac{n+1}{(\omega + \Omega_z)^2 + (\gamma/2)^2} + \frac{n}{(\omega - \Omega_z)^2 + (\gamma/2)^2} \right]. \quad (162)$$

The scattering rates of the two competing processes ( $\Gamma_S, \Gamma_{aS}$ ) correspond to the powers detected in the sidebands of the heterodyne measurement (Supplementary Figure 32), allowing from such a measurement, direct evaluation of the motional energy of the thermal harmonic oscillator.

#### Heterodyne noise analysis

By identification of all noise sources in our heterodyne measurement, we are able to isolate the signal component originating from the optomechanical interaction. From that we can evaluate the asymmetry of the Stokes and anti-Stokes peaks. The heterodyne local oscillator is generated by a sequence of two acousto-optical modulators (AOMs) driven by two locked signal generators at 205 MHz and 195.8 (or 214.2) MHz, aligned to order -1 and +1 respectively, in order to produce a local oscillator shifted by -9.2 (or +9.2) MHz. The noise contributions in the heterodyne spectra are determined by: the spectrum analyzer dark noise ( $\text{DN}_{\text{sa}}$ ), the detector

dark noise ( $DN_{\text{det}}$ ), the optical shot noise (SN) (Supplementary Figure 31a), the heterodyne signal generator phase noise ( $PN_{\text{sg}}$ ) and finally the particle's motional signal (SIG). In addition one has to also consider the detector transfer function  $f_{\text{det}}(\Omega)$ , arising from the 75 MHz cut off frequency. The total noise is

$$S_{\text{raw}} = DN_{\text{sa}} + DN_{\text{det}} + f_{\text{det}}(\Omega)(SN + PN_{\text{sg}} + \text{SIG}) \quad (163)$$

Switching on the noise contributions one by one, we are able to directly measure their progressive sum, and evaluate the contribution of each component (Supplementary Figure 31c). As the optical shot noise is white by definition, we can evaluate the detector transfer function (linear in a band of 1 MHz around the heterodyne frequency) by measuring the detector's response to this white noise. Next we want to characterize the  $PN_{\text{sg}}$ , which only appears in the heterodyne measurement together with the motional sidebands. We thus evaluate this noise source ( $PN_{\text{sg}}$ ) directly, by mixing the signals driving the AOMs and rescaling the carrier peak to that measured in the optical heterodyne measurement (see Supplementary Figure 31b). This contribution is then transformed by  $f_{\text{det}}(\Omega)$  and added to the total noise (green component in Supplementary Figure 31c-d). The sum of separately evaluated noise contributions fits very well to the raw measured data.

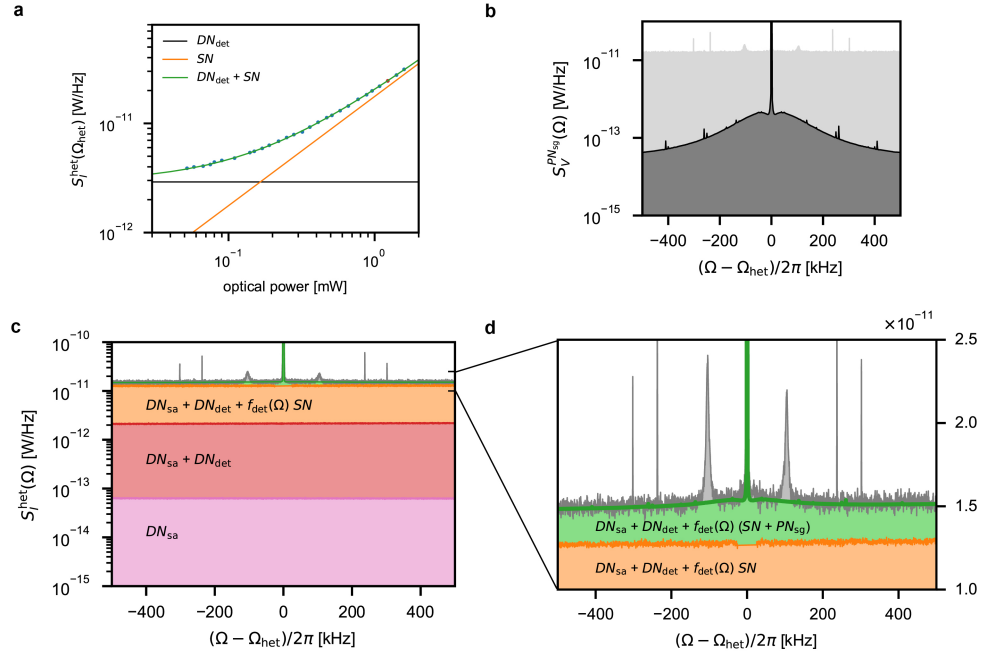


**Figure 31: Noise components in the heterodyne spectra.** **a**, Linear dependence of the shot-noise power as a function of optical power in the heterodyne local oscillator. The red point shows our operating condition, almost a factor 10 above dark noise. **b**, Phase noise of the heterodyne signal generators, directly measured after a mixer, and renormalized to the optical carrier amplitude. The lighter background shows comparison with the raw optical signal. Even though at the relevant frequencies this is almost a factor 100 smaller than the measured signal, its contribution is fundamental (green area in **c** and **d**) given low scattering rates in the ground state. **c-d**, Detail of all of the noises contributing to the heterodyne spectrum.

We can now isolate the signal of interest. We note that the signal generator phase noise is not the only source of phase noise into our heterodyne. After subtraction of all independently characterized noise contributions, and normalization to shot noise, we notice a residual noise contribution falling off as  $1/f$ . This noise is compatible to what we expected from the laser phase noise in our unbalanced ( $\sim 1$  m) interferometer. We fit to the clean spectra the sum of a double lorentian (162), and a symmetric  $1/f$  noise component, with a fixed offset of 1. For each fit we evaluate the quality of the model by checking the Gaussianity of the residuals (Supplementary Figure 32a-b). In addition we verify quantum consistency by noting that, while

the ratio (asymmetry) of blue to red side-band changes as cooling improves, their difference, remains constant (Supplementary Figure 32c). In order to acquire higher statistical significance, we perform repeated measurements for a subset of points, and extract the asymmetry and occupation from the mean value of red and blue side-band powers (Figure 1b in the main text) [Sud+17a]. In order to exclude any other source of uncorrelated noise that may be altering the observed asymmetry we perform our measurements at both  $\Omega_{\text{het}} = \pm 9.2 \text{ MHz}$ . Except from the swapping of the Stokes and anti-Stokes sidebands in the spectra, we observe no difference in the ratio or in the absolute difference of the scattering rates, confirming correct identification of all of the significant noise sources.

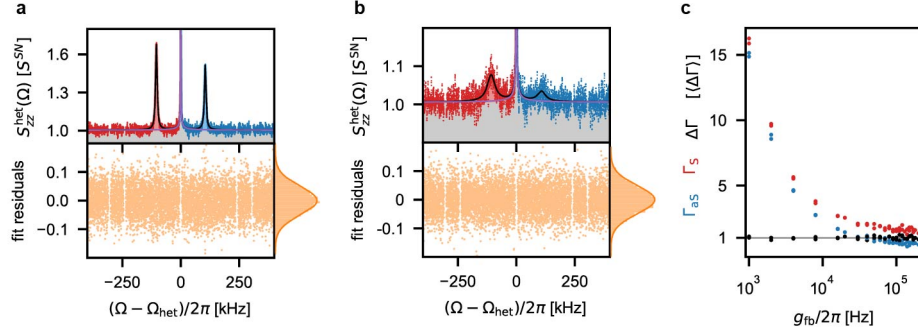
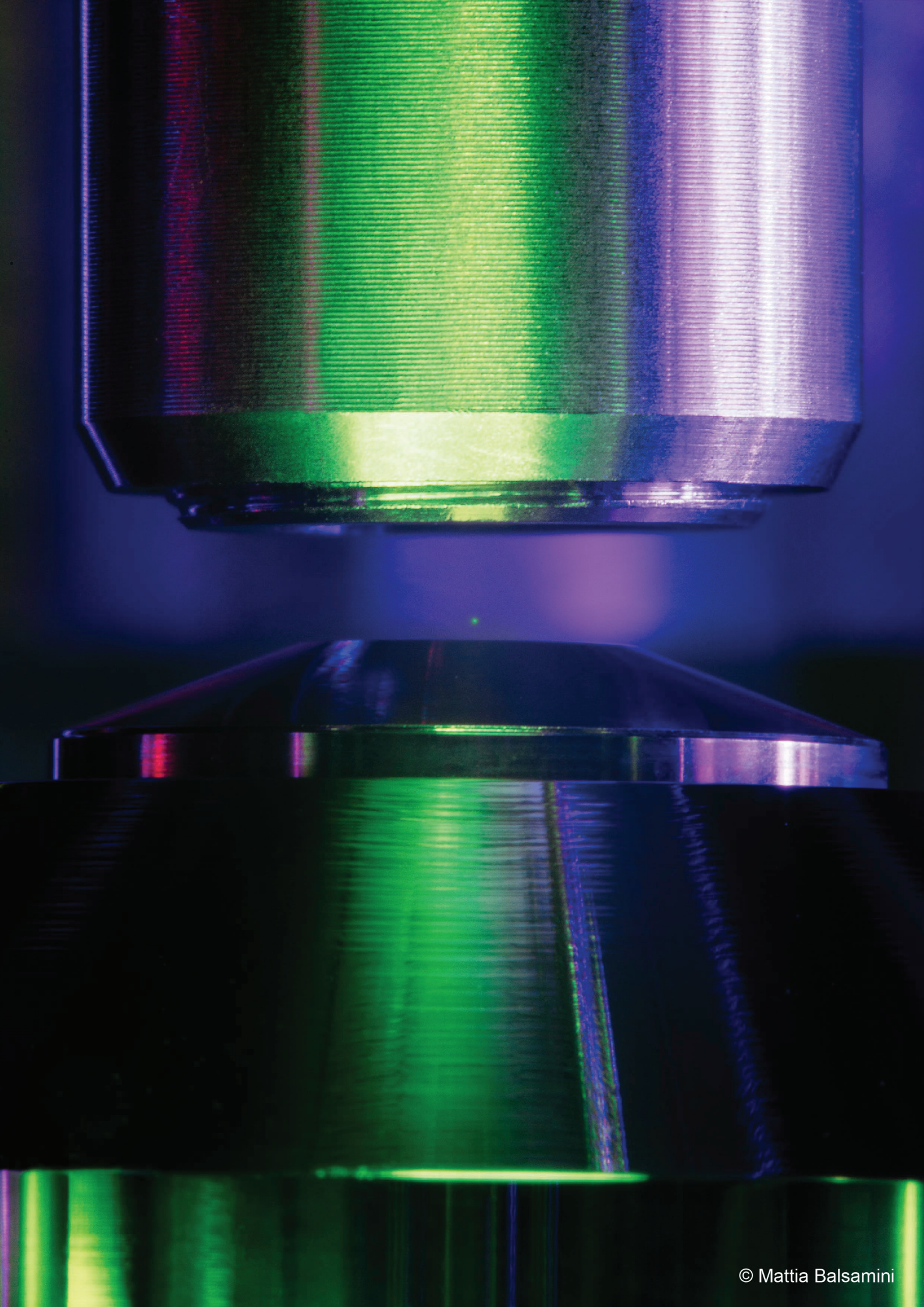


**Figure 32: Side-band asymmetry fit.** **a-b**, Heterodyne spectra after noise subtraction, application of the inverse detector transfer function  $f_{\text{det}}^{-1}(\omega)$  (whitening). The fit (black line) is a 4 parameter fit of a double lorentian plus a  $1/f$  symmetric noise (shown also separately as purple line and gray area). The Gaussian distribution of the residuals shows good agreement of the measured spectra to the noise model. **c**, Power of the red and blue sideband normalized by their average difference, as a function of the LQG feedback gain for both positive and negative heterodyne frequencies (2 points per colour per gain). The constant difference in the power of the 2 side-bands represents a sanity check of the noise analysis.

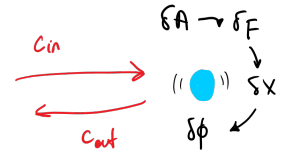




# 5

## ROOM TEMPERATURE PONDEROMOTIVE SQUEEZING WITHOUT A CAVITY

Quantum mechanical radiation pressure fluctuations disturb the motion of a mechanical oscillator [Cav80]<sup>1</sup>. In chapter 2 we have seen how the quantum nature of light (in general of a measurement device) sets a bound to the precision that a measurement involving such device can achieve. But let's continue the argument: Quantum mechanical radiation pressure fluctuations disturb the motion of a mechanical oscillator, which in turn defines the phase fluctuations of the scattered radiation. This logic is what defines ponderomotive squeezing. Specifically, random quantum fluctuations in the photon number (amplitude) of the optical field define a fluctuating force noise driving the motion of the oscillator. While the interaction leaves the optical amplitude unchanged, position fluctuations of the oscillator are transduced to the optical phase. Since the force noise scales with the amplitude of the incoming field, the optomechanical interaction results correlations between the outgoing amplitude and phase quadratures. If the input noise fluctuations are limited by vacuum noise, as it is the case for pure optical states, these correlations will result, for some linear combination of amplitude and phase, in a reduction of the total noise of the field quadrature below the shot noise level: a squeezed state of light. The term *ponderomotive* refers to the fact that the radiation pressure force that is relevant for this effect is only amplified by the mechanical response on time scales much slower than the optical oscillations.



Ponderomotive squeezing of light was derived by Fabre *et al.* [Fab+94] and by Mancini and Tombesi [MT94]. They showed the formal equivalence of optomechanical squeezing with squeezing achieved in a Kerr medium, where correlations between amplitude and phase arise from the intensity dependent index of refraction of a  $\chi^{(3)}$  nonlinearity. These results, shortly followed by more advanced studies on the generation of macroscopic optical [MMT97] and mechanical quantum states [BJK97], defined the formalism of modern quantum optomechanics. Ponderomotive squeezing was later also proposed as a source for noise reduction in gravitational wave detectors [Cor+06]. The first experimental observation of correlations between radiation-pressure force noise and the position of a mechanical resonator was achieved by Marino *et al.* [Mar+10] and Verlot *et al.* [Ver+10] using an input field with an increased amplitude noise with respect to the vacuum state in order to amplify the correlation term. Observation of quantum noise reduction by ponderomotive squeezing was achieved two years later by Brooks *et al.* using ultracold atoms in an optical cavity [Bro+12], and shortly after demonstrated in solid state optomechanical systems in a cryogenic environment [SN+13; Pur+13; Sud+17a; OK+18; Mas+19]. At room temperature, noise reduction due to the radiation pressure-position correlation was observed [Pur+17; Sud+17b], even on kg-scale objects [Yu+20], however the high thermal noise contribution did not allow to obtain squeezed light. Recently the first demonstration of optomechanical ponderomotive squeezing was achieved at room temperature by Aggarwal *et al.* [Agg+20], with a movable mirror inside an optical cavity.

Thermal noise of the mechanical system and optical losses in the measurement degrade the squeezing of light. To minimize optical losses and enhance the measurement strength, all ponderomotive squeezing experiments to date make use of an optical cavity. In addition, most of them are carried out in a cryogenic environ-

<sup>1</sup> Here we are paraphrasing the words of Caves, who in this work [Cav80] actually demonstrated that radiation pressure fluctuations disturb the measurement of the position of kg masses in gravitational wave detectors.



ment to minimize thermal noise. Here I show ponderomotive squeezing at room temperature and without an optical cavity. Even though the qualitative results are similar, the details of the derivation in of this effect in free space do have some differences. For this reason, in the first section of this chapter I will derive the basic theory leading to ponderomotive squeezing in the absence of a cavity. In the second section I will show preliminary measurement data, that demonstrates quantum noise squeezing of light resulting from correlations between the optical force and the mechanical displacement noises.

## 5.1 THEORY

We want to derive the time dependent output optical field after the interaction with a mechanical oscillator. This is conveniently done in the Heisenberg picture, with the quantum operators evolving in time, according to the Heisenberg equation (20). In this section I will start by (re-)deriving the quantum langevin equations of motion of the optical and mechanical creation-and annihilation operators. This is equivalent to the derivation showed in section 4.7.5, however, for the sake of simplicity I will neglect spatial mode considerations. The effects of imperfect overlap of the output modes and the detection modes are being absorbed into an overall measurement efficiency. This is justified by the final results of 4.7.5 and allows me to follow with more detail the mathematical steps, without losing sight of the physical meaning, hopefully giving the more inexperienced reader a tool to independently begin addressing problems of this kind. The time dependent equations of motion of the mechanical oscillator and the output optical quadratures are then analysed in frequency space, where the main approximations are considered and the effects of ponderomotive squeezing can be easily recognized.

### 5.1.1 The quantum langevin equations

We start by defining the Hamiltonian of the optomechanical system: a mechanical oscillator (described by the operators  $a, a^\dagger$ ) that is dissipatively coupled to an external thermal environment or bath (described by the operators  $b, b^\dagger$ ), and dispersively coupled to a measurement apparatus, in our case an optical field (described by the operators  $c, c^\dagger$ ):

$$\begin{aligned}
 H = & \underbrace{\hbar\Omega_q a^\dagger a}_{\text{system}} + \underbrace{\hbar \int d\omega \omega b^\dagger b}_{\text{bath}} + \underbrace{\hbar \int d\omega \omega c^\dagger c}_{\text{meter}} \\
 & + \underbrace{i\hbar\sqrt{\frac{\gamma}{2\pi}} \int d\omega (b^\dagger a + ba^\dagger)}_{\text{thermal coupling}} + \underbrace{\hbar g \int d\omega (a^\dagger + a)(c^\dagger + c)}_{\text{measurement interaction}}
 \end{aligned} \tag{164}$$

*Notation: the frequency mode label of the creation and annihilation operators is omitted.*

where the optomechanical coupling  $g$  and damping  $\gamma$  rates are assumed to be real and independent of frequency. We can now write the the Heisenberg equations of motion (20) for  $a, b$  and  $c$ :

$$\dot{a}(t) = \frac{i}{\hbar} [H, a] = \underbrace{-i\Omega_q a(t)}_{A1} - \underbrace{\sqrt{\frac{\gamma}{2\pi}} \int d\omega b(t)}_{B1} + \underbrace{ig \int d\omega (c^\dagger(t) + c(t))}_{C1} \tag{165a}$$

$$\dot{b}(t) = \frac{i}{\hbar} [H, b] = \underbrace{-i\omega b(t)}_{A1} + \underbrace{\sqrt{\frac{\gamma}{2\pi}} a}_{B1} \tag{165b}$$

$$\dot{c}(t) = \frac{i}{\hbar} [H, c] = \underbrace{-i\omega c(t)}_{A1} - \underbrace{ig(a^\dagger + a)}_{B1} \tag{165c}$$

*Math reminder:*  
 $[a^\dagger a, a] = a^\dagger a a - a a^\dagger a =$   
 $[a^\dagger, a] a + a a^\dagger a - a a^\dagger a =$   
 $[a^\dagger, a] a = -a$

### 5.1.2 The system evolution

At this point the strategy is as follows: we formally solve the linear differential equations (165b) and (165c) by integrating them up to the interaction time  $t$ . These solutions can then be used into the terms B and C in equation (165a). Here it is convenient to identify (and define) the input modes for the thermal and optical interaction, which allow us to simplify the notation. Equations (165b) and (165c) are a couple of linear, first order differential equations. Their solution is:

$$b(t) = b(0)e^{-i\omega t} + \sqrt{\frac{\gamma}{2\pi}} \int_0^t dt' e^{-i\omega(t-t')} a(t') \quad (166a)$$

$$c(t) = c(0)e^{-i\omega t} - ig \int_0^t dt' e^{-i\omega(t-t')} (a^\dagger(t') + a(t')) \quad (166b)$$

*Math reminder:*

$$\begin{aligned} \dot{x}(t) &= \lambda x(t) + f(t), \\ \text{substitution: } y(t) &= x e^{-\lambda t}, \\ \text{derivative: } \dot{y}(t) &= (x(t) - \lambda) e^{-\lambda t} = f(t) e^{-\lambda t} \\ \text{solution: } y(t) &= y(0) + \int_0^t dt' e^{-\lambda t'} f(t') \\ \text{substitute back: } x(t) &= x(0) e^{\lambda t} + \int_0^t dt e^{\lambda(t-t')} f(t') \end{aligned}$$

We can now plug equation (166a) into the B1 term of equation (165a):

$$\begin{aligned} B1 &= \sqrt{\frac{\gamma}{2\pi}} \int d\omega b(t) \\ &= \sqrt{\frac{\gamma}{2\pi}} \int d\omega \left( b(0)e^{-i\omega t} + \sqrt{\frac{\gamma}{2\pi}} \int_0^t dt' e^{-i\omega(t-t')} a(t') \right) \\ &= \underbrace{\sqrt{\gamma} \int d\omega b(0)e^{-i\omega t}}_{-b_{\text{in}}(t)} + \underbrace{\frac{\gamma}{2\pi} \int_0^t dt' a(t') \int d\omega e^{-i\omega(t-t')}}_{2\pi\delta(t-t')} \\ &= -\sqrt{\gamma} b_{\text{in}}(t) + \frac{\gamma}{2} a(t) \end{aligned} \quad (167)$$

*Math reminder:*

$$\int_a^b dx \delta(x - b) f(x) = \frac{1}{2} f(b)$$

where we have defined the input mode of the thermal bath :

$$b_{\text{in}}(t) = -\sqrt{\frac{1}{2\pi}} \int d\omega b(0)e^{-i\omega t}. \quad (168)$$

We proceed similarly with the optical field: we use (166b) into the C1 term of equation (165a):

$$\begin{aligned} C1 &= ig \int d\omega (c^\dagger(t) + c(t)) \\ &= ig \int d\omega \left[ \left( c^\dagger(0)e^{i\omega t} + ig \int_0^t dt' e^{i\omega(t-t')} (a^\dagger(t') + a(t')) \right) + \text{H.c.} \right] \\ &= ig \left( \underbrace{\int d\omega c^\dagger(0)e^{i\omega t}}_{\sqrt{2\pi}c_{\text{in}}^\dagger(t)} + \underbrace{\int d\omega c(0)e^{-i\omega t}}_{\sqrt{2\pi}c_{\text{in}}(t)} \right) \\ &\quad - g^2 \int_0^t dt' (a^\dagger(t') + a(t')) \underbrace{\int d\omega e^{i\omega(t-t')} - e^{-i\omega(t-t')}}_{2\pi\delta(t-t') - 2\pi\delta(t-t')=0} \\ &= i\sqrt{2\pi}g (c_{\text{in}}^\dagger(t) + c_{\text{in}}(t)) \end{aligned} \quad (169)$$

where we have defined the input mode of the optical field, up to the interaction time  $t$  as:

$$c_{\text{in}}(t) = \sqrt{\frac{1}{2\pi}} \int d\omega c(0)e^{-i\omega t}. \quad (170)$$

*Properties [GC85]*

$$\begin{aligned} \langle b_{\text{in}}(t) b_{\text{in}}(0) \rangle &= 0 \\ \langle b_{\text{in}}^\dagger(t) b_{\text{in}}^\dagger(0) \rangle &= 0 \\ \langle b_{\text{in}}^\dagger(t) b_{\text{in}}(0) \rangle &= n_{\text{th}} \delta(t) \\ \langle b_{\text{in}}(t) b_{\text{in}}^\dagger(0) \rangle &= (n_{\text{th}} + 1) \delta(t) \end{aligned}$$

*Properties [Lou00]:*

$$\begin{aligned} \langle c_{\text{in}}(t) c_{\text{in}}(0) \rangle &= 0 \\ \langle c_{\text{in}}^\dagger(t) c_{\text{in}}^\dagger(0) \rangle &= 0 \\ \langle c_{\text{in}}^\dagger(t) c_{\text{in}}(0) \rangle &= 0 \\ \langle c_{\text{in}}(t) c_{\text{in}}^\dagger(0) \rangle &= \delta(t) \end{aligned}$$

We can finally write the evolution of the  $a$  operator inserting the results for B1 (167) and C1 (169) into equation (165a):

$$\dot{a}(t) = -\left(i\Omega_q + \frac{\gamma}{2}\right) a(t) + \sqrt{\gamma} b_{\text{in}}(t) + i\sqrt{\Gamma_{\text{ba}}} \left(c_{\text{in}}^\dagger(t) + c_{\text{in}}(t)\right) \quad (171)$$

where  $\Gamma_{\text{ba}} = 2\pi g^2$  is the backaction-induced decoherence rate. The solution of this linear differential equation is conveniently solved in the Fourier domain. This is done by writing the operators in terms of their Fourier components, allowing one to apply the time derivative to the exponential term only. This yields:

*Math reminder:*

$$\mathcal{F}[a(t)] = a(\omega) = \sqrt{\frac{1}{2\pi}} \int dt e^{-i\omega t} a(t)$$

$$\mathcal{F}^{-1}[a(\omega)] = a(t) = \sqrt{\frac{1}{2\pi}} \int d\omega e^{i\omega t} a(\omega)$$

$$\dot{a}(\omega) = -i\omega a(\omega)$$

$$(a(\omega))^\dagger = a^\dagger(-\omega)$$

$$a(\omega) = \frac{\sqrt{\gamma} b_{\text{in}}(\omega) + i\sqrt{\Gamma_{\text{ba}}} \left(c_{\text{in}}^\dagger(\omega) + c_{\text{in}}(\omega)\right)}{i(\Omega_q - \omega) + \frac{\gamma}{2}} \quad (172a)$$

$$a^\dagger(\omega) = \frac{\sqrt{\gamma} b_{\text{in}}^\dagger(\omega) - i\sqrt{\Gamma_{\text{ba}}} \left(c_{\text{in}}^\dagger(\omega) + c_{\text{in}}(\omega)\right)}{-i(\Omega_q + \omega) + \frac{\gamma}{2}}, \quad (172b)$$

and the correlators of the bath and input field in Fourier space become [HMD15]:

$$\begin{aligned} \langle b_{\text{in}}(\omega) b_{\text{in}}(\omega') \rangle &= \langle b_{\text{in}}^\dagger(\omega) b_{\text{in}}^\dagger(\omega') \rangle = 0 \\ \langle b_{\text{in}}^\dagger(\omega) b_{\text{in}}(\omega') \rangle &= n_{\text{th}} \delta(\omega + \omega') \end{aligned} \quad (173a)$$

$$\begin{aligned} \langle b_{\text{in}}(\omega) b_{\text{in}}^\dagger(\omega') \rangle &= (n_{\text{th}} + 1) \delta(\omega + \omega') \\ \langle c_{\text{in}}(\omega) c_{\text{in}}(\omega') \rangle &= \langle c_{\text{in}}^\dagger(\omega) c_{\text{in}}^\dagger(\omega') \rangle = \langle c_{\text{in}}^\dagger(\omega) c_{\text{in}}(\omega') \rangle = 0 \\ \langle c_{\text{in}}(\omega) c_{\text{in}}^\dagger(\omega') \rangle &= \delta(\omega + \omega'). \end{aligned} \quad (173b)$$

### 5.1.3 The output field

We can now turn our attention to the output mode of the optical field. It is in the end the only quantity we experimentally have access to! We can define the output optical field as a function of the field operators at the moment of interaction, similarly to what was done for the input optical field in equation (166b). This time, rather than defining an earlier time 0 and integrating up to the interaction time  $t$ , we define a late time  $T$ , and integrate backwards in time, back to the onset of interaction. The field operator  $c(t)$  at interaction time  $t$ , defined in equation (166b) can equivalently be written as:

$$c(t) = c(T) e^{-i\omega(t-T)} - ig \int_T^t dt' e^{-i\omega(t-t')} \left(a^\dagger(t') + a(t')\right) \quad (174)$$

We can now integrate  $c(t)$  over all frequencies. Using definition (166b) or (174) we obtain respectively:

$$\begin{aligned} \int c(t) d\omega &= \int d\omega c(0) e^{-i\omega t} - ig \int_0^t dt' \left(a^\dagger(t') + a(t')\right) \int d\omega e^{-i\omega(t-t')} \\ &= -\sqrt{2\pi} c_{\text{in}}(t) - i\pi g \left(a^\dagger(t) + a(t)\right) \end{aligned} \quad (175a)$$

$$\begin{aligned} \int c(t) d\omega &= \underbrace{\int d\omega c(T) e^{-i\omega(t-T)}}_{\sqrt{2\pi} c_{\text{out}}} - ig \int_T^t dt' \left(a^\dagger(t') + a(t')\right) \int d\omega e^{-i\omega(t-t')} \\ &= \sqrt{2\pi} c_{\text{out}}(t) + i\pi g \left(a^\dagger(t) + a(t)\right) \end{aligned} \quad (175b)$$

where we have defined the input mode of the optical field, after the interaction as:

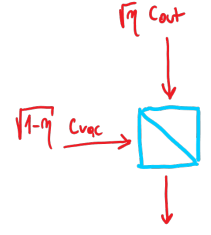
$$c_{\text{out}}(t) = \sqrt{\frac{1}{2\pi}} \int d\omega c(0) e^{-i\omega t} \quad (176)$$

Imposing continuity at the time of interaction (175a must be equal to 175b) we finally get the output mode as a function of the input optical mode and the interaction with the mechanical system:

$$c_{\text{out}}(t) = c_{\text{in}}(t) - i\sqrt{\Gamma_{\text{ba}}} \left( a^\dagger(t) + a(t) \right) \quad (177)$$

In real experiments we likely will not be able to detect the output field with unity efficiency. Losses due to imperfect mode matching between the optical output mode and the mode we detect, or due to non unity conversion efficiency of the photo-detectors can be modelled by a single beam splitter with transmissivity  $\eta_d$ . Unitarity of the detected mode function is ensured by considering a fraction  $(1 - \eta_d)$  of the optical vacuum coupling in via the orthogonal port. We therefore redefine the detected optical mode as:

$$\begin{aligned} c_{\text{det}}(t) &= \sqrt{1 - \eta_d} c_{\text{vac}}(t) + \sqrt{\eta_d} c_{\text{out}}(t) \\ &= \sqrt{1 - \eta_d} c_{\text{vac}}(t) + \sqrt{\eta_d} c_{\text{in}}(t) - i\sqrt{\Gamma_{\text{meas}}} \left( a^\dagger(t) + a(t) \right) \end{aligned} \quad (178)$$



Properties:

$$\begin{aligned} c_{\text{vac}} c_{\text{vac}} &= c_{\text{vac}}^\dagger c_{\text{vac}} = 0 \\ c_{\text{vac}}^\dagger c_{\text{vac}}^\dagger &= 0 \\ c_{\text{vac}} c_{\text{vac}}^\dagger &= 1 \\ c_{\text{vac}} c_{\text{in}} &= c_{\text{vac}}^\dagger c_{\text{in}} = 0 \\ c_{\text{vac}}^\dagger c_{\text{in}} &= c_{\text{vac}} c_{\text{in}}^\dagger = 0 \end{aligned}$$

where  $\Gamma_{\text{meas}} = \eta_d \Gamma_{\text{ba}} = \eta_d 2\pi g^2$ . Equation (176) (and (178)) define the output (detected) optical field after the interaction with the mechanical oscillator. It depends on the input field and on the dynamics of the mechanical oscillator. As introduced earlier in this chapter, ponderomotive squeezing is a phenomenon that appears on timescales defined by the mechanical motion, and therefore much slower than the optical frequency. For this reason it is convenient to work in a low-frequency limit, close to mechanical resonance, and ignore the rest. The natural way of operating such a frequency cut-off is analysing the fields in their spectral domain. In the next section we will therefore first study the motional spectrum of the position of the harmonic oscillator, deriving it from equations (172) in the high-Q and low frequency limit. We will then use this result to write the spectrum of the quadratures of the output (or detected) field.

#### 5.1.4 The motional spectrum of the quantum harmonic oscillator

The position and momentum operators for the quantum mechanical oscillator can be written in terms of the  $a$  and  $a^\dagger$  operators as

$$q = \underbrace{\sqrt{\frac{\hbar}{2m\Omega_q}}}_{q_{\text{zpf}}} (a^\dagger + a), \quad \text{and} \quad p = i \underbrace{\sqrt{\frac{\hbar m \Omega_q}{2}}}_{p_{\text{zpf}}} (a^\dagger - a). \quad (179)$$

These definitions, together with equations (172), allow us to write the motional spectrum of the harmonic oscillator. The computation is greatly simplified by observing that owing to the correlators (173) most terms vanish. The motional spectrum is[HMD15]:

Definition:

$$S_{XX}(\omega) = \int d\omega' \langle X^\dagger(\omega) X(\omega') \rangle$$

$$\begin{aligned}
S_{qq}(\omega) &= \int d\omega' \langle q(\omega) q(\omega') \rangle \\
&= q_{zpf}^2 \int \left[ \frac{\gamma \langle b_{in}(\omega) b_{in}^\dagger(\omega') \rangle}{(i(\Omega_q - \omega) + \frac{\gamma}{2})(-i(\Omega_q + \omega') + \frac{\gamma}{2})} + \frac{\gamma \langle b_{in}^\dagger(\omega) b_{in}(\omega') \rangle}{(-i(\Omega_q + \omega) + \frac{\gamma}{2})(i(\Omega_q - \omega') + \frac{\gamma}{2})} \right. \\
&\quad + \frac{\Gamma_{ba} \langle c(\omega) c^\dagger(\omega') \rangle}{(i(\Omega_q - \omega) + \frac{\gamma}{2})(-i(\Omega_q + \omega') + \frac{\gamma}{2})} + \frac{\Gamma_{ba} \langle c(\omega) c^\dagger(\omega') \rangle}{(-i(\Omega_q + \omega) + \frac{\gamma}{2})(i(\Omega_q - \omega') + \frac{\gamma}{2})} \\
&\quad \left. - \frac{\Gamma_{ba} \langle c(\omega) c^\dagger(\omega') \rangle}{(i(\Omega_q - \omega) + \frac{\gamma}{2})(i(\Omega_q - \omega') + \frac{\gamma}{2})} - \frac{\Gamma_{ba} \langle c(\omega) c^\dagger(\omega') \rangle}{(-i(\Omega_q + \omega) + \frac{\gamma}{2})(-i(\Omega_q + \omega') + \frac{\gamma}{2})} \right] d\omega' \\
&= q_{zpf}^2 \left[ \frac{\gamma(n_{th} + 1)}{(\Omega_q - \omega)^2 + (\frac{\gamma}{2})^2} + \frac{\gamma n_{th}}{(\Omega_q + \omega)^2 + (\frac{\gamma}{2})^2} + \frac{\Gamma_{ba}}{(\Omega_q - \omega)^2 + (\frac{\gamma}{2})^2} + \frac{\Gamma_{ba}}{(\Omega_q + \omega)^2 + (\frac{\gamma}{2})^2} \right. \\
&\quad \left. - \frac{\Gamma_{ba}}{\Omega_q^2 - \omega^2 + (\frac{\gamma}{2})^2 - i\Omega_q \gamma} - \frac{\Gamma_{ba}}{\Omega_q^2 - \omega^2 + (\frac{\gamma}{2})^2 + i\Omega_q \gamma} \right] \\
&\approx q_{zpf}^2 \frac{\gamma n_{th} 4\Omega_q^2}{(\Omega_q^2 - \omega^2)^2 + \omega^2 \gamma^2} + q_{zpf}^2 \frac{\Gamma_{ba} 4\Omega_q^2}{(\Omega_q^2 - \omega^2)^2 + \omega^2 \gamma^2} \\
&= (q_{zpf}^2 \gamma n_{th} 4\Omega_q^2 + q_{zpf}^2 \Gamma_{ba} 4\Omega_q^2) m^2 |\chi_m(\omega)|^2 \\
&\stackrel{\text{Definition:}}{=} \frac{1}{m(\Omega_q^2 - \omega^2 + i\gamma\omega)} = (2k_B T \gamma m + 4\Gamma_{ba} p_{zpf}) |\chi_m(\omega)|^2 \\
&= (S_{FF}^{th} + S_{FF}^{ba}) |\chi_m(\omega)|^2
\end{aligned} \tag{180}$$

Approximations:  
 $n_{th} \gg 1$   
 $\Omega_q \gg \gamma$   
 $\omega \approx \Omega_q$

Later in this chapter, when using these approximate results, we will use  $\Omega$  to indicate frequencies in order to remind us that derivations are valid in a limited frequency range close to the mechanical resonance.

### 5.1.5 The spectrum of the output quadratures

At this point we can finally analyse the properties of the quadratures of the output field, which one can detect experimentally by homodyne or heterodyne detection. In the following steps we will discuss for simplicity the properties of the output field, defined by (176). The derivation for the spectrum of the quadratures of the detected mode (178) follows exactly the same steps, so I will only write the final result. The generalized quadrature of angle  $\theta$  of the optical field is defined as:

$$X_\theta^j = c_j e^{-i\theta} + c_j^\dagger e^{i\theta} \tag{181}$$

Using equation (176) we can write the generalized quadrature of the output mode as:

$$\begin{aligned}
X_\theta^{\text{out}}(t) &= c_{\text{out}} e^{-i\theta} + c_{\text{out}}^\dagger e^{i\theta} \\
&= c_{\text{in}} e^{-i\theta} + c_{\text{in}}^\dagger e^{i\theta} + i\sqrt{\Gamma_{ba}} (a^\dagger(t) + a(t)) (e^{i\theta} - e^{-i\theta}) \\
&= X_\theta^{\text{in}}(t) - 2 \frac{\sqrt{\Gamma_{ba}}}{q_{zpf}} q(t) \sin(\theta)
\end{aligned} \tag{182}$$

Math reminder:  
 $\frac{e^{i\theta} - e^{-i\theta}}{2i} = \sin(\theta)$

and its autocorrelation function:

$$\begin{aligned}
\langle X_\theta^{\text{out}}(t) X_\theta^{\text{out}}(0) \rangle &= \overbrace{\langle X_\theta^{\text{in}}(t)^\dagger X_\theta^{\text{in}}(0) \rangle}^{A2} + \overbrace{\frac{4\Gamma_{ba}}{q_{zpf}^2} \sin^2(\theta) \langle q(t)^\dagger q(0) \rangle}^{B2} \\
&\quad + \underbrace{\frac{2\sqrt{\Gamma_{ba}}}{q_{zpf}} \sin(\theta) [\langle X_\theta^{\text{in}}(t)^\dagger q(0) \rangle + \langle q(t)^\dagger X_\theta^{\text{in}}(0) \rangle]}_{C2}
\end{aligned} \tag{183}$$



This allows us, together with the Wiener-Khinchin theorem, to compute the power spectral density of the output quadrature. We compute the spectral contributions for the separate terms. The term A2 results in the trivial white spectrum:

$$S_{A2} = S_{XX}^{\text{in}} = \int dt e^{-i\omega t} \langle X_0^{\text{in}}(t)^\dagger X_0^{\text{in}}(0) \rangle = \int d\tau e^{i\omega\tau} \delta(\tau) = 1. \quad (184)$$

The term B2 represents the autocorrelation of the position of the mechanical oscillator imprinted on the output field. Its spectrum is:

$$S_{B2} = S_{qq}^{\text{out}}(\omega, \theta) = \frac{4\Gamma_{ba}}{q_{\text{zpf}}^2} \sin^2(\theta) \int dt e^{-i\omega t} \langle q(t)^\dagger q(0) \rangle = \frac{4\Gamma_{ba}}{q_{\text{zpf}}^2} \sin^2(\theta) S_{qq}(\omega), \quad (185)$$

where the motional spectral density  $S_{qq}(\omega)$  is derived in equation (180). The last term (C2) in equation (183) is the one showing the correlations between the amplitude fluctuations of the input field and the motion of the oscillator: the squeezing term. To derive its power spectrum it is convenient to write the input field as linear combination  $\cos(\theta)$  and  $\sin(\theta)$ :

$$X_\theta^j = c_j e^{i\theta} + c_j^\dagger e^{-i\theta} = X_0^j \cos(\theta) + X_{\frac{\pi}{2}}^j \sin(\theta) \quad (186)$$

where the coefficients  $X_0^j = c_j^\dagger + c_j$  and  $X_{\frac{\pi}{2}}^j = i(c_j^\dagger - c_j)$  represent the amplitude and phase quadrature of the field respectively. This decomposition allows us to immediately identify the Hermitian and anti-Hermitian components of the quadrature. Because the  $q$  operator is also Hermitian, one immediately sees in that all terms proportional to  $X_{\frac{\pi}{2}}^j$  vanish in equation (183), leaving only:

$$C2 = \frac{2\sqrt{\Gamma_{ba}}}{q_{\text{zpf}}} \sin(2\theta) \langle X_0^{\text{in}}(t) q(0) \rangle = \frac{2}{\hbar} \sin(2\theta) \langle F^{\text{ba}}(t), q(0) \rangle. \quad (187)$$

To help the physical interpretation we have defined the radiation pressure (or ponderomotive) force determined by the optical amplitude fluctuations on to the mechanical oscillator as [SN+13]

$$F^{\text{ba}}(t) = \frac{\hbar\sqrt{\Gamma_{ba}}}{q_{\text{zpf}}} X_0^{\text{in}}(t). \quad (188)$$

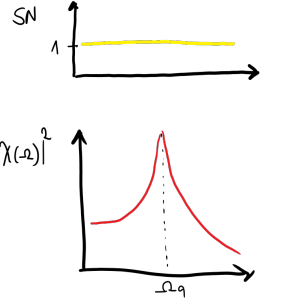
From equation (187) we see that the C2 term in (183) represents the correlations between the input optical amplitude and the position of the oscillator. Using (172) and (173), the spectrum of C2 can be calculated (via the convolution theorem):

$$\begin{aligned} S_{C2} = S_{qX}^{\text{out}}(\omega, \theta) &= \frac{2\sqrt{\Gamma_{ba}}}{q_{\text{zpf}}} \sin(2\theta) \int dt e^{-i\omega t} \langle X_0^{\text{in}}(t) q(0) \rangle \\ &= \frac{2\sqrt{\Gamma_{ba}}}{q_{\text{zpf}}} \sin(2\theta) X_0^{\text{in}}(\omega) q(\omega) \\ &= \frac{2\sqrt{\Gamma_{ba}}}{q_{\text{zpf}}} \sin(2\theta) (c_{\text{in}}^\dagger + c_{\text{in}}) q_{\text{zpf}} (a^\dagger + a) \\ &= 2\Gamma_{ba} \sin(2\theta) \left( \frac{c_{\text{in}} c_{\text{in}}^\dagger}{(\Omega_q + \omega) + i\frac{\gamma}{2}} + \frac{c_{\text{in}} c_{\text{in}}^\dagger}{(\Omega_q - \omega) - i\frac{\gamma}{2}} \right) \\ &\approx 4\Gamma_{ba} \sin(2\theta) \Omega_q m \chi_m^*(\omega) \\ &= \frac{4\Gamma_{ba}}{q_{\text{zpf}}^2} \frac{\hbar}{2} \chi_m^*(\omega) \sin(2\theta) \end{aligned} \quad (189)$$

where again we have used the high-Q approximation in the vicinity of resonance. Putting together (184), (185) and (189), the real part of the total output spectrum of the output quadrature becomes:

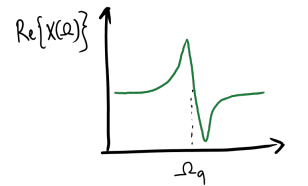
$$S_{XX}^{\text{det}}(\Omega, \theta) = 1 + \frac{4\Gamma_{ba}}{q_{\text{zpf}}^2} \left[ S_{qq}(\Omega) \sin^2(\theta) + \frac{\hbar}{2} \text{Re}\{\chi_m(\Omega)\} \sin(2\theta) \right]. \quad (190)$$

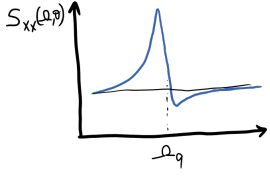
Wiener-Khinchin theorem:  
 $\int dt \langle x(t)^\dagger x(0) \rangle e^{-i\omega t} = S_{xx}(\omega)$



Math reminder:  
 $2 \sin(\theta) \cos(\theta) = \sin(2\theta)$

$$\begin{aligned} c_{\text{in}} c_{\text{in}} &= c_{\text{in}}^\dagger c_{\text{in}} = c_{\text{in}}^\dagger c_{\text{in}}^\dagger = 0 \\ c_{\text{in}} c_{\text{in}}^\dagger &= 1 \\ a^\dagger c_{\text{in}}^\dagger &= \frac{\sqrt{\Gamma_{ba}} c_{\text{in}} c_{\text{in}}^\dagger}{(\Omega_q + \omega) + i\frac{\gamma}{2}} \\ a^\dagger c_{\text{in}} &= 0 \\ a c_{\text{in}}^\dagger &= \frac{\sqrt{\Gamma_{ba}} c_{\text{in}} c_{\text{in}}^\dagger}{(\Omega_q - \omega) - i\frac{\gamma}{2}} \\ a c_{\text{in}} &= 0 \end{aligned}$$





As expected, this is the same result that one gets if one considers a mechanical oscillator coupled to an optical resonator in the bad cavity limit and driven on resonance [SN+13]. The spectrum of the detected quadratures in the case of non-unity detection efficiency can be derived by following the same steps, starting from the definition of  $c_{\text{det}}$  in (178) rather than using  $c_{\text{out}}$  from (182), and remembering that the vacuum and the input field are uncorrelated. The result is:

$$\begin{aligned} S_{XX}^{\text{det}}(\Omega, \theta) &= 1 + \frac{4\Gamma_{\text{meas}}}{q_{\text{zpf}}^2} \left[ S_{qq}(\Omega) \sin^2(\theta) + \frac{\hbar}{2} \text{Re}\{\chi_m(\Omega)\} \sin(2\theta) \right] \\ &= 1 + \frac{4\eta_d \Gamma_{\text{ba}}}{q_{\text{zpf}}^2} \left[ \left(1 + \frac{1}{C_q}\right) S_{\text{FF}}^{\text{ba}} |\chi_m(\Omega)|^2 \sin^2(\theta) + \frac{\hbar}{2} \text{Re}\{\chi_m(\Omega)\} \sin(2\theta) \right] \end{aligned} \quad (191)$$

In this definition the measured spectrum is given in units of the detected shot noise which is the first term of the equation. The second term in (191) represents the motion of the harmonic oscillator and is certainly positive. The third term is the result of correlations between the motion of the particle and the input field which, for certain frequency and quadrature angles, can become negative. This may lead, under certain conditions, to a total noise that is below 1, i.e. smaller than the optical vacuum fluctuations. The optical mode at that frequency is therefore a squeezed optical state. Lets quickly study the function. Equation (191) is a function of two variables, defined on the domain  $\Omega \in [0, \infty)$  and  $\theta \in [-\pi/2, \pi/2]$ . In this domain the function is maximized in  $(\Omega_q, \pm\pi/2)$  and has two local minima at  $(\Omega_q + \Delta_{\text{sq}}, \theta_{\text{sq}})$  and  $(\Omega_q - \Delta_{\text{sq}}, -\theta_{\text{sq}})$ . At  $(\Omega_q, 0)$  is a saddle point. The two minima represent two frequency modes  $\Omega_{\text{sq}} = \Omega_q \pm \Delta_{\text{sq}}$  where light is maximally squeezed in its quadrature defined by the angle  $\pm\theta_{\text{sq}}$ . In particular in the limit high  $Q$  ( $\gamma \ll \Omega$ )

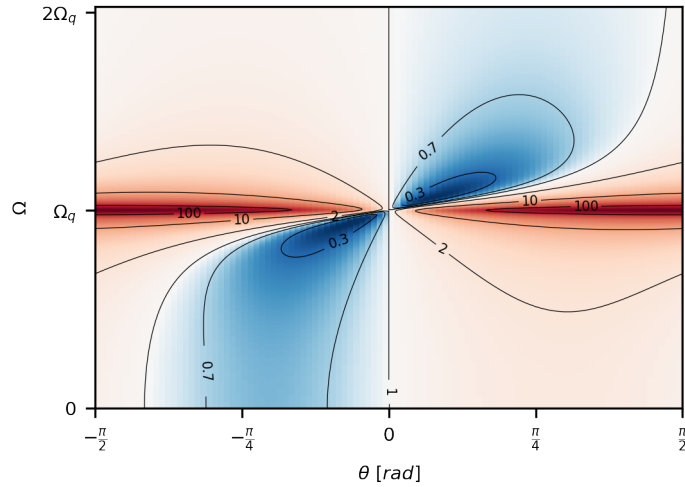


Figure 33: The spectrogram of the output quadrature as a function of the angle of analysis.

and high cooperativity ( $C_q \gg 1$ ), assuming perfect detection efficiency  $\eta_d = 1$  and high occupancy  $n \gg 1$ , the correlation term is strong enough to maximally suppress both the thermal noise and the shot noise contributions at two specific frequencies. Equation (191) is sometimes written in the units of the displacement spectrum. Using the definition of measurement rate given in chapter 2, equation (36) we can multiply equation (191) with  $S_{qq}^{\text{imp}}$ , to obtain the spectrum of the output quadrature in units of displacement noise [Mas+19]:

$$S_{XX}^{\text{out}}(\Omega, \theta) = S_{qq}^{\text{imp}} + \sin^2(\theta) \left[ \left( S_{\text{FF}}^{\text{ba}} + S_{\text{FF}}^{\text{th}} \right) |\chi_m(\Omega)|^2 - 2\text{Re} \left\{ \chi_m(\Omega) S_{qF}^{\text{ba}}(\theta) \right\} \right], \quad (192)$$

where the force-displacement correlations spectrum is  $S_{qF}^{\text{ba}}(\theta) = -\frac{\hbar}{2} \cot(\theta)$ .

## 5.2 EXPERIMENT

Up to now we have seen how the optomechanical interaction can, similarly to what happens in a Kerr medium, establish correlations between perpendicular quadratures of the optical field, leading to squeezed optical states. In this section I will briefly describe the detection and analysis of squeezed light from the interaction of a silica particle levitated in an optical tweezer. The detailed technical description of the setup is the same as the one given in chapter 4. The only difference is that now all the collected light scattered by the particle is directed to the heterodyne receiver.

### 5.2.1 Heterodyne demodulation

The quadrature spectrum is extracted by demodulation of the heterodyne time trace: the output field (oscillating at frequency  $\omega_{\text{in}}$ ) is interfered on a 50/50 beam splitter with a reference field (local oscillator) oscillating at a frequency  $\omega_{\text{lo}} = \omega_{\text{in}} + \Omega_{\text{het}}$ . The intensity at two outputs is then recorded by two photodiodes, resulting in a photocurrent:

$$i_{\text{het}} \propto X_0^{\text{out}}(t) \cos(\Omega_{\text{het}}t + X_{\frac{\pi}{2}}^{\text{out}}(t) + \varphi(t)) \quad (193)$$

*Heterodyne photocurrent*

where  $\varphi(t)$  is a slowly varying phase ( $d\varphi(t)/dt \ll \Omega_z, \Omega_{\text{het}} \forall t$ ) that takes into account the drifts in the optical path length. In contrast to homodyne detection, where the phase relation between two fields is fixed, in a heterodyne measurement the local oscillator is continuously scanning between the amplitude and phase quadratures of the output signal. If the phase scan (or heterodyne frequency) is much faster than the frequencies of the dynamics of interest ( $\Omega_{\text{het}} \gg \Omega_z$ ), a demodulation of the heterodyne signal by  $\sin(\Omega_{\text{het}}t)$  and  $\cos(\Omega_{\text{het}}t)$  will result in a simultaneous recording of the in-phase (I) and quadrature (Q) components of the signal. From these equation (186) allows us to reconstruct the time evolution of any optical quadrature  $X_0^{\text{out}}(t)$ . A complete optical tomography can be equivalently obtained using 2 homodyne receivers with a fixed  $\pi/2$  phase relation, identical detectors and identical power in the local oscillators. The advantage of a heterodyne measurement is that power balancing and active phase stabilization of the interferometer are not longer required as a single local oscillator is evenly shared between orthogonal quadratures. It is important to keep in mind, that as the heterodyne measurement is sharing the local oscillator between two orthogonal quadratures, the detection efficiency for each one is reduced by a factor 2, just as if we were splitting the signal between 2 homodyne detectors. The demodulation can easily done with analog

*Heterodyne demodulation*

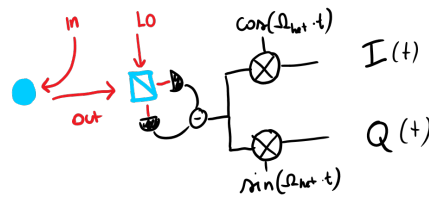


Figure 34: Heterodyne IQ-demodulation

components by use of an IQ mixer and low pass filters or even digitally using a Hilbert transform signal decomposition.

### 5.2.2 Detection

As a drawback, a heterodyne measurement that can resolve the quantum fluctuations of the optical field scattered by the particle requires a large dynamic range. This is because the strong local oscillator that is necessary to amplify the quantum noise will also amplify the heterodyne carrier which may lead to a saturation the detector electronics. The required dynamic range can be gauged by the total de-

*Dynamic range*

tection efficiency  $\eta_d^2$  over the square of the Lamb-Dicke parameter  $\eta_{LD} = \alpha k z_{zpf}$  ( $\alpha$ : geometric factor of order 1,  $k$ : wavevector,  $z_{zpf} = \sqrt{\hbar/(2m\Omega_z)}$ : position zero-point fluctuation) which defines the ratio of the inelastic to elastic scattering rates for the optomechanical interaction. In order to reduce the required dynamic range we choose for this experiment a smaller particle size ( $r = 43 \text{ nm}$ ) and a lower mechanical frequency ( $\Omega_z/2\pi \sim 75 \text{ kHz}$ ). With  $\alpha \sim 1.5$  and  $\eta_d \sim 0.3$  we have:

$$\eta_d/\eta_{LD}^2 \sim 2.1 \cdot 10^7, \quad (194)$$

which is still small enough for a 16 bit oscilloscope which has a dynamic range of  $2^{16} = 4.2 \cdot 10^9$ .

It is also important to choose the appropriate detector: in order to achieve a shot noise limited detection one must be able to amplify the scattered light with a local oscillator that is strong enough that its associated shot noise exceeds the detector dark noise by one order of magnitude, without damaging the photodiodes or saturating the transimpedance amplifier:

*Detector limits: photodiode  
damage and electronic  
saturation*

$$P_{lo} < \min \left\{ 2P_{\max}, \frac{\Delta P_{\text{sat}}^2}{P_{\text{sig}}} \right\} \quad (195)$$

where  $P_{\max}$  is the single photodiode damage power,  $\Delta P_{\text{sat}}$  is the power difference between the photodiodes that saturates the detector amplifier, and  $P_{\text{sig}}$  the power of the signal that is being heterodyned. Sometimes the saturation power is in terms of the maximum voltage swing ( $\Delta V$ ) at the output of the detector:

$$\Delta P_{\text{sat}} = \frac{-e\eta_q}{h\nu} \frac{\Delta V}{g_t} \quad (196)$$

where  $g_t$  is the detectors transimpedance gain,  $e$  is the electron charge,  $\eta_q$  the detector quantum efficiency,  $h$  the Plank constant and  $\nu$  the optical frequency. In terms of the induced photocurrent we will have a shot noise and a dark noise level of (in units of  $A/\sqrt{\text{Hz}}$ ):

$$\sqrt{S_i^{\text{sn}}} = -e\sqrt{2\eta_q \frac{P_{lo}}{h\nu}} \quad \text{and} \quad \sqrt{S_i^{\text{dn}}} = \text{NEP} \frac{\eta_q e}{h\nu}, \quad (197)$$

with NEP the noise equivalent power of the detector. The ratio of optical shot noise to dark noise is the figure of merit that has to be maximized in the choice of a detector. Putting together definitions (195), (196) and (197) we find:

$$\frac{S_i^{\text{sn}}}{S_i^{\text{dn}}} = \frac{2h\nu P_{lo}}{\eta_q \text{NEP}^2} < \min \left\{ \frac{4h\nu}{\eta_q} \frac{P_{\max}}{\text{NEP}^2}, \frac{2h^3\nu^3}{e^2\eta_q^2} \frac{\Delta V^2}{g_t^2 \text{NEP}^2 P_{\text{sig}}} \right\}. \quad (198)$$

We use a Thorlabs PDB 471 balanced detector, with a maximum NEP of  $8 \text{ pW}/\sqrt{\text{Hz}}$  a maximum voltage swing of  $\Delta V \pm 3.6 \text{ V}$ , a transimpedance gain of  $g_t = 10^4$  and a maximum power per diode of  $P_{\max} = 5 \text{ mW}$ . With a signal power of only  $P_{\text{sig}} \sim 100 \text{ nW}$  we are limited by the power threshold of the diodes to a maximum shot noise level of about 15 dB above dark noise. In practice, operating well below threshold and considering digitization noise, the total technical noise is still 11 dB below the shot noise level.

### 5.2.3 Results

With a heterodyne frequency of  $\Omega_{\text{het}}/2\pi = 6 \text{ MHz}$  we record traces of the heterodyne interference, optical shot noise and detector dark noise. For each measurement we record a 500 s long trace at a sampling frequency of  $f_s = 62.5 \text{ MHz}$ . A

<sup>2</sup> here we consider the total detection efficiency of the heterodyne measurement

low-pass filter at  $f_{lp} = 15$  MHz is used to prevent aliasing of high-frequency noise onto our signal. After digital demodulation of the recorded trace we reconstruct the quadrature spectrum at all angles, and observe a maximum squeezing of about 10%, slightly less than what is expected in our experimental conditions at a pressure of  $1.5 \cdot 10^{-8}$  mbar. This is because, at the optimal quadrature angle, the strongest squeezing is expected in a very narrow band very close to resonance. Here, the small frequency fluctuations due to mechanical drifts in our setup are enough to wash out this narrow feature at the optimal angle. At larger angles the squeezing is distributed over a broader band, and further away from resonance.

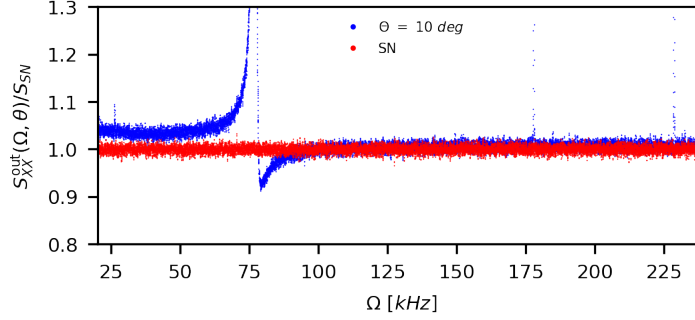


**Figure 35:** Spectrum of the output light. The spectrum of the optical quadrature (blue) at angle  $\theta = 10$  deg. The red points indicate the shot noise level independently measured by covering the signal path in the interferometric detection. The noise reduction below the shot noise level is evident close to resonance.

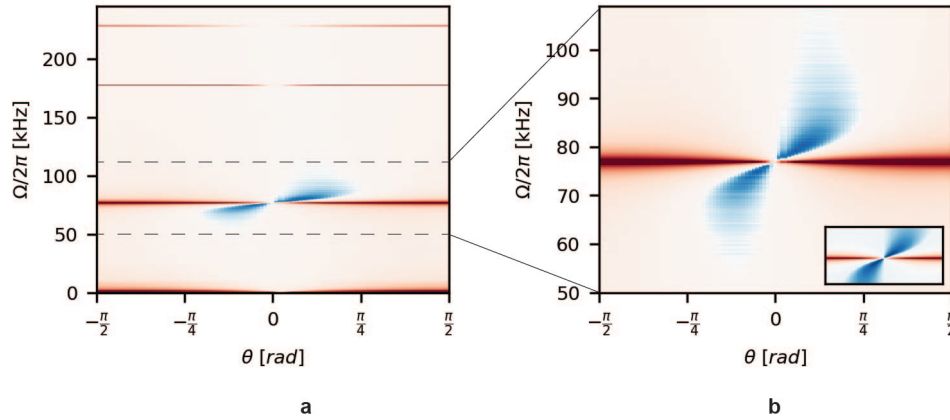


**Figure 36:** Spectrogram of the measured output quadratures as a function of the analyser angle where the warm and cold colours represent noise above and below the shot noise level, respectively. **a** Starting from the the bottom, the first dark red line is defined by the low frequency phase noise (minimized at  $\theta = 0$ ). The second dark red horizontal line is the main resonance  $\Omega_z/2\pi = 77$  kHz. Close to  $\theta = 0$ , also this noise is reduced and the negative contribution of the squeezed light becomes relevant taking the spectrum below the shot noise level (blue shades). The third and fourth dark line are the noise contributions from the transverse motion at  $\Omega_x$  and  $\Omega_y$ . **b** Detail of the spectrogram close to  $\Omega_z$ . The inset shows the theoretical plot expected in our experimental conditions, confirming both the quantitative and qualitative agreement of theory and experiment.

As mentioned before, the heterodyne detection and its demodulation allow us, with a single measurement, to simultaneously record and reconstruct the output quadratures at all angles  $\theta$ , and plot an experimental spectrogram and to appreciate the excellent qualitative and quantitative agreement of our measurement with the predicted model (Figure 33). One last interesting representation is the phase space plot of a squeezed mode oscillating at frequency  $\Omega_{sq}$ : a horizontal section in Figure

36. In polar representation we can easily recognize the non-gaussian phase space distribution of a two-mode squeezed state [And+16].

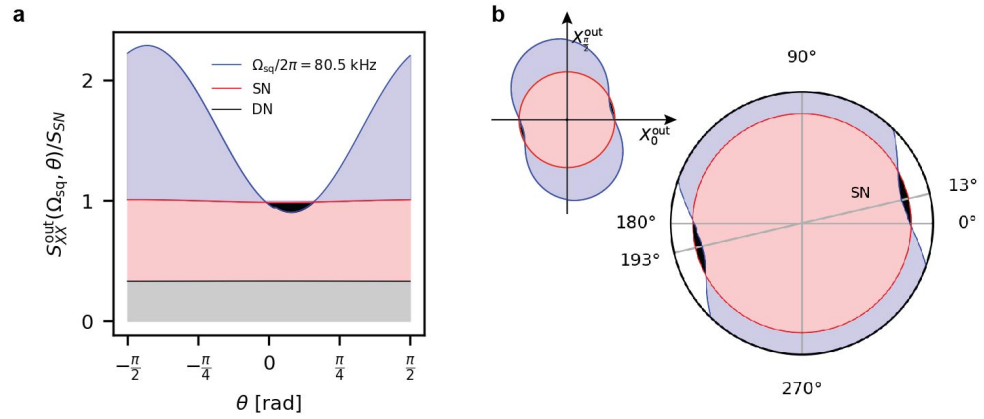


**Figure 37:** **a**, Noise variance as a function of the quadrature angle for the optical mode at  $\Omega_{sq}/2\pi = 80$  kHz. **b**, Quadrature noise (standard deviation) in polar representation and with dark noise subtracted.

In summary I have here shown the first preliminary evidence of radiation-pressure squeezing of light without a cavity and with a room temperature oscillator. The agreement between experiment and theory is excellent, with a residual discrepancy of about 0.5%. We expect to further reduce this discrepancy with a careful modelling of technical phase noise and of transverse mode contributions. Observation of ponderomotive squeezing via a full heterodyne based optical tomography represents a promising step towards the observation of entanglement between light and a room temperature mechanical oscillator [Gut+20].

In this thesis I presented three optomechanical experiments involving a levitated system at room temperature. In chapter 3 (reference [Mag+18]) we coupled the motion of a levitated nanoparticle to the evanescent field of a photonic crystal cavity, showing high coupling strength and high detection efficiency. Although the system is far from operating in the quantum regime our levitated probe allows us to image the three dimensional electric field intensity gradient of the nanophotonic structure in super-resolution. As also recently discussed by Montoya *et al.* [Mon+21], surface scanning, together with the high force sensitivity provided by levitated particles, will allow the developments of short range force sensors, possibly surpassing the current performance of atomic force microscopes. In chapter 4 (reference [Mag+21]) we bring a levitated particle into the quantum regime. In contrast to the first demonstration of ground-state cooling of a levitated particle by Delić *et al.*, where a cavity is used to coherently control the particle motion, we do so by measurement and feedback. While the cavity approach ultimately will yield higher state purity, the advantage of our feedback scheme is its extreme robustness and versatility. Moreover quantum filtering and optimal control allows us to condition the quantum state on the measurement outcome, and control the quantum trajectory of the particle in real time. Implementation of optimal control algorithms in quantum mechanical experiments represents a milestone in the development of quantum technologies, for both sensing and fundamental purposes. A natural follow up experiment is the preparation of squeezed mechanical states. This would allow faster evolution of the wavepacket in free space or nonlinear potentials as well as an enhanced force sensitivity. Another intriguing possibility is given by the extremely high impulse sensitivity of our system [Car+20]. The advantage of quantum filtering is that it allows conditioning of a very pure quantum state and maintain a quantum limited sensitivity even with moderate cooling. The demonstrated sensitivity is already enough to study the energetic statistics of single molecule impulses, possibly allowing to shed light on the poorly understood mechanisms that govern decoherence processes by gas scattering. In addition, extending the techniques developed here to larger masses would greatly benefit the current searches for gravitationally interacting dark matter particles [Mon+20b]. Finally in chapter 5 (manuscript in preparation), I demonstrate room temperature ponderomotive squeezing without a cavity. Although the squeezing is moderate, this result is particularly interesting as it is the first time that this is done without an optical resonator. Besides, our measurement scheme is based on the demodulation of a single heterodyne detection. This allows us to recover, at all times, a full optical state tomography and potentially to reconstruct the optomechanical density matrix in search of evidences of quantum correlations (or entanglement) between light and mechanics [Gut+20].

[...continues (from the introduction)] In the introduction of this thesis I tried to convince the reader about the macroscopicity of the glass particles I have dedicated my doctorate to. Yet looking at them now, and back at the work I describe in this thesis, my arguments have become weaker, their “macroscopic” behaviour almost negligible, and I might have convinced myself of the opposite: they can now go into to the basket of the microscopic! so who’s next?

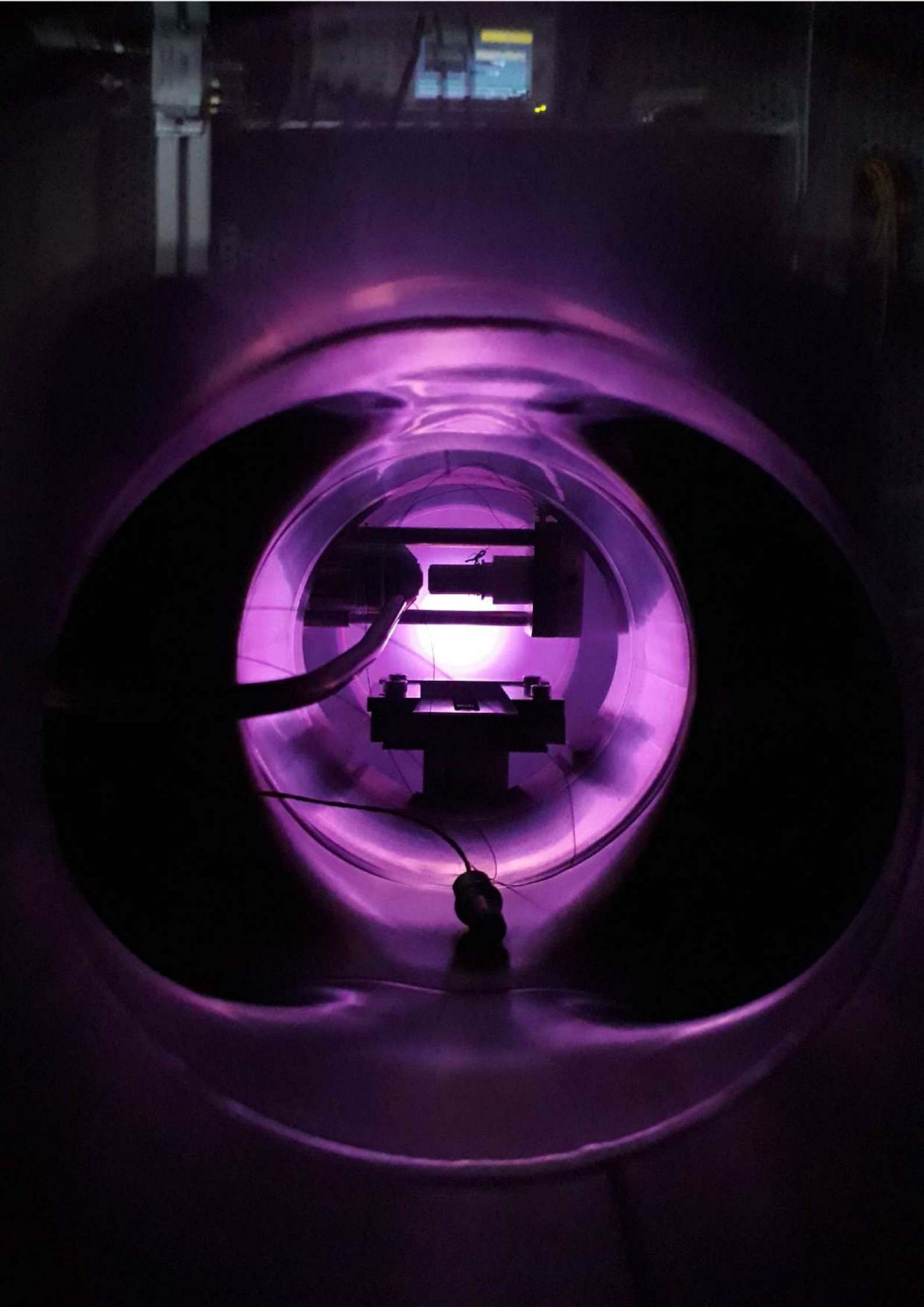




## SOME MORE FIGURES

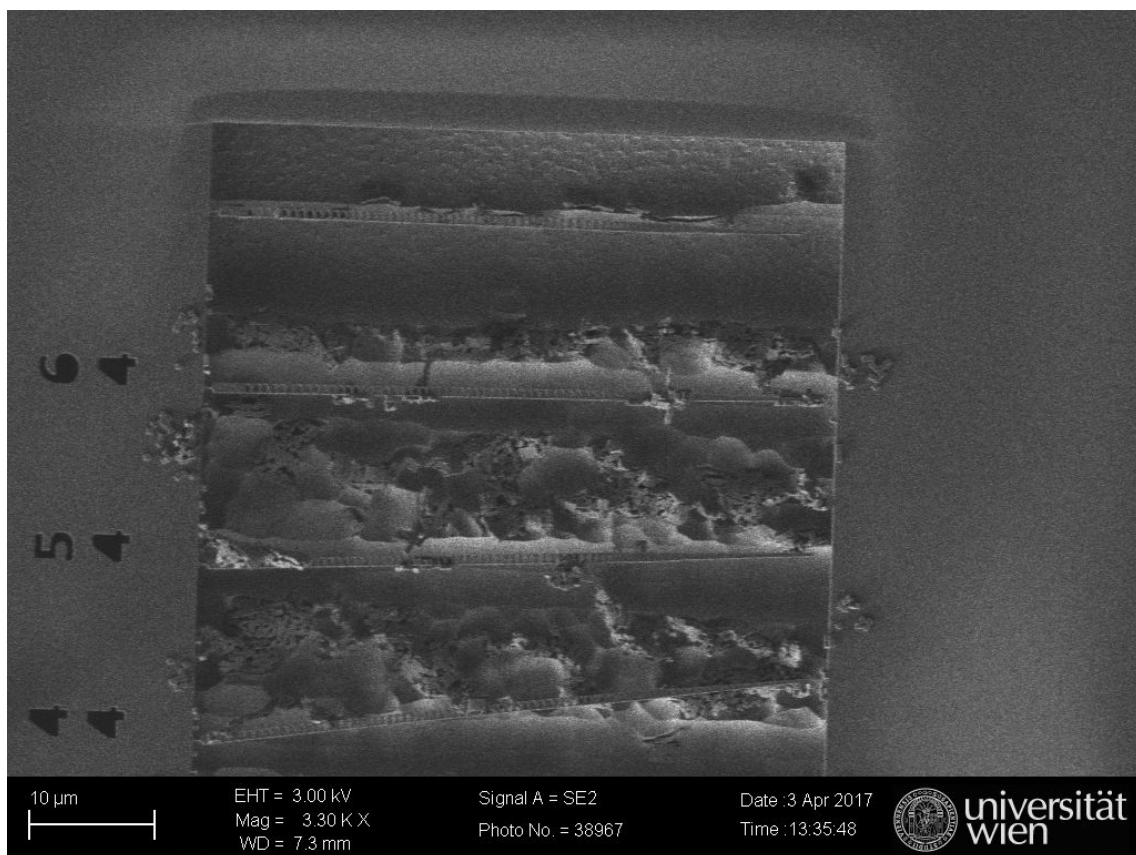
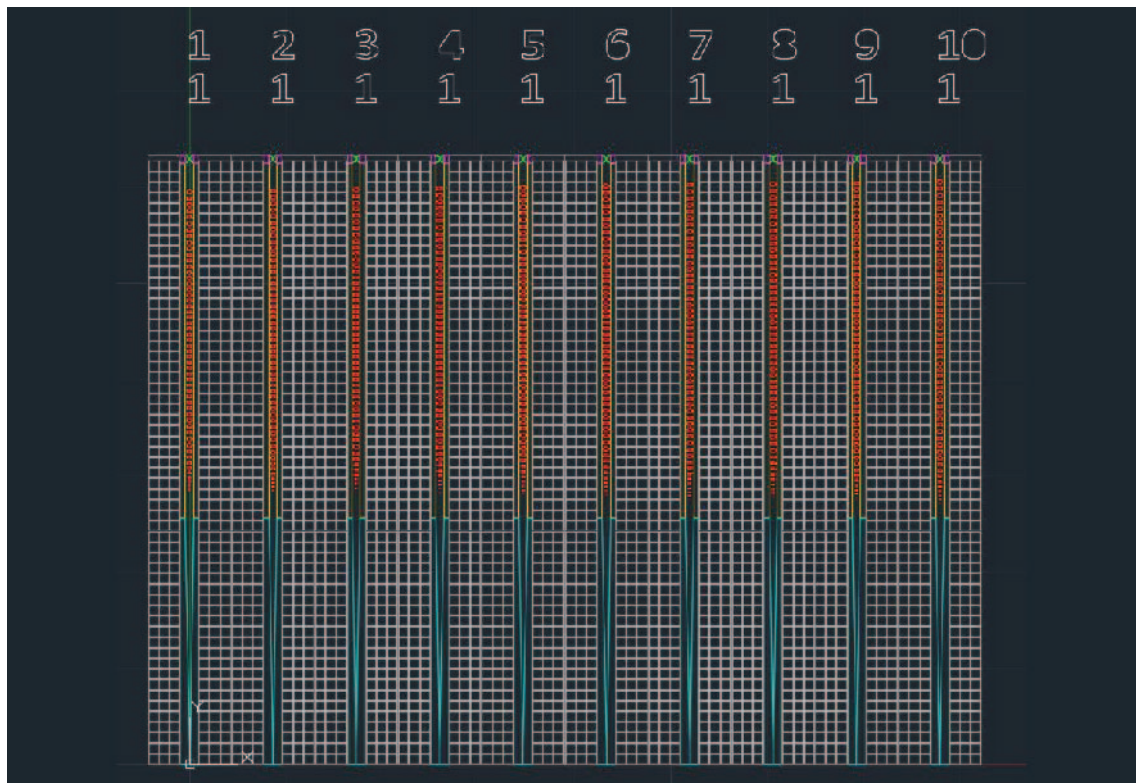
I include some figures here, taken during the years in the lab. Some may be useful to understand details of the experiments, some because I find them pretty.

Picture of the inside of the vacuum chamber. Nitrogen plasma for charge control is ignited by applying about 2 kV at 0.1 mbar resulting in the typical purple glow. At the center one can see the microscope objective and collimating lens. Below the holder for the stage controlling the photonic crystal cavity. On the left the tube delivering the particles to the trap.



CAD drawing of the photonic crystal cavities. As the device number grows, the distance between holes is increased. Together with other parameter sweeps, this helps to find a device with ideal optical properties. The small squares (1  $\mu$ m edge) serve to facilitate the etching process.

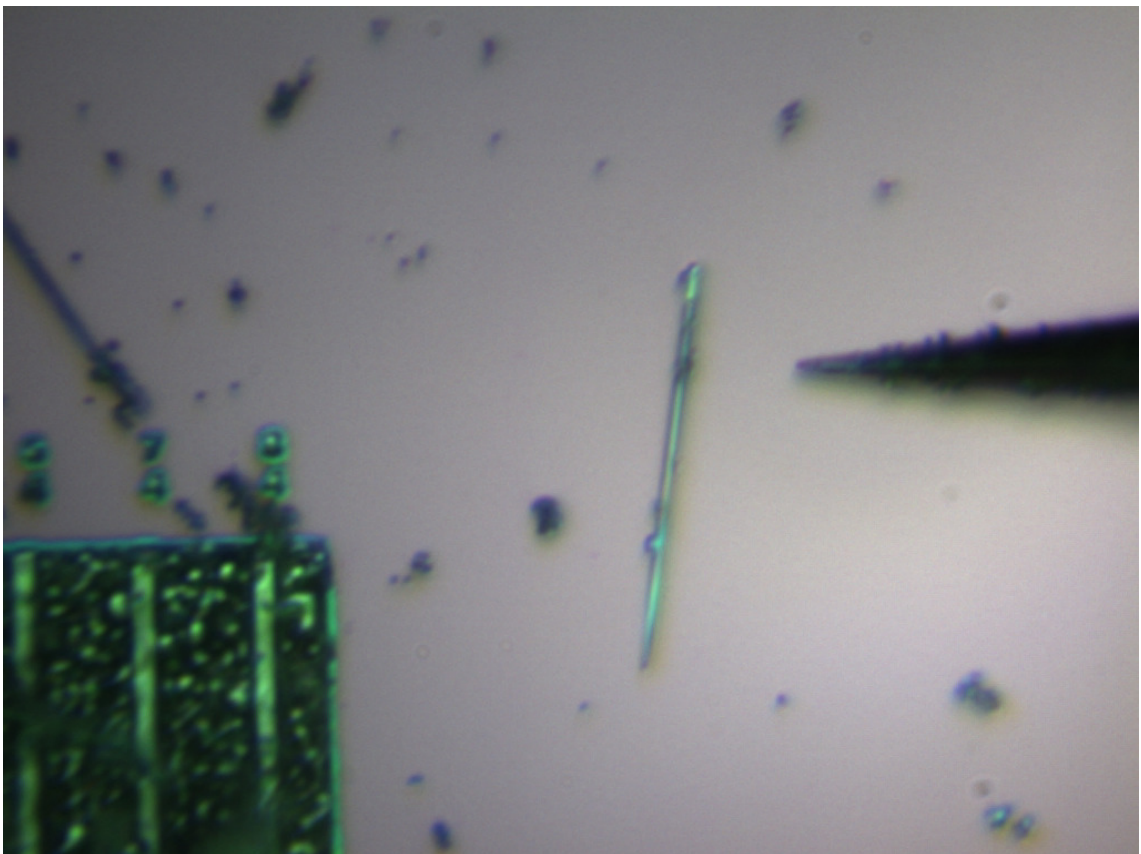
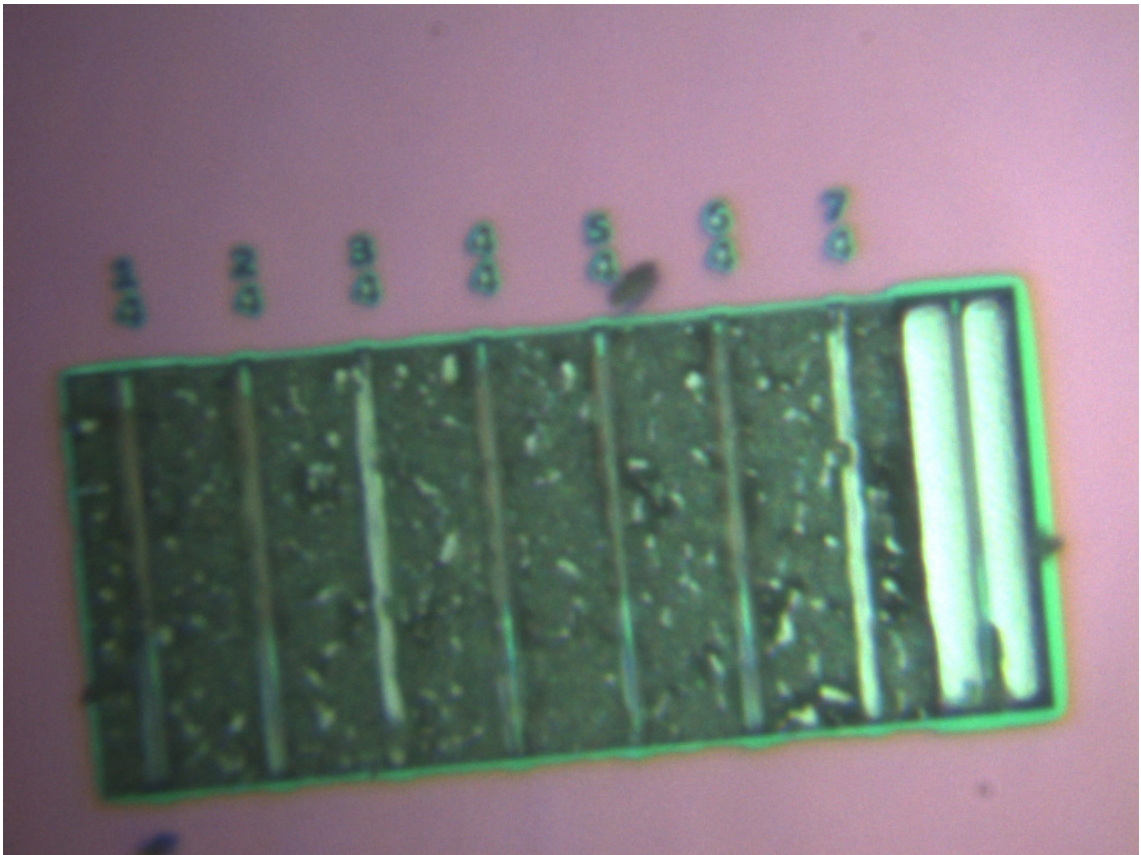
Scanning electron microscope (SEM) picture of the first batches of photonic crystal cavities. The small cubes designed to facilitate the etching process were not removed properly, and often attached to the structures, making them unusable.



Optical picture of the same chip. Even here the etching leftovers are evident. Only the rightmost part appears to be clean

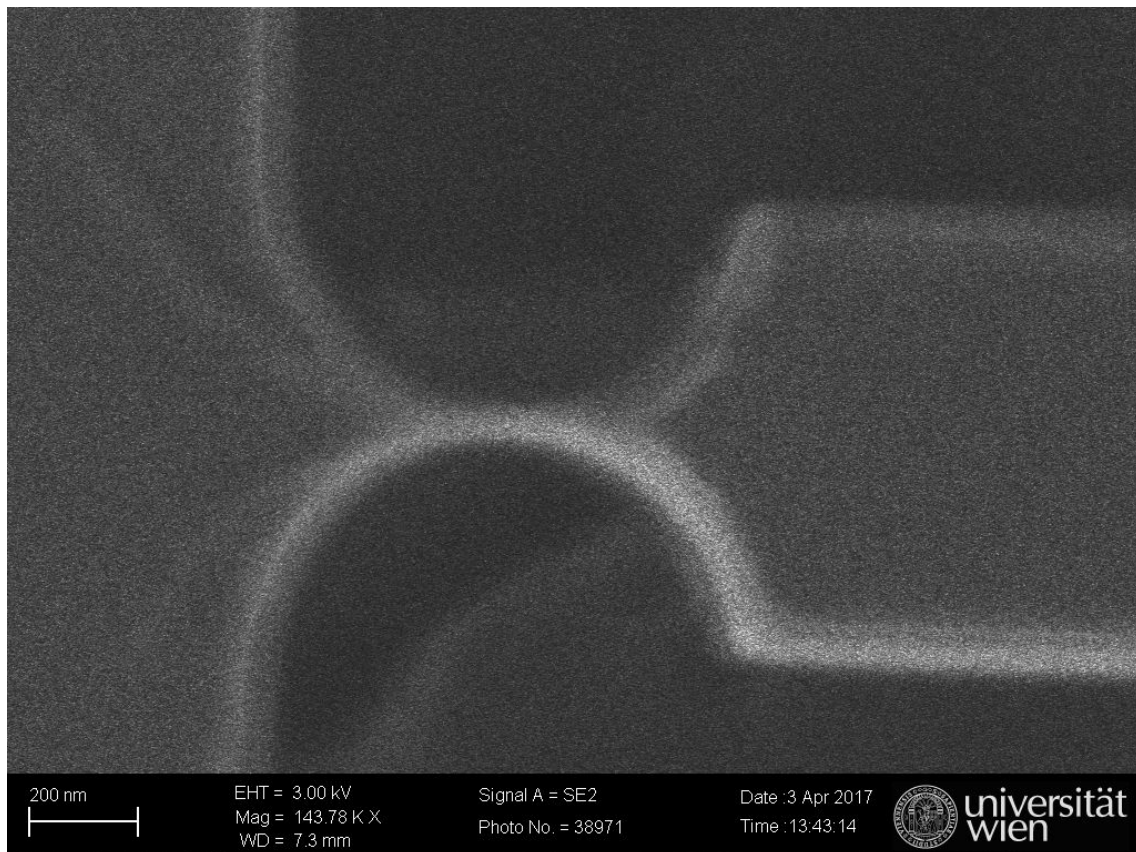
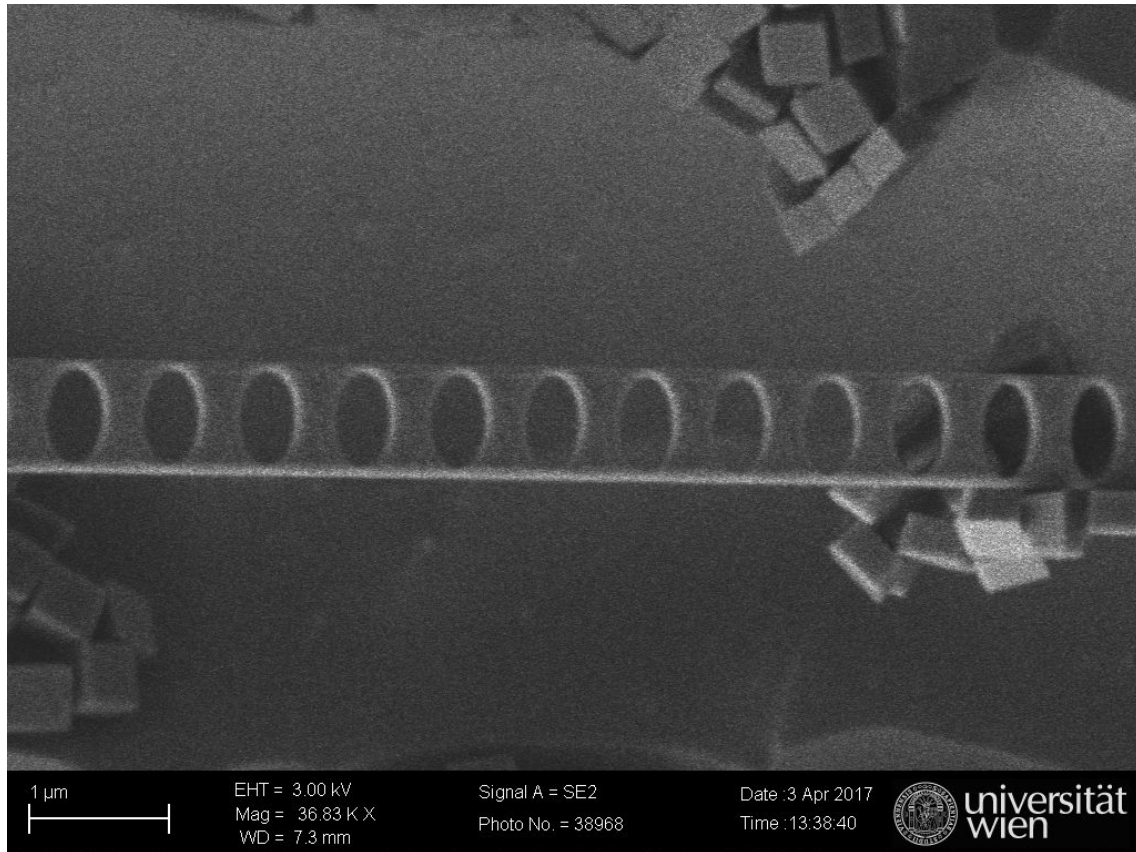
Attempt to pick up a photonic crystal: etching leftovers are everywhere! On the right the tungsten tip used to break the connection of the cavities to the chip.





The etched cubes sticking to the photonic crystal.

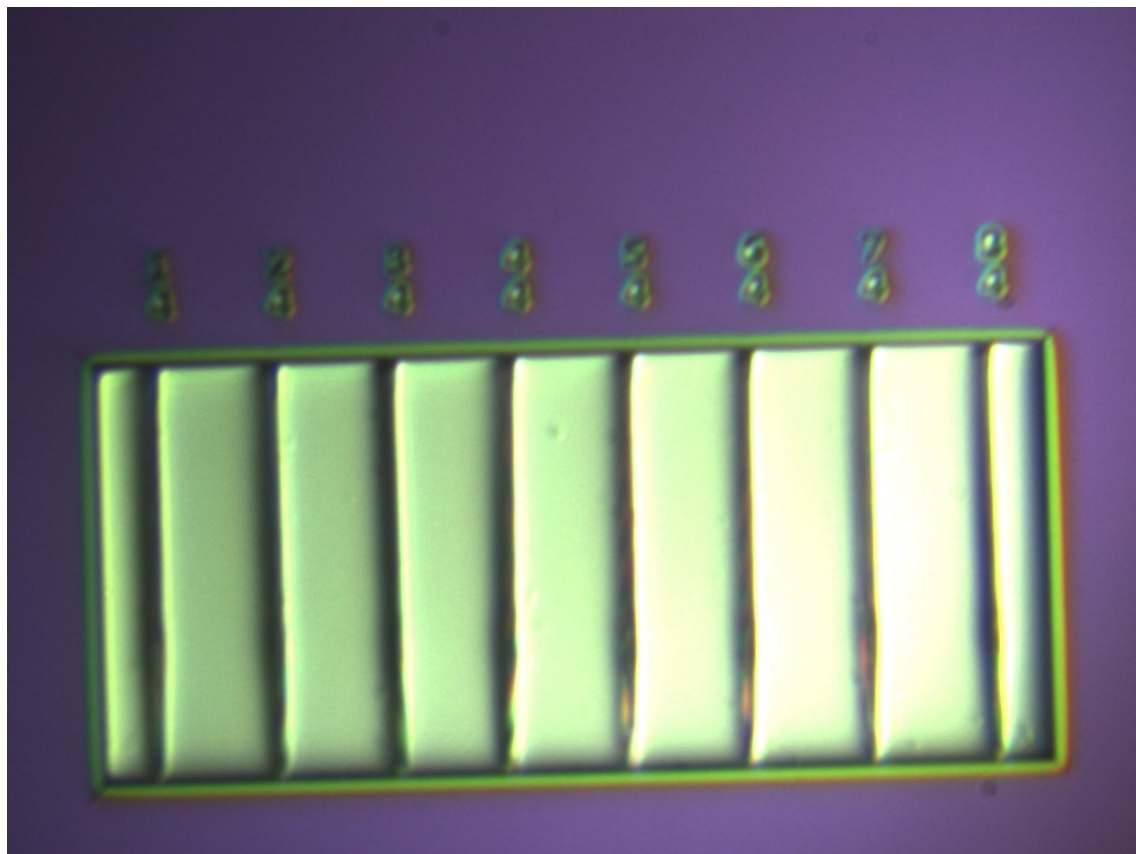
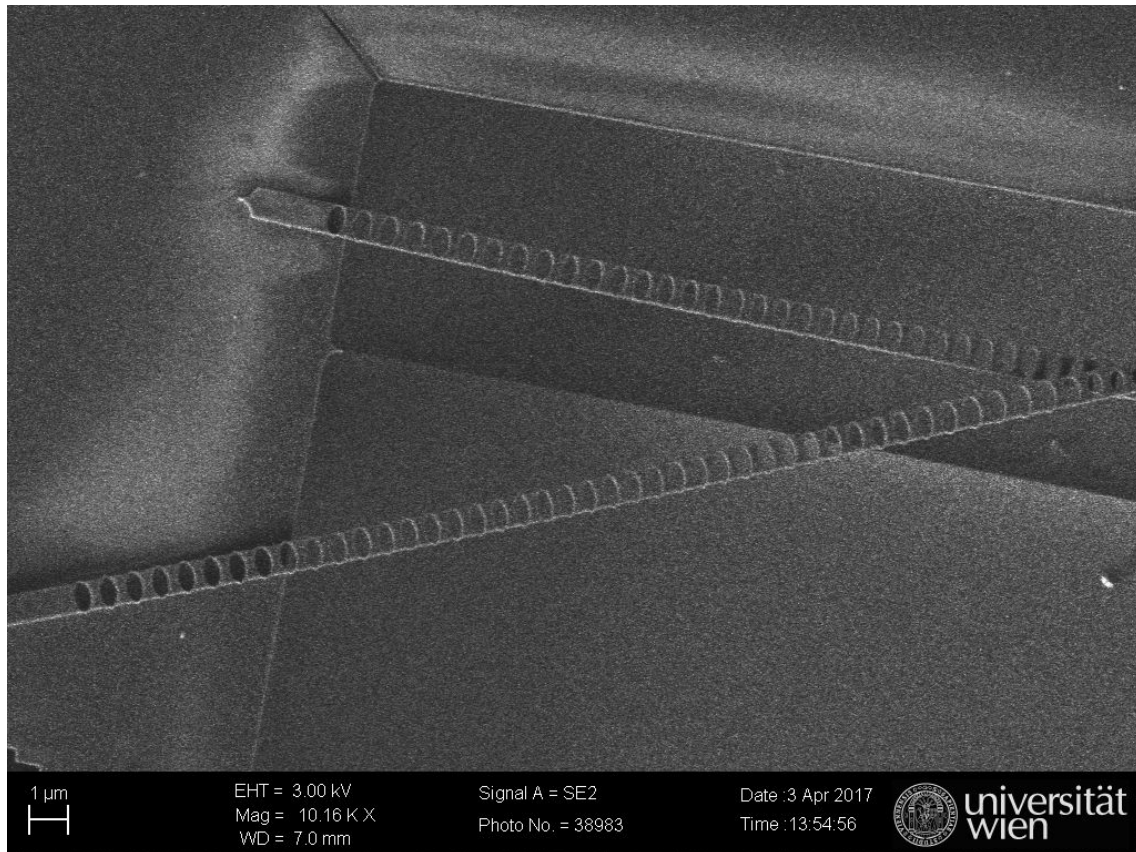
Detail of the connection holding keeping the photonic ctystals connected to the chip. This was broken by pressing with a tungsten tip, while the other side (with taper) was kept in contact with the fiber.



SEM image of a clean chip.

Optical microscope image of a clean chip. No etching leftovers are visible.

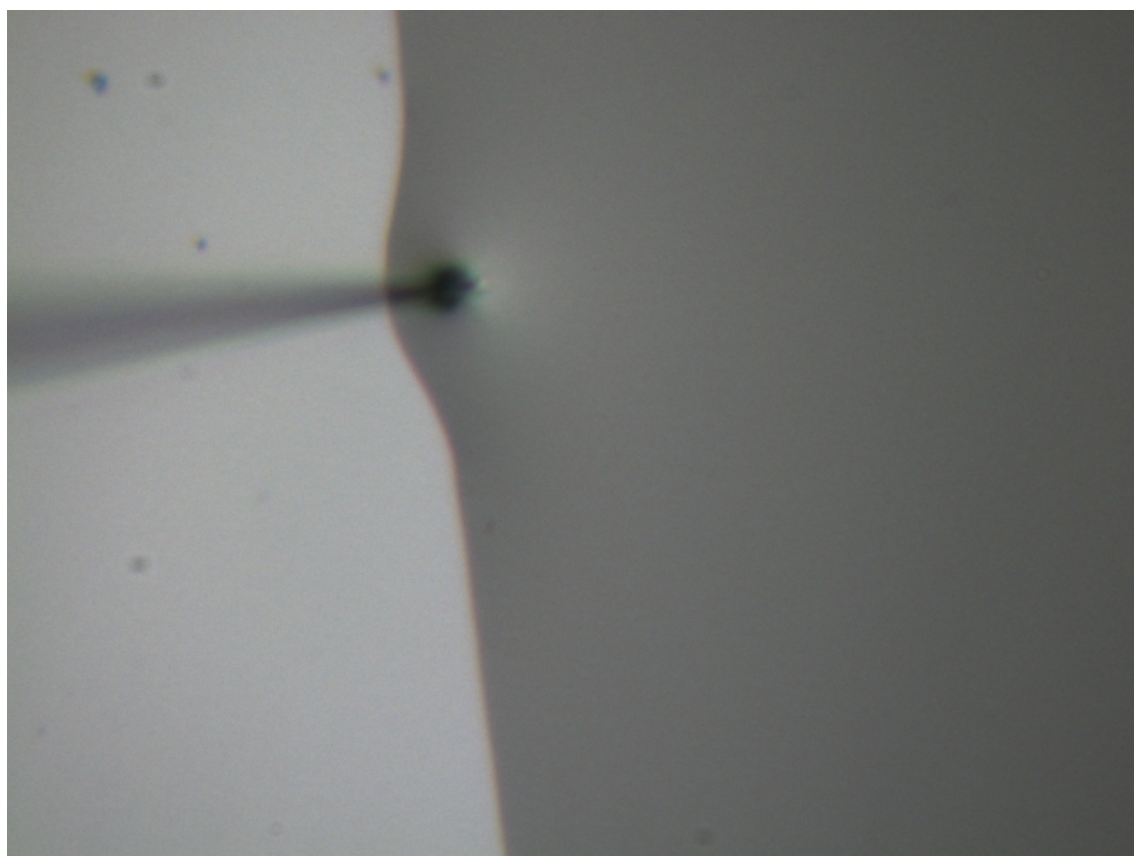




SEM image of a tapered fiber after it was dipped in UV glue to increase the contact surface with the photonic crystal. The droplets of glue evident on the fiber far from the tip are not cause of increased losses.

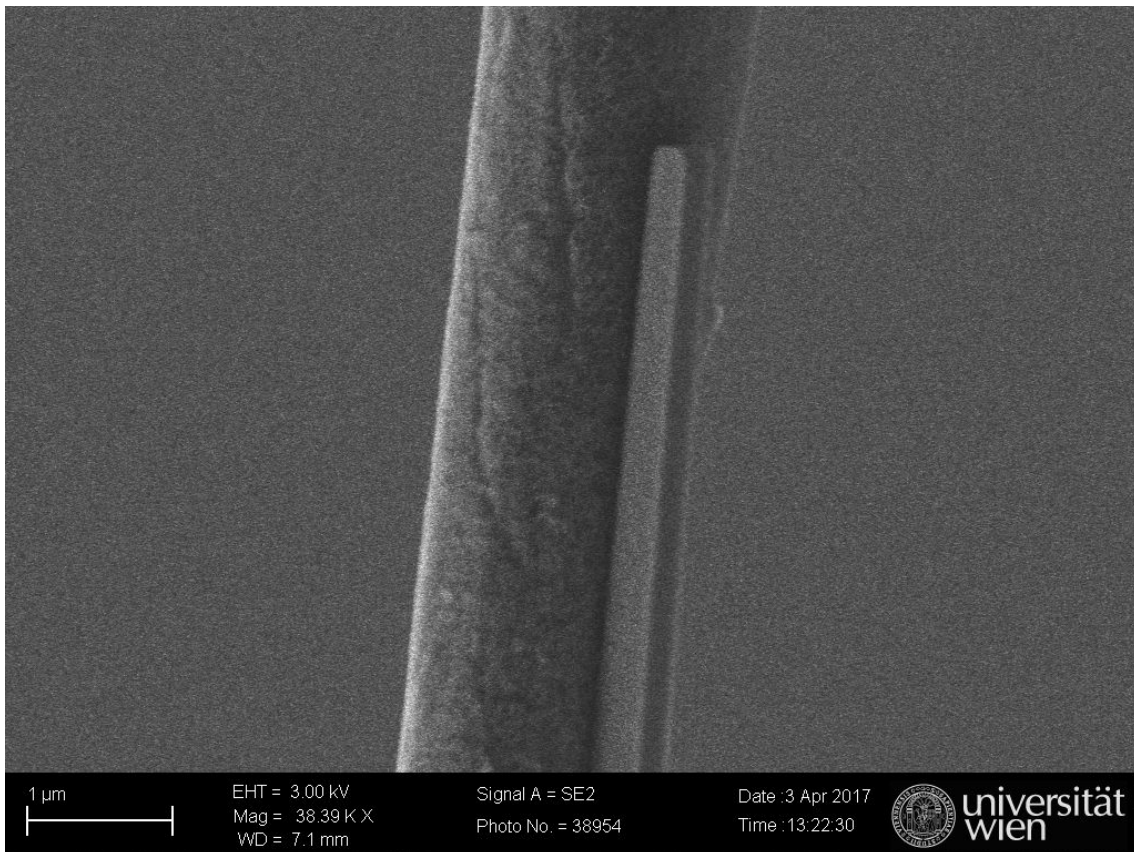
Optical microscope image of the tapered fiber as it is pushed into a droplet of UV glue. Its important to choose the glue with a low viscosity in order not to break the tip of the tapered fiber.





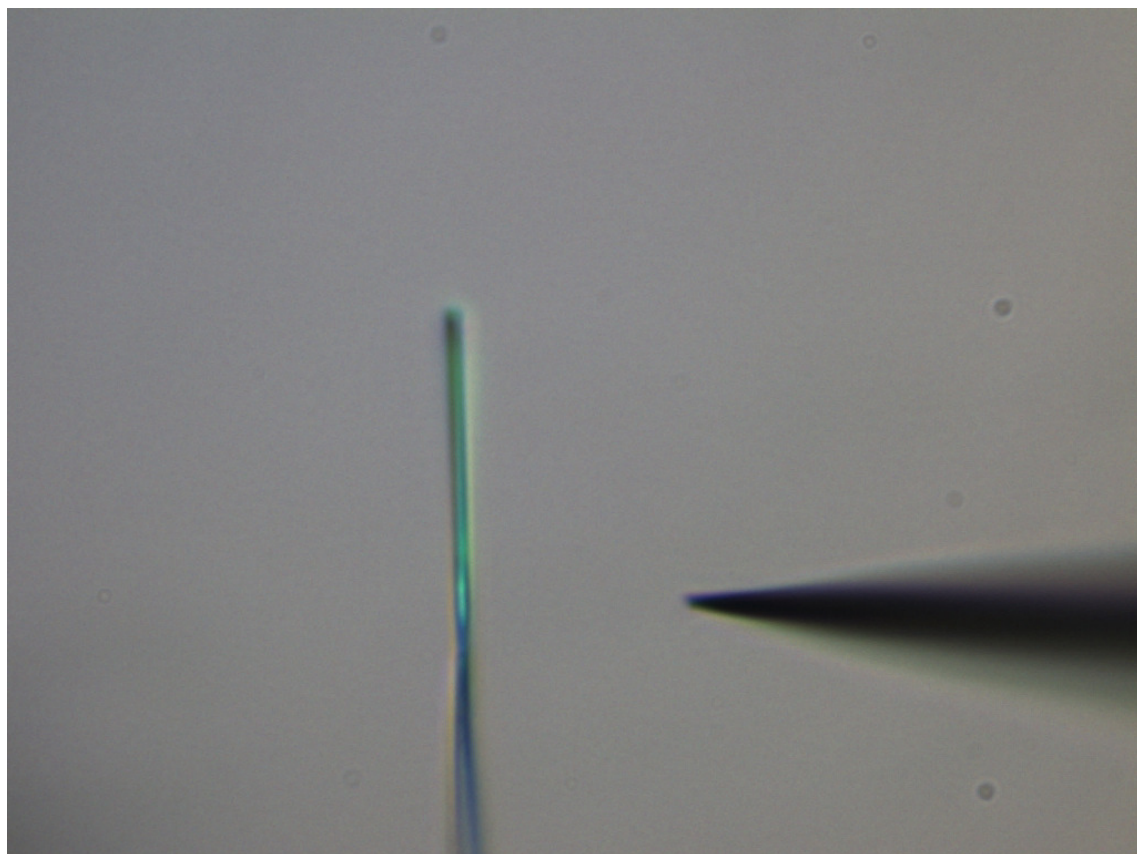
After being dipped into UV glue, the surface of the fiber is smoothened, and the contact surface is increased. This greatly enhances the bonding between the photonic crystal and the fiber. Note that the glue is cured before contact with the cavity.

SEM image of the contract point between fiber and cavity.



SEM image of the photonic crystal cavity on the tapered fiber.

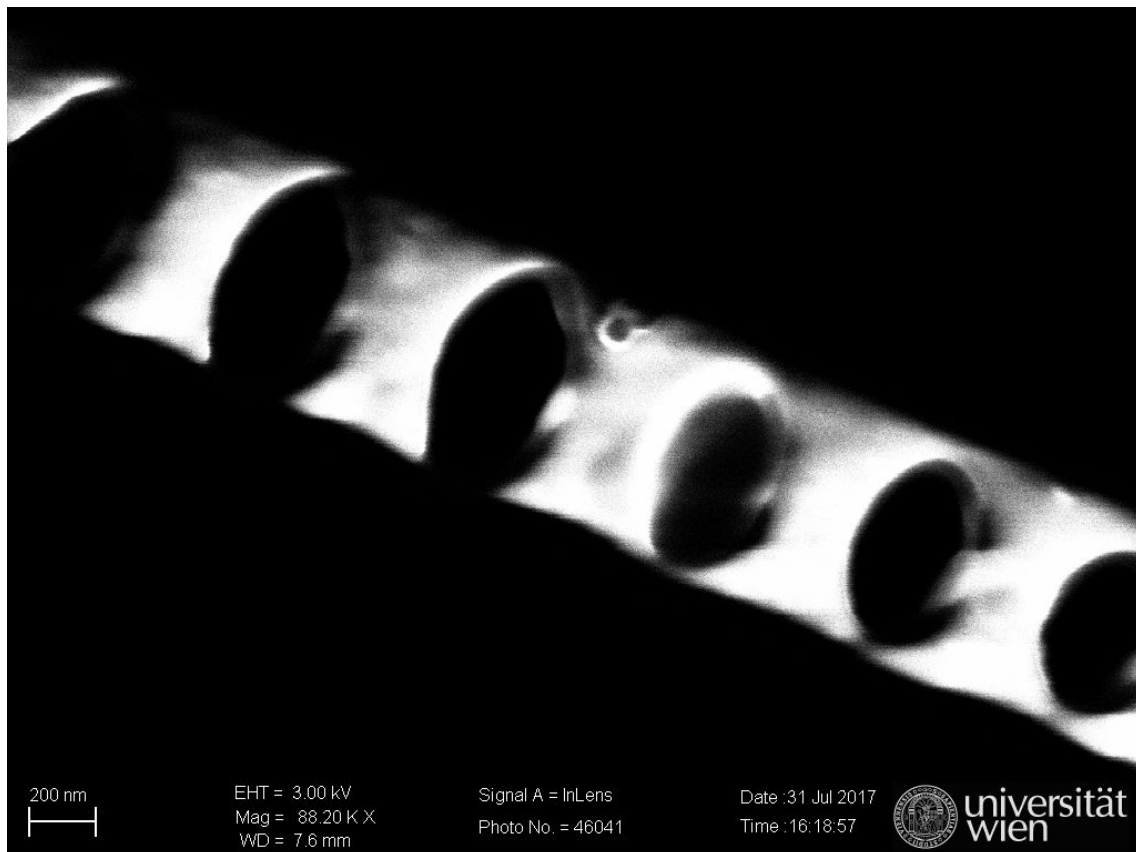
Optical image of the photonic crystal cavity as it was placed and aligned on to the tapered fiber with the help of a tungsten tip (right).



SEM image of the photonic crystal cavity after being used in an experiment. It seems that a particle got stuck to the cavity after it was lost! The image looks very bad as the sample was not gold coated before imaging causing it to charge up, deflecting electrons.

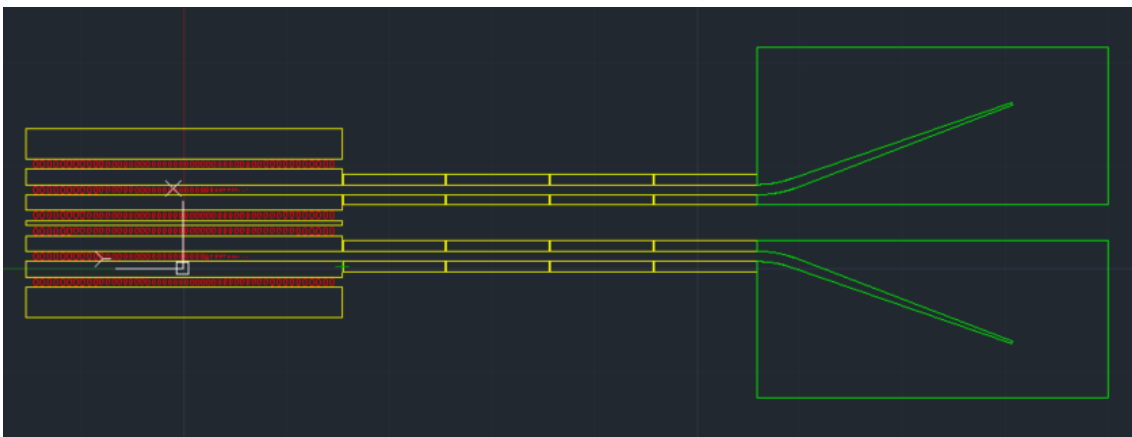
A gold coated (cracks on the surface) sample can be imaged very well.





Drawing of the cavities for future experiments. This kind of device was designed to remain on chip, for better thermalization and mechanical stability. Cavities were also designe in pairs for the study of self induced backaction dynamics (SIBA) as proposed by Neumeyer *et al.* [NQC15].

The CAD version of the new devices.





## BIBLIOGRAPHY

- [Abb+09] B. Abbott et al. “Observation of a kilogram-scale oscillator near its quantum ground state”. In: *New Journal of Physics* 11 (2009), pp. 0–13. ISSN: 13672630. DOI: [10.1088/1367-2630/11/7/073032](https://doi.org/10.1088/1367-2630/11/7/073032). URL: <http://iopscience.iop.org/1367-2630/11/7/073032> (cit. on pp. 47, 62).
- [Abb+16] B. P. Abbott et al. “Observation of Gravitational Waves from a Binary Black Hole Merger”. In: *Phys. Rev. Lett.* 116 (6 2016), p. 061102. DOI: [10.1103/PhysRevLett.116.061102](https://doi.org/10.1103/PhysRevLett.116.061102). URL: <https://link.aps.org/doi/10.1103/PhysRevLett.116.061102> (cit. on p. 3).
- [Agg+20] Nancy Aggarwal et al. “Room-temperature optomechanical squeezing”. In: *Nature Physics* 16.7 (2020), pp. 784–788. ISSN: 1745-2481. DOI: [10.1038/s41567-020-0877-x](https://doi.org/10.1038/s41567-020-0877-x). URL: <https://doi.org/10.1038/s41567-020-0877-x> (cit. on p. 89).
- [AKM14] Markus Aspelmeyer, Tobias J. Kippenberg, and Florian Marquardt. “Cavity optomechanics”. In: *Rev. Mod. Phys.* 86 (4 2014), pp. 1391–1452. DOI: [10.1103/RevModPhys.86.1391](https://doi.org/10.1103/RevModPhys.86.1391). URL: <https://link.aps.org/doi/10.1103/RevModPhys.86.1391> (cit. on pp. 15, 16, 21, 28, 29, 37, 81).
- [Alt+11] D. J. Alton et al. “Strong interactions of single atoms and photons near a dielectric boundary”. In: *Nature Physics* 7.2 (2011), pp. 159–165. ISSN: 1745-2481. DOI: [10.1038/nphys1837](https://doi.org/10.1038/nphys1837). URL: <https://doi.org/10.1038/nphys1837> (cit. on p. 21).
- [And+16] Ulrik L Andersen et al. “30 years of squeezed light generation”. In: *Physica Scripta* 91.5 (2016), p. 053001. DOI: [10.1088/0031-8949/91/5/053001](https://doi.org/10.1088/0031-8949/91/5/053001). URL: <https://doi.org/10.1088/0031-8949/91/5/053001> (cit. on p. 100).
- [Ane+09] G. Anetsberger et al. “Near-field cavity optomechanics with nanomechanical oscillators”. In: *Nature Physics* 5 (2009), p. 909. URL: <http://dx.doi.org/10.1038/nphys1425> (cit. on pp. 21, 24).
- [Arc+06] O. Arcizet et al. “Radiation-pressure cooling and optomechanical instability of a micromirror”. In: *Nature* 444.7115 (2006), pp. 71–74. ISSN: 1476-4687. DOI: [10.1038/nature05244](https://doi.org/10.1038/nature05244). URL: <https://doi.org/10.1038/nature05244> (cit. on p. 4).
- [Arm+03] D. K. Armani et al. “Ultra-high-Q toroid microcavity on a chip”. In: *Nature* 421.6926 (2003), pp. 925–928. ISSN: 1476-4687. DOI: [10.1038/nature01371](https://doi.org/10.1038/nature01371). URL: <https://doi.org/10.1038/nature01371> (cit. on p. 4).
- [Asa+17] Takashi Asano et al. “Photonic crystal nanocavity with a Q factor exceeding eleven million”. In: *Opt. Express* 25.3 (2017), pp. 1769–1777. DOI: [10.1364/OE.25.001769](https://doi.org/10.1364/OE.25.001769). URL: <http://www.opticsexpress.org/abstract.cfm?URI=oe-25-3-1769> (cit. on p. 29).
- [Ase+13] Peter Asenbaum et al. “Cavity cooling of free silicon nanoparticles in high vacuum”. In: *Nature Communications* 4 (2013), p. 2743. URL: <http://dx.doi.org/10.1038/ncomms3743> (cit. on pp. 4, 21, 23, 25).
- [ÅW13] Karl J Åström and Björn Wittenmark. *Computer-controlled systems: theory and design*. Courier Corporation, 2013 (cit. on pp. 44, 45, 76).

- [Baw+15] Mateusz Bawaj et al. “Probing deformed commutators with macroscopic harmonic oscillators”. In: *Nature Communications* 6.1 (2015), p. 7503. ISSN: 2041-1723. DOI: [10.1038/ncomms8503](https://doi.org/10.1038/ncomms8503). URL: <https://doi.org/10.1038/ncomms8503> (cit. on p. 3).
- [BCF90] S. A. Beresnev, V. G. Chernyak, and G. A. Fomyagin. “Motion of a spherical particle in a rarefied gas. Part 2. Drag and thermal polarization”. In: *Journal of Fluid Mechanics* 219 (1990), 405–421. DOI: [10.1017/S0022112090003007](https://doi.org/10.1017/S0022112090003007) (cit. on p. 84).
- [Bel+16] Alessio Belenchia et al. “Testing Quantum Gravity Induced Nonlocality via Optomechanical Quantum Oscillators”. In: *Phys. Rev. Lett.* 116 (16 2016), p. 161303. DOI: [10.1103/PhysRevLett.116.161303](https://link.aps.org/doi/10.1103/PhysRevLett.116.161303). URL: <https://link.aps.org/doi/10.1103/PhysRevLett.116.161303> (cit. on p. 3).
- [Bel80] Viacheslav Pavlovich Belavkin. “Optimal filtering of Markov signals with quantum white noise”. In: *Radio Eng. Electron. Phys. (USSR)* 25 (1980), p. 1445 (cit. on p. 3).
- [Bel95] VP Belavkin. “Quantum filtering of Markov signals with white quantum noise”. In: *Quantum communications and measurement*. Springer, 1995, pp. 381–391 (cit. on pp. 12, 43, 46, 49, 76).
- [Bel98] VP Belavkin. “Measurement, filtering and control in quantum open dynamical systems”. In: *Reports on Mathematical Physics* 43.3 (1998), A405–A425 (cit. on p. 76).
- [BHo8] Luc Bouten and Ramon van Handel. “On the Separation Principle of Quantum Control”. In: *Quantum Stochastics and Information: Statistics, Filtering and Control*. Ed. by V. P. Belavkin and M. I. Guta. Singapore: World Scientific, 2008 (cit. on p. 76).
- [BJK97] S. Bose, K. Jacobs, and P. L. Knight. “Preparation of nonclassical states in cavities with a moving mirror”. In: *Phys. Rev. A* 56 (5 1997), pp. 4175–4186. DOI: [10.1103/PhysRevA.56.4175](https://link.aps.org/doi/10.1103/PhysRevA.56.4175). URL: <https://link.aps.org/doi/10.1103/PhysRevA.56.4175> (cit. on p. 89).
- [BK95] Vladimir Borisovich Braginsky and Farid Ya Khalili. *Quantum measurement*. Cambridge University Press, 1995 (cit. on pp. 12, 13).
- [BLP82] Alberto Barchielli, L Lanz, and GM Prosperi. “A model for the macroscopic description and continual observations in quantum mechanics”. In: *Il Nuovo Cimento B* (1971-1996) 72.1 (1982), pp. 79–121 (cit. on p. 11).
- [BLP83] A. Barchielli, L. Lanz, and G. M. Prosperi. “Statistics of continuous trajectories in quantum mechanics: Operation-valued stochastic processes”. In: *Foundations of Physics* 13.8 (1983), pp. 779–812. ISSN: 1572-9516. DOI: [10.1007/BF01906270](https://doi.org/10.1007/BF01906270). URL: <https://doi.org/10.1007/BF01906270> (cit. on pp. 3, 11).
- [BM04] Gunnar Björk and Piero G Luca Mana. “A size criterion for macroscopic superposition states”. In: *Journal of Optics B: Quantum and Semi-classical Optics* 6.11 (2004), p. 429 (cit. on p. 3).
- [Bow+13] Richard W. Bowman et al. “Optical Trapping at Gigapascal Pressures”. In: *Phys. Rev. Lett.* 110 (9 2013), p. 095902. DOI: [10.1103/PhysRevLett.110.095902](https://link.aps.org/doi/10.1103/PhysRevLett.110.095902). URL: <https://link.aps.org/doi/10.1103/PhysRevLett.110.095902> (cit. on p. 23).
- [Bro+12] Daniel W. C. Brooks et al. “Non-classical light generated by quantum-noise-driven cavity optomechanics”. In: *Nature* 488.7412 (2012), pp. 476–480. ISSN: 1476-4687. DOI: [10.1038/nature11325](https://doi.org/10.1038/nature11325). URL: <https://doi.org/10.1038/nature11325> (cit. on p. 89).



- [BS10] P. F. Barker and M. N. Shneider. “Cavity cooling of an optically trapped nanoparticle”. In: *Phys. Rev. A* 81 (2 2010), p. 023826. DOI: [10.1103/PhysRevA.81.023826](https://doi.org/10.1103/PhysRevA.81.023826). URL: <https://link.aps.org/doi/10.1103/PhysRevA.81.023826> (cit. on pp. 4, 21).
- [BSLK04] Yaakov Bar-Shalom, X Rong Li, and Thiagalingam Kirubarajan. *Estimation with applications to tracking and navigation: theory algorithms and software*. John Wiley & Sons, 2004 (cit. on p. 46).
- [Bur+17] Michael J. Burek et al. “Fiber-Coupled Diamond Quantum Nanophotonic Interface”. In: *Phys. Rev. Applied* 8 (2 2017), p. 024026. DOI: [10.1103/PhysRevApplied.8.024026](https://doi.org/10.1103/PhysRevApplied.8.024026). URL: <https://link.aps.org/doi/10.1103/PhysRevApplied.8.024026> (cit. on pp. 24, 28, 34–36).
- [Bus+13] P. Bushev et al. “Shot-Noise-Limited Monitoring and Phase Locking of the Motion of a Single Trapped Ion”. In: *Phys. Rev. Lett.* 110 (13 2013), p. 133602. DOI: [10.1103/PhysRevLett.110.133602](https://doi.org/10.1103/PhysRevLett.110.133602). URL: <https://link.aps.org/doi/10.1103/PhysRevLett.110.133602> (cit. on pp. 47, 62).
- [BV75] Vladimir B Braginskii and Yurii I Vorontsov. “Quantum-mechanical limitations in macroscopic experiments and modern experimental technique”. In: *Soviet Physics Uspekhi* 17.5 (1975), pp. 644–650. DOI: [10.1070/pu1975v017n05abeh004362](https://doi.org/10.1070/pu1975v017n05abeh004362). URL: <https://doi.org/10.1070/pu1975v017n05abeh004362> (cit. on pp. 3, 13, 52).
- [BVH09] Luc Bouten, Ramon Van Handel, and Matthew R James. “A discrete invitation to quantum filtering and feedback control”. In: *SIAM review* 51.2 (2009), pp. 239–316 (cit. on p. 12).
- [BVJ07] Luc Bouten, Ramon Van Handel, and Matthew R. James. “An introduction to quantum filtering”. English (US). In: *SIAM Journal on Control and Optimization* 46.6 (2007). Copyright: Copyright 2011 Elsevier B.V., All rights reserved., pp. 2199–2241. ISSN: 0363-0129. DOI: [10.1137/060651239](https://doi.org/10.1137/060651239) (cit. on pp. 12, 43, 76).
- [Car+20] Daniel Carney et al. “Mechanical quantum sensing in the search for dark matter”. In: *Quantum Science and Technology* (2020). URL: <http://iopscience.iop.org/article/10.1088/2058-9565/abcfcf> (cit. on pp. 3, 52, 101).
- [Car93] Howard Carmichael. *An open systems approach to quantum optics: lectures presented at the Université Libre de Bruxelles, October 28 to November 4, 1991*. Vol. 18. Springer Science & Business Media, 1993 (cit. on pp. 3, 11, 45, 76).
- [Cav80] Carlton M. Caves. “Quantum-Mechanical Radiation-Pressure Fluctuations in an Interferometer”. In: *Phys. Rev. Lett.* 45 (2 1980), pp. 75–79. DOI: [10.1103/PhysRevLett.45.75](https://doi.org/10.1103/PhysRevLett.45.75). URL: <https://link.aps.org/doi/10.1103/PhysRevLett.45.75> (cit. on pp. 3, 89).
- [Cav+80] Carlton M. Caves et al. “On the measurement of a weak classical force coupled to a quantum-mechanical oscillator. I. Issues of principle”. In: *Rev. Mod. Phys.* 52 (2 1980), pp. 341–392. DOI: [10.1103/RevModPhys.52.341](https://doi.org/10.1103/RevModPhys.52.341). URL: <https://link.aps.org/doi/10.1103/RevModPhys.52.341> (cit. on pp. 3, 13).
- [Cav82] Carlton M. Caves. “Quantum limits on noise in linear amplifiers”. In: *Phys. Rev. D* 26 (8 1982), pp. 1817–1839. DOI: [10.1103/PhysRevD.26.1817](https://doi.org/10.1103/PhysRevD.26.1817). URL: <https://link.aps.org/doi/10.1103/PhysRevD.26.1817> (cit. on pp. 1, 7).

- [Cav85] Carlton M. Caves. “Defense of the Standard Quantum Limit for Free-Mass Position”. In: *Phys. Rev. Lett.* 54 (23 1985), pp. 2465–2468. DOI: [10.1103/PhysRevLett.54.2465](https://doi.org/10.1103/PhysRevLett.54.2465). URL: <https://link.aps.org/doi/10.1103/PhysRevLett.54.2465> (cit. on pp. 3, 13).
- [Cav86] Carlton M. Caves. “Quantum mechanics of measurements distributed in time. A path-integral formulation”. In: *Phys. Rev. D* 33 (6 1986), pp. 1643–1665. DOI: [10.1103/PhysRevD.33.1643](https://doi.org/10.1103/PhysRevD.33.1643). URL: <https://link.aps.org/doi/10.1103/PhysRevD.33.1643> (cit. on p. 12).
- [Cav87] Carlton M. Caves. “Quantum mechanics of measurements distributed in time. II. Connections among formulations”. In: *Phys. Rev. D* 35 (6 1987), pp. 1815–1830. DOI: [10.1103/PhysRevD.35.1815](https://doi.org/10.1103/PhysRevD.35.1815). URL: <https://link.aps.org/doi/10.1103/PhysRevD.35.1815> (cit. on p. 12).
- [CGS03] A. A. Clerk, S. M. Girvin, and A. D. Stone. “Quantum-limited measurement and information in mesoscopic detectors”. In: *Phys. Rev. B* 67 (16 2003), p. 165324. DOI: [10.1103/PhysRevB.67.165324](https://doi.org/10.1103/PhysRevB.67.165324). URL: <https://link.aps.org/doi/10.1103/PhysRevB.67.165324> (cit. on pp. 1, 3, 24, 62).
- [Cha+10] D. E. Chang et al. “Cavity opto-mechanics using an optically levitated nanosphere”. In: *Proceedings of the National Academy of Sciences* 107.3 (2010), pp. 1005–1010. DOI: [10.1073/pnas.0912969107](https://doi.org/10.1073/pnas.0912969107). eprint: <http://www.pnas.org/content/107/3/1005.full.pdf>. URL: <http://www.pnas.org/content/107/3/1005.abstract> (cit. on pp. 4, 21).
- [Cha+11] Jasper Chan et al. “Laser cooling of a nanomechanical oscillator into its quantum ground state”. In: *Nature* 478 (2011), p. 89. URL: <http://dx.doi.org/10.1038/nature10461> (cit. on pp. 3, 16, 24).
- [Che13] Yanbei Chen. “Macroscopic quantum mechanics: theory and experimental concepts of optomechanics”. In: *Journal of Physics B: Atomic, Molecular and Optical Physics* 46.10 (2013), p. 104001. ISSN: 0953-4075. DOI: [10.1088/0953-4075/46/10/104001](https://doi.org/10.1088/0953-4075/46/10/104001). arXiv: [arXiv: 1302.1924v1](https://arxiv.org/abs/1302.1924v1). URL: <http://stacks.iop.org/0953-4075/46/i=10/a=104001?key=crossref.f6fb280b25ca177dd9c80e4daf9cd4e0> (cit. on p. 52).
- [Cle+10] A. A. Clerk et al. “Introduction to quantum noise, measurement, and amplification”. In: *Rev. Mod. Phys.* 82 (2 2010), pp. 1155–1208. DOI: [10.1103/RevModPhys.82.1155](https://doi.org/10.1103/RevModPhys.82.1155). URL: <https://link.aps.org/doi/10.1103/RevModPhys.82.1155> (cit. on pp. 3, 14, 15, 47, 58, 59, 62, 85).
- [CM87] Carlton M. Caves and G. J. Milburn. “Quantum-mechanical model for continuous position measurements”. In: *Phys. Rev. A* 36 (12 1987), pp. 5543–5555. DOI: [10.1103/PhysRevA.36.5543](https://doi.org/10.1103/PhysRevA.36.5543). URL: <https://link.aps.org/doi/10.1103/PhysRevA.36.5543> (cit. on pp. 3, 7, 8, 10–12).
- [Cor+06] Thomas Corbitt et al. “Squeezed-state source using radiation-pressure-induced rigidity”. In: *Phys. Rev. A* 73 (2 2006), p. 023801. DOI: [10.1103/PhysRevA.73.023801](https://doi.org/10.1103/PhysRevA.73.023801). URL: <https://link.aps.org/doi/10.1103/PhysRevA.73.023801> (cit. on p. 89).
- [Deb+17] Kapil Debnath et al. “Ultrahigh-Q photonic crystal cavities in silicon rich nitride”. In: *Opt. Express* 25.22 (2017), pp. 27334–27340. DOI: [10.1364/OE.25.027334](https://doi.org/10.1364/OE.25.027334). URL: <http://www.opticsexpress.org/abstract.cfm?URI=oe-25-22-27334> (cit. on p. 29).
- [Del+19] Uroš Delić et al. “Cavity Cooling of a Levitated Nanosphere by Coherent Scattering”. In: *Phys. Rev. Lett.* 122 (12 2019), p. 123602. DOI: [10.1103/PhysRevLett.122.123602](https://doi.org/10.1103/PhysRevLett.122.123602). URL: <https://link.aps.org/doi/10.1103/PhysRevLett.122.123602> (cit. on p. 46).

- [Del+20a] Uroš Delić et al. “Cooling of a levitated nanoparticle to the motional quantum ground state”. In: *Science* 367.6480 (2020), pp. 892–895. ISSN: 0036-8075. DOI: [10.1126/science.aba3993](https://doi.org/10.1126/science.aba3993). eprint: <https://science.sciencemag.org/content/367/6480/892.full.pdf>. URL: <https://science.sciencemag.org/content/367/6480/892> (cit. on pp. 3, 16, 46).
- [Del+20b] Uroš Delić et al. “Levitated cavity optomechanics in high vacuum”. In: *Quantum Science and Technology* 5.2 (2020), p. 025006 (cit. on p. 21).
- [Des+13] Nicolas Deschannes et al. “Observation of Backaction and Self-Induced Trapping in a Planar Hollow Photonic Crystal Cavity”. In: *Phys. Rev. Lett.* 110 (12 2013), p. 123601. DOI: [10.1103/PhysRevLett.110.123601](https://doi.org/10.1103/PhysRevLett.110.123601). URL: <https://link.aps.org/doi/10.1103/PhysRevLett.110.123601> (cit. on p. 24).
- [DFT13] John C Doyle, Bruce A Francis, and Allen R Tannenbaum. *Feedback control theory*. Courier Corporation, 2013 (cit. on p. 76).
- [Die+18] Rozenn Diehl et al. “Optical potential mapping with a levitated nanoparticle at sub-wavelength distances from a membrane”. In: *arXiv:1803.04917 [physics.optics]* (2018) (cit. on pp. 24, 35).
- [DJ99] A. C. Doherty and K. Jacobs. “Feedback control of quantum systems using continuous state estimation”. In: *Physical Review A - Atomic, Molecular, and Optical Physics* 60.4 (1999), pp. 2700–2711. ISSN: 10941622. DOI: [10.1103/PhysRevA.60.2700](https://doi.org/10.1103/PhysRevA.60.2700). arXiv: [9812004](https://arxiv.org/abs/9812004) (cit. on pp. 49, 76).
- [DSC02] Wolfgang Dür, Christoph Simon, and J. Ignacio Cirac. “Effective Size of Certain Macroscopic Quantum Superpositions”. In: *Phys. Rev. Lett.* 89 (21 2002), p. 210402. DOI: [10.1103/PhysRevLett.89.210402](https://doi.org/10.1103/PhysRevLett.89.210402). URL: <https://link.aps.org/doi/10.1103/PhysRevLett.89.210402> (cit. on p. 3).
- [EB03] S.C. Edwards and V.P. Belavkin. “On the Duality of Quantum Filtering and Optimal Feedback Control in Quantum Open Linear Dynamical Systems”. In: *Physics and Control, 2003. Proceedings. 2003 International Conference*. Vol. 3. Aug. 2003, 768 –772 vol.3. DOI: [10.1109/PHYCON.2003.1237001](https://doi.org/10.1109/PHYCON.2003.1237001) (cit. on pp. 77, 78).
- [EB05] S. C Edwards and V. P Belavkin. “Optimal Quantum Filtering and Quantum Feedback Control”. In: *arXiv:0506018 [quant-ph]* (2005). arXiv: [quant-ph/0506018](https://arxiv.org/abs/quant-ph/0506018) (cit. on p. 76).
- [EFV05] Dirk Englund, Ilya Fushman, and Jelena Vuckovic. “General recipe for designing photonic crystal cavities”. In: *Optics express* 13.16 (2005), pp. 5961–5975 (cit. on p. 22).
- [Eng+05] Dirk Englund et al. “Controlling the Spontaneous Emission Rate of Single Quantum Dots in a Two-Dimensional Photonic Crystal”. In: *Phys. Rev. Lett.* 95 (1 2005), p. 013904. DOI: [10.1103/PhysRevLett.95.013904](https://doi.org/10.1103/PhysRevLett.95.013904). URL: <https://link.aps.org/doi/10.1103/PhysRevLett.95.013904> (cit. on p. 24).
- [EWP17] Muhammad F Emzir, Matthew J Woolley, and Ian R Petersen. “A quantum extended Kalman filter”. In: *Journal of Physics A: Mathematical and Theoretical* 50.22 (2017), p. 225301. DOI: [10.1088/1751-8121/aa6e5e](https://doi.org/10.1088/1751-8121/aa6e5e). URL: <https://doi.org/10.1088/1751-8121/aa6e5e> (cit. on p. 12).
- [Fab+94] C. Fabre et al. “Quantum-noise reduction using a cavity with a movable mirror”. In: *Phys. Rev. A* 49 (2 1994), pp. 1337–1343. DOI: [10.1103/PhysRevA.49.1337](https://doi.org/10.1103/PhysRevA.49.1337). URL: <https://link.aps.org/doi/10.1103/PhysRevA.49.1337> (cit. on p. 89).

- [Fla+15] Fulvio Flamini et al. “Thermally reconfigurable quantum photonic circuits at telecom wavelength by femtosecond laser micromachining”. In: *Light: Science & Applications* 4.11 (2015), e354–e354. ISSN: 2047-7538. DOI: [10.1038/lsa.2015.127](https://doi.org/10.1038/lsa.2015.127). URL: <https://doi.org/10.1038/lsa.2015.127>.
- [Fri+17] Martin Frimmer et al. “Controlling the net charge on a nanoparticle optically levitated in vacuum”. In: *Phys. Rev. A* 95 (6 2017), p. 061801. DOI: [10.1103/PhysRevA.95.061801](https://link.aps.org/doi/10.1103/PhysRevA.95.061801). URL: <https://link.aps.org/doi/10.1103/PhysRevA.95.061801> (cit. on pp. 24, 47, 58).
- [GA10] Mohinder Grewal and Angus Andrews. “Applications of Kalman Filtering in Aerospace 1960 to the Present [Historical Perspectives”. In: *Control Systems, IEEE* 30 (July 2010), pp. 69 –78. DOI: [10.1109/MCS.2010.936465](https://doi.org/10.1109/MCS.2010.936465) (cit. on p. 44).
- [GB+19] C. Gonzalez-Ballester et al. “Theory for Cavity Cooling of Levitated Nanoparticles via Coherent Scattering: Master Equation Approach”. In: *Physical Review A* 100 (2019), p. 013805. ISSN: 2469-9926, 2469-9934. DOI: [10.1103/PhysRevA.100.013805](https://doi.org/10.1103/PhysRevA.100.013805) (cit. on p. 71).
- [GC85] C. W. Gardiner and M. J. Collett. “Input and Output in Damped Quantum Systems: Quantum Stochastic Differential Equations and the Master Equation”. In: *Physical Review A* 31.6 (1985), p. 3761. DOI: [10.1103/PhysRevA.31.3761](https://doi.org/10.1103/PhysRevA.31.3761) (cit. on pp. 71, 91).
- [Gen+08] C. Genes et al. “Ground-state cooling of a micromechanical oscillator: Comparing cold damping and cavity-assisted cooling schemes”. In: *Phys. Rev. A* 77 (3 2008), p. 033804. DOI: [10.1103/PhysRevA.77.033804](https://link.aps.org/doi/10.1103/PhysRevA.77.033804). URL: <https://link.aps.org/doi/10.1103/PhysRevA.77.033804> (cit. on pp. 15, 28).
- [Gen+15] Marco G Genoni et al. “Quantum cooling and squeezing of a levitating nanosphere via time-continuous measurements”. In: *New Journal of Physics* 17.7 (2015), p. 073019. ISSN: 1367-2630. DOI: [10.1088/1367-2630/17/7/073019](https://doi.org/10.1088/1367-2630/17/7/073019). arXiv: 1503.05603. URL: <https://iopscience.iop.org/article/10.1088/1367-2630/17/7/073019> (cit. on p. 52).
- [Ger+03] JM Geremia et al. “Quantum Kalman Filtering and the Heisenberg Limit in Atomic Magnetometry”. In: *Phys. Rev. Lett.* 91 (25 2003), p. 250801. DOI: [10.1103/PhysRevLett.91.250801](https://link.aps.org/doi/10.1103/PhysRevLett.91.250801). URL: <https://link.aps.org/doi/10.1103/PhysRevLett.91.250801> (cit. on p. 45).
- [Ger+08] Andrew A. Geraci et al. “Improved constraints on non-Newtonian forces at 10 microns”. In: *Phys. Rev. D* 78 (2 2008), p. 022002. DOI: [10.1103/PhysRevD.78.022002](https://link.aps.org/doi/10.1103/PhysRevD.78.022002). URL: <https://link.aps.org/doi/10.1103/PhysRevD.78.022002> (cit. on p. 3).
- [Ger+96] JMea Gerard et al. “Quantum boxes as active probes for photonic microstructures: The pillar microcavity case”. In: *Applied Physics Letters* 69.4 (1996), pp. 449–451 (cit. on p. 22).
- [Gha+18] A. H. Ghadimi et al. “Elastic strain engineering for ultralow mechanical dissipation”. In: *Science* 360.6390 (2018), pp. 764–768. ISSN: 0036-8075. DOI: [10.1126/science.aar6939](https://doi.org/10.1126/science.aar6939). eprint: <https://science.sciencemag.org/content/360/6390/764.full.pdf>. URL: <https://science.sciencemag.org/content/360/6390/764> (cit. on p. 4).
- [Gie+12] Jan Gieseler et al. “Subkelvin Parametric Feedback Cooling of a Laser-Trapped Nanoparticle”. In: *Phys. Rev. Lett.* 109 (10 2012), p. 103603. DOI: [10.1103/PhysRevLett.109.103603](https://link.aps.org/doi/10.1103/PhysRevLett.109.103603). URL: <https://link.aps.org/doi/10.1103/PhysRevLett.109.103603> (cit. on pp. 4, 17, 21, 23, 43).

- [Gie+14] Jan Gieseler et al. “Dynamic relaxation of a levitated nanoparticle from a non-equilibrium steady state”. In: *Nature Nanotechnology* 9 (2014), p. 358. URL: <http://dx.doi.org/10.1038/nnano.2014.40> (cit. on pp. 43, 83).
- [Gig+06] S. Gigan et al. “Self-cooling of a micromirror by radiation pressure”. In: *Nature* 444.7115 (2006), pp. 67–70. ISSN: 1476-4687. DOI: [10.1038/nature05273](https://doi.org/10.1038/nature05273). URL: <https://doi.org/10.1038/nature05273> (cit. on p. 4).
- [Gla+15] Steffen J. Glaser et al. “Training Schrödinger’s cat: quantum optimal control”. In: *The European Physical Journal D* 69.12 (2015), p. 279. ISSN: 1434-6079. DOI: [10.1140/epjd/e2015-60464-1](https://doi.org/10.1140/epjd/e2015-60464-1). URL: <https://doi.org/10.1140/epjd/e2015-60464-1> (cit. on p. 45).
- [GLS16] Marco G. Genoni, Ludovico Lami, and Alessio Serafini. “Conditional and Unconditional Gaussian Quantum Dynamics”. In: *Contemporary Physics* 57.3 (July 2, 2016), pp. 331–349. ISSN: 0010-7514. DOI: [10.1080/00107514.2015.1125624](https://doi.org/10.1080/00107514.2015.1125624). URL: <https://doi.org/10.1080/00107514.2015.1125624> (visited on 03/09/2021) (cit. on p. 76).
- [GNG19] Jingkun Guo, Richard Norte, and Simon Gröblacher. “Feedback Cooling of a Room Temperature Mechanical Oscillator close to its Motional Ground State”. In: *Phys. Rev. Lett.* 123 (22 2019), p. 223602. DOI: [10.1103/PhysRevLett.123.223602](https://link.aps.org/doi/10.1103/PhysRevLett.123.223602). URL: <https://link.aps.org/doi/10.1103/PhysRevLett.123.223602> (cit. on p. 4).
- [GNQ13] Jan Gieseler, Lukas Novotny, and Romain Quidant. “Thermal nonlinearities in a nanomechanical oscillator”. In: *Nature Physics* 9 (2013), p. 806. URL: <http://dx.doi.org/10.1038/nphys2798> (cit. on pp. 21, 47, 70).
- [Gob+15] A. Goban et al. “Superradiance for Atoms Trapped along a Photonic Crystal Waveguide”. In: *Phys. Rev. Lett.* 115 (6 2015), p. 063601. DOI: [10.1103/PhysRevLett.115.063601](https://link.aps.org/doi/10.1103/PhysRevLett.115.063601). URL: <https://link.aps.org/doi/10.1103/PhysRevLett.115.063601> (cit. on p. 24).
- [GPK10] Andrew A. Geraci, Scott B. Papp, and John Kitching. “Short-Range Force Detection Using Optically Cooled Levitated Microspheres”. In: *Phys. Rev. Lett.* 105 (10 2010), p. 101101. DOI: [10.1103/PhysRevLett.105.101101](https://link.aps.org/doi/10.1103/PhysRevLett.105.101101). URL: <https://link.aps.org/doi/10.1103/PhysRevLett.105.101101> (cit. on pp. 3, 23, 29).
- [GSM04] JM Geremia, John K. Stockton, and Hideo Mabuchi. “Real-Time Quantum Feedback Control of Atomic Spin-Squeezing”. In: *Science* 304.5668 (2004), pp. 270–273. ISSN: 0036-8075. DOI: [10.1126/science.1095374](https://science.sciencemag.org/content/304/5668/270.full.pdf). eprint: <https://science.sciencemag.org/content/304/5668/270.full.pdf>. URL: <https://science.sciencemag.org/content/304/5668/270> (cit. on p. 44).
- [Gut+20] C. Gut et al. “Stationary optomechanical entanglement between a mechanical oscillator and its measurement apparatus”. In: *Phys. Rev. Research* 2 (3 2020), p. 033244. DOI: [10.1103/PhysRevResearch.2.033244](https://link.aps.org/doi/10.1103/PhysRevResearch.2.033244). URL: <https://link.aps.org/doi/10.1103/PhysRevResearch.2.033244> (cit. on pp. 100, 101).
- [GVK12] E. Gavartin, P. Verlot, and T. J. Kippenberg. “A hybrid on-chip optomechanical transducer for ultrasensitive force measurements”. In: *Nature Nanotechnology* 7 (2012), p. 509. URL: <http://dx.doi.org/10.1038/nnano.2012.97> (cit. on p. 21).
- [GZ04] Crispin W. Gardiner and Peter Zoller. *Quantum Noise*. Third. Berlin: Springer, 2004. ISBN: 978-3-540-22301-6 (cit. on pp. 8, 73, 76).



- [Ham+15] P. Hamilton et al. “Atom-interferometry constraints on dark energy”. In: *Science* 349.6250 (2015), pp. 849–851. ISSN: 0036-8075. DOI: [10.1126/science.aaa8883](https://doi.org/10.1126/science.aaa8883). eprint: <https://science.sciencemag.org/content/349/6250/849.full.pdf>. URL: <https://science.sciencemag.org/content/349/6250/849> (cit. on p. 3).
- [Hau+13] B. J. M. Hausmann et al. “Coupling of NV Centers to Photonic Crystal Nanobeams in Diamond”. In: *Nano Letters* 13.12 (2013), pp. 5791–5796. DOI: [10.1021/nl402174g](https://doi.org/10.1021/nl402174g). eprint: <http://dx.doi.org/10.1021/nl402174g>. URL: <http://dx.doi.org/10.1021/nl402174g> (cit. on p. 24).
- [Heb+18] Erik Hebestreit et al. “Calibration and energy measurement of optically levitated nanoparticle sensors”. In: *Review of Scientific Instruments* 89.3 (2018), p. 033111 (cit. on p. 81).
- [Hei27] W Heisenberg. “Über den anschaulichen Inhalt der quantentheoretischen Kinematik und Mechanik”. In: *Zeitschrift für Physik* 43.3 (1927), pp. 172–198 (cit. on p. 13).
- [Hem+17] David Hempston et al. “Force sensing with an optically levitated charged nanoparticle”. In: *Applied Physics Letters* 111.13 (2017), p. 133111. DOI: [10.1063/1.4993555](https://doi.org/10.1063/1.4993555). eprint: <https://doi.org/10.1063/1.4993555>. URL: <https://doi.org/10.1063/1.4993555> (cit. on pp. 23, 29).
- [HH17] Sebastian G. Hofer and Klemens Hammerer. “Chapter Five - Quantum Control of Optomechanical Systems”. In: *Advances In Atomic, Molecular, and Optical Physics*. Ed. by Chun C. Lin and Susanne F. Yelin Ennio Arimondo. Vol. 66. Academic Press, 2017, pp. 263–374. DOI: [10.1016/bs.aamop.2017.03.003](https://doi.org/10.1016/bs.aamop.2017.03.003). URL: <http://www.sciencedirect.com/science/article/pii/S1049250X17300149> (visited on 06/09/2017) (cit. on pp. 12, 76).
- [HKY01] Christina J. Hood, H. J. Kimble, and Jun Ye. “Characterization of high-finesse mirrors: Loss, phase shifts, and mode structure in an optical cavity”. In: *Phys. Rev. A* 64 (3 2001), p. 033804. DOI: [10.1103/PhysRevA.64.033804](https://doi.org/10.1103/PhysRevA.64.033804). URL: <https://link.aps.org/doi/10.1103/PhysRevA.64.033804> (cit. on p. 21).
- [HMD15] B.D. Hauer, J. Maciejko, and J.P. Davis. “Nonlinear power spectral densities for the harmonic oscillator”. In: *Annals of Physics* 361 (2015), pp. 148 –183. ISSN: 0003-4916. DOI: <https://doi.org/10.1016/j.aop.2015.05.031>. URL: <http://www.sciencedirect.com/science/article/pii/S0003491615002304> (cit. on pp. 85, 92, 93).
- [Hry+15] Aaron C. Hryciw et al. “Tuning of nanocavity optomechanical coupling using a near-field fiber probe”. In: *Optica* 2.5 (2015), pp. 491–496. DOI: [10.1364/OPTICA.2.000491](https://doi.org/10.1364/OPTICA.2.000491). URL: <http://www.osapublishing.org/optica/abstract.cfm?URI=optica-2-5-491> (cit. on p. 27).
- [Iwa+13] Kohjiro Iwasawa et al. “Quantum-Limited Mirror-Motion Estimation”. In: *Phys. Rev. Lett.* 111 (16 2013), p. 163602. DOI: [10.1103/PhysRevLett.111.163602](https://doi.org/10.1103/PhysRevLett.111.163602). URL: <https://link.aps.org/doi/10.1103/PhysRevLett.111.163602> (cit. on p. 46).
- [Jai+16] Vijay Jain et al. “Direct Measurement of Photon Recoil from a Levitated Nanoparticle”. In: *Phys. Rev. Lett.* 116 (24 2016), p. 243601. DOI: [10.1103/PhysRevLett.116.243601](https://doi.org/10.1103/PhysRevLett.116.243601). URL: <https://link.aps.org/doi/10.1103/PhysRevLett.116.243601> (cit. on pp. 4, 17, 21, 23, 28, 36, 43, 83).



- [JD96] P.S. Jessen and I.H. Deutsch. “Optical Lattices”. In: ed. by Benjamin Bederson and Herbert Walther. Vol. 37. *Advances In Atomic, Molecular, and Optical Physics*. Academic Press, 1996, pp. 95–138. DOI: [https://doi.org/10.1016/S1049-250X\(08\)60099-3](https://doi.org/10.1016/S1049-250X(08)60099-3). URL: <http://www.sciencedirect.com/science/article/pii/S1049250X08600993> (cit. on p. 85).
- [Jia+17] Junyi Jiao et al. “Single-Molecule Protein Folding Experiments Using High-Precision Optical Tweezers”. In: *Methods Mol Biol* 1486 (2017), pp. 357–390. ISSN: 1064-3745. DOI: [10.1007/978-1-4939-6421-5\\_14](https://doi.org/10.1007/978-1-4939-6421-5_14). URL: <http://www.ncbi.nlm.nih.gov/pmc/articles/PMC5508109/> (cit. on p. 23).
- [JM+18] Ricardo Jiménez-Martínez et al. “Signal Tracking Beyond the Time Resolution of an Atomic Sensor by Kalman Filtering”. In: *Phys. Rev. Lett.* 120 (4 2018), p. 040503. DOI: [10.1103/PhysRevLett.120.040503](https://doi.org/10.1103/PhysRevLett.120.040503). URL: <https://link.aps.org/doi/10.1103/PhysRevLett.120.040503> (cit. on p. 45).
- [Joh+19] Aisling Johnson et al. “Observation of Collective Superstrong Coupling of Cold Atoms to a 30-m Long Optical Resonator”. In: *Phys. Rev. Lett.* 123 (24 2019), p. 243602. DOI: [10.1103/PhysRevLett.123.243602](https://doi.org/10.1103/PhysRevLett.123.243602). URL: <https://link.aps.org/doi/10.1103/PhysRevLett.123.243602> (cit. on p. 22).
- [JSo6] Kurt Jacobs and Daniel A. Steck. “A straightforward introduction to continuous quantum measurement”. In: *Contemporary Physics* 47.5 (2006), pp. 279–303. DOI: [10.1080/00107510601101934](https://doi.org/10.1080/00107510601101934). eprint: <https://doi.org/10.1080/00107510601101934>. URL: <https://doi.org/10.1080/00107510601101934> (cit. on p. 11).
- [Jun+13] Christian Junge et al. “Strong Coupling between Single Atoms and Nontransversal Photons”. In: *Phys. Rev. Lett.* 110 (21 2013), p. 213604. DOI: [10.1103/PhysRevLett.110.213604](https://doi.org/10.1103/PhysRevLett.110.213604). URL: <https://link.aps.org/doi/10.1103/PhysRevLett.110.213604> (cit. on p. 21).
- [Kal+12] Rainer Kaltenbaek et al. “Macroscopic quantum resonators (MAQRO)”. In: *Experimental Astronomy* 34.2 (2012), pp. 123–164. ISSN: 1572-9508. DOI: [10.1007/s10686-012-9292-3](https://doi.org/10.1007/s10686-012-9292-3). URL: <https://doi.org/10.1007/s10686-012-9292-3> (cit. on pp. 4, 23).
- [Kal+60] Rudolf Emil Kalman et al. “Contributions to the theory of optimal control”. In: *Boletín de la Sociedad Matemática Mexicana* 5.2 (1960), pp. 102–119 (cit. on pp. 43, 46, 49, 76).
- [Kal60] Rudolph Emil Kalman. “A new approach to linear filtering and prediction problems”. In: *J. Basic Eng.* 82 (1960), pp. 35–45 (cit. on pp. 43, 46, 76).
- [Kam+21] M. Kamba et al. “Recoil-limited feedback cooling of single nanoparticles near the ground state in an optical lattice”. In: *Phys. Rev. A* 103 (5 2021), p. L051701. DOI: [10.1103/PhysRevA.103.L051701](https://doi.org/10.1103/PhysRevA.103.L051701). URL: <https://link.aps.org/doi/10.1103/PhysRevA.103.L051701> (cit. on pp. 46, 47, 62).
- [KBo6] Dustin Kleckner and Dirk Bouwmeester. “Sub-kelvin optical cooling of a micromechanical resonator”. In: *Nature* 444.7115 (2006), pp. 75–78. ISSN: 1476-4687. DOI: [10.1038/nature05231](https://doi.org/10.1038/nature05231). URL: <https://doi.org/10.1038/nature05231> (cit. on p. 4).

- [Kie+13] Nikolai Kiesel et al. “Cavity cooling of an optically levitated submicron particle”. In: *Proceedings of the National Academy of Sciences* 110.35 (2013), pp. 14180–14185. DOI: [10.1073/pnas.1309167110](https://doi.org/10.1073/pnas.1309167110). eprint: <http://www.pnas.org/content/110/35/14180.full.pdf>. URL: <http://www.pnas.org/content/110/35/14180.abstract> (cit. on pp. 4, 16, 17, 21, 23, 25).
- [Kni+95] JC Knight et al. “Mapping whispering-gallery modes in microspheres with a near-field probe”. In: *Optics Letters* 20.14 (1995), pp. 1515–1517 (cit. on p. 22).
- [Kor+07] Jan Ivar Korsbakken et al. “Measurement-based measure of the size of macroscopic quantum superpositions”. In: *Phys. Rev. A* 75 (4 2007), p. 042106. DOI: [10.1103/PhysRevA.75.042106](https://doi.org/10.1103/PhysRevA.75.042106). URL: <https://link.aps.org/doi/10.1103/PhysRevA.75.042106> (cit. on p. 3).
- [Kra+83] Karl Kraus et al. *States, effects, and operations: fundamental notions of quantum theory. Lectures in mathematical physics at the University of Texas at Austin*. Vol. 190. Springer, 1983 (cit. on p. 8).
- [KSV04] TJ Kippenberg, SM Spillane, and KJ Vahala. “Demonstration of ultra-high-Q small mode volume toroid microcavities on a chip”. In: *Applied Physics Letters* 85.25 (2004), pp. 6113–6115 (cit. on p. 22).
- [Kuh+15] Stefan Kuhn et al. “Cavity-Assisted Manipulation of Freely Rotating Silicon Nanorods in High Vacuum”. In: *Nano Letters* 15.8 (2015), pp. 5604–5608. DOI: [10.1021/acs.nanolett.5b02302](https://doi.org/10.1021/acs.nanolett.5b02302). eprint: <http://dx.doi.org/10.1021/acs.nanolett.5b02302>. URL: <http://dx.doi.org/10.1021/acs.nanolett.5b02302> (cit. on p. 21).
- [Kuh+17] Stefan Kuhn et al. “Nanoparticle detection in an open-access silicon microcavity”. In: *Applied Physics Letters* 111.25 (2017), p. 253107. DOI: [10.1063/1.5008492](https://doi.org/10.1063/1.5008492). eprint: <https://doi.org/10.1063/1.5008492>. URL: <https://doi.org/10.1063/1.5008492> (cit. on pp. 22, 23).
- [LaH+04] M. D. LaHaye et al. “Approaching the Quantum Limit of a Nanomechanical Resonator”. In: *Science* 304.5667 (2004), pp. 74–77. ISSN: 0036-8075. DOI: [10.1126/science.1094419](https://doi.org/10.1126/science.1094419). eprint: <https://science.sciencemag.org/content/304/5667/74.full.pdf>. URL: <https://science.sciencemag.org/content/304/5667/74> (cit. on p. 3).
- [Lam18] Jonas Lammers. *State preparation and verification in continuously measured quantum systems*. Leibniz Universität Hannover, 2018 (cit. on p. 11).
- [Lee+20] J. G. Lee et al. “New Test of the Gravitational  $1/r^2$  Law at Separations down to 52  $\mu\text{m}$ ”. In: *Phys. Rev. Lett.* 124 (10 2020), p. 101101. DOI: [10.1103/PhysRevLett.124.101101](https://doi.org/10.1103/PhysRevLett.124.101101). URL: <https://link.aps.org/doi/10.1103/PhysRevLett.124.101101> (cit. on p. 3).
- [Leg02] A J Leggett. “Testing the limits of quantum mechanics: motivation, state of play, prospects”. In: *J. Phys. Condens. Matter* 14 (2002), R415–R451 (cit. on p. 52).
- [Leg80] A. J. Leggett. “Macroscopic Quantum Systems and the Quantum Theory of Measurement”. In: *Progress of Theoretical Physics Supplement* 69 (Mar. 1980), pp. 80–100. ISSN: 0375-9687. DOI: [10.1143/PTP.69.80](https://doi.org/10.1143/PTP.69.80). eprint: <https://academic.oup.com/ptps/article-pdf/doi/10.1143/PTP.69.80/5356381/69-80.pdf>. URL: <https://doi.org/10.1143/PTP.69.80> (cit. on p. 3).
- [Lei+17] Rick Leijssen et al. “Nonlinear cavity optomechanics with nanomechanical thermal fluctuations”. In: *Nature Communications* 8 (2017), p. 16024. URL: <http://dx.doi.org/10.1038/ncomms16024> (cit. on p. 29).

- [Li+10] Tongcang Li et al. “Measurement of the Instantaneous Velocity of a Brownian Particle”. In: *Science* 328.5986 (2010), pp. 1673–1675. ISSN: 0036-8075. DOI: [10.1126/science.1189403](https://doi.org/10.1126/science.1189403). eprint: <http://science.sciencemag.org/content/328/5986/1673.full.pdf>. URL: <http://science.sciencemag.org/content/328/5986/1673> (cit. on p. 23).
- [Lia+19] J. Liao et al. “FPGA Implementation of a Kalman-Based Motion Estimator for Levitated Nanoparticles”. In: *IEEE Transactions on Instrumentation and Measurement* 68.7 (2019), pp. 2374–2386 (cit. on p. 46).
- [LJ11] Chang-Woo Lee and Hyunseok Jeong. “Quantification of Macroscopic Quantum Superpositions within Phase Space”. In: *Phys. Rev. Lett.* 106 (22 2011), p. 220401. DOI: [10.1103/PhysRevLett.106.220401](https://doi.org/10.1103/PhysRevLett.106.220401). URL: <https://link.aps.org/doi/10.1103/PhysRevLett.106.220401> (cit. on p. 3).
- [LKR11] Tongcang Li, Simon Kheifets, and Mark G. Raizen. “Millikelvin cooling of an optically trapped microsphere in vacuum”. In: *Nature Physics* 7 (2011), p. 527. URL: <http://dx.doi.org/10.1038/nphys1952> (cit. on p. 23).
- [Lne16] Lneuhau. *Shards of Silicon — Red Pitaya DAC performance*. <https://ln1985blog.wordpress.com/2016/02/07/red-pitaya-dac-performance/s> [online]. Accessed: 2020-11-30. 2016 (cit. on p. 80).
- [Lou00] R. Loudon. *Quantum Theory of Light*. Oxford: Oxford University Press, 2000 (cit. on pp. 13, 59, 91).
- [Mab05] Hideo Mabuchi. “Quantum feedback and the quantum–classical transition”. In: *Science and ultimate reality: quantum theory, cosmology, and complexity*. Repr. Cambridge University Press, 2005. ISBN: 0-521-83113-X, 9780521831130 (cit. on pp. 7, 11).
- [Mac+20] Gregory S. MacCabe et al. “Nano-acoustic resonator with ultralong phonon lifetime”. In: *Science* 370.6518 (2020), pp. 840–843. ISSN: 0036-8075. DOI: [10.1126/science.abc7312](https://doi.org/10.1126/science.abc7312). eprint: <https://science.sciencemag.org/content/370/6518/840.full.pdf>. URL: <https://science.sciencemag.org/content/370/6518/840> (cit. on p. 4).
- [Mag+18] Lorenzo Magrini et al. “Near-field coupling of a levitated nanoparticle to a photonic crystal cavity”. In: *Optica* 5.12 (2018), pp. 1597–1602. DOI: [10.1364/OPTICA.5.001597](https://doi.org/10.1364/OPTICA.5.001597). URL: <http://www.osapublishing.org/optica/abstract.cfm?URI=optica-5-12-1597> (cit. on pp. 4, 17, 21, 101).
- [Mag+21] Lorenzo Magrini et al. “Real-time optimal quantum control of mechanical motion at room temperature”. In: *Nature* 595.7867 (2021), pp. 373–377. ISSN: 1476-4687. DOI: [10.1038/s41586-021-03602-3](https://doi.org/10.1038/s41586-021-03602-3). URL: <https://doi.org/10.1038/s41586-021-03602-3> (cit. on pp. 4, 17, 43, 101).
- [Mar+10] Francesco Marino et al. “Classical Signature of Ponderomotive Squeezing in a Suspended Mirror Resonator”. In: *Phys. Rev. Lett.* 104 (7 2010), p. 073601. DOI: [10.1103/PhysRevLett.104.073601](https://doi.org/10.1103/PhysRevLett.104.073601). URL: <https://link.aps.org/doi/10.1103/PhysRevLett.104.073601> (cit. on p. 89).
- [Mas+19] David Mason et al. “Continuous force and displacement measurement below the standard quantum limit”. In: *Nature Physics* 15.8 (2019), pp. 745–749. ISSN: 1745-2481. DOI: [10.1038/s41567-019-0533-5](https://doi.org/10.1038/s41567-019-0533-5). URL: <https://doi.org/10.1038/s41567-019-0533-5> (cit. on pp. 62, 89, 96).
- [MG21] David C. Moore and Andrew A. Geraci. “Searching for new physics using optically levitated sensors”. In: *Quantum Sci. Technol.* 6 (2021), p. 014008. URL: <https://doi.org/10.1088/2058-9565/abcf8a> (cit. on pp. 3, 52).

- [Mil+15] J. Millen et al. “Cavity Cooling a Single Charged Levitated Nanosphere”. In: *Phys. Rev. Lett.* 114 (12 2015), p. 123602. DOI: [10.1103/PhysRevLett.114.123602](https://doi.org/10.1103/PhysRevLett.114.123602). URL: <https://link.aps.org/doi/10.1103/PhysRevLett.114.123602> (cit. on pp. 21, 23, 25).
- [Min61] M. Minsky. “Microscopy apparatus”. In: *US Patent No. 3013467* (1961) (cit. on p. 43).
- [MMT97] S. Mancini, V. I. Man’ko, and P. Tombesi. “Ponderomotive control of quantum macroscopic coherence”. In: *Phys. Rev. A* 55 (4 1997), pp. 3042–3050. DOI: [10.1103/PhysRevA.55.3042](https://doi.org/10.1103/PhysRevA.55.3042). URL: <https://link.aps.org/doi/10.1103/PhysRevA.55.3042> (cit. on p. 89).
- [Mon+20a] Fernando Monteiro et al. “Force and acceleration sensing with optically levitated nanogram masses at microkelvin temperatures”. In: *Phys. Rev. A* 101 (5 2020), p. 053835. DOI: [10.1103/PhysRevA.101.053835](https://doi.org/10.1103/PhysRevA.101.053835). URL: <https://link.aps.org/doi/10.1103/PhysRevA.101.053835> (cit. on p. 52).
- [Mon+20b] Fernando Monteiro et al. “Search for Composite Dark Matter with Optically Levitated Sensors”. In: *Phys. Rev. Lett.* 125 (18 2020), p. 181102. DOI: [10.1103/PhysRevLett.125.181102](https://doi.org/10.1103/PhysRevLett.125.181102). URL: <https://link.aps.org/doi/10.1103/PhysRevLett.125.181102> (cit. on pp. 52, 101).
- [Mon+21] Cris Montoya et al. “Scanning force sensing at  $\mu\text{m}$ -distances from a conductive surface with nanospheres in an optical lattice”. In: *arXiv preprint arXiv:2103.03420* (2021) (cit. on pp. 17, 101).
- [MP09] Victor M Moreno and Alberto Pigazo. *Kalman filter: recent advances and applications*. In-Teh, 2009 (cit. on p. 76).
- [MRG14] David C. Moore, Alexander D. Rider, and Giorgio Gratta. “Search for Millicharged Particles Using Optically Levitated Microspheres”. In: *Phys. Rev. Lett.* 113 (25 2014), p. 251801. DOI: [10.1103/PhysRevLett.113.251801](https://doi.org/10.1103/PhysRevLett.113.251801). URL: <https://link.aps.org/doi/10.1103/PhysRevLett.113.251801> (cit. on pp. 3, 23).
- [MT94] S. Mancini and P. Tombesi. “Quantum noise reduction by radiation pressure”. In: *Phys. Rev. A* 49 (5 1994), pp. 4055–4065. DOI: [10.1103/PhysRevA.49.4055](https://doi.org/10.1103/PhysRevA.49.4055). URL: <https://link.aps.org/doi/10.1103/PhysRevA.49.4055> (cit. on p. 89).
- [MVT98] Stefano Mancini, David Vitali, and Paolo Tombesi. “Optomechanical Cooling of a Macroscopic Oscillator by Homodyne Feedback”. In: *Phys. Rev. Lett.* 80 (4 1998), pp. 688–691. DOI: [10.1103/PhysRevLett.80.688](https://doi.org/10.1103/PhysRevLett.80.688). URL: <https://link.aps.org/doi/10.1103/PhysRevLett.80.688> (cit. on p. 16).
- [Neu32] Johann von Neumann. *Mathematische Grundlagen der Quantenmechanik*. Berlin, 1932 (cit. on p. 7).
- [NH06] Lukas Novotny and Bert Hecht. *Principles of Nano-Optics*. Cambridge University Press, 2006. DOI: [10.1017/CB09780511813535](https://doi.org/10.1017/CB09780511813535) (cit. on p. 68).
- [NH13] Stefan Nimmrichter and Klaus Hornberger. “Macroscopicity of Mechanical Quantum Superposition States”. In: *Phys. Rev. Lett.* 110 (16 2013), p. 160403. DOI: [10.1103/PhysRevLett.110.160403](https://doi.org/10.1103/PhysRevLett.110.160403). URL: <https://link.aps.org/doi/10.1103/PhysRevLett.110.160403> (cit. on p. 3).
- [Nov17] Lukas Novotny. “Radiation damping of a polarizable particle”. In: *Phys. Rev. A* 96 (3 2017), p. 032108. DOI: [10.1103/PhysRevA.96.032108](https://doi.org/10.1103/PhysRevA.96.032108). URL: <https://link.aps.org/doi/10.1103/PhysRevA.96.032108> (cit. on pp. 68, 71, 73, 83).

- [NQC15] Lukas Neumeier, Romain Quidant, and Darrick E Chang. “Self-induced back-action optical trapping in nanophotonic systems”. In: *New Journal of Physics* 17.12 (2015), p. 123008. URL: <http://stacks.iop.org/1367-2630/17/i=12/a=123008> (cit. on pp. 29, 122).
- [OK+18] C. F. Ockeloen-Korppi et al. “Revealing Hidden Quantum Correlations in an Electromechanical Measurement”. In: *Phys. Rev. Lett.* 121 (24 2018), p. 243601. DOI: 10.1103/PhysRevLett.121.243601. URL: <https://link.aps.org/doi/10.1103/PhysRevLett.121.243601> (cit. on p. 89).
- [Ove+18] Chris Overstreet et al. “Effective Inertial Frame in an Atom Interferometric Test of the Equivalence Principle”. In: *Phys. Rev. Lett.* 120 (18 2018), p. 183604. DOI: 10.1103/PhysRevLett.120.183604. URL: <https://link.aps.org/doi/10.1103/PhysRevLett.120.183604> (cit. on p. 3).
- [Oza89] M. Ozawa. *Realization of Measurement and the Standard Quantum Limit*. Tombesi P., Pike E.R. (eds) Squeezed and Nonclassical Light. NATO ASI Series (Series B: Physics), vol 190. Boston, MA: Springer, 1989 (cit. on pp. 3, 13).
- [Pal+13] TA Palomaki et al. “Entangling mechanical motion with microwave fields”. In: *Science* 342.6159 (2013), pp. 710–713 (cit. on pp. 15, 17).
- [Par12] M. G. A. Paris. “The modern tools of quantum mechanics”. In: *The European Physical Journal Special Topics* 203.1 (2012), pp. 61–86. ISSN: 1951-6401. DOI: 10.1140/epjst/e2012-01535-1. URL: <https://doi.org/10.1140/epjst/e2012-01535-1> (cit. on p. 9).
- [Pau88] H. Paul. “Shot Noise in Photodetectors and Vacuum Fluctuations”. In: *Journal of Modern Optics* 35.7 (1988), pp. 1225–1235. DOI: 10.1080/09500348814551291. eprint: <https://doi.org/10.1080/09500348814551291>. URL: <https://doi.org/10.1080/09500348814551291> (cit. on p. 38).
- [Pik+12] Igor Pikovski et al. “Probing Planck-scale physics with quantum optics”. In: *Nature Physics* 8.5 (2012), pp. 393–397. ISSN: 1745-2481. DOI: 10.1038/nphys2262. URL: <https://doi.org/10.1038/nphys2262> (cit. on p. 3).
- [Pog+07] M. Poggio et al. “Feedback Cooling of a Cantilever’s Fundamental Mode below 5 mK”. In: *Phys. Rev. Lett.* 99 (1 2007), p. 017201. DOI: 10.1103/PhysRevLett.99.017201. URL: <https://link.aps.org/doi/10.1103/PhysRevLett.99.017201> (cit. on pp. 4, 50, 69, 81).
- [Pot16] Anton Potočnik. *Redpitaya Guide*. <http://antonpotocnik.com> [online]. Accessed: 2020-09-25. 2016 (cit. on p. 80).
- [Pur+13] T. P. Purdy et al. “Strong Optomechanical Squeezing of Light”. In: *Phys. Rev. X* 3 (3 2013), p. 031012. DOI: 10.1103/PhysRevX.3.031012. URL: <https://link.aps.org/doi/10.1103/PhysRevX.3.031012> (cit. on p. 89).
- [Pur+17] T. P. Purdy et al. “Quantum correlations from a room-temperature optomechanical cavity”. In: *Science* 356.6344 (2017), pp. 1265–1268. ISSN: 0036-8075. DOI: 10.1126/science.aag1407. eprint: <https://science.sciencemag.org/content/356/6344/1265.full.pdf>. URL: <https://science.sciencemag.org/content/356/6344/1265> (cit. on p. 89).
- [Qia+86] Shi-Xiong Qian et al. “Lasing droplets: highlighting the liquid-air interface by laser emission”. In: *Science* 231.4737 (1986), pp. 486–488 (cit. on p. 22).
- [Qua+13] Qimin Quan et al. “Single particle detection in CMOS compatible photonic crystal nanobeam cavities”. In: *Opt. Express* 21.26 (2013), pp. 32225–32233. DOI: 10.1364/OE.21.032225. URL: <http://www.opticsexpress.org/abstract.cfm?URI=oe-21-26-32225> (cit. on pp. 21, 24).



- [Ral+18] Jason F Ralph et al. “Dynamical model selection near the quantum-classical boundary”. In: *Physical Review A* 98.1 (2018), p. 010102. ISSN: 2469-9926. DOI: [10.1103/PhysRevA.98.010102](https://doi.org/10.1103/PhysRevA.98.010102). URL: <https://link.aps.org/doi/10.1103/PhysRevA.98.010102> (cit. on p. 52).
- [Ran+16] Gambhir Ranjit et al. “Zeptonewton force sensing with nanospheres in an optical lattice”. In: *Phys. Rev. A* 93 (5 2016), p. 053801. DOI: [10.1103/PhysRevA.93.053801](https://doi.org/10.1103/PhysRevA.93.053801). URL: <https://link.aps.org/doi/10.1103/PhysRevA.93.053801> (cit. on pp. 23, 29, 52).
- [RF19] Andrey A Rakhubovsky and Radim Filip. “Stroboscopic high-order nonlinearity in quantum optomechanics”. In: *arXiv:1904.00773v1 [physics.optics]* 1 (2019), pp. 1–9. eprint: [arXiv:1904.00773v1](https://arxiv.org/abs/1904.00773v1) (cit. on p. 52).
- [RI+10] Oriol Romero-Isart et al. “Toward quantum superposition of living organisms”. In: *New Journal of Physics* 12.3 (2010), p. 033015. URL: <http://stacks.iop.org/1367-2630/12/i=3/a=033015> (cit. on pp. 4, 21, 23).
- [RI+11a] O. Romero-Isart et al. “Large Quantum Superpositions and Interference of Massive Nanometer-Sized Objects”. In: *Phys. Rev. Lett.* 107 (2 2011), p. 020405. DOI: [10.1103/PhysRevLett.107.020405](https://doi.org/10.1103/PhysRevLett.107.020405). URL: <https://link.aps.org/doi/10.1103/PhysRevLett.107.020405> (cit. on p. 4).
- [RI+11b] O. Romero-Isart et al. “Optically levitating dielectrics in the quantum regime: Theory and protocols”. In: *Phys. Rev. A* 83 (1 2011), p. 013803. DOI: [10.1103/PhysRevA.83.013803](https://doi.org/10.1103/PhysRevA.83.013803). URL: <https://link.aps.org/doi/10.1103/PhysRevA.83.013803> (cit. on pp. 4, 85).
- [Ric+17] F. Ricci et al. “Optically levitated nanoparticle as a model system for stochastic bistable dynamics”. In: *Nature Communications* 8 (2017), p. 15141. URL: <http://dx.doi.org/10.1038/ncomms15141> (cit. on p. 23).
- [Rie+16] Ralf Riedinger et al. “Non-classical correlations between single photons and phonons from a mechanical oscillator”. In: *Nature* 530 (2016), p. 313. URL: <http://dx.doi.org/10.1038/nature16536> (cit. on pp. 15, 17).
- [RK14] N. Rotenberg and L. Kuipers. “Mapping nanoscale light fields”. In: *Nature Photonics* 8 (2014), 919 EP. URL: <http://dx.doi.org/10.1038/nphoton.2014.285> (cit. on p. 27).
- [Ron+17] Loïc Rondin et al. “Direct measurement of Kramers turnover with a levitated nanoparticle”. In: *Nature Nanotechnology* 12 (2017), p. 1130. URL: <http://dx.doi.org/10.1038/nnano.2017.198> (cit. on p. 23).
- [Ros+18] Massimiliano Rossi et al. “Measurement-based quantum control of mechanical motion”. In: *Nature* 563.7729 (2018), pp. 53–58. ISSN: 1476-4687. DOI: [10.1038/s41586-018-0643-8](https://doi.org/10.1038/s41586-018-0643-8). URL: <https://doi.org/10.1038/s41586-018-0643-8> (cit. on pp. 3, 4, 28, 44, 46, 64, 69).
- [Ros+19] Massimiliano Rossi et al. “Observing and Verifying the Quantum Trajectory of a Mechanical Resonator”. In: *Phys. Rev. Lett.* 123 (16 2019), p. 163601. DOI: [10.1103/PhysRevLett.123.163601](https://doi.org/10.1103/PhysRevLett.123.163601). URL: <https://link.aps.org/doi/10.1103/PhysRevLett.123.163601> (cit. on p. 46).
- [RSMQ21] Andrés de los Ríos Sommer, Nadine Meyer, and Romain Quidant. “Strong optomechanical coupling at room temperature by coherent scattering”. In: *Nature Communications* 12.1 (2021), p. 276. ISSN: 2041-1723. DOI: [10.1038/s41467-020-20419-2](https://doi.org/10.1038/s41467-020-20419-2). URL: <https://doi.org/10.1038/s41467-020-20419-2> (cit. on p. 46).
- [Rup+16] M. G. Ruppert et al. “A Kalman Filter for Amplitude Estimation in High-Speed Dynamic Mode Atomic Force Microscopy”. In: *IEEE Transactions on Control Systems Technology* 24.1 (2016), pp. 276–284. DOI: [10.1109/TCST.2015.2435654](https://doi.org/10.1109/TCST.2015.2435654) (cit. on p. 46).



- [Sako4] Kazuaki Sakoda. *Optical properties of photonic crystals*. Vol. 80. Springer Science & Business Media, 2004 (cit. on p. 22).
- [Say+11] Clément Sayrin et al. “Real-time quantum feedback prepares and stabilizes photon number states”. In: *Nature* 477.7362 (2011), pp. 73–77. ISSN: 1476-4687. DOI: [10.1038/nature10376](https://doi.org/10.1038/nature10376). URL: <https://doi.org/10.1038/nature10376> (cit. on pp. 44, 45).
- [SC92] Dean F. Sittig and Kei-Hoi Cheung. “A parallel implementation of a multi-state Kalman filtering algorithm to detect ECG arrhythmias”. In: *International journal of clinical monitoring and computing* 9.1 (1992), pp. 13–22. ISSN: 0167-9945. DOI: [10.1007/BF01145898](https://doi.org/10.1007/BF01145898). URL: <https://doi.org/10.1007/BF01145898> (cit. on p. 46).
- [Sch+06] A. Schliesser et al. “Radiation Pressure Cooling of a Micromechanical Oscillator Using Dynamical Backaction”. In: *Phys. Rev. Lett.* 97 (24 2006), p. 243905. DOI: [10.1103/PhysRevLett.97.243905](https://link.aps.org/doi/10.1103/PhysRevLett.97.243905). URL: <https://link.aps.org/doi/10.1103/PhysRevLett.97.243905> (cit. on p. 4).
- [Sch+14] Sydney Schreppler et al. “Optically measuring force near the standard quantum limit”. In: *Science* 344.6191 (2014), pp. 1486–1489. ISSN: 0036-8075. DOI: [10.1126/science.1249850](https://science.sciencemag.org/content/344/6191/1486.full.pdf). eprint: <https://science.sciencemag.org/content/344/6191/1486.full.pdf>. URL: <https://science.sciencemag.org/content/344/6191/1486> (cit. on p. 3).
- [Sch+16] R. Schilling et al. “Near-Field Integration of a SiN Nanobeam and a SiO<sub>2</sub> Microcavity for Heisenberg-Limited Displacement Sensing”. In: *Phys. Rev. Applied* 5 (5 2016), p. 054019. DOI: [10.1103/PhysRevApplied.5.054019](https://link.aps.org/doi/10.1103/PhysRevApplied.5.054019). URL: <https://link.aps.org/doi/10.1103/PhysRevApplied.5.054019> (cit. on p. 62).
- [Sch+19] Björn Schränski et al. “Macroscopicity of quantum mechanical superposition tests via hypothesis falsification”. In: *Phys. Rev. A* 100 (3 2019), p. 032111. DOI: [10.1103/PhysRevA.100.032111](https://link.aps.org/doi/10.1103/PhysRevA.100.032111). URL: <https://link.aps.org/doi/10.1103/PhysRevA.100.032111> (cit. on p. 3).
- [Set+18] Ashley Setter et al. “Real-time Kalman filter: Cooling of an optically levitated nanoparticle”. In: *Phys. Rev. A* 97 (3 2018), p. 033822. DOI: [10.1103/PhysRevA.97.033822](https://link.aps.org/doi/10.1103/PhysRevA.97.033822). URL: <https://link.aps.org/doi/10.1103/PhysRevA.97.033822> (cit. on p. 46).
- [SN+12] Amir H. Safavi-Naeini et al. “Observation of Quantum Motion of a Nanomechanical Resonator”. In: *Phys. Rev. Lett.* 108 (3 2012), p. 033602. DOI: [10.1103/PhysRevLett.108.033602](https://link.aps.org/doi/10.1103/PhysRevLett.108.033602). URL: <https://link.aps.org/doi/10.1103/PhysRevLett.108.033602> (cit. on p. 50).
- [SN+13] Amir H. Safavi-Naeini et al. “Squeezed light from a silicon micromechanical resonator”. In: *Nature* 500 (2013), p. 185. URL: <http://dx.doi.org/10.1038/nature12307> (cit. on pp. 16, 17, 89, 95, 96).
- [SR20] T. Seberston and F. Robicheaux. “Distribution of laser shot-noise energy delivered to a levitated nanoparticle”. In: *Phys. Rev. A* 102 (3 2020), p. 033505. DOI: [10.1103/PhysRevA.102.033505](https://link.aps.org/doi/10.1103/PhysRevA.102.033505). URL: <https://link.aps.org/doi/10.1103/PhysRevA.102.033505> (cit. on pp. 43, 47, 58, 60, 84).
- [SS20] Kanupriya Sinha and Yiğit Subaşı. “Quantum Brownian motion of a particle from Casimir-Polder interactions”. In: *Phys. Rev. A* 101 (3 2020), p. 032507. DOI: [10.1103/PhysRevA.101.032507](https://link.aps.org/doi/10.1103/PhysRevA.101.032507). URL: <https://link.aps.org/doi/10.1103/PhysRevA.101.032507> (cit. on p. 85).
- [Ste94] Robert F Stengel. *Optimal control and estimation*. New York: Dover Publications, 1994 (cit. on p. 76).

- [Sud+17a] V. Sudhir et al. “Appearance and Disappearance of Quantum Correlations in Measurement-Based Feedback Control of a Mechanical Oscillator”. In: *Phys. Rev. X* 7 (1 2017), p. 011001. DOI: [10.1103/PhysRevX.7.011001](https://doi.org/10.1103/PhysRevX.7.011001). URL: <https://link.aps.org/doi/10.1103/PhysRevX.7.011001> (cit. on pp. 15, 46, 64, 87, 89).
- [Sud+17b] V. Sudhir et al. “Quantum Correlations of Light from a Room-Temperature Mechanical Oscillator”. In: *Phys. Rev. X* 7 (3 2017), p. 031055. DOI: [10.1103/PhysRevX.7.031055](https://doi.org/10.1103/PhysRevX.7.031055). URL: <https://link.aps.org/doi/10.1103/PhysRevX.7.031055> (cit. on p. 89).
- [Tan+20] Wen-Hai Tan et al. “Improvement for Testing the Gravitational Inverse-Square Law at the Submillimeter Range”. In: *Phys. Rev. Lett.* 124 (5 2020), p. 051301. DOI: [10.1103/PhysRevLett.124.051301](https://doi.org/10.1103/PhysRevLett.124.051301). URL: <https://link.aps.org/doi/10.1103/PhysRevLett.124.051301> (cit. on p. 3).
- [Teb+20] Felix Tebbenjohanns et al. “Motional Sideband Asymmetry of a Nanoparticle Optically Levitated in Free Space”. In: *Phys. Rev. Lett.* 124 (1 2020), p. 013603. DOI: [10.1103/PhysRevLett.124.013603](https://doi.org/10.1103/PhysRevLett.124.013603). URL: <https://link.aps.org/doi/10.1103/PhysRevLett.124.013603> (cit. on pp. 46, 47, 62, 81).
- [Teu+11] J. D. Teufel et al. “Sideband cooling of micromechanical motion to the quantum ground state”. In: *Nature* 475.7356 (2011), pp. 359–363. ISSN: 1476-4687. DOI: [10.1038/nature10261](https://doi.org/10.1038/nature10261). URL: <https://doi.org/10.1038/nature10261> (cit. on pp. 3, 16).
- [TFN19] Felix Tebbenjohanns, Martin Frimmer, and Lukas Novotny. “Optimal position detection of a dipolar scatterer in a focused field”. In: *Phys. Rev. A* 100 (4 2019), p. 043821. DOI: [10.1103/PhysRevA.100.043821](https://doi.org/10.1103/PhysRevA.100.043821). URL: <https://link.aps.org/doi/10.1103/PhysRevA.100.043821> (cit. on pp. 18, 43, 47, 60, 61).
- [Tho+08] J. D. Thompson et al. “Strong dispersive coupling of a high-finesse cavity to a micromechanical membrane”. In: *Nature* 452 (2008), p. 72. URL: <http://dx.doi.org/10.1038/nature06715> (cit. on pp. 4, 16).
- [Tho+13] J. D. Thompson et al. “Coupling a Single Trapped Atom to a Nanoscale Optical Cavity”. In: *Science* 340.6137 (2013), pp. 1202–1205. ISSN: 0036-8075. DOI: [10.1126/science.1237125](https://doi.org/10.1126/science.1237125). eprint: <http://science.sciencemag.org/content/340/6137/1202.full.pdf>. URL: <http://science.sciencemag.org/content/340/6137/1202> (cit. on pp. 21, 24, 29, 39).
- [Tie+14] T. G. Tiecke et al. “Nanophotonic quantum phase switch with a single atom”. In: *Nature* 508 (2014), p. 241. URL: <http://dx.doi.org/10.1038/nature13188> (cit. on p. 21).
- [Vam+07] A. N. Vamivakas et al. “Phase-sensitive detection of dipole radiation in a fiber-based high numerical aperture optical system”. In: *Opt. Lett.* 32.8 (2007), pp. 970–972. DOI: [10.1364/OL.32.000970](https://doi.org/10.1364/OL.32.000970). URL: <http://ol.osa.org/abstract.cfm?URI=ol-32-8-970> (cit. on pp. 47, 65).
- [Van+11] M. R. Vanner et al. “Pulsed quantum optomechanics”. In: *Proceedings of the National Academy of Sciences* 108.39 (2011), pp. 16182–16187. DOI: [10.1073/pnas.1105098108](https://doi.org/10.1073/pnas.1105098108). eprint: <http://www.pnas.org/content/108/39/16182.full.pdf>. URL: <http://www.pnas.org/content/108/39/16182.abstract> (cit. on p. 29).
- [Van+13] M. R. Vanner et al. “Cooling-by-measurement and mechanical state tomography via pulsed optomechanics”. In: *Nature Communications* 4 (2013), 2295 EP –. URL: <http://dx.doi.org/10.1038/ncomms3295> (cit. on p. 36).

- [Ver+10] P. Verlot et al. “Backaction Amplification and Quantum Limits in Optomechanical Measurements”. In: *Phys. Rev. Lett.* 104 (13 2010), p. 133602. DOI: [10.1103/PhysRevLett.104.133602](https://doi.org/10.1103/PhysRevLett.104.133602). URL: <https://link.aps.org/doi/10.1103/PhysRevLett.104.133602> (cit. on p. 89).
- [Vet+10] E. Vetsch et al. “Optical Interface Created by Laser-Cooled Atoms Trapped in the Evanescent Field Surrounding an Optical Nanofiber”. In: *Phys. Rev. Lett.* 104 (20 2010), p. 203603. DOI: [10.1103/PhysRevLett.104.203603](https://doi.org/10.1103/PhysRevLett.104.203603). URL: <https://link.aps.org/doi/10.1103/PhysRevLett.104.203603> (cit. on p. 21).
- [Vij+12] R. Vijay et al. “Stabilizing Rabi oscillations in a superconducting qubit using quantum feedback”. In: *Nature* 490.7418 (2012), pp. 77–80. ISSN: 1476-4687. DOI: [10.1038/nature11505](https://doi.org/10.1038/nature11505). URL: <https://doi.org/10.1038/nature11505> (cit. on p. 44).
- [Vov+17] Jamie Vovrosh et al. “Parametric feedback cooling of levitated optomechanics in a parabolic mirror trap”. In: *J. Opt. Soc. Am. B* 34.7 (2017), pp. 1421–1428. DOI: [10.1364/JOSAB.34.001421](https://doi.org/10.1364/JOSAB.34.001421). URL: <http://josab.osa.org/abstract.cfm?URI=josab-34-7-1421> (cit. on p. 23).
- [Vuč+01] Jelena Vučković et al. “Design of photonic crystal microcavities for cavity QED”. In: *Physical Review E* 65.1 (2001), p. 016608 (cit. on p. 22).
- [Vuc+02] Jelena Vuckovic et al. “Optimization of the Q factor in photonic crystal microcavities”. In: *IEEE Journal of Quantum Electronics* 38.7 (2002), pp. 850–856 (cit. on p. 22).
- [Wan+97] M. D. Wang et al. “Stretching DNA with optical tweezers.” In: *Biophys J* 72.3 (1997), pp. 1335–1346. ISSN: 0006-3495. URL: <http://www.ncbi.nlm.nih.gov/pmc/articles/PMC1184516/> (cit. on p. 23).
- [Wei+14] A. J. Weinstein et al. “Observation and Interpretation of Motional Sideband Asymmetry in a Quantum Electromechanical Device”. In: *Phys. Rev. X* 4 (4 2014), p. 041003. DOI: [10.1103/PhysRevX.4.041003](https://doi.org/10.1103/PhysRevX.4.041003). URL: <https://link.aps.org/doi/10.1103/PhysRevX.4.041003> (cit. on p. 85).
- [Wie+15] Witlef Wieczorek et al. “Optimal State Estimation for Cavity Optomechanical Systems”. In: *Phys. Rev. Lett.* 114 (22 2015), p. 223601. DOI: [10.1103/PhysRevLett.114.223601](https://doi.org/10.1103/PhysRevLett.114.223601). URL: <https://link.aps.org/doi/10.1103/PhysRevLett.114.223601> (cit. on pp. 46, 49, 79, 80).
- [Wil+15] D. J. Wilson et al. “Measurement-based control of a mechanical oscillator at its thermal decoherence rate”. In: *Nature* 524 (2015), p. 325. URL: <http://dx.doi.org/10.1038/nature14672> (cit. on pp. 16, 17, 21, 28, 64, 69).
- [Win+19] Dominik Windey et al. “Cavity-Based 3D Cooling of a Levitated Nanoparticle via Coherent Scattering”. In: *Phys. Rev. Lett.* 122 (12 2019), p. 123601. DOI: [10.1103/PhysRevLett.122.123601](https://doi.org/10.1103/PhysRevLett.122.123601). URL: <https://link.aps.org/doi/10.1103/PhysRevLett.122.123601> (cit. on p. 46).
- [WM10] Howard M. Wieseman and Gerard J. Milburn. *Quantum measurement and control*. Cambridge: Cambridge University Press, 2010 (cit. on pp. 45, 46, 75).
- [Wol+15] Emma Edwina Wollman et al. “Quantum squeezing of motion in a mechanical resonator”. In: *Science* 349.6251 (2015), pp. 952–955 (cit. on p. 16).
- [Yon+12] Hidehiro Yonezawa et al. “Quantum-Enhanced Optical-Phase Tracking”. In: *Science* 337.6101 (2012), pp. 1514–1517. ISSN: 0036-8075. DOI: [10.1126/science.1225258](https://doi.org/10.1126/science.1225258). eprint: <https://science.sciencemag.org/content/337/6101/1514.full.pdf>. URL: <https://science.sciencemag.org/content/337/6101/1514> (cit. on pp. 44, 45).

- [Yu+20] Haocun Yu et al. “Quantum correlations between light and the kilogram-mass mirrors of LIGO”. In: *Nature* 583.7814 (2020), pp. 43–47. ISSN: 1476-4687. DOI: [10.1038/s41586-020-2420-8](https://doi.org/10.1038/s41586-020-2420-8). URL: <https://doi.org/10.1038/s41586-020-2420-8> (cit. on p. 89).
- [Yue83] Horace P. Yuen. “Contractive States and the Standard Quantum Limit for Monitoring Free-Mass Positions”. In: *Phys. Rev. Lett.* 51 (9 1983), pp. 719–722. DOI: [10.1103/PhysRevLett.51.719](https://link.aps.org/doi/10.1103/PhysRevLett.51.719). URL: <https://link.aps.org/doi/10.1103/PhysRevLett.51.719> (cit. on pp. 3, 13).
- [YV16] Benjamin Yadin and Vlatko Vedral. “General framework for quantum macroscopicity in terms of coherence”. In: *Phys. Rev. A* 93 (2 2016), p. 022122. DOI: [10.1103/PhysRevA.93.022122](https://link.aps.org/doi/10.1103/PhysRevA.93.022122). URL: <https://link.aps.org/doi/10.1103/PhysRevA.93.022122> (cit. on p. 3).
- [ZG97] Peter Zoller and Crispin W. Gardiner. “Quantum Noise in Quantum Optics: The Stochastic Schrödinger Equation”. In: *Quantum Fluctuations, Volume 63*. Ed. by S. Reynaud, E. Giacobino, and F. David. First. Amsterdam: North Holland, 1997. ISBN: 0-444-82593-2 (cit. on p. 72).

# CURRICULUM VITAE

last updated on October 15<sup>th</sup> 2021

## EDUCATION

- Jan 2016 – Dec 2021 **Doctoral studies in Physics**, University of Vienna, Austria  
Sep 2012 – Jan 2015 **MSc. in Physic**, Sapienza Università di Roma, Italy  
Sep 2008 – Jan 2012 **BSc. in Physic**, Sapienza Università di Roma, Italy  
Sep 2003 – Jul 2008 **Diploma Scientifico**, Liceo Scientifico “A. Volta”, Spoleto, Italy

## RESEARCH EXPERIENCE

- Sep 2015 – Dec 2021 **Research Assistant**  
Prof. Markus Aspemeyer, Univeristy of Vienna  
Topic: optical levitation, near-field sensing and quantum control
- Jun 2014 – Jan 2015 **Project Student**  
Prof. Fabio Sciarrino, Sapienza Università di Roma  
Topic: integrated quantum optics
- Sep 2013 – Mar 2014 **Project Student**  
Prof. Roberto Di Leonardo, Sapienza Università di Roma  
Topic: optical trapping of bacteria

## TEACHING EXPERIENCE

- Summer term 2019 **Teaching Assistant**  
Seminar “Challenges in Research II - from practical work to publication”, PhD curriculum
- 2017 – 2021 Co-supervisor for one Master and two Bachelor thesis.
- 2009 – 2020 Mathematics and physics tutor for middle and high school students

## HONORS

- Oct 2016 – Sep 2021 **Affiliated to CoQuS Doctoral School**  
Doctoral school for research in Complex Quantum Systems
- May 2016 – Sep 2021 **Affiliated to VDS-P Doctoral School**  
Vienna Doctoral School for research in Physics
- May 6<sup>th</sup> 2019 **Best student talk award**, International Student Workshop on Quantum Technologies 2019, Shanghai, China.

## PUBLICATIONS

- [Mag+21] Lorenzo Magrini et al. “Real-time optimal quantum control of mechanical motion at room temperature”. In: *Nature* 595.7867 (2021), pp. 373–377. ISSN: 1476-4687. DOI: [10.1038/s41586-021-03602-3](https://doi.org/10.1038/s41586-021-03602-3). URL: <https://doi.org/10.1038/s41586-021-03602-3> (cit. on pp. 4, 17, 43, 101).
- [Car+20] Daniel Carney et al. “Mechanical quantum sensing in the search for dark matter”. In: *Quantum Science and Technology* (2020). URL: <http://iopscience.iop.org/article/10.1088/2058-9565/abcfd> (cit. on pp. 3, 52, 101).
- [Mag+18] Lorenzo Magrini et al. “Near-field coupling of a levitated nanoparticle to a photonic crystal cavity”. In: *Optica* 5.12 (2018), pp. 1597–1602. DOI: [10.1364/OPTICA.5.001597](https://doi.org/10.1364/OPTICA.5.001597). URL: <http://www.osapublishing.org/optica/abstract.cfm?URI=optica-5-12-1597> (cit. on pp. 4, 17, 21, 101).
- [Fla+15] Fulvio Flamini et al. “Thermally reconfigurable quantum photonic circuits at telecom wavelength by femtosecond laser micromachining”. In: *Light: Science & Applications* 4.11 (2015), e354–e354. ISSN: 2047-7538. DOI: [10.1038/lsa.2015.127](https://doi.org/10.1038/lsa.2015.127). URL: <https://doi.org/10.1038/lsa.2015.127>.

## CONFERENCE CONTRIBUTIONS

- Oct 12<sup>th</sup> 2021 **Invited Talk**, QuSCo International Conference: Quantum Control in Quantum Technologies, Obergurgl, Austria.
- Sept 20<sup>th</sup> 2021 **Contributed Talk**, Thermodynamics of Information Workshop, University of Vienna, Vienna, Austria.
- Sept 2<sup>nd</sup> 2021 **Invited Seminar Talk**, Yale University, New Haven (CT), USA.
- Jun 2<sup>nd</sup> 2021 **Contributed Talk**, APS DAMOP meeting, 2021, Virtual meeting, USA.
- Apr 9<sup>th</sup> 2021 **Contributed Talk**, Optomechanics for dark matter detection, 2nd edition, Virtual workshop, USA.
- Oct 30<sup>th</sup> 2019 **Invited Talk**, Vienna Graduate Conference on Complex Quantum Systems 2019, Vienna, Austria.
- May 6<sup>th</sup> 2019 **Contributed Talk**, International Student Workshop on Quantum Technologies 2019, Shanghai, China.
- Apr 6<sup>th</sup> 2019 **Contributed Talk**, Quantum Information and Measurement (QIM) V: Quantum Technologies Conference, Rome, Italy.
- Mar 7<sup>th</sup> 2019 **Contributed Talk**, APS march meeting, Boston, USA.
- Sep 21<sup>st</sup> 2018 **Contributed Talk**, YQIS conference and CoQus summer school, Vienna, Austria.
- Nov 30<sup>th</sup> 2017 **Contributed Talk**, Workshop Quantum Foundations: New frontiers testing quantum mechanics from underground to space, Frascati, Italy.



- Feb 2018 **Poster**, Gordon Research Conference (GRC): Mechanical Systems in the Quantum Regime, Ventura (CA), USA.
- Feb 2018 **Poster**, Gordon Research Seminars (GRS): Mechanical Systems in the Quantum Regime, Ventura (CA), USA.
- Feb 2018 **Poster**, Frontiers of Circuit QED and Optomechanics (FCQO18), Klosteneuburg, Austria.
- Sep 2018 **Poster**, Quantum Engineering of Levitated Systems, Benasque, Spain.
- Sep 2017 **Poster**, CoQuS and IMPRS-QST Vienna Summer School on Complex Quantum Systems, Vienna, Austria.